Universidade de Brasília – UnB

Instituto de Geociências – IG

Programa de Pós-Graduação em Geologia

“Evolução tectônica e metalogenética no contexto do depósito aurífero de Fazenda Nova, Arco Magmático de Arenópolis, Goiás”.

Gustavo Campos Marques

Tese de doutorado Nº 137

Orientador: Prof. Claudinei Gouveia de Oliveira

Banca Examinadora: Prof. Prof. Roberto Xavier (Unicamp)
Prof. Nilson F. Botelho (UnB)
Dr. Evandro Klein (CPRM)
Suplente: Prof[a]. Adalene M. Silva (UnB)

Brasília, DF, 2017

Agradecimentos

A Deus e ao *Reiki*, que sempre me trouxeram boas energias e as bençãos de cada dia.

À minha esposa Bárbara, minha companheira, pelo amor, amizade, cumplicidade e apoio, sempre me motivando para concluir esta tese de douturado, especialmente neste momento, grávida da minha pequena alegria chamada Sofia.

À minha mãe Ivete, pelo amor, amizade, confiança e apoio constantes em todos os momentos. Devo tudo a você!

Ao meu pai Roberto, pelo amor, amizade e companheirismo estabelecidos por toda a vida. Obrigado por tudo!

À Universidade de Brasília, instituição pública que me ofereceu da graduação ao douturado um ensino de qualidade e uma boa formação, atualmente muito bem aplicada na minha profissão.

Ao meu orientador Claudinei Gouveia Oliveira, pela experiência transmitida nas infinitas discussões geológicas, assim como pelo incentivo no aprendizado e no desenvolvimento da pesquisa, e, principalmente, na confiança depositada no meu trabalho científico.

Aos professores Márcio Pimentel, Maria Emília e ao geólogo Eugênio Espada, pelas revisões detalhadas nos *papers.*

À equipe de trabalho da Yamana, Iris, Leonardo, Kaká, Emerson, Tiago Eloi, Leandro (Dumdum), Diego, Igor, Rafael, Artur, Patrícia, Samuel (Bala), Eduardo e Jhony – que, diga-se de passagem, me ajudou muito- pela experiência e amizade. De forma especial, agradeço André Oliveira e Juliano Souza e pela compreensão profissional que tiveram na conclusão desta tese.

Aos meus irmãos Daniel, Fernando, Helena e Ana que são parte da minha existência e história.

Minhas “tias” Zulmira e Mirian pelo incentivo e carinho.

Aos meus sogro e sogra, Helvécio e Simone, pelo carinho e apoio para terminar essa tese.

À geologia, ciência que cada dia me apaixono mais, por mostrar os segredos da Mãe Terra!

Meus sinceros agradecimentos e dedicação especial para vocês duas Bárbara e Sofia .

Gustavo Campos Marques

Resumo

O Arco Magmático de Goiás é hoje um terreno estratégico para exploração de ouro pela *Yamana Gold*, razão pela qual boa parte dos orçamentos de exploração vem sendo aplicados neste local, visando o avanço do conhecimento cientifico e a descoberta de novos depósitos. Uma descoberta recente foi o depósito aurífero de Fazenda Nova, localizado na Faixa Jaupaci (180 km a oeste de Goiânia), uma das sequências vulcânicas do Arco Magmático de Arenópolis (porção sul do Arco Magmático de Goiás). Motivado pela referida descoberta, esta tese objetivou entender o contexto geológico da Faixa Jaupaci, assim como a gênese da mineralização aurífera de Fazenda Nova. Para atingir esse objetivo foram realizados mapeamentos geológicos, descrição de testemunhos de sondagem, interpretação de seção de sondagem, descrições petrográficas, análise química de rocha total, química de minério, química mineral, imageamento em microscópio eletrônico de varredura (MEV), análise isotópica Sm-Nd, análise isotópica C-O, imageamento de zircões por catodo luminescência (CL) e datação U-Pb por LA-ICP-MS.

Foram definidos dois eventos de magmatismo na Faixa Jaupaci: o primeiro, ocorrido em ambiente de arco magmático, se deu entre 770-750 Ma; e o segundo, gerado em um ambiente pós-colisional que ocorreu entre 597-506 Ma.

O magmatismo em ambiente de arco pode ser subdividido em dois principais pulsos: um mais antigo denominado Suíte Tipo 1, que compreende tonalitos e granodioritos com ilmenita, afinidade peraluminosa e calci-alcalina cristalizados em ~770 Ma; e um mais recente, que engloba magmas félsicos com magnetita, afinidade adakítica e metaluminosa representando pelos granitoides da Suíte Tipo 2 com idade de 753 ± 12 Ma , assim como os metariolitos basais da Sequência Jaupaci datados com idade de 748 ± 10 Ma. Os dados isótopos de Sm-Nd da Suíte Tipo 1 mostraram idades modelos T_{DM} de 0,86 até 0,91 Ga e ε_{Nd} (T) positivo com valores variando de +4,6 até + 5,4. Tais rochas foram interpretadas como sendo provenientes da fusão da crosta juvenil em estágios finais de colisão em um ambiente intra-oceânico. A Suíte Tipo 2 e os metariolitos s apresentam idades modelo T_{DM} um pouco mais antiga, variando de 1,1 até 1,21 Ga e o ε_{Nd} (T) positivo com valores variando de +1,1 até + 2,08, sendo a origem interpretada como proveniente de baixa fusão parcial de uma crosta juvenil muito espessa em um ambiente de arco continental.

O magmatismo pós-colisional foi divido em três eventos relacionados temporalmente à geração da Zona de Cisalhamento Moiporá Novo-Brasil: o pré-cinemático (~597-587 Ma), o sin-cinemático (~577-539 Ma) e o pós-cinématico (~511-506 Ma). O evento pré-cinemático ocorre em um ambiente extensional com ascensão mantélica e posterior delaminação da crosta inferior. Associado a este evento ocorrem vulcanismo bimodal, granitos tipo-A assim como um conjunto de diques denominados de Intrusivas Bacilândia (composto por diques de gabros doleritos, traquitos, dioritos pórfiro e sienitos pórfiro). As rochas do evento pré-cinemático apresentam idade modelos T_{DM} variando entre 0,75 Ga e 0,9 e ε_{Nd}(T) variando de +2,3 to +6,6. O evento sin-cinématico ocorre em um regime compressional no qual é registrada uma fase deformacional D_n com desenvolvimento de metamorfismo em fácies xisto verde e o desenvolvimento de grandes estruturas *strike-slip*. Dentre essas, a mais importantes é a Zona de Cisalhamento Moiporá-Novo Brasil, interpretada como uma estrutura litosférica profunda que permitiu a interação do manto com a base da litosfera, gerando um novo pulso de granitos tipo-A e um grande volume de diques alcalinos de Intrusivas Bacilândia. Os granitos tipo-A do evento sin-cinématicos apresentam a mesma assinatura geoquímica que o evento pré-cinemático, entretanto com idades modelos mais antigas com T_{DM} 1,27 – 2,25 Ga e ε_{Nd} (T) negativo com valores variando -1.0 até -20.0. De outra forma, as Intrusivas Bacilândia deste evento apresentam idade modelo T_{DM} entre 0.75 – 0.88 Ga e ε_{Nd} (T) positivo com valores variando entre +3,51 e +4,5. O evento pós-cinemático ocorre em um ambiente extensional com a geração de granitos tipo-A e lamprófiros sem deformação com idades modelos variando entre 0.9 até 1.2 Ga e ε_{Nd} (T) com valores negativos a positivos (-4,0 até +1,88).

A lavra da mineralização aurífera de Fazenda Nova teve seu inicio em 2004, entretanto os recursos oxidados foram exauridos e a lavra interrompida no final de 2006. No inicio de 2010 foi

reconhecido o potencial sulfetado nesse deposito e definido um recurso inferido de 650 koz com 4,0 g/t Au (cut-off de 2,0 g/t Au). A mineralização de Fazenda Nova está hospedada em diques das Intrusivas Bacilândia (principalmente em doleritos e diorito pórfiros) apresentando três estágios de alteração hidrotermal: i) o estágio inicial, ou mineralizante, consiste de uma alteração pervasiva biotítica e sericitização dos feldspatos acompanhada por *stock-work* de quartzo e brechas silificadas. A alteração pervasiva ocorre associada com uma disseminação de sulfeto composta por arsenopirita-pirrotita-scheelita-stibinita, além de siderita e apatita hidrotermal. A arsenopirita desse estágio apresenta formato acicular e apresenta ouro invisível além de inclusões de grãos de galena, pirita e ouro, que origina o caráter refratário do minério. A temperatura estimada para cristalização de arsenopirita, pirrotita junto ao ouro foi de 340°C; ii) O estágio intermediário é composto *stock-work* de calcita e quartzo com uma assembleia hidrotermal de clorita, epidoto, turmalina e titanita associado a sulfetos como pirrotita-pirita-arsenopirita. A arsenopirita neste estágio é tabular não apresenta inclusões de sulfetos e nem de ouro. A temperatura estimada para o par de sulfetos arsenopirita-pirita foi de 305°C; iii) O último estágio é composto por veios e brechas composto apenas por calcita-ankerita sem alteração hidrotermal ou mineralização aurífera.

Tantos os diques como a mineralização apresentam uma forte relação espacial com a Falha Bacilândia, uma estrutura NNW de segunda ordem da Zona de Cisalhamento Moiporá-Novo Brasil. A Falha Bacilândia deve ter atuado como uma estrutura profunda que canalizou os magmas das Intrusivas Bacilândia assim como os fluidos hidrotermais. A maior atividade desta falha ocorreu em aproximadamente 574-572 Ma e está associado à geração de maior volume de diques, tal como os estágios hidrotermais no depósito de Fazenda Nova. Processos magmáticos atuaram de forma crucial na fertilidade do Au e concentração de fluidos hidrotermais: O depósito de Fazenda Nova foi classificado como *Reduced Intrusion Related* epizonal baseado nos seguintes aspectos: i) mineralização hospedada em magma reduzido pós-colisional;ii) processos magmáticos atuando na concentração de Au e outros metais; iii) textura epizonal de veios como *stock-work*/brechas associadas a sulfetos com temperaturas de cristalização entre 340-305 °C, indicando um alto gradiente hidrotermal; iv) associação metálica de Au-As-W-Sb; v) Isótopos de C-O em veios de calcita com valores equivalentes a carbonatos magmáticos ou hidrotermais mantélicos.

Palavra Chave: Arco Magmático de Goiás, magmatismo pós-colisional, depósito do tipo Au Reduced Intrusion Related, zona de cisalhamento strike-slip intracontinental

Abstract

The Goiás Magmatic Arc became recently a strategic terrain for gold exploration by Yamana Gold, for this reason the substantial exploration budget has been invest in this terrain, aiming the advanced of scientific knowledge and the discovery of new deposits. The most recent discovery was the Fazenda Nova Gold deposit, located in Jaupaci Belt (180 km west from Goiânia), one of the volcanic sequences in the Arenópolis Arc (southern portion of Goiás Magmatic Arc). Motivated by discovery of Fazenda Nova deposit, this thesis aims to understand the geological setting of Jaupaci Belt as well as the mineralization model of Fazenda Nova gold deposit. Thus, to achieve these proposed goals were performed geological mapping, drilling section interpretation, drill core descriptions, thin section description, whole rock analysis, ore and mineral chemistry, electronic petrography using MEV, Sm-Nd isotopic analysis, zircon petrography using CL image and U-Pb aging of rocks using LA-ICP-MS method.

Two events of magmatic events were defined in Jaupaci Belt: the first, in arc setting that took place between ca. 770-750 Ma and the second, generated in post-collisional setting, occurred between 597-506 Ma.

The arc setting magmatism was separated in two main pulses: the first encompasses Type-1 Suite Ma represented by 770 Ma old ilmenite-bearing tonalities and granodiorites with peraluminous and calc-alkaline affinity. The second encompasses Type 2 Suite magnetite-bearing, metaluminous magmas represented by orthogneisses (753 ± 12 Ma) and basal metarhyolites (748 ± 10 Ma) of the Jaupaci Sequence. The Sm-Nd isotopes of Type-1 Suite display T_{DM} ages from 0.86 to 0.91 Ga and positive ε_{Nd} (T) with values ranging from +4.6 to + 5.4. The sources from these rocks were interpreted from melting of juvenile crust in late stage of intra-oceanic arc. The Type-2 Sm-Nd data showed slightly old T_{DM} ages with 1.1 to 1.21 Ga old and positive ε_{Nd} (T) values ranging from +1.1 to +2.08. The sources of these rocks were interpreted as melting of overthickned juvenile crust in a continental arc setting.

The post-collisional event was divided in three events temporally related to generation of Moiporá Novo-Brasil Shear Zone: the pre-kinematics (~597-587 Ma), the sin-kinematics (~577-539 Ma) and the post-kinematics (~511-506 Ma) events. The pre-kinematic event took place in extensional setting with mantle upwelling and delamination of sub-continental mantle lithosphere. The magmatic rocks from this event comprise I- and A-type granitoids, bimodal volcanism, as well as set of dikes called as Bacilândia Intrusives (composed by dykes of gabbros, dolerites, trachyte, diorite porphyry and syenite porphyry). The Sm-Nd isotopic data from the pre-kinematic rocks showed T_{DM} ages ranging from 0.75 Ga to 0.9 and ε_{Nd}(T) with positive values ranging from +2.3 to +6.6. The sin-kinematics event occurred in compressional regime with development of green-schist metamorphism, development of D_n deformation event and deep translithospheric strike-slip shear zones. The most paramount structure is Moiporá Novo-Brasil Shear Zone, this deep shear zones allowed the interaction of mantle and lower crust, inducing the generation of A-type sin-kynematic granitoids as well as a large volume of Bacilândia Intrusive dikes. The sin-kinematics A-type granites display the same geochemical feature of pre-kinematics granites, however Sm-Nd T_{DM} ages are older with values ranging from 1.27 to 2.25 Ga and negative ε_{Nd} (T) with values varying -1.0 to -20. On the other hand, the dikes of Bacilândia Intrusives from this event showed T_{DM} ages between 0.75 – 0.88 Ga and positive ε_{Nd} (T) with values ranging between +3.51 to +4.5. The post-kinematic event took place in extensional setting with generation of undeformed type-A granite and lamprophyre. The T_{DM} ages showed variation of 0.9 – 1.2 Ga, while ε_{Nd} (T) values varying between negative to positive (-4.0 to +1.88).

The mining of gold mineralization of Fazenda Nova have been started in 2004, however, the oxidized resources were depleted and the mining was interrupted in late 2006. In early 2010, was recognized sulphide potential in this deposit and the exploratory works defined an inferred resource of 650 koz with 4.0 g/t Au (cut-off of 2.0 g/t Au). The mineralization is hosted in dikes of Bacilândia Intrusives (mainly in dolerites and diorite porphyries) with three hydrothermal stages: i) the early or mineralized stage, comprise pervasive sericitization of feldspar and biotitization with stock-work of quartz and silicified breccias associated with disseminated sulfide assemblage of arsenopyrite-

pyrrhotite-scheelite-stibinite in addition to hydrothermal siderite and apatite. The most common sulfide in this stage is fine-grained acicular arsenopyrite that hosted invisible gold and inclusion of gold, galena and pyrite grains. The temperature estimated for crystallization of acicular arsenopyrite and pyrrhotite along with gold was of 340°C;ii) intermediate stage is represented by stockworks of calcite-quartz veins associated with hydrothermal assemblage of chlorite, tourmaline, epidote, titanite and disseminated sulfide assemblage of pyrrhotite-arsenopyrite-pyrite. The arsenopyrite at this stage display tabular texture with no sulfides or gold inclusion. The crystallization temperature of tabular arsenopyrite-pyrite was estimated with 305°C; iii) the late stage is veining and brecciation infilled by monotonous calcite-ankerite with no gold mineralization or hydrothermal alteration

The dikes and gold mineralization present strong relationship with the Bacilândia Fault. The Bacilândia Fault is a second order crustal-scale shear zone that branch out of the major crustal-scale Moiporá-Novo Brasil shear system along the NNW direction. The Bacilândia fault play important role to channelize melts to uppercrust and mineralized hydrothermal fluids. The major activity took place at ~574-572 Ma with emplacement of large volume of dikes of Bacilândia Intrusives and most likely development of hydrothermal stages in Fazenda Nova deposit. The Fazenda Nova deposit was classified as epizonal Reduced Intrusion Related based on the follow evidences: i) mineralization developed during post-collisional tectonic setting above previously metasomatized subcontinental lithosphere mantle; ii) high geothermal gradients indicate by ore deposition at temperatures of 340° to 300°C and veins textures formed only shallow depths (<4 km); iii) metal association of Au-As-W-Sb iv) volatile saturation induced by magmatic processes such as fractional crystallization, magma mixing, or crustal assimilation; v) CO_2 hydrothermal veins with C-O isotopes displaying magmatic/mantle fluids affinities

Keywords : Goiás Magmatic Arc, post-collisional magmatism, Reduced Intrusion Related gold deposit, intracontinental strike-slip

Lista de Figuras

Lista de Tabelas

Sumário

1.INTRODUÇÃO

A aglutinação de fragmentos crustais no Neoproterozoico, para formar o Gondwana, está associada a mineralizações auríferas e à geração de arcos juvenis. Destes, destacam-se: *Arabian-Nubian Shield* ao longo do Mar Vermelho (com 880-550 Ma, Botros 2001, Doebrich *et al*., 2004,); *Carolina Terrane* no sudeste dos Apalaches (535 Ma - Hibbard *et. al.*, 2002); *Sayan-Baikal-Muya* Belt no SW da plataforma da Siberia (Zhmodik *et al.*, 2006); e o *Arco Magmático de Goiás* no Brasil Central (886-630 Ma, Oliveira *et al.*, 2004; Oliveira *et al*., 2015,). A descoberta recente de depósitos de ouro do tipo classe mundial, como por exemplo*:* Sukary Hill com 10 Moz (43-101 report) no *Arabian Nubian-Shield* explorado pela Centamin; e Cu-Au Chapada (Oliveira *et al.*, 2015) com 7 Moz, no Arco Magmático de Goiás, explorado pela *Yamana Gold*, tornou arcos juvenis Neoproterozóicos estratégicos para as empresas de exploração mineral. Nesse contexto, a *Yamana Gold* vem investindo de maneira sistemática na exploração do Arco Magmático de Goiás, no qual se destaca o depósito aurífero de Fazenda Nova (denominado internamente pela Yamana como projeto Arco Sul), como a mais nova (re) descoberta de ouro nesse tipo de ambiente.

1.1. Justificativa do tema

O depósito aurífero de Fazenda Nova está hospedado nas rochas vulcânicas da Sequência Jaupaci (Amaro, 1989), e localiza-se na porção leste do Arco Magmático de Arenópolis (Fig.1.1), segmento meridional do Arco Magmático de Goiás. Estas rochas vulcânicas foram prospectadas pela WMC (*Western Mining Company*), no início da década de 90, com a realização de uma campanha de sedimento de corrente regional, posteriormente delimitada em um *follow-up* de amostragem de solo. Em 1995, a concessão mineral foi passada para a Santa Elina, quando foi delimitado um corpo de minério oxidado por meio de sondagem reversa. Em 2003, a *Yamana Gold* adquiriu os direitos minerais da Santa Elina, produzindo entre os anos de 2004 a 2006 um total de 163 koz a um teor 0,89 ppm de minério oxidado de ouro. Contudo, no final do ano de 2006, as atividades de mineração e exploração naquele depósito foram encerradas, pois o minério oxidado foi exaurido.

A partir de 2010, a equipe de exploração da *Yamana Gold* realizou uma reavaliação dos dados existentes do depósito de Fazenda Nova, na qual se observou um potencial para minério de ouro sulfetado naquela região, motivo pelo qual foram realizados furos diamantados exploratórios que interceptaram compósitos de alto teor de ouro (>10 g/t Au).

Atualmente, foram definidos recursos inferidos sulfetados com 646.000 oz @ 4,02 g/t Au (cut-off de 2,0 g/t de Au , conforme a NI-43-101) e ainda possui potencial para adicionar novos recursos. Além do referido depósito, nos trabalhos regionais de exploração foram encontrados outros prospectos de Au na Sequência Jaupaci, mostrando o grande potencial metalogenético para ouro nesta porção do Arco Magmático de Goiás (Fig.1.1).

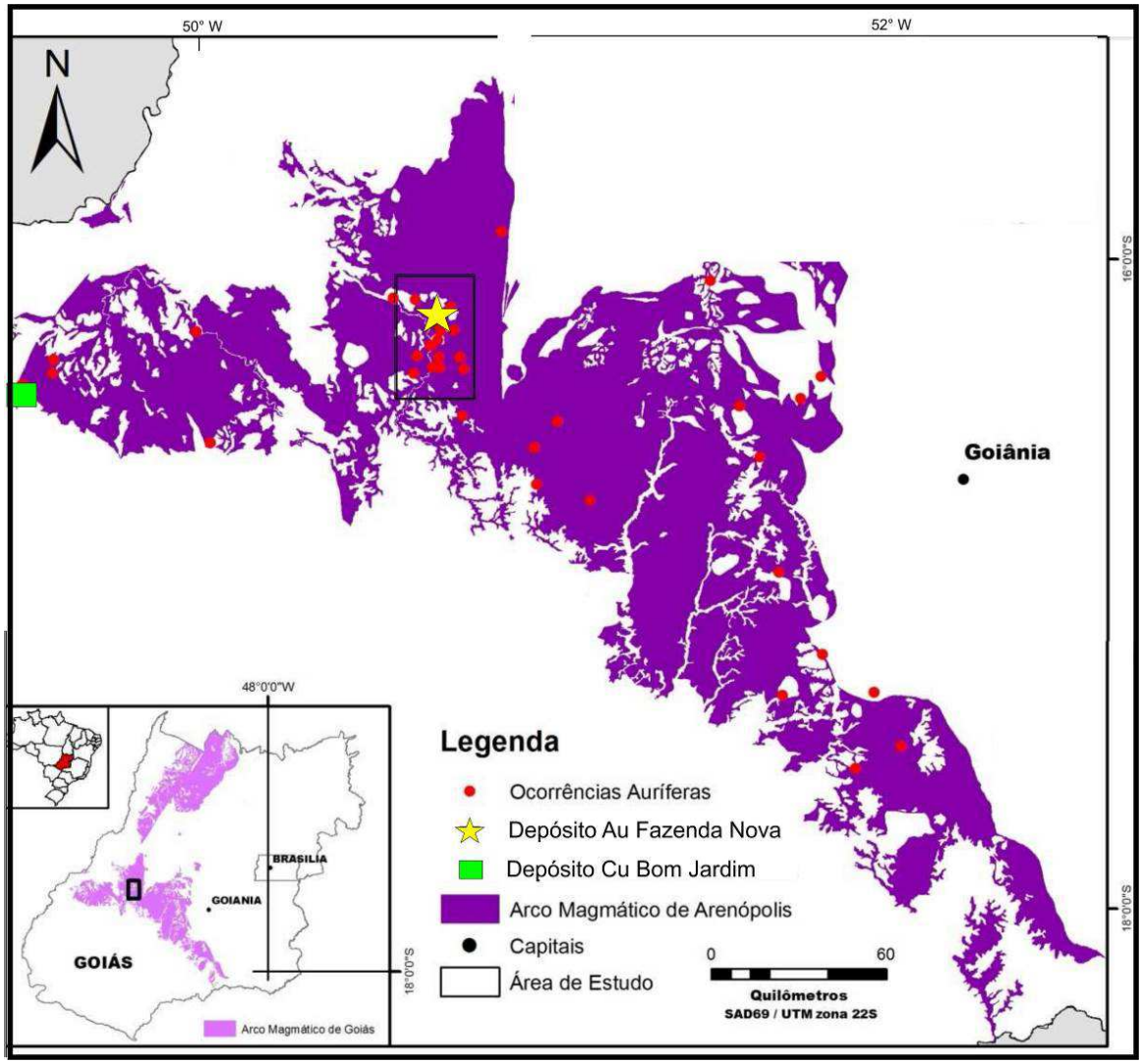

Figura 1.1 - Localização das ocorrências auríferas e do depósito de Au-Fazenda Nova no Arco Magmático de Arenópolis, a área de estudo encontra-se 150 km de distância de Goiânia, GO (Adaptado do SIG de Góias).

Apesar do potencial prospectivo de ouro na Sequência Jaupaci, os únicos trabalhos que descreveram a geologia nesta área foram os de Amaro (1989), Pimentel *et al.,* (1991) e mais recentemente Ramos (2010). Estes trabalhos apenas descreveram a mineralização

aurífera de Fazenda Nova hospedada em microdioritos (andesitos) e dioritos pórfiros associados a rochas metavulcânicas ácidas da Sequência Jaupaci.

Contudo, com o avanço dos mapeamentos regionais e a realização de furos de sondagem pela Yamana no citado depósito, foi possível chegar a novas constatações, quais sejam: i) a mineralização de ouro está associada a um sistema complexo de diques/*sills* com diferentes composições (além de dioritos foram mapeados gabros, traquitos e sienitos) que intrudem diferentes tipos de rochas plutônicas além das metavulcânicas félsicas; (ii) observou-se a relação espacial de falhas transcorrentes com as ocorrências de ouro, diques/*sills* e granitos tipo A; (iii) caracterizou-se a mineralização com um zoneamento proximal e distal. O proximal está associado a um sistema *stock-work/*brecha, com intensa alteração hidrotermal representada por silicificação, sericitização, biotitização e sulfetos (arsenopirita, pirrotita e pirita), no qual o ouro está diretamente associado à ocorrência de arsenopirita. No distal, os veios passam a apresentar e alteração clorítica com carbonatação associado a uma sulfetação incipiente.

Ocorre que, apesar dos avanços, ainda existiam questionamentos que motivaram a elaboração desta tese de doutoramento:

1- Qual a idade dos diques e de suas rochas encaixantes (Sequência Jaupaci)?
2- Em qual contexto tectônico essas rochas se formaram?
3- Qual a relação de falhas transcorrentes e geração dos diques e granitos tipo-A? Essas falhas são condutos de magma e fluido hidrotermais?
4- Qual o modelo metalogénetico para o depósito Fazenda Nova?

1.2. Estrutura da tese e objetivos

A tese está divida em quatro capítulos além deste tópico introdutório. Os capítulos 3 e 4 estão na forma de artigos que já foram ou ainda serão submetidos para publicação em periódicos científicos internacionais especializados nos temas abordados. Os artigos contemplam os objetivos, resultados e metodologias aplicadas para responder as perguntas acima mencionadas. A tese está divida da seguinte forma:

O **capítulo 2** contempla a introdução teórica para explicitar os conceitos utilizados nos capítulos subsequentes. Nele será abordada a definição de orogênese acrescionária e os seus principais tipos de depósitos auríferos, além dos principais controles na metalogênese do ouro, como a fertilidade do manto, eventos de remobilização e grandes estruturas litosféricas.

Ademais, serão listadas as diferenças entre o sistema do tipo Au-orogênico e Au-*Intrusion related,* com o qual o depósito de Fazenda Nova compartilha características.

O **capítulo 3** visa definir a idade das rochas hospedeiras da mineralização de Fazenda Nova, e o contexto tectônico em que elas se formaram, os quais foram expostos na forma do 1° artigo submetido em periódico internacional (*Precambriam Research),* denominado ***"Evolution of the Neoproterozoic Goiás Magmatic Arc: from island arc to post-collisional intracontinental magmatism***". Este artigo traz novos dados de U-Pb em zircão, Sm-Nd e geoquímica de rocha total da Faixa Jaupaci, onde foram reconhecidos cinco eventos magmáticos, sendo os dois primeiros eventos relacionados ao ambiente de arco definido com idade entre 770 a 750 Ma, e os três últimos ao ambiente pós-colisional, definidos entre 597 até 504 Ma. Adicionalmente, foram correlacionadas as idades obtidas com eventos tectônicos no Arco Magmático de Goiás, e com outros arcos Neoproterozoicos no mundo.

O **capítulo 4** define a relação de estruturas transcorrentes com a formação de depósitos de ouro e discorre sobre o modelo metalogenético do depósito de Fazenda Nova, assunto que será tratado no 2° artigo a ser publicado em periódico internacional, chamado "***The Fazenda Nova Au deposit, Goiás Magmatic Arc: Cambriam Intrusion Related auriferous mineralization controlled by intracontinental strike-slip fault" –***. Este artigo aborda dados de petrografia, e associações hidrotermais do depósito de Fazenda Nova, fornece idades de U-Pb, Sm-Nd e geoquímica de rocha total dos diques associado a mineralização aurífera, além de definir um modelo metalogenético para o depósito de Fazenda Nova.

O **capítulo 5** contempla as conclusões obtidas na tese.

As referências dos capítulos 2 e 5 estarão no final da tese, enquanto as referências dos (capítulos 3 e 4) estarão no final de cada capítulo.

2.OROGÊNESE ACRESCIONÁRIA E DEPÓSITOS AURÍFEROS RELACIONADOS.

A geração de supercontinentes está diretamente relacionada ao desenvolvimento de orogêneses acrescionárias. Este tipo de orogênese é caracterizado pela subducção de litosfera oceânica em margens continentais ou em ambientes intra-oceânicos, associados aos sistemas de falhas complexas (empurrões e transcorrências) com um ou mais eventos tectônico-termais. Tal fato resulta no espessamento e na estabilização da litosfera com a significativa acresção de terrenos juvenis (Windley 1995; Cawood & Buchan, 2007; Cawood *et al.,* 2009). Contudo, cabe destacar que embora exista a predominância de arcos juvenis nesta orogênese, eles representam estreitas crostas obductadas sobre um embasamento litosférico antigo, eventualmente denominados microcontinentes (Griffin *et al.,* 2009; Hronsky *et al.,* 2012). Como exemplos de orogêneses acrescionárias, podemos citar: no Arqueano, a Província Superior e o Craton Yalgarn (Sengör & Natal'in 2004); no Neoproterozoico, a porção nordeste da Orogênese Pan-Africana (Stern 1994) e o Arco Magmático de Goiás (Oliveira *et al.,* 2015); e como exemplo atual, a margem e a paleomargem do Oceano Pacífico.

2.1 Orogênese Acrescionária no Neoproterozoico e a formação do Gondwana.

A amalgamação do supercontinente Gondwana ocorreu no final do Neoproterozoico. Neste período ocorreu o fechamento do oceano Goiás-Farusiano em decorrência da convergência dos crátons Amazônico, São Francisco-Congo, Kalahari, Rio de La Plata e do Oeste do Cráton Africano, dando origem ao Gondwana ocidental. Ao mesmo tempo, ocorreu o fechamento do oceano Moçambique, decorrente da aproximação dos escudos Núbio, Antártica, Austrália e Índia, formando Gondwana Oriental (Cordani *et al.,* 2013, Jonhson *et al.,* 2011). Os cratons e escudos que formam Gondwana são compostos por fragmentos continentais provenientes da fragmentação do Supercontinente Rodínia, processo que se iniciou há aproximadamente 900 Ma e terminou há cerca de 570 Ma. Neste processo, diversos complexos acrecionários e possíveis microcontinentes foram aprisionados nos cinturões móveis brasiliano-pan-africanos, e agora estão expostos na América do Sul, na porção oeste e Central da África, e na porção ocidental do Oriente Médio. Eles podem ser classificados em dois tipos de unidades orogênicas: i) Uma unidade antiga (com idade de 900-650 Ma), composta por faixas de orogênese acrescionária, que é constituída essencialmente por rochas

sedimentares e magmáticas intraoceânicas com assinatura juvenil. No Gondwana ocidental, é representada pelos arcos magmáticos de Iskel, Tilemsi, Amalaoulaou, Kabyé e Goiás (Dostal *et al.,* 1994; Caby 2003, Pimentel *et al.,* 2000, Laux *et al.,* 2005); no Gondwana Oriental é representada pelos terrenos Arábico-Núbico como Midyan, Hijaz, Asir, Ar Ryan e Afif (Meert ,2003; Doebrich *et al.,* 2007, Robinson *et al.,* 2014); ii) uma unidade mais jovem (com idade de 700-520 Ma), formada pela colagem de faixas orogênicas localizadas nas margens cratônicas, compreendendo embasamento retrabalhado e cinturões de dobras e empurrões. Esta unidade tectônica é composta por sequências ofiolíticas, prismas acrescionários e suítes magmáticas com assinaturas de arco continental, a exemplo das faixas Trans-Saharan, Dahomeyan, Araguaia, Brasília e Paraguai.

A aglutinação dessas unidades ocorreu devido ao fechamento do Oceano Goiás-Farusiano, que é marcado por assembleias metamórficas de baixa temperatura/ alta pressão, como coesita-eclogitos, evidenciando um ambiente colisional continente-continente do tipo *deep-continental subduction* (Ganade de Araújo *et al,.* 2014). As idades obtidas nestas rochas metamórficas no oeste da África (Togo e Mali) são de ~621-611 Ma (Berger *et al.,* 2014), crono-correlatas com as idades obtidas na Província Borborema ~616 Ma (Ganade de Araújo *et al.,* 2014), indicando um *front* colisional de mais 2500 km, podendo ser comparado com o tamanho da cordilheira atual dos Himalaias

Posteriormente a este estágio colisional, desenvolve-se um mega-cisalhamento denominado Lineamento Transbrasiliano (Schobbenhaus 1975) ou Transbransiliano-Kandi (Cordani *et al.,* 2013), estendendo-se da América do Sul (desde a Argentina até o nordeste do Brasil) à África (Togo e Argélia). Este lineamento é composto por diversas zonas de cisalhamentos profundas que reutilizaram zonas de fraquezas litosféricas geradas pelo estágio de colisão continental. Esta zonas de cisalhamento podem ser profundas o suficiente e estenderem-se até a base da litosfera (*sub-continental lithospheric mantle-SCLM*), agindo como condutos para o manto ascender e fundir o material litosférico, originando magmatismo bimodal e granitos do Tipo A (Vauchez & Tommasi, 2003; Pirajno, 2010). Exemplos de magmatismo Tipo A ao longo do Lineamento Transbrasiliano: o Granitos Mucambo com 535 Ma e Merouca 520 Ma no Ceará (Archanjo *et al.,* 2009); o Granito Serra Negra com 525 Ma (Guimarães *et al.,*, 2012) e Iporá com 490 Ma na região do Arco Magmático de Goiás (Pimentel *et al.,* 1996); e os granitos São Vicente com 521 Ma e Coxim com 542 Ma na Faixa Paraguai com (McGee *et al.,* 2012).

Estruturas semelhantes ao Lineamento Transbrasiliano também são observadas no *Arabian Nubian-Shield*, como a Falha Nadj, associados a granitos Tipo-A, datados em ~ 525 Ma (Robinson *et al.*, 2014).

2.2. Depósitos auríferos associados à orogênese acrescionária

Uma grande variedade de depósitos auríferos é formada em orogênese acrescionária relacionados a ambientes tectono-magmáticos distintos, como pórfiros e epitermais do tipo (Au-Cu-Ag) *High sulphidation* ou (Au-Ag) *Low-Suphidation*; intrusões alcalinas com Au *Low-Sulphidation*, depósitos de Au-tipo *Carlin*, vulcanogênico com sulfetos maciços rico em Au, depósitos orogênicos de Au, depósitos do tipo Au *Intrusion Related* e depósitos do tipo IOCG ou Cu-Au-Oxido de Ferro (Bierlien *et al.*, 2006). Devido às alternâncias dos estados de extensão e de compressão nesta orogênese, os depósitos supracitados podem ser formados em ambientes e tempos distintos, e, posteriormente, serem justapostos ou até mesmo se sobreporem (*overprinting*). Por outro lado, esses depósitos podem ser formados sincronicamente e separados espacialmente dentro de um mesmo orógeno.

Hronsky *et al.*, (2012) sintetizaram uma orogênese acrescionária em 4 principais domínios metalogenéticos e tectono-magmáticos: i) magmatismo de arco relacionado a margem ativa de subducção; ii) superposto a rifte; iii) inversão de arco e rifte pericontinental; iv) superposto a impacto de ascensão mantélica. Cada ambiente tectono-magmático é explicitado na tabela 2.1.

Tabela 2.1 – Depósitos formados em orogênese acrescionária, tabela adaptada de Hronsky *et al.*, (2012).

Ambiente tectno-magmático	Tipos de Depósitos	Regimesgeodinâmico favoráveis	Exemplos	Comentários
Magmatismo de arco relacionado a margem ativa de subducção	Pórfiros e depósitos epitermais relacionados, como (Au-Cu-Ag) High sulphidation, (Au-Ag) Low-Suphidation	Transição de extensão para compressão oblíqua , também relacionados a placas com subducção pouco inclinada (Tosdal & Richards ,2001).	Tampankam ,Bingham Canyon, Grassberg	Predomínio de pórfiros e depósitos relacionados com magmas calci-alcalinos a alcalinos , no qual magmas mineralizados alcalinos são tipicamente ricos em Au.
				Geralmente estão associados com falhas transformantes ou outras estruturas profundas que representam conexões com a litosfera.
				A diversidade de depósitos depende da relação espacial (distal ou proximal) do centro magmático.
Rifte superposto a uma margem continental ativa	Intrusões alcalinas com Au *Low-Sulphidation* relacionados a depósitos vulcanogênicos (VMS) com sulfetos maciços ricos em Au	Extensão associada a *roll-back* da crosta subductada ou extensão local em ambiente colisional (Richards 1990)	Ladoham-Lihir , Henty, Porgera ,Cripple Creek	Rifte ocorre com em uma fase extensional, devido a retração da placa subductante , formando back-arc e depósitos do tipo VMS, ou com extensão incipiente com magmatismo alcalino em orógenos colisionais formando depósitos do tipo low-sulphidation
				Tipos de depósitos estão fortemente relacionado com grau de extensão.
Inversão de arco e rift-pericontinental	depósitos orogênicos de Au, depósitos do tipo Au *Intrusion Related*	Últimos estágios de inversão colisional e extensão limitada pós-orogênica.	Dolin Creek , Kalgoorlie, Muruntau, Ashanti, , Bendigo	Ocorre devido a inversão de rifts pericontinentais formados na bacia retro-arco, que apresenta sequências vulcano-sedimentares com assembleia metamórfica de alta temperatura e baixa pressão
				Geralmente ocorrem adjacentes a margens continentais ou fragmentos de crosta continental
				Significativa contribuição magmática, predominando magmas derivados do manto
Impacto de pluma ou ascenção mantélica	IOCG ou Cu-Au-óxido de Ferro	Estágios iniciais de impacto de *hot-spot* sob a crosta	Olympic Dam	

2.3. Ligação do enriquecimento do manto superior e controles em escala regional com a formação de depósitos auríferos.

Todos os depósitos supracitados na tabela 2.1, independentemente do ambiente tectono-magmático em que se formaram, apresentam três fatores em comum para formação de depósitos auríferos em orogêneses acrescionárias (Bierlien *et al.*, 2009, McCuaig *et al.*, 2010, Hronsky et al., 2012): i) a fertilidade do manto litosférico superior; ii) o evento de remobilização dos fluidos previamente enriquecidos em ouro, e; iii) as grandes estruturas litosféricas que canalizam os fluidos mineralizados para a crosta superior. Esses três fatores atuam como componentes chaves formando "reservatórios" auríferos que posteriormente podem ser acessados em diferentes ambientes tectono-magmáticos (Tabela 2.1).

2.3.1.Fertilidade do Manto

Com intuito de elucidar a metalogenia do ouro com uma fonte mantélica, Loucks & Ballard (2003) mostraram dados de rocha total de basaltos de arcos do Quaternário em dois tipos de ambientes: ambientes relacionados a depósitos de ouro e sem relação com a mineralização aurífera. Os resultados mostraram que basaltos relacionados a ambientes auríferos apresentaram geoquímica distinta, caracterizada por altos valores de Nb e Th e por outros elementos litófilos incompatíveis, com altas razões Nb/Y, Th/Yb e Ba/Zr. O mesmo padrão geoquímico foi observado em lamprófiros shoshoníticos em depósitos auríferos na Austrália (Hillgrove) e na China (Laowangzhay).

Loucks & Ballard (2003) mostraram que essas anomalias geoquímicas dos magmas associados a depósitos auríferos não estão relacionadas às contribuições de fluidos aquosos ou magmas derivados da fusão da placa subductada. A contribuição de fluidos aquosos foi descartada devido ao fato de que magmas "férteis" em ouro mostram-se com pouca adição de elementos incompatíveis solúveis em água, como, por exemplo, K, Pb, Sr e Cs (Figura 2.1). A outra possiblidade de anomalia, associada à fusão da placa subductada, também foi descartada devido ao fato de os elementos terras rara pesados, como Y, Ho, Er, Tm e Yb, apresentarem o mesmo padrão tanto para os magmas "férteis" em ouro quanto para os "estéreis" nesses elementos.

Analisando as evidências supracitadas, Loucks & Ballard (2003) concluíram que o magma parental de ambientes férteis em ouro é produzido por dois fatores: baixo grau

de fusão parcial do manto astenosférico e/ou a fusão de regiões do manto litosférico, que são pré-enriquecidas em elementos incompatíveis (fertilizados) gerados previamente pelo baixo grau de fusão parcial do manto profundo. Outras evidências do manto como um reservatório fertilizado são: i) a associação entre magmas alcalinos, que por definição são enriquecidos em elementos incompatíveis, e mineralização auríferas (Jensen & Barton 2000; Sillitoe, 2002; Muller, 2002); ii) evidencias diretas de enriquecimento primário de ouro em magmas alcalinos, como, por exemplo, lavas alcalinas recentes do vulcão Kilauea, no Havaí, onde são documentadas concentrações de 36 ppb de ouro (Loucks & Ballard 2003); iii) estudos em xenólitos peridotíticos, no norte do Craton da China, que apresentam valores relativamente altos de ouro, com concentrações de 10,4 a 13,5 ppb de ouro (Zheng *et al.,* 2005).

Percebe-se, portanto, que o ouro se comporta como um elemento incompatível durante fusão parcial baixa ou moderada do manto superior, sendo que as concentrações máximas de ouro estão relacionadas com a menor taxa de fusão parcial, enquanto as menores concentrações de ouro estão relacionadas com o aumento da taxa de fusão (Figura 2.2).

Kay *et al.,* (2005) descreve que subducção de baixo ângulo, ou *flat-subduction,* é conceitualmente favorável para a fertilização do manto superior descrito acima por dois principais motivos: primeiro, porque neste ambiente a geração de magma relacionado à subducção é diminuída devido ao resfriamento da cunha mantélica induzida pela crosta, gerando, desta forma, magmas de baixa fusão parcial e, consequentemente, enriquecidos em ouro; segundo, porque a subducção de baixo ângulo é tipicamente associada com a tectônica compressional, que inibe a passagem de magma derivado do manto para a superfície (Figura 2.2).

Outro processo de fertilização em subducção de baixo ângulo está relacionado aos magmas adakíticos descritos por Defant & Drummond (1990) e Martin *et al.,* (2005) que consistem em magmas atribuídos à fusão parcial de crosta oceânica (metabasalto hidratado) subductantes em pressões altas o suficiente para estabilizarem granada ± anfibólito residuais (baixos valores de Y), e fundirem plagioclásios (altos valores de Sr). Segundo Sun et. al. (2010), a crosta oceânica apresenta concentrações de Cu duas vezes maior do que a crosta continental inferior e a cunha mantélica. Desta forma, o magma adakitico e os fluidos associados à fusão da crosta oceânica podem liberar grande quantidade de Cu (presumidamente ouro também) com grande potencial de formação de mineralizações de Cu-Au ou também de apenas Au. Um exemplo de

magma com afinidade adakítica relacionado à mineralização Cu-Au (pórfiro neoproterozóico deformado) é o depósito de Chapada, descrito por Oliveira *et al.* (2015), no Arco Magmático de Goiás.

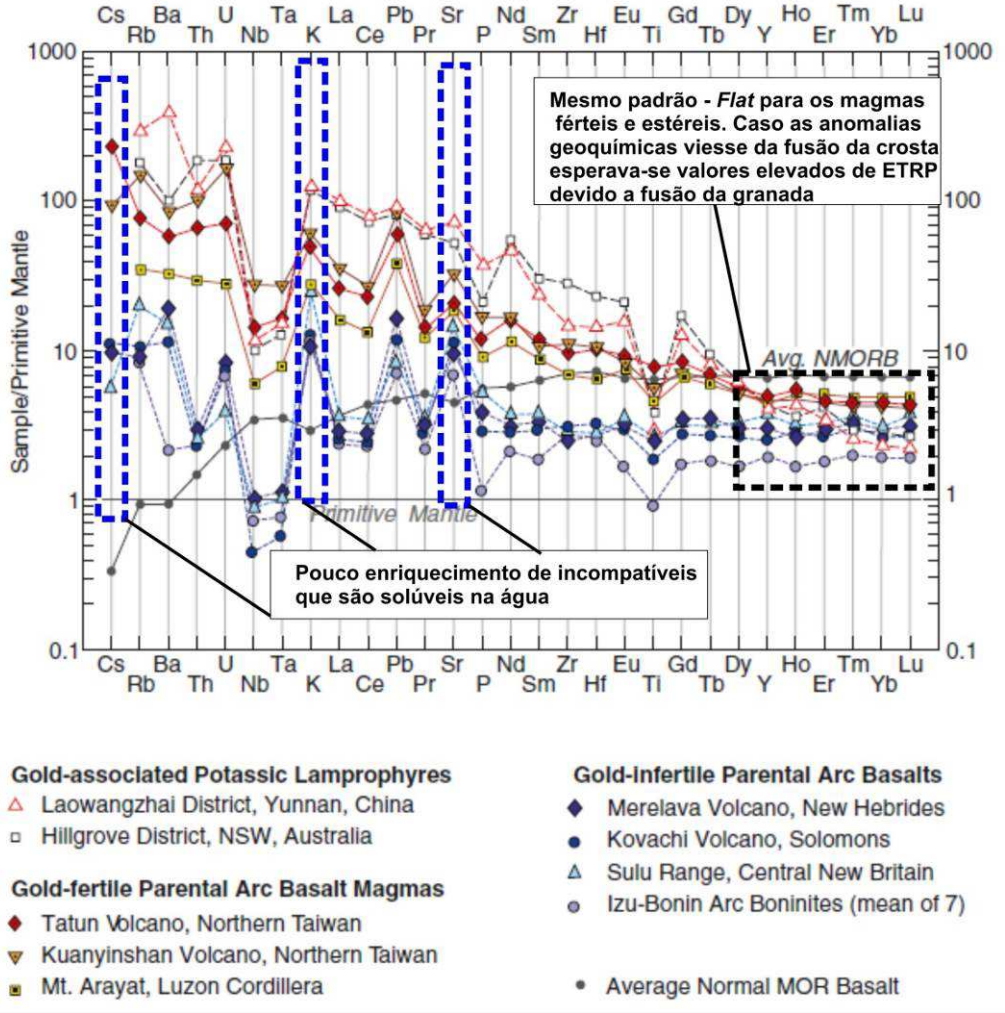

Figura 2.1 - Gráfico multielementar adaptado de Loucks & Ballard (2003) com a comparação entre basaltos N-MORB, basaltos relacionados a depósitos de ouro, lamprófiros relacionados a depósitos de ouro e basaltos sem relação com mineralizações auríferas. Nota-se o enriquecimento de elementos incompatíveis, principalmente de elementos insolúveis HFSE como Nb, Ta e Zr, nos basaltos relacionados às mineralizações auríferas.

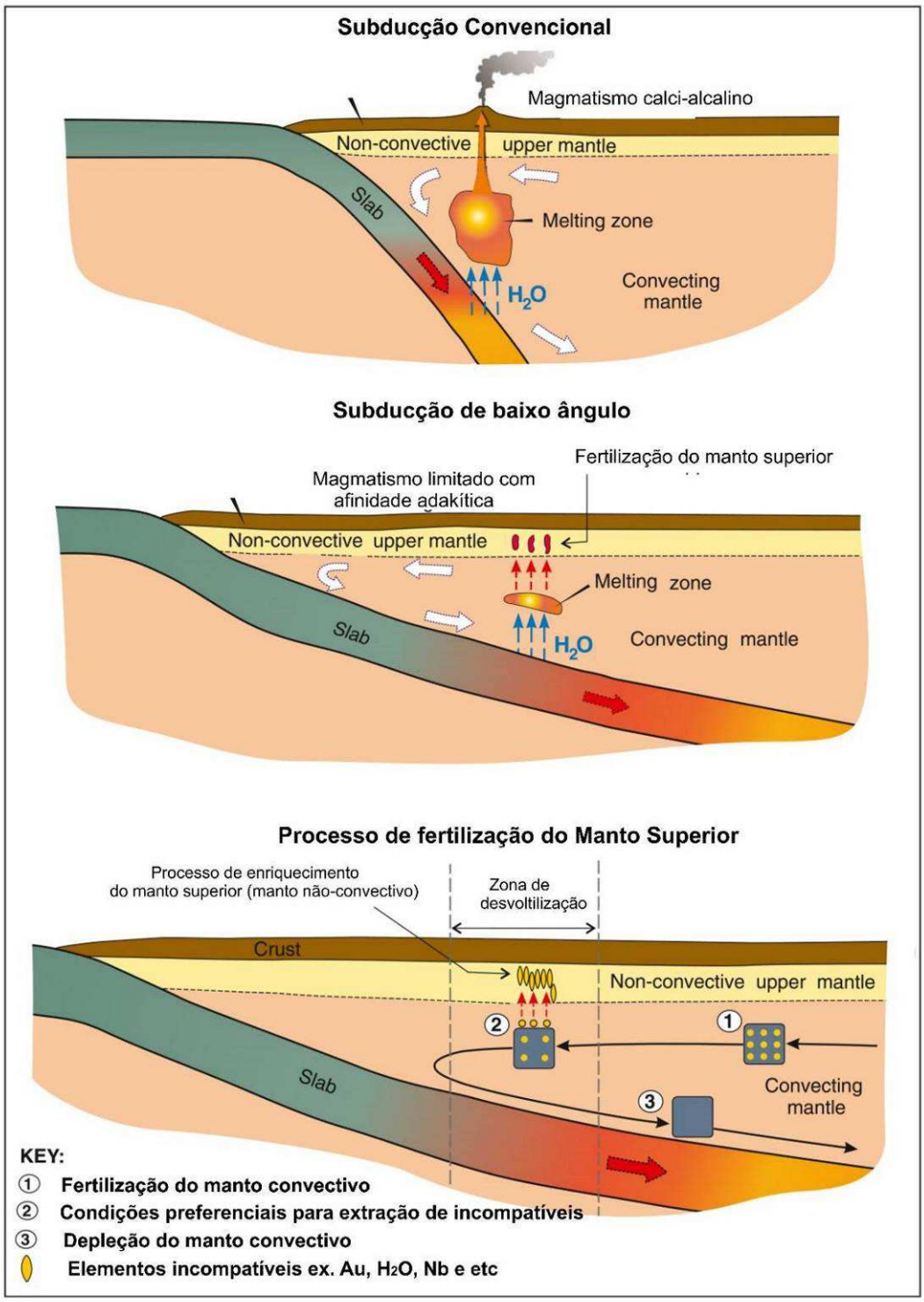

Figure 2.2 - Modelo esquemático de Hronsky *et al.* (2012) mostrando uma subducção convencional (ou de alto ângulo) no qual estão relacionados intenso magmatismo, geralmente de composição calci-alcalina, e com elevada fusão parcial, sendo elevadas devido a grande quantidade de fluidos liberados da placa subductada. Em uma subducção de baixo ângulo ocorre pouca fusão parcial e magmatismo limitado, podendo ter composição adakítica. Esse processo enriquece o manto não-convectivo com elementos incompatíveis

2.3.2. Evento de Remobilização

O segundo evento importante é a remobilização de magmas ou fluidos enriquecidos em ouro para o manto superior, via refusão de porções pré-enriquecidas em ouro. Um fator crítico, segundo Richards (2009), é a não diluição por outros magmas derivados do manto profundo, favorecidos por situações onde apenas pequenas quantidades de magmas profundos são geradas e fortemente focalizadas para a crosta superior (um exemplo de ambiente onde é favorecido este fator é a subducção de baixo ângulo discutido acima).

Segundo Goldfarb *et al.* (2001) e Bierlein *et al.* (2006), os quatro principais fatores que controlam a remobilização de litosfera previamente fertilizada para a crosta superior são: i) o impacto de pluma mantélica; ii) a delaminação do manto litosférico em evento pós-colisional; iii) a erosão do manto litosférico ; iv) a retração da placa subductante (*slab rollback*) com posterior ascensão astenosférica (Figura 2.3 A, B, C e D).

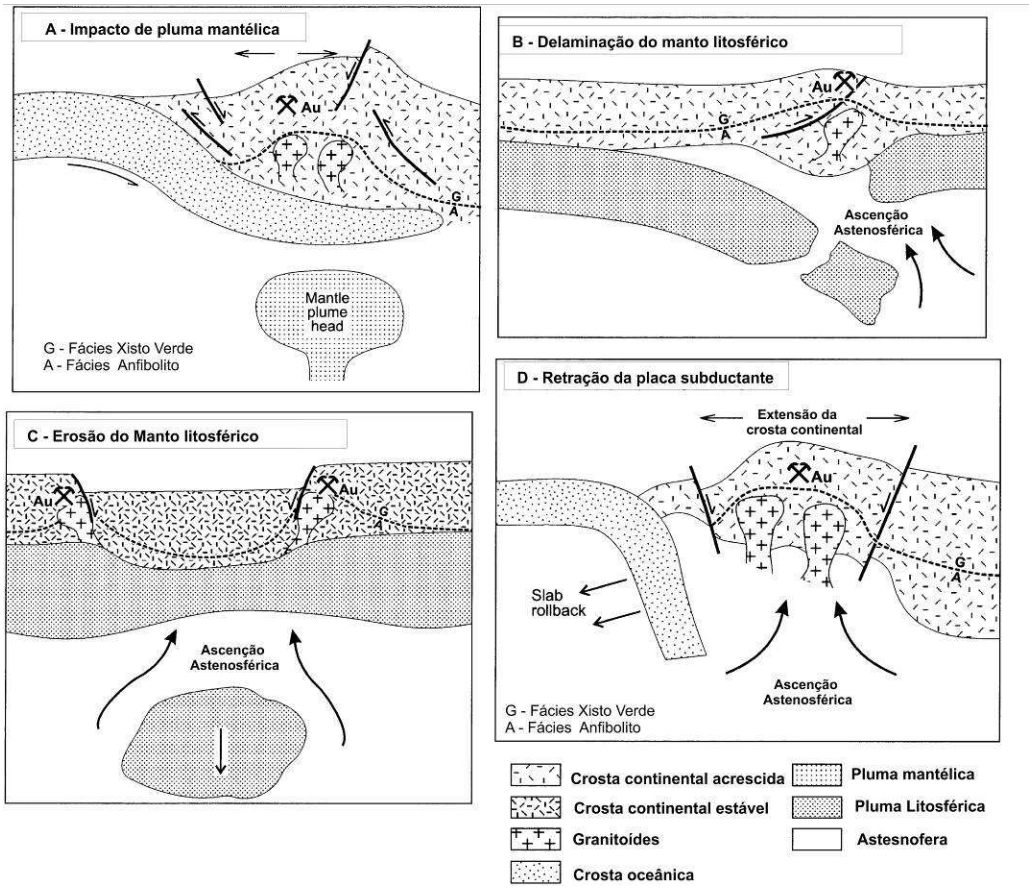

Figura 2.3- Eventos tectônicos segundo Goldfarb *et al.*, (2001) que levam a remobilização do manto pré-fertilizado: A) Impacto de pluma, B) Delaminação do manto;C) erosão do manto; D) retração da placa subductante.

2.3.3. Grandes estruturas litosféricas

O terceiro fator está relacionado a grandes estruturas litosféricas que canalizam os magmas/fluidos fertilizados para crosta superior. Estas estruturas ocorrem, geralmente, próximas à margem de blocos tectônicos ou associadas a fragmentos de crosta continental (Hronsky *et al.* 2012). São contínuas logintudinalmente e profundidade, e bem marcadas por lineamentos gravimétricos ou por isótopos radiogênicos, como mapas de Sm-Nd utilizados por Mole *et al.* (2013) na Austrália (Figura 2.4).

Como exemplo de estrutura transcorrente intracontinental com influência na área de estudo, destaca-se o Lineamento Transbrasiliano e estruturas secundárias a esse lineamento Transbrasiliano, como a Zona de Cisalhamento Moiporá-Novo Brasil, localizada na área de estudo (Fig 3.1).

Adicionalmente, estruturas litosféricas como zonas de cisalhamento transcorrente intracontinentais, canalizam fluidos e magmatismo. Estas zonas de cisalhamento delimitam blocos litosféricos e zonas de deformação continental originadas durante estágios finais da colisão (decorrentes do escape lateral desses blocos), podendo ser reativados durantes novas fases de tectonismo e acresção (Storti *et al.,* 2003). Geralmente apresentam feições dúcteis a rúptil-dúcteis, com foliações miloníticas com mergulho vertical a sub-vertical. As assinaturas geofísicas (sísmica e gravimetria) indicam ligação com o manto superior. Falhas transcorrente podem atuar como condutos de magmas, que por sua vez induzem à formação de sistemas hidrotermais-magmáticos. Geralmente, magmatismo associado às falhas transcorrente apresenta fontes mantélicas e/ou do manto litosférico metasomatizado e incluem granitoides de alto-K, granitoides do tipo A, lavas shoshoníticas e lamprófíros (Vaughan & Sacrow, 2003;). Comumente, este tipo de magmatismo ocorre em regimes tectônicos pós-colisionais (Bonin *et al.*, 1998).

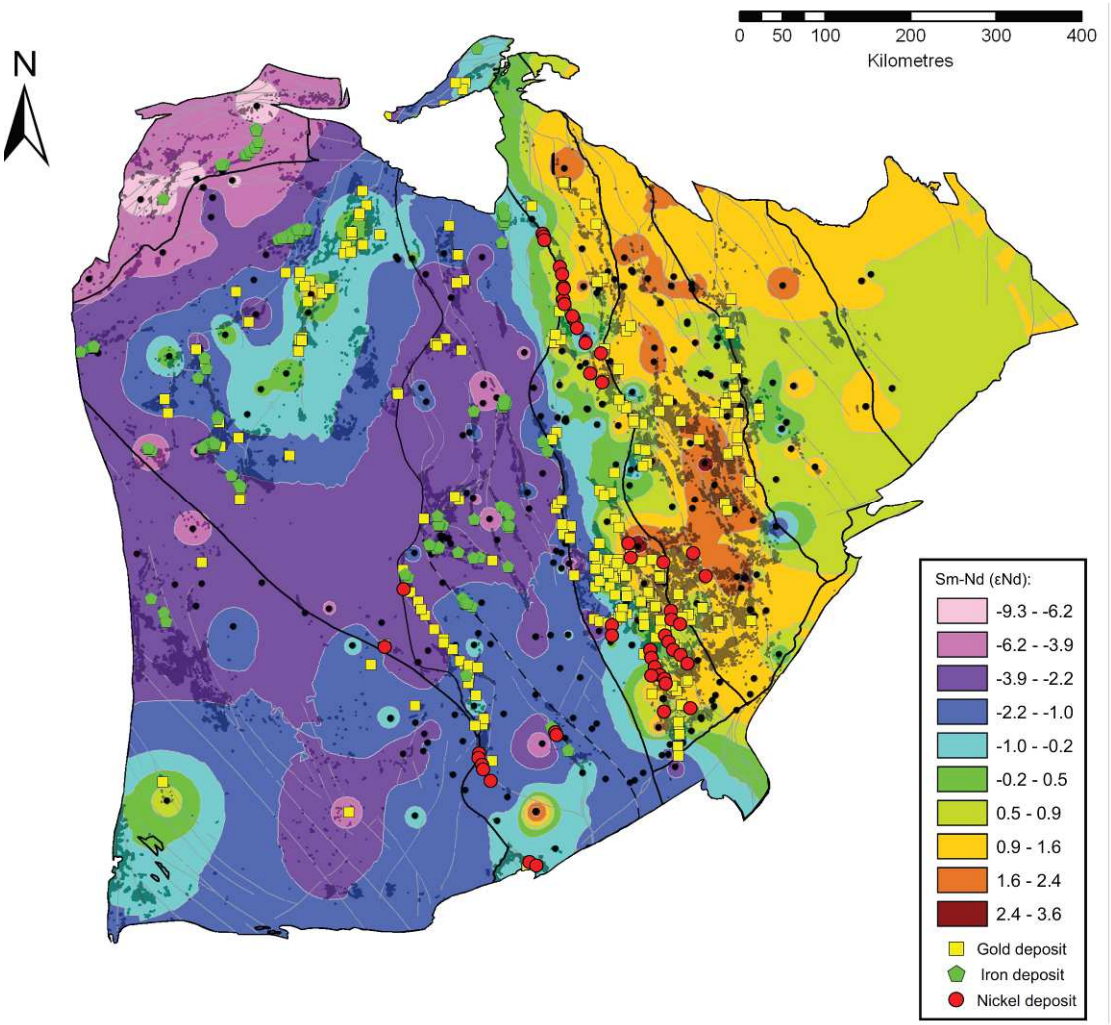

Figura 2.4 - Mapa isotópico de Épsilon-Neodímio de Mole *et al.*, (2013) no Craton Yialgarn , Austrália Ocidental, mostrando a distribuição de depósitos auríferos, ferríferos e de níquel. O limite NNW é interpretado como a margem de um paleocraton de 2.7 Ga estando os depósitos auríferos principalmente confinados entre a crosta juvenil a leste e crosta evoluída a oeste. Mapas como este definem grandes suturas litosféricas e mostram a arquitetura da crosta como um todo.

Segundo Pirajno (2010) o magmatismo associado a esses sistemas transcorrente intracontinentais desenvolvem-se, inicialmente, devido ao impacto de pluma mantélica ou ascenção astenosférica devido a delaminação da crosta inferior. Posteriormente, ocorre a migração lateral da pluma que é canalizada para as estruturas transcorrente profundas (Figura 2.5A). O material da pluma reage com o manto listosférico subcontinental, geralmente metassomatisado, ou previamente enriquecido, induzindo a um sistema magmático-hidrotermal que pode ser divido em: i) intrusões sin-cinemáticas que originam complexos máficos-ultramáficos e granitoides Tipo A, associados

principalmente à mineralização do tipo Ni-Cu-EGP, Au-*lode*; ii) e em intrusões pós-cinemáticas, que são associadas a depósitos do tipo Au-*Intrusion Related*, Au-epitermal e depósitos do tipo Cu-Au pórfiro e skarn. Entretanto, pode ocorrer a reativação dessas zonas de cisalhamento com nova ascenção de material mantélico, que resulta em novo ciclo de magmatismo, deformando pulsos anteriores, inclusive originando ortognaisses (Figura 2.5B). Sistemas com muitas reativações fazem com que o magmatismo associado ao regime transcorrente seja muito prolongado, variando de 15 a 50 Ma.

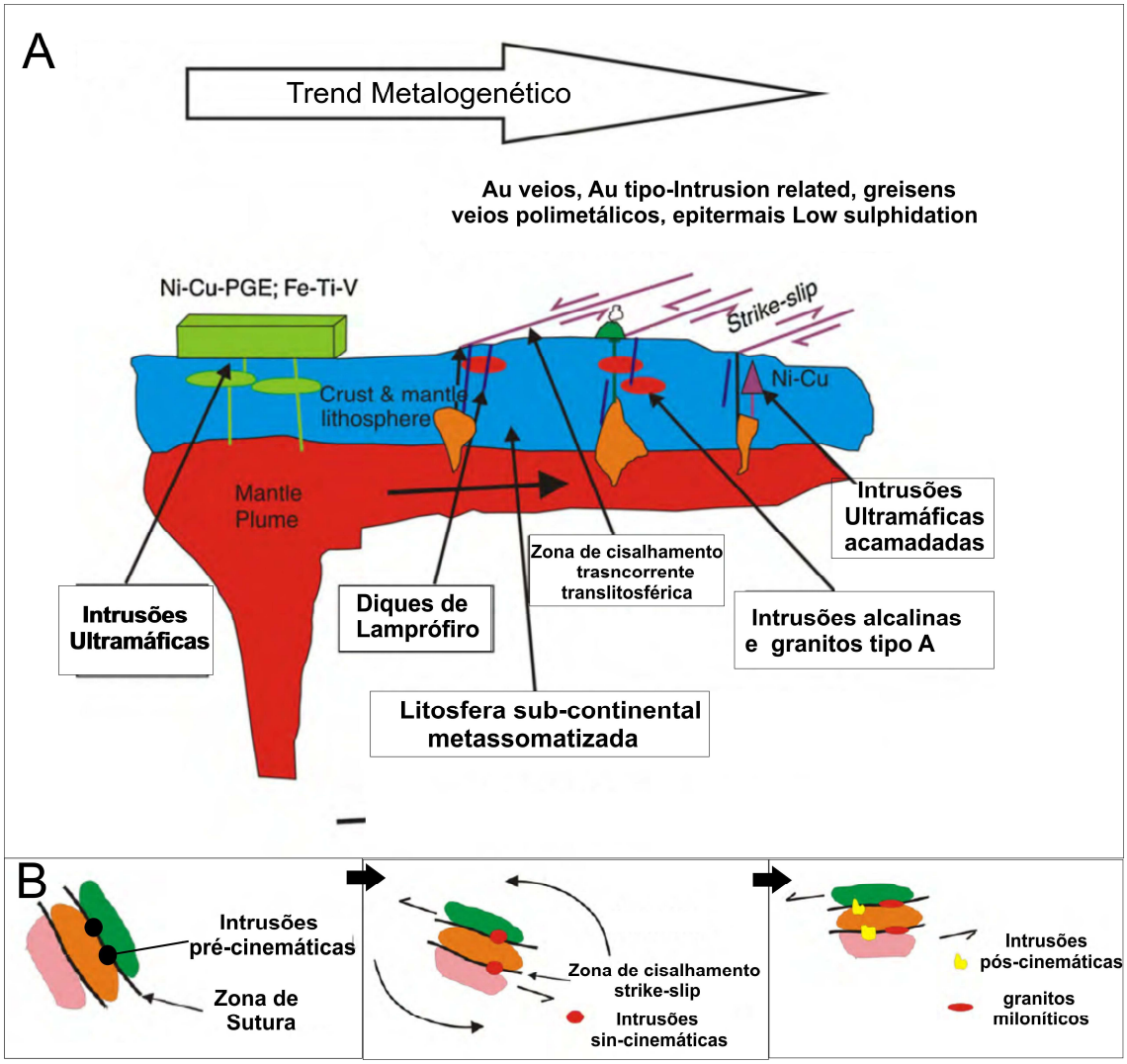

Figura 2.5. - A) modelo proposto por Pirajno (2010) ilustrando o impacto de pluma e posterior migração lateral para zonas de cisalhamento translitosféricas. A interação da pluma com o manto litosférico subcontinental (SCLM) metassomatizado origina magmas tipos A, magmatismo máfico ultramáfico e depósitos hidrotermais associados. B) Etapas de formação de zonas de cisalhamento e geração de intrusões granticas tipo A pré, sin e pós-cinemáticas,

2.4. Diferenças entre depósitos de Au orogênico e depósitos de Au do tipo Intrusion Related

Como foi citado acima, os depósitos de Au-orogênico e do Au-*Intrusion-Related* compartilham do mesmo ambiente tectono-magmático (retro-arco e inversão peri-continental), assim como da mesma associação de metais, alteração da rocha-encaixante, fluidos mineralizantes e controles estruturais (Groves *et al.,* 2003). Entretanto, algumas características são próprias de cada tipo:

Os depósitos de Au orogênico foram definidos por Groves *et al.,* (1998) como depósitos formados durante tectônica compressional a transtensional em estágio sin-orogênico. Apresentam forte controle estrutural e zoneamento hidrotermal limitado, já que os fluidos aquo-carbônicos apresentam-se em equilíbrio com as rochas encaixantes. Posteriormente, Groves *et al.,* (2003) definiram zoneamento vertical para estes depósitos, dividindo-os em: epizonal, mesozonal e hipozonal (Figura 2.6A). O depósito **Epizonal** ocorre entre 2 a 5 km de profundidade em fácies xisto-verde baixo, com típica associação metálica Au-Sb (Hg), estruturas rúpteis como brechas e *stock-works* e associação hidrotermal típica com pirita-carbonato-sericita. O depósito **Mesozonal** ocorre entre 5 a 10 km de profundidade, em facies xisto verde (xisto verde alto), com associação metálica de Au-As-Te, associado à estrutura rúptil-dúctil como veios do tipo *fault-fill*, veios laminados e associação hidrotermal típica com clorita-biotita-arsenopirita-pirita. O depósito **Hipozonal** ocorre em profundidade de 10 a 20 km, em fácies anfibolito, com associação metálica Au-As, associado a estruturas tipicamente dúcteis (como veios do tipo paralelos ao acamamento e veios disseminados) e associação hidrotermal de mais alta temperatura com pirrotita-arsenopirita-(loellingita)-diopsídio-biotita-anfibólio

A intrusão de batólitos, stocks, sills e diques de composição félsica a intermediária, e até lamprófiros, é bem documentada na literatura (Rock & Groves 1988; Goldfarb *et al.,* 2001; Goldfarb *et al.,* 2005), como sendo temporalmente associados à evolução de muitos distritos de depósitos orogênicos. Entretanto, não existem evidências de magmas que sejam diretamente responsáveis pela mineralização aurífera em depósitos orogênicos. Hoje é aceito que a associação dos magmas e fluidos orogênicos compartilha grandes estruturas de primeira ordem, que viabiliza a associação espacial e temporal de ambos.

Os fluidos formadores dos depósitos orogênicos são unicamente ricos em CO_2 e com baixa a moderada salinidade. Depósitos orogênicos do Arqueano apresentam veios

com temperatura de formação de 325° a 400°C, enquanto veios formados no Paleoproterozoico a Fanerozoico são de mais baixa temperatura, de 250° a 350°. Vale ressaltar que esta temperatura pode variar, dependendo da profundidade de ocorrência, de 2 a 20 km (epizonal-hipozonal). Os fluidos mineralizantes, na maioria das vezes, apresentam valores de $\delta^{18}O$ entre 6 a 13 por mil e δD de -80 até -20 por mil, indicando contribuições significativas de fluidos aquo-carbônicos metamórficos nos sistemas hidrotermais auríferos. Isótopos de $\delta^{34}S$ relacionados a sulfetos com valores de 0 a 10 por mil com algumas exceções de valores mais altos ou mais baixos, indicando pouca influência do manto na formação do enxofre (Goldfarb *et al.,* 2005).

A classificação de depósitos de ouro do tipo *intrusion-related* (IRGD) sempre foi controversa desde sua concepção (Thompson *et al,* 1999; Thompson & Newberry 2000; Lang *et al.,* 2000; Hart *et al.,* 2002) devido às sua semelhanças com depósitos do tipo Au-orogênico, principalmente porque em alguns casos estão espacialmente associados (Groves et, al., 2003 Goldfarb *et, al*., 2005). Contudo, os autores supracitados concordam com as seguintes características específicas dos IRGD: i) forte associação temporal e espacial com magmatismo reduzido; ii) associação metálica de Bi, As, W, Te e assembleia de sulfetos reduzidos; iii) sistemas granitóides anômalos indicando alguma contribuição de magmas derivados do manto (alcalino máficos) na base da crosta; iv) ocorrência em ambiente pós-colisional associado a margens pericontinentais; v) ocorrência em estruturas profundas como limites de blocos litosféricos ou zonas cisalhamento translitosféricas transcorrente*;* vi) típica alteração hidrotermal composta por sericitização, carbonatação, potassificação (K-feldspato e/ou biotita) e albitização; vii) formação de fluidos com salinidade baixa e ouro transportado por tio-complexos de H_2O-CO_2-CH_4-N_2.

Hart *et al.,* (2002), devido ao forte zoneamento hidrotermal e termal, definiram os IRGD de acordo com a proximidade das intrusões, definindo-os como: ***Intrusion-hosted,*** que se caracteriza pelo fato de a mineralização estar hospedada na própria intrusão, assim como pelo fato de possuir associação metálica de Au-Bi-Te-W e alterações do tipo disseminada/substituição e *veois;* **Proximal,** definido por ser uma alteração do tipo skarn (Au-As) e possuir veios epizonais com associação de Au-As-Sb; e, por último, **Distal,** representado por veios com associação Ag-Pb-Zn hospedados nas encaixantes das intrusivas (Figura 2.6B).

Goldfarb *et al.* (2005) e Mair *et al.* (2011) mencionam que para a distinção entre depósitos de Au orogênicos e IRGD, o principal critério seria a análise dos depósitos em

escala de distrito, e não apenas a análise de um depósito isolado. Em escala de distrito é possível observar o amplo zoneamento hidrotermal e metálico dos IRGD´s, enquanto os depósitos de Au-orogênico apresentam zoneamento hidrotermal muito mais uniforme (tanto lateralmente quanto verticalmente) e raramente apresentam alguma variação na associação metálica.

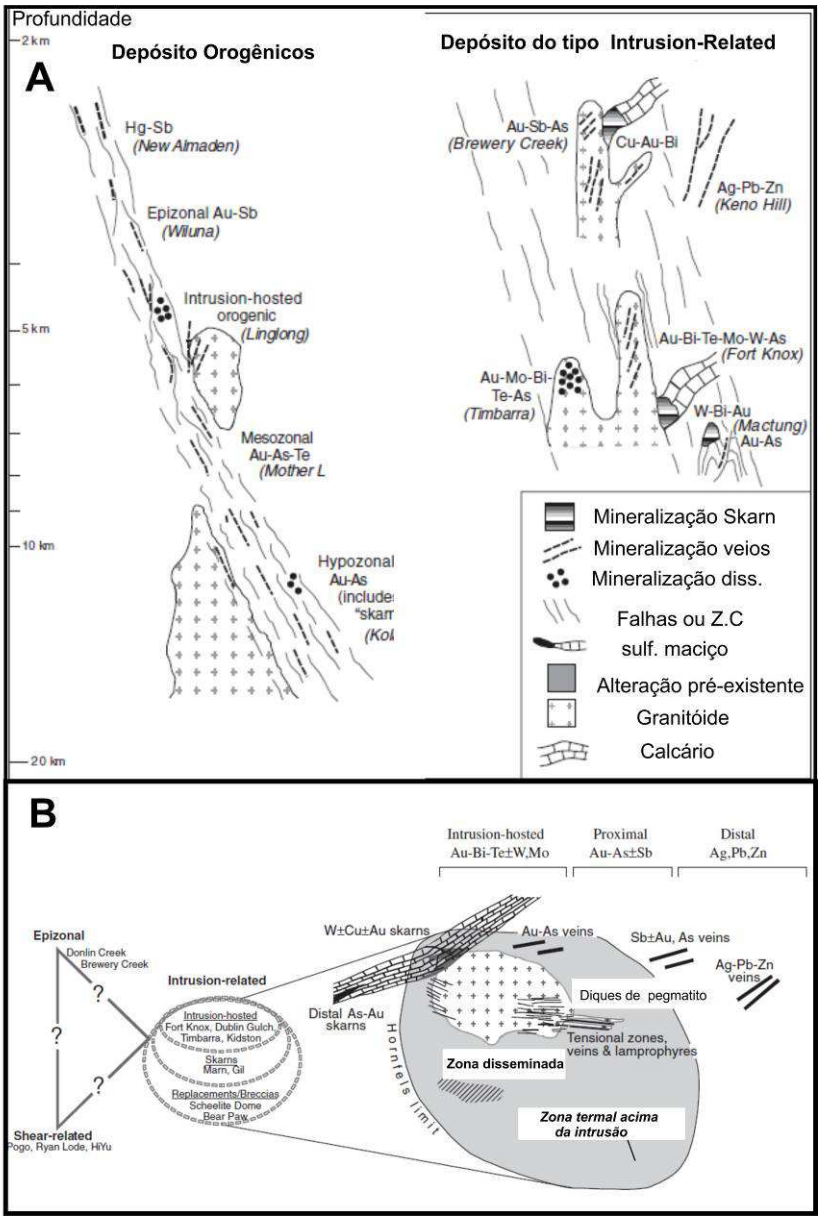

Figura 2.6 - A) Zoneamento vertical dos depósitos de Au orogênico e dos IRGD segundo Groves *et al.* (2003), ao lado dos exemplos de depósitos auríferos no mundo para cada profundidade e modelo B) zoneamento espacial da alteração hidrotermal e associação metálica dos IRGD segundo Hart *et al.* (2002) em relação à proximidade da intrusão.

3. EVOLUTION OF NEOPROTEROZOIC GOIÁS MAGMATIC ARC, CENTRAL BRAZIL: FROM ISLAND ARC TO POST-COLLISIONAL INTRACONTINENTAL MAGMATISM

Abstract

The Goiás Magmatic Arc is one of the main components of the Neoproterozoic Brasília Belt, in central Brazil. It records a protracted magmatic history involving the amalgamation of juvenile terranes comprising early Neoproterozoic to Cambrian granitoids emplaced into volcano-sedimentary sequence. New U-Pb, Sm-Nd and geochemical data obtained in the Jaupaci Belt, one the best preserved sequence in the southern part of this Magmatic Arc, allowed a better understanding of its tectonic setting and crustal evolution. We recognized two main magmatic setting: the first, in arc-related magmatism that took place between 770 and 750 Ma and the second, generated in post-collisional setting, occurred between 597 and 506 Ma. The arc related magmatism was divided into two main events: *the oldest is represented by 770 Ma old ilmenite-bearing granitoids emplaced during the late stage of intra-oceanic arc; the youngest event encompasses 750 Ma old formed most likely in a continental arc-back arc setting comprising magnetite-bearing, metaluminous intrusions presently represented by orthogneisses and basal metarhyolites of the Jaupaci Sequence. The post-collisional event was divided into three events temporally related to generation of major intracontinental translithospheric strike-slip fault: i) the pre-kinematic event (597-587 Ma) in extensional regime associated with mantle upwelling* or *delamination of sub-continental lithospheric mantle, where I- and A-type granitoids and bimodal volcanism were generated; ii) the sin-kinematic event occurred in compressional regime with development of green-schist metamorphism, folding and deep translithospheric strike-slip shear zones. These deep shear zones channelized and induced the generation of 577-539 Ma A-type sin-kynematic granitoids as well as*; v) *511-506 Ma old post-kynematic undeformed A-type granite intrusions, representing the youngest granitoid identified so far in the Goiás Magmatic Arc. The magmatic events have correlative ages in other parts of Gondwana showing that tectonic events: Island Arc (900-800 Ma), Continental Arc (750-630 Ma), post-collisional (597-585 Ma), and granites associated with intracontinental strike-slip (577-539 Ma) are roughly coeval throughout the Neoproterozoic and early Cambrian.*

Key words: Goiás Magmatic Arc, post-collisional magmatism, intracontinental strike-slip, Assembly of West Gondwana.

3.1. Introduction

The assembly of Gondwana, during the Neoproterozoic, involved the amalgamation of several continental blocks with the closure of ocean basins, subduction of oceanic lithosphere and accretion of juvenile arcs along a number of convergent margins. Examples of Neoproteroic juvenile arcs are found in the Dom Feliciano Belt ,southern Brazil (Babinski et al., 1997, Saalmann et al., 2005), in east of Africa represented by the Tuareg Shield (Amalaoulaou Complex, Tilemsi Arc and Kindal-Iskel terranes) in West Africa (Caby 2003; Liégeois 2005, Henry et al., 2008, Berger et al., 2011, Bosch et al .,2015); in north Africa in the Anti-Atlas Belt (Triantafyllou et al., 2015) and in the Arabian Nubian Shield (Stern and Jonhson 2010, Johnson et al., 2011, Stern et al., 2012, Cox et al., 2012, Fritz et al., 2013).

Episode of Neoproterozoic crustal accretion in West Gondwana is mainly represented by the Goiás Magmatic Arc (GMA), formed during the convergence of the São Francisco, Paranapanema and Amazonian cratons. This accretionary convergent margin records protracted tectonic/magmatic history, starting during the Tonian, between ca. 920 and 800 Ma, with the development of intra-oceanic arcs and ending with continental arc magmatism (660-630 Ma). This was followed by continental collision at ca. 630 Ma during the so-called Brasiliano orogeny resulting from the closure of the Brasilides or Goiás-Pharusian Ocean (Pimentel et al., 1991, Pimentel and Fuck 1992, Pimentel et al., 2000, Kroner and Cordani 2003, Laux et al., 2005, Cordani et al., 2013a, Brito Neves et al., 2014)

Following the collisional stage an important set of intracontinental strike slip shear zones, collectively known as the Transbrasiliano Lineament (Schobbenhaus 1975) or Transbrasiliano-Kandi Lineament were developed. They extend from South America (Argentina and central and NE Brazil) to Africa (Cordani et al 2013a). The Transbrasiliano Lineament is defined by a series of deep ductile shear zones that probably reachs the base of the lithosphere, as indicated by deep seismic, gravimetric and magnetic regional surveys (Assumpção et al., 2004, Soares et al., 2006, Feng et al., 2007, Curto et al., 2014). These deep structures acted as conduits for hot asthenospheric mantle to reach the base of SCLM (sub-continental lithospheric mantle) providing the necessary heat to melt the base of lithosphere, where mafic magmas, which in turn, possibly promoted melting of the continental crust generating high-K to A-type granites (Pirajno 2010). The relationship between post-collisional high-K and A-type intrusion

and the development of the Transbrasiliano strike-slip system has not yet been investigated in detail in the GMA.

In this paper, we studied the Jaupaci Belt one the best preserved supracrustal sequence in the GMA hosting important A-type intrusions spatially related with the translithospheric strike-slip system. We present new U-Pb geochronological data (LA-ICPMS and ID-TIMS), as well as Sm-Nd isotopic and whole-rock geochemical data from metavolcanic and granitoid rocks of the Jaupaci Belt. The following aspects were investigated: (1) the precise timing and nature of the different post-collisional magmatic events in an attempt to establish the relationship between the strike-slip system and the generation of post-orogenic melts; (2) the nature and tectonic setting of each magmatic event predating the post-collisional magmatism and its relevance for the evolution of the Goiás Magmatic Arc; (3) the comparison of tectonic events in the GMA with other Neoproterozoic juvenile arcs, delivering a new insight on the assembly of Gondwana.

3.2. Geological Setting

The Tocantins province is a Neoproterozoic Brasiliano/Pan-African orogen resulting from the convergence and collision of three major continental blocks: the Amazonian in the west, São Francisco to the east, and the Paranapanema in the south, which is covered by Phanerozoic sedimentary rocks of the Paraná Basin. The province is composed of three Neoproterozoic fold belts: the Araguaia and Paraguay belts, extending along the eastern and southeastern margins of the Amazonian Craton, respectively, and the Brasília Belt, exposed along the western edge of the São Francisco Craton (Fig 3.1).

The Brasilia Fold Belt divided into two tectonic zones the external and internal. The eastern external zone is a craton-verging fold-and-thrust belt, comprising thick passive margin sedimentary deposits, deformed and metamorphosed under greenschist facies or lower P-T conditions. The internal, western part of the belt comprises: (i) the metamorphic core of the belt including the Neoproterozoic ultra-high temperature (UHT) Anápolis-Itauçu granulites separated by faults from the mainly turbiditic lower grade metasedimentary rocks of the Araxá Group, which includes small ophiolite remnants; (ii) the Goiás Massif made of Archean granite-greenstone terrains, Paleoproterozoic orthogneisses largely covered by folded metasedimentary sequences , recently interpreted as the São Francisco epicratonic western margin; (iii) and in the

western part the Goiás Magmatic Arc (Pimentel and Fuck 1992, Fuck et al., 1994; Pimentel et al., 2000, Dardenne, 2000, Pimentel et al., 2004; Laux et al., 2005, Valeriano et al., 2008, Giustina et al., 2009, Jost et al., 2010 Fuck et al., 2014, Cordeiro 2014).

The western limit of the Brasilia Belt (Fig. 3.1) is roughly defined by the Transbrasiliano Lineament (TBL), characterized by an imbricated network of blocks, mostly gneisses and granulites, with ages varying from Archean to Neoproterozoic (Gorayeb et al., 2013, Frasca 2015). The nature of the TBL is ambiguous, being interpreted either as a collisional suture (Cordani et al., 2003), or as a first order strike-slip zone generated due to lateral scape along the collision zone between the Amazonian and São Francisco cratons (Hasui et al., 2012). However, the most accepted model interprets it as a dextral intracontinental strike slip deformational system (Fuck et al., 2013), or even as a transform plate boundary (Ganade de Araújo et al., 2014b). In the study region the TBL includes strong N30°E-trending gravity and magnetic gradients represented by the Serra Negra fault zone (Fig. 3.2). This structure separates two crustal tectonic domains, the Paranapanema Block to the east, and the Amazon paleocontinent to the west (Curto et al., 2015).

3.3. The Goiás Magmatic Arc

The Goiás Magmatic Arc is exposed in two segments, the Mara Rosa Arc, in the north and the Arenópolis Arc, to the south (Fig. 3.1), separated by the Archean Goiás Massif (Pimentel et al., 1997).

Available geochronological data reveal a complex evolution of arc system, with four main magmatic episodes: (i) the earliest took place between ca. 900 and 820 Ma, comprising tonalitic/dioritic/dacitic rocks formed in an intra-oceanic setting with $\varepsilon_{Nd(T)}$ values between +3.0 and +6.0 and T_{DM} model ages mostly between 0.8 and 1.1 Ga (Pimentel et, al., 1991 , Pimentel and Fuck 1992, Pimentel et al., 2000, Laux et al., 2005); (ii) the second episode is represented by arc volcanism at ca. 750 Ma (Pimentel et al., 1991, Guimarães et al., 2012); (iii) the third episode, also dominated by tonalitic rocks but showing continental arc geochemical and isotopic affinities, occurred between 660 and 630 Ma ; iv) after that, syn-orogenic to post-orogenic magmatism took place, representing the transition from calc-alkaline to alkaline/peraluminous dominated

assemblages. Despite the coeval tectonic events, the Mara Rosa and the Arenópolis arcs display remarkable differences shown in Table 3.1.

:

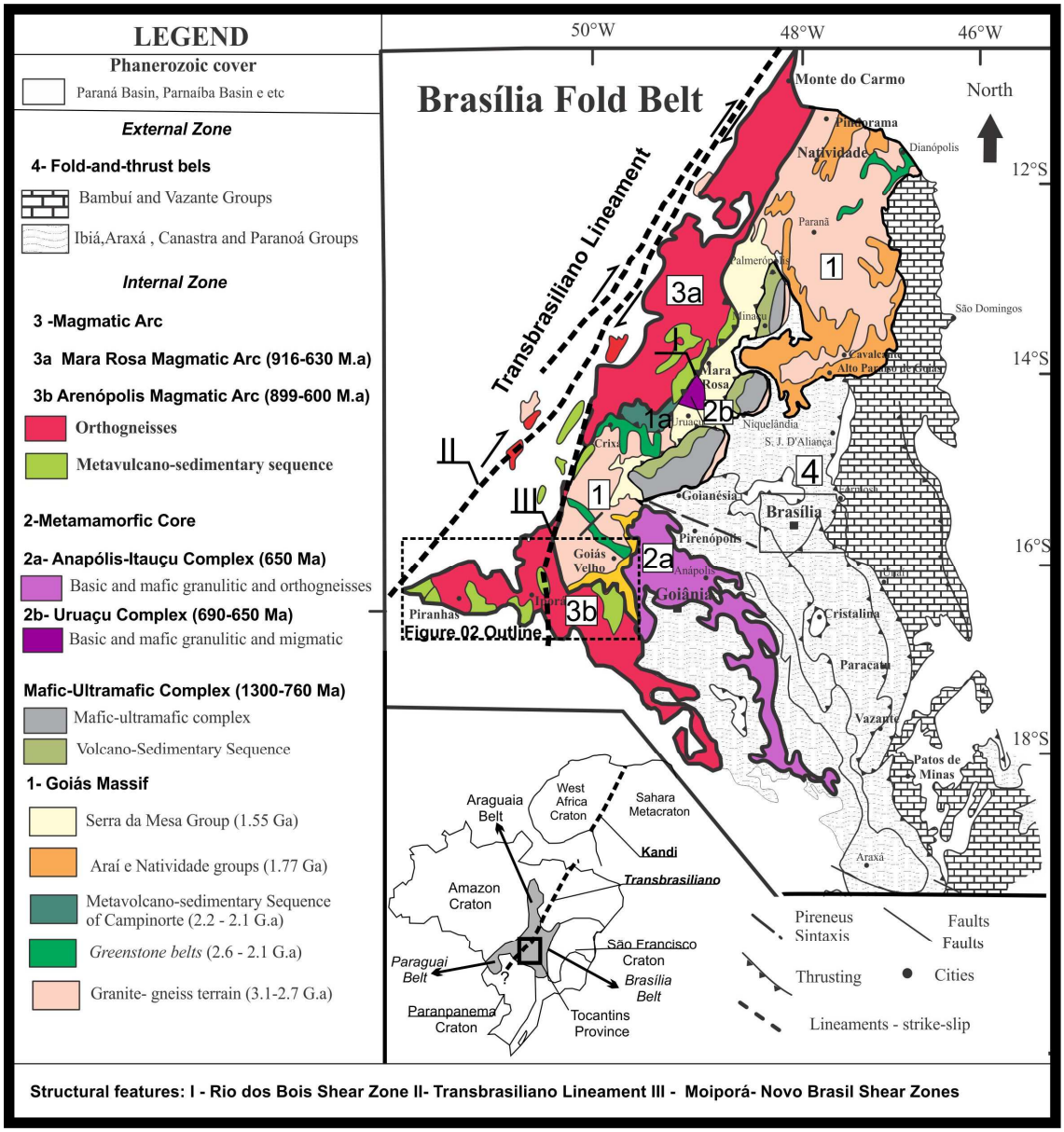

Figure. 3.1 – Geological sketch map of the Brasilia Fold Belt (modified from Fuck et al., 1994, Dardenne 2000, Fuck et al., 2014).

The Arenópolis Magmatic Arc comprises orthogneisses and late to post-tectonic intrusions exposed between narrow NNW to NNE belts of volcano-sedimentary arc sequences (Pimentel and Fuck, 1992; Pimentel et al., 1999). The arc is limited in the west by the Transbrasiliano Lineament and in the east by granulites of the Anápolis-

Itauçu Complex (Fig. 3.2). Table 3.2 presents a summary of the available isotopic data for the Arenópolis Arc.

Table 3.1 - showing the differences of two segments in the Goiás Magmatic Arc

Setting	Mara Rosa Arc	Arenópolis Arc
Sequences	Abundance of detrital metasedimentary rocks, whereas felsic/intermediate volcanic rocks are less voluminous.	Predominance of rhyolitic/dacitic volcanic rocks with subordinate metassedimentary rocks.
Nature of post-tectonic intrusion	Commonly leucocratic and have primary muscovite, indicating their peraluminous nature.	Bimodal intrusions with metaluminous nature, high-K and A-type affinities.
Structural Setting	Low angle foliation related to the development of isoclinal folding and thrust to reverse faults.	High angle foliation related to the development of strike-slip faults in the western segment. Low angle related to isoclinal folding in the eastern segment
Metamorphism	Regional amphibolite facies	Regional greenschist facies (some plutonic rocks display amphibolite facies)

The metavolcano-sedimentary sequences in the Arenópolis Magmatic Arc comprises, from west to east (Fig3.2): i) the Bom Jardim Sequence, represented by juvenile arc rocks dated at 749 ± 6 Ma (U-Pb in zircon from a crystal tuff; Guimarães et al., 2012); ii) the Arenópolis-Piranhas Sequence, composed of ophiolite fragments associated with pelitic metasedimentary rocks, interpreted as an accretionary prism. Felsic volcanic rocks yielded the U-Pb zircon age of 899 ± 6 Ma (Pimentel and Fuck, 1987, Pimentel et al., 1991); iii) the Iporá-Amorinopólis Sequence, represented by bimodal volcanics and metasediments, in which a metarhyolite yielded the U-Pb zircon age of 636 ± 6 Ma (Rodrigues et al., 1999); iv) the Jaupaci Sequence, which is a bimodal volcanic sequence composed of interbedded–metabasalt, metarhyolite and minor metadacite. Contrasting with the other sequences, the absence of metasedimentary rocks is remarkable. One metarhyolite sample yielded the U-Pb zircon age of 764 ± 14 Ma (Pimentel et al., 1991); and v) the Anicuns-Itaberaí and Córrego da Boa Esperança sequences, marked by predominance of mafic volcanics rocks and chemical metasediments suggesting an oceanic forearc setting. U-Pb zircon ages vary from 815 ± 10 Ma to 886 ± 5 Ma (Laux et al., 2005).

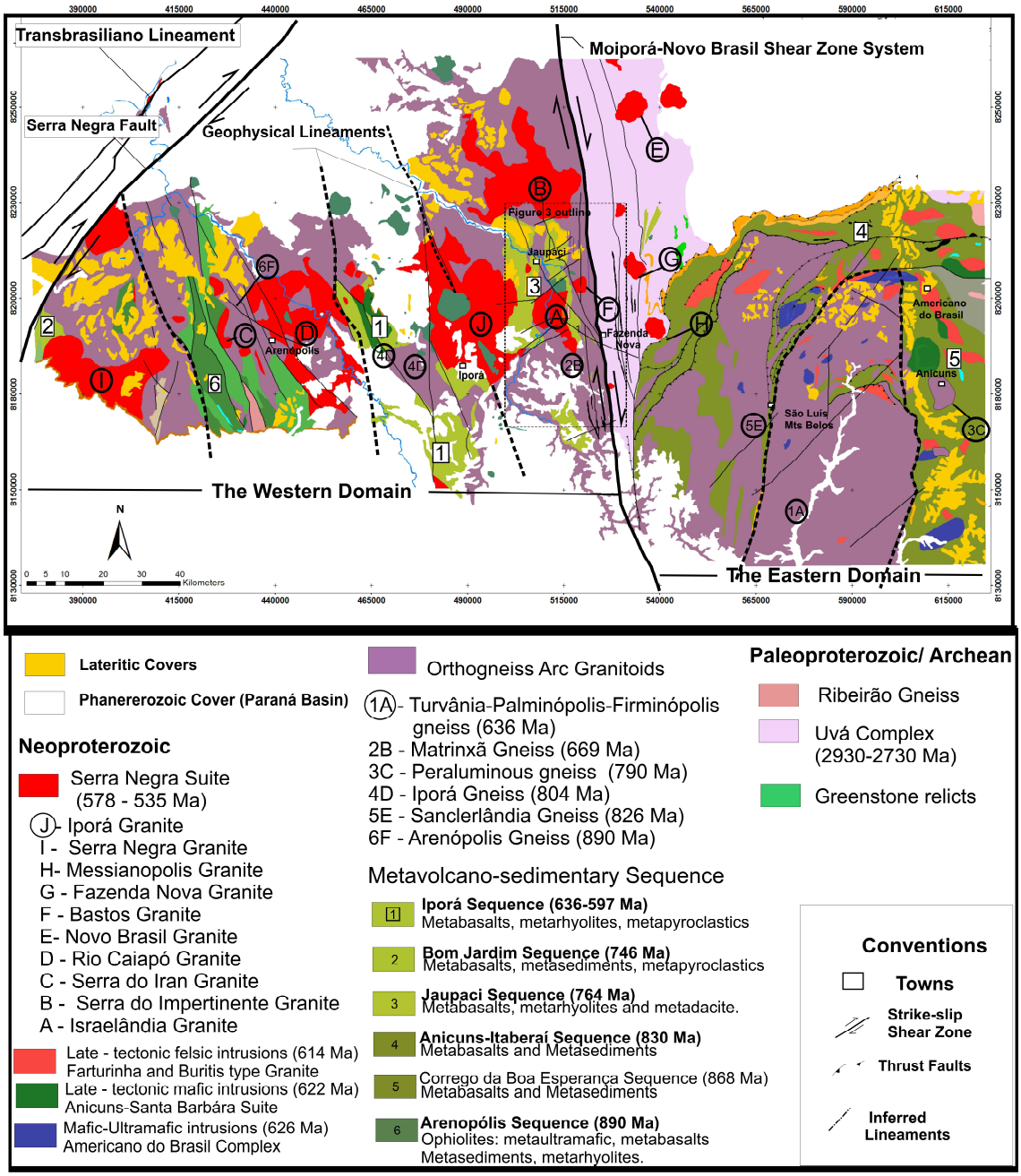

Figure 3.2 - Geological map of Arenópolis Arc showing the metavolcano-sedimentary sequences and the arc granitoids, as well as its western and eastern limits

The orthogneisses are dominantly hornblende- and biotite-bearing metadiorites, metatonalites and metagranodiorites. They show mineral assemblages indicative of metamorphism under amphibolite facies conditions; locally, they display relict igneous textures and structures, but frequently show mylonitic textures. U-Pb zircon ages indicate that the igneous protholiths crystallized in three distinct events: i) the oldest occurred between 899 and 804 Ma with primitive M-type granitoids generated in intra-

oceanic island arc setting (e.g. Arenópolis and Sanclerlândia gneisses). The Nd isotopic data indicate T_{DM} ages ranging from 0.89 to 1.2 Ga and ε_{Nd} (T) values between +0.37 and +6.0 (Pimentel and Fuck, 1992; Pimentel et al., 1996; Rodrigues et al., 1999, Laux et al., 2005); ii) the second event is represented by peraluminous muscovite-bearing metagranitoids generated between 790 and 786 Ma . The Nd isotopic data indicate T_{DM} ages ranging from 0.89 to 1.4 Ga and ε_{Nd} (T) values between -1.8 and +4.8 (Laux et al., 2005) ;and iii) the youngest event took place between 669 and 630 Ma, being represented by the metaluminous and peraluminous gneiss (e.g. Matrinxã and Firminópolis gneisses). The ε_{Nd} values vary from +2.2 to -15.1 with T_{DM} ages between 1.1 and 2.2 Ga, showing assimilation of older crustal material (Laux et al., 2005).

Syn- to late-tectonic intrusions are represented by mafic-ultramafic intrusions (Americano do Brasil U-Pb zircon age of 626 ± 8 Ma), gabbro-dioritic and granitic plutons (U-Pb age of 622 ± 5 Ma) intruded during and after the final deformational events of the Brasiliano orogeny (Laux et al., 2004).

The last magmatic event is characterized by the Serra Negra Suite**,** comprising batholithic high-K granite intrusions, associated with dikes or plugs of mafic composition. They are divided into three emplacement episodes. The early episode is represented by high-K, I-type granites with U-Pb and Rb-Sr isochron ages ranging from 588 to 576 Ma. Nd isotopes render model ages between 0.84 to 1.4 Ga and ε_{Nd} (T) from -2.0 to +3.0 (Pimentel and Fuck, 1994, Pimentel et al., 1996). The second (ca. 550-539 Ma) includes high-K, A-type granites, locally showing mylonitic textures, as exposed in the Moiporá-Novo Brasil shear zones, occurring as N-S elongated bodies or even forming large batholiths (Fig. 3.3). Nd isotopes indicate model ages of 0.9 Ga, 1.46 Ga and 2.61 Ga, and ε_{Nd} (T) between -21.6 and +0.3 (Mota-Araújo 2013). The younger episode represented by undeformed A-type granites with Rb-Sr ages varying of 490 to 485 Ma old (Pimentel et al., 1996).

.

ARENOPOLIS ARC ISOTOPIC DATA SUMMARY										
Volcano-sedimentary sequences	**Rock type**	**Age: U-Pb Zircon (Ma)**	**Model Age - T_{DM} Sm-Nd (Ga)**	**ε_{Nd} (T)**	**Late to pos-tectonic intrusions**	**Rock type**	**Age: U-Pb Zircon (Ma)**	**Age :Rb-Sr**	**Model Age - T_{DM} Sm-Nd (Ga)**	**ε_{Nd} (T)**
Bom - Jardim	Acid metavolcanic rock	749 ± 6 (11)	1.0 to 1.68 (11)	-5.97 to + 4.6	Americano do Brasil Mafic-Ultramafic Complex	Norite	626 ± 8 (9)			+ 2.4 to + 3.0 (5)
Arenopólis – Piranha	Metarhyolite	900 ± 8 (2)	1.1 to 1.4 (2)	+2.5 to + 6.9	Anicuns Santa-Barbara Suíte	Gabbro e metadiorite	623 ± 13 (9)		1.0 to 1.13 (9)	+ 1.8 to + 2.6
	Gabbro (Morro do Baú)	890 ± 6 SHRIMP (7)					622 ± 6 (9)			
					Farturinha Granite	Biotita Granite	614 ± 5 (9)		1.2 (9)	0.4
Iporá - Amorinopolis	Metarhyolite	636 ± 3; 597 (6)	0.76 to 1.0 (5)	+1.8 to + 5.3	Buriti de Goiás Granite	Biotite Granite	614 ± 20 (11)		0.97-1.19 (11)	+1.2 to + 2.7
Jaupaci	Metarhyolite	764 ± 14 (1)			Suite Serra Negra Intrusions					
					Israêlandia Granite	Biotite Tonalite	587± 20 (4)		0.84 to 0.92 (4)	+ 2.3 to + 3.0
Anicuns Itaberaí	Metagabbro	830 ± 8 (9)	0.98 (9)	+4.3 to + 5.0	Rio Caiapó Granite	Granite and Granodiorite		587 ± 17 (4)	0.93 to 1.24 (4)	- 3.3to +2.3
	Metadiorite	815 ± 10 (9)			Serra do Iran Granite	Biotite Granite		588 ± 19 (4)	0.93 to 1.4 (4)	-2.7 to 2.0
Córrego da Boa Esperança	Amphibolite	886 ± 5 (9)	1.0 (9)	+4.0 to + 5.0	Impertinente Granite (porphyritic facies)	Porphyry biotite-Granite		576 ± 18(4)	2.1 to 2.7 (4)	-16 to -19
	Amphibole schist	862 ± 5 (9)			Impertinente Granite (equigranular Facies)	Biotite granite		485± 18(4)	0.9 to 1.2 (4)	-4.6 to +1.1
Arc Granitoids / Orthogneisses					Iporá Granito	Biotite Horblende granite to sienite		490± 24(4)	1.0 to 1.2 (4)	-3.3 to 0.7
Arenópolis	Granite Gneiss	899 ± 7 (1 e 3)	1.0 to 1.2(1 e 3)	+ 1.9 até + 3.2	Serra Negra Granite	Bt –Horblende granite	538± 14 (11)		1.23 to 1.92 (4,11)	-3.0 to -4.0
					Granito Ivolândia		550± 11 (12)		1.35 (12)	-3.2
Sanclerlândia	Tonalite Gneiss	820 ± 7 (8)	0.9 to 1.0 (5,8)	+ 4.0 to + 6.0	Novo Brasil Granite	Biotite Granite			2.35 (12)	-21.7
		828± 7 (12)			Córrego do Ouro Granite	Biotite Granite			1.49 to 2.61 (12)	-4.6 to -20.7
		822± 7 (12)			Messianópolis Granite	Biotita Granite	542 ± 4 SHRIMP (12)		2.25 (12)	-20
Iporá	Granodiorite Gneiss	804 ± 6 (10)	1.18 (1,6)	+ 0.37 to + 1.85						
Granito Lavrinha	Granite Gneiss	799 ± 14 (10)	0.89 (10)	4.8	Piloândia Granite	Mylonitic Granite	539± 6 (12)		1.12 to 1.27 (12)	-1.0 to -2.2
Granito São João	Biotite metagranite	792 ± 5 (10)	1.05 (10)	3.8						
Granito Creoulos	Metagranite	782± 12 (10)	1.07 (10)	3.6	Moipora Granite	Metagranodiorite	556± 4 (12)		1.0 (12)	-0.8
	Muscovite gneisse	790± 14 (10)	1.47 (9)	-1.8						
Matrinxã	Hornblende metagranite	669 ± 3 (10)	0.99 (10)	2.2	**(References): 1 - Pimentel et al. (1991); 2 - Pimentel and Fuck (1992a); 3 - Pimentel and Fuck (1994); 4 - Pimentel et. al., (1996); 5 - Gioia et al. (1997) 6 - Rodrigues et al. (1999) 7- Pimentel et. al., (2003) 8 - Motta-Araújo and Pimentel (2003); 9 - Laux et. al.,(2004); 10 -Laux et. al., (2005); 11 - Guimarães et. al,. (2012); 12- Motta-Araújo (2013).**					
Firminópolis	Granite gneiss	634 ± 8 (5,10)	1.39 (6,10)	-4.6						
Palminópolis	Tonalite gneiss	637 ± 20 (10)	1.48 and 2.21 (10)	-6.4 and -15.1						
Turvânia	Tonalite gneiss	630 ± 5 (10)	1.11(10)	0.3						

Table 3.2 - Summary of isotopic data of the Arenópolis Arc.

3.4. Geology of the Jaupaci Belt

In this section the Jaupaci Sequence metavolcanic rocks and related intrusions are described and called collectively as the Jaupaci Belt. The sequence is well exposed and hosts A-type intrusions spatially related to strike-slip zone, which motivated the present study. The eastern border of the Jaupaci Belt is separated from the Goiás Archean block by the Moiporá-Novo Brasil Shear Zone and the western contact with the Iporá Sequence is poorly exposed and remains unclear. To the south, the sequence is covered by Paleozoic sedimentary rocks of the Paraná Basin (Fig. 3.3).

3.4.1. Jaupaci Metavolcanic Sequence

The Jaupaci Sequence comprises a ~1 km thick succession of metamorphosed volcanic rocks, folded and sheared along strike-slip faults. The succession is stratigraphically well preserved, comprising basal metarhyolites, followed by metabasalts intercalated with felsic metavolcanics. The stratigraphy differ from west to east in the Jaupaci Belt; in the west the basal metarhyolite is succeeded by intercalation of thin layers (<100 m) of felsic metavolcanics with metabasalts, whereas in the east these layers are relatively thicker (~300 m).

The basal metarhyolite is grey to white in color, fine-grained to porphyritic, and is composed of orthoclase, albite, quartz, muscovite and plagioclase, with minor apatite and magnetite (Fig. 3.4A and 3.4B). Deformation produced a flattened fabric in the groundmass, where muscovite lamellaes are developed. In regions where deformation was more intense, folding and mylonitic foliation developed. This is marked by quartz-feldspar porphyroclasts forming pressure shadows as well as by ribbon-shaped quartz.

The metabasalts are represented by fine-grained mafic schists composed of chlorite, epidote, plagioclase, quartz, actinolite and magnetite. The foliation is defined by chlorite and actinolite, indicating metamorphic conditions under greenschist facies. The metamorphic recrystallization was intense, leaving rare relict textural features, including poorly preserved plagioclase phenocrysts (Fig. 3.4C).

The felsic metavolcanics are interpreted as metamorphic products of dacites and rhyolites. The metadacites are formed by quartz-plagioclase-biotite-sericite and traces of ilmenite, pyrrhotite and apatite. In places, the volcanic texture is marked by preserved feldspar phenocrysts (Fig. 3.4D). The metarhyolites are formed by muscovite, quartz,

orthoclase and plagioclase and traces of apatite. Locally the felsic metavolcanics were submitted to strong deformation, developing mylonitic textures.

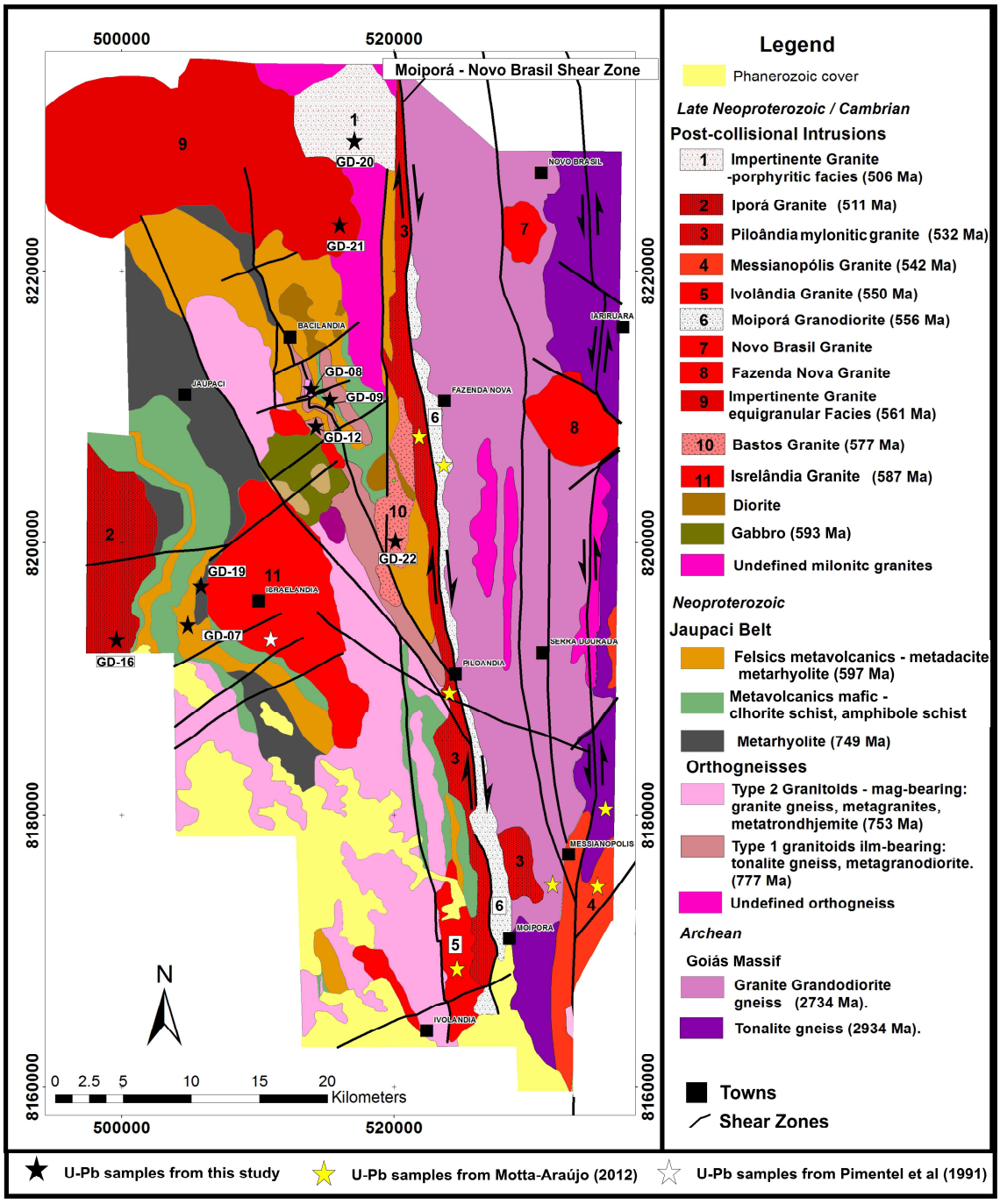

Figure 3.3 – Geological map of the Jaupaci Belt showing the location of U-Pb samples collected in study area.

3.4.2. Orthogneisses (Arc Granitoids)

This suite comprises deformed TTG-type plutonic rocks and two petrographic groups are identified: (i) type 1 includes a tonalite to granodiorite association and (ii) type 2 composed of trondhjemite to granite.

Type 1 intrusions are ilmenite-bearing metagranitoids exposed as tectonic slices within the Jaupaci Sequence. Type 1 intrusions present tonalite/granodiorite composition ,whitish, coarse-grained and composed by microcline-plagioclase-quartz-muscovite with ilmenite and trace amounts of titanite (Fig. 3.4E). They usually show strong deformation with folding and interference features between two foliations (Fig. 3.4F).

Type 2 intrusions are magnetite-bearing metagranitoids largely confined within a narrow belt along the central part of the Jaupaci Sequence or forming small plutons which are, in general, associated with exposures of basal metarhyolites of the Jaupaci sequence (Fig. 3.3). The trondhjemite member is characterized by leucocratic intrusions composed by assemblage of albite-biotite-quartz, the latter commonly showing a smoky aspect (Fig. 3.5A), as well as trace amounts of apatite and magnetite. Quartz is mostly recrystallized and biotite defines the foliation, eventually developing a mylonitic fabric. Granitic rocks are grey, medium- to coarse-grained, composed by orthoclase-albite-quartz-biotite-hornblende and magnetite. The foliation is marked by alternating bands of biotite and quartz-feldspar (Fig. 3.5B).

3.4.3. Serra Negra Suite

The Serra Negra suite is represented by large plutons emplaced into the Jaupaci Sequence and orthogneisses. Although these plutons exhibit isotropic texture, they are locally recrystallized and deformed especially along their margins. The Serra Negra intrusion in the Jaupaci Belt encompasses the Israelândia, Bastos, Piloândia, Iporá, Impertinente, and Moiporá granites, as well as some other smaller plutons.

Israelândia granite is emplaced into the central part of the Jaupaci Belt, separating its western and eastern parts. The Israelândia granite is composed of several different facies with compositions that vary between granite, quartz monzonite, biotite monzogranite, granodiorite and gabbro. The predominant facies is represented by a biotite granodiorite, which is whitish, coarse-grained, phaneritic and equigranular,

composed of orthoclase, plagioclase, quartz, biotite and trace amounts of zircon and apatite. Microgranular mafic enclaves (MMEs) are widespread in the Isrealândia Granite, but their spatial distribution is heterogeneous and highly concentrated in some of the margins of the pluton. Enclaves are most commonly centimeters to decimeters in size and their mineralogy is identical to that of host granites, but with higher amounts of mafic minerals (~15 vol.% biotite).

Bastos granite is emplaced along the eastern margin of the Jaupaci Belt, in the vicinities of the Moipóra-Novo Brasil fault, commonly showing mylonitic textures (Fig. 3.5C). It consists of pinkish, medium-grained biotite-bearing granite with K-feldspar macro-crystals in a groundmass of quartz, plagioclase and biotite.

Iporá granite is emplaced in the western margin of the Jaupaci sequence, separating it from the Iporá Sequence. The Iporá granite comprises reddish, equigranular, coarse-grained biotite-bearing monzo- to alkali-granite (Fig. 3.5D), formed by microcline, quartz, plagioclase and biotite with trace amounts of titanite, apatite and zircon and, locally, fluorite. They also contain centimenter and decimeter size mafic enclaves.

Impertinente Granite forms a large batholith in the northern portion of the Jaupaci Belt, comprising two facies: an early phase represented by deformed equigranular granite and a later phase formed by porphyritic coarse-grained granite. Both are biotite-bearing granites with similar composition: microcline, quartz, plagioclase and biotite and traces of apatite and zircon.

Moiporá Granodiorite is emplaced along the Moipóra-Novo Brasil fault, in the eastern margin of the Piloândia granite. It consists of a medium-grained deformed greyish granodiorite formed by K-feldspar, plagioclase, quartz, biotite and small amounts of titanite.

Piloândia Granite: comprises a NNW elongated intrusion along the Moipóra-Novo Brasil fault, showing remarkable mylonitic to ultramylonitic textures. It consists of two facies; the first is strongly deformed, fine- to medium-grained, pinkish granite, with elongated quartz marking the stretching lineation (Fig. 3.5E), whereas the second phase is a magnetite-rich, whitish, less deformed granite.

These felsic intrusions are commonly associated with dykes and small mafic intrusions (plugs) (Fig. 3.5F). Dolerite and gabbros are the most common rock type, showing euhedral plagioclase and hornblende phenocrysts in a groundmass of biotite,

plagioclase, quartz, and rutile/ilmenite, with trace amounts of pyrrhotite and chalcopyrite.

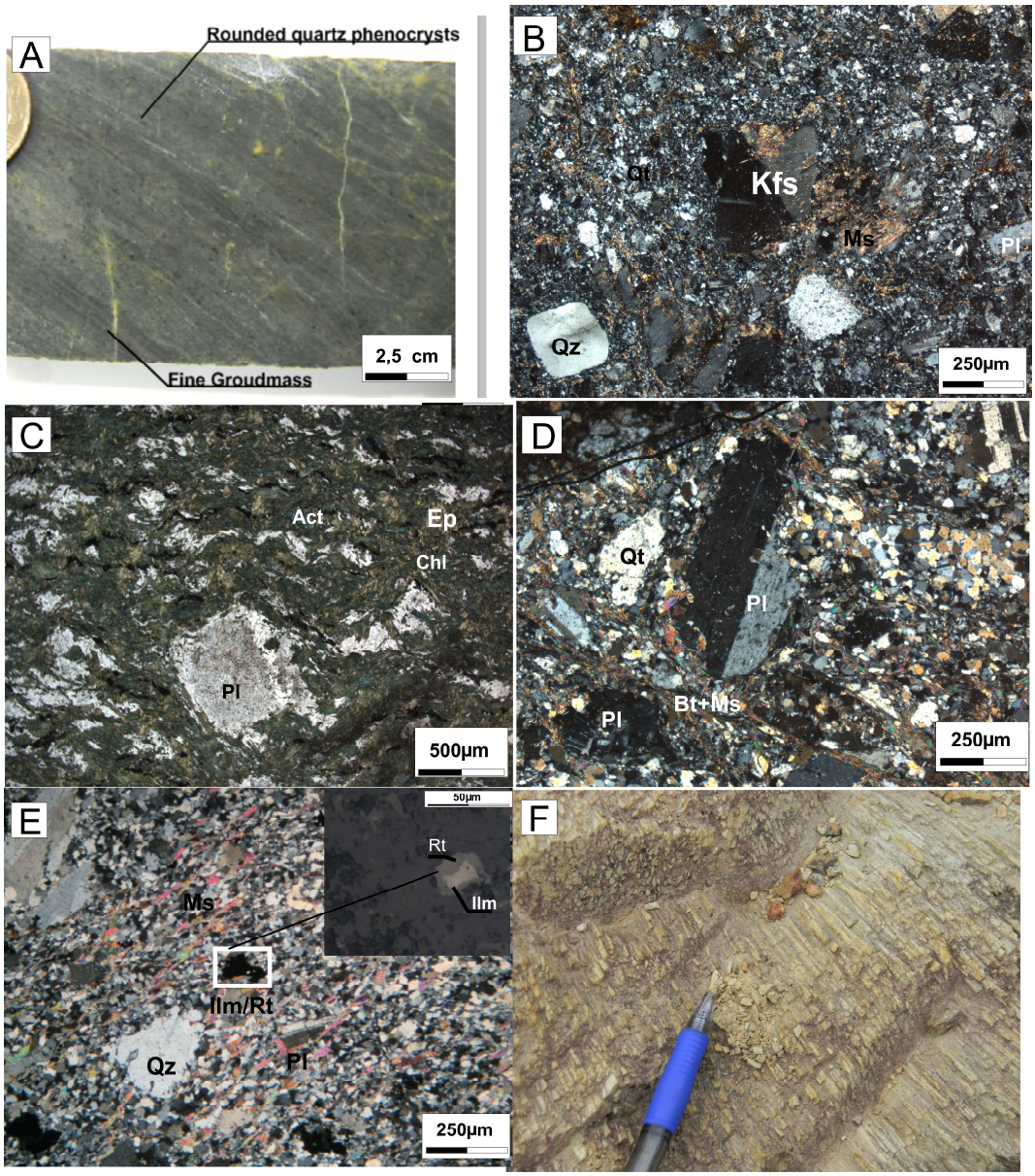

Figure 3.4 - A) Photograph of hand specimen of metarhyolite showing rounded quartz phenocrysts in greyish microcrystalline groundmass. B) Photomicrograph of the metarhyolite with preserved volcanic texture: rounded quartz and k-feldspar phenocrysts in a fine grained groundmass of plagioclase, quartz, muscovite and K-feldspar. C) Photomicrograph of the metabasalt with preserved plagioclase phenocrysts (Pl), foliation defined by chlorite (Chl), actinolite (Act) and minor epidote (Ep). D) Photomicrograph of felsic metavolcanic showing preserved volcanic texture with plagioclase phenocrysts in fine grained groundmass composed by quartz, feldspar, biotite and muscovite. E) Photomicrograph of Type 1 metatonalite showing phenocrysts of quartz (Qz) and plagioclase (Pl) in a quartz-rich groundmass, foliation is marked by muscovite (Ms). The

opaque minerals are ilmenite and rutile (Ilm/Rt). F) Outcrop of a strongly deformed metatonalite developing pencil-like structures due to the intersection of two foliations (Sn-1 and Sn).

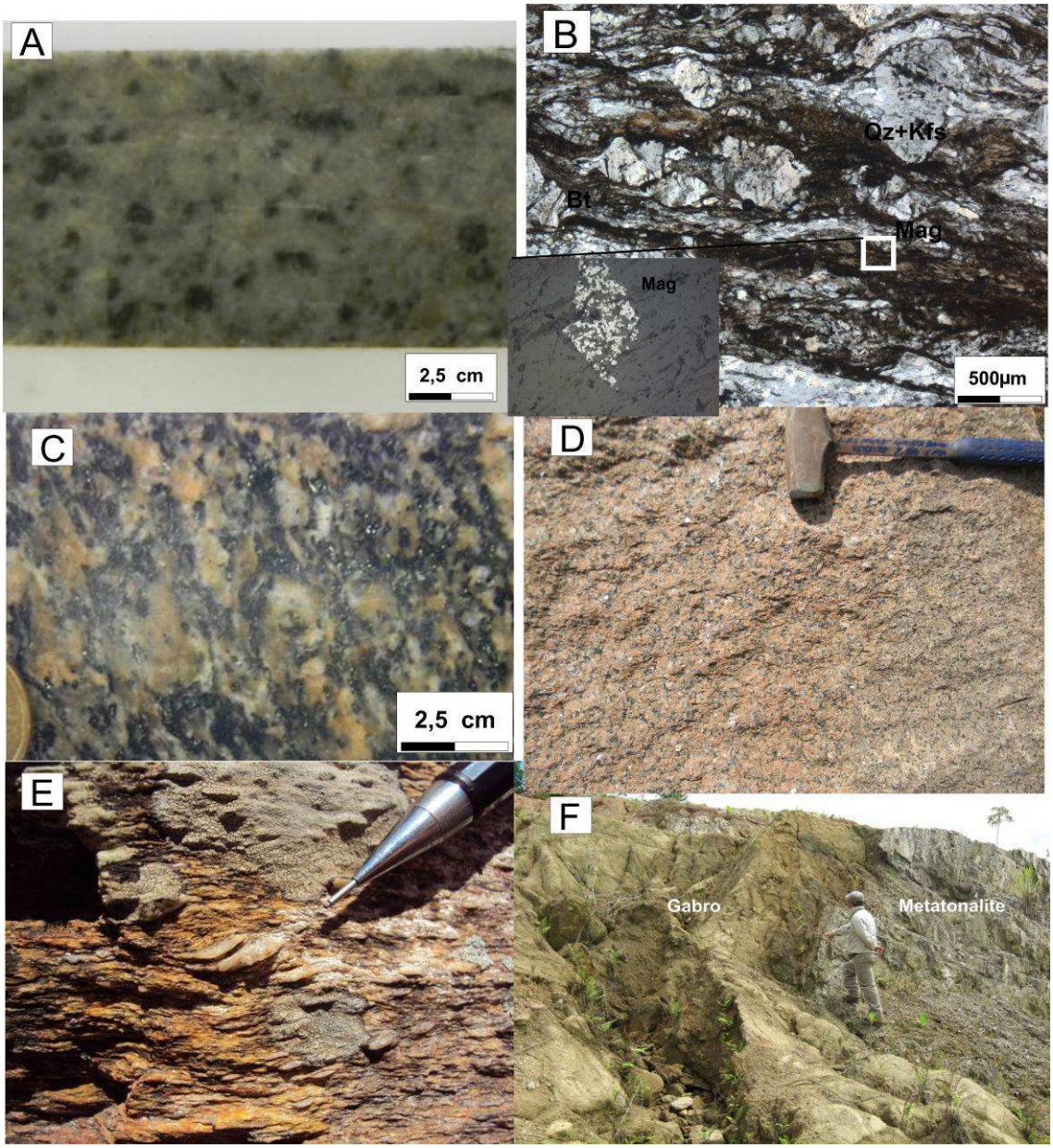

Figure 3.5 - A) Drill core sample of type 2 Trondhjemite with typical black-colored quartz; B) Photomicrograph of mylonitic granite gneiss showing banding of quartz and K-feldspar (Kfs) with biotite (Bt). The opaque minerals are commonly represented by magnetite (Mag). C) Deformed Bastos granite with feldspar porphyroclasts and foliation defined by biotite. D) Outcrop of the Iporá granite with its typical reddish color. E) Outcrop of mylonitic Piloândia granite in the Moiporá-Novo Brasil Shear Zone, showing stretched quartz indicating dextral displacement (Plan View foliation – 080/88); F) Outcrop of a small gabbro plug intruding the metatonalite of type 1 Suite.

3.5. Analytical procedures

3.5.1. U–Pb and Sm-Nd isotopic analyses

Zircon concentrates were extracted from ca. 10 kg rock samples using conventional gravimetric and magnetic techniques at the Geochronology Laboratory of the University of Brasília. Mineral fractions were hand-picked under a binocular microscope to obtain fractions of similar size, shape and color. For in situ U-Pb analyses, hand-picked zircon grains were mounted in epoxy mounts and polished to obtain a smooth surface. Before analyses, mounts were cleaned with dilute (ca. 2%) HNO_3. Backscattered electron images or cathodoluminescence images were obtained using a FEI-QUANTA 450 working at 10 kV at the University of Brasília.

The U-Pb LA-ICPMS analyses followed the analytical procedure described by Buhn et al., (2009) and were carried out at the Geochronology Laboratory of the University of Brasília. For LA-ICPMS U-Pb analyses, samples were placed in an especially adapted laser cell. A New Wave UP213 Nd: YAG laser (λ = 213 nm), linked to a Thermo Finnigan Neptune Multi-collector ICPMS was used. Helium was used as the carrier gas and mixed with argon before entering the ICPMS. The laser was run at a frequency of 10 Hz and energy of ~100 mJ/cm2 with a spot diameter of 30μm.

For the U-Pb LA-ICPMS zircon analyses, a fragment of zircon standard GJ-1 (Jackson et al., 2004) was used as the primary reference material in a standard-sample bracketing method, accounting for mass bias and drift correction. The resulting correction factor for each sample analysis considers the relative position of each 199 analysis within the sequence of 4 samples bracketed by two standard and two blank analyses (Albarède et al., 2004). An internal standard was run at the start and at the end of each analytical session, yielding accuracy around 2% and precision in the range of 1% (1σ). Uncertainties in sample analyses were propagated by quadratic addition of the external uncertainty observed for the standards to the reproducibility and within-run precision of each unknown analysis. Zircon grains with $^{206}Pb/^{204}Pb$ lower than 1000 were rejected. U–Pb age data were calculated and plotted using ISOPLOT v.3 (Ludwig, 2003) and errors for isotopic ratios are presented at the 1σ level.

Sm-Nd isotopic analyses followed the method described by Gioia and Pimentel (2000) and were carried out at the Geochronology Laboratory of the University of Brasília. Whole rock powders (ca. 50 mg) were mixed with ^{149}Sm-^{150}Nd spike solution

and dissolved in Savillex capsules. Sm and Nd extraction of whole-rock samples followed conventional cation exchange techniques. Sm and Nd samples were loaded on Re evaporation filaments of double filament assemblies and the isotopic measurements were carried out on a multi-collector Finnigan MAT 262 mass spectrometer in static mode. Uncertainties for Sm/Nd and $^{143}Nd/^{144}Nd$ ratios are better than ±0.5% (2σ) and ±0.005% (2σ),respectively, based on repeated analyses of international rock standards BHVO-1 and BCR-1. The $^{143}Nd/^{144}Nd$ ratios were normalized to $^{146}Nd/^{144}Nd$ of 0.7219 and the decay constant used was 6.54×10^{-12} a^{-1}. The T_{DM} values were calculated using the model of DePaolo (1981). Nd procedure blanks were better than 100 pg.

3.5.2.Geochemistry

Whole rock analyses were performed at ALS Chemex, Peru. Major oxides and minor elements were obtained by ICP-AES spectrometry following a lithium metaborate/tetrabortate fusion and dilute nitric digestion of a sample aliquot of 0.1 g. Rare earth and refractory elements were determined by ICPMS following a lithium metaborate / tetraborate fusion and nitric acid digestion of 0.1 g samples. Loss on ignition (LOI) was measured after ignition at 1000°C. All rocks analysed were subjected to regional metamorphism, and some of them also to hydrotermalism. Volcanic rocks were submitted to metamorphism under greenschist facies conditions and, thus, the primary geochemical compositions are liable to subsequent modifications. Large ion lithophile elements (e.g. Rb, Ba, K, Sr) are generally considered mobile under metamorphic conditions whereas rare earth elements and high field strength elements (e.g. Th, Nb, Ti, Zr, Y) are considered the least mobile or immobile (Rollinson, 1993).

Given these considerations, only those elements generally considered to be immobile are used in geochemical diagrams. To minimize secondary effects, all samples were carefully selected to exclude veining and recent weathering. Samples with LOI greater than 5.0 were discarded.

3.6. Isotopic Results

U–Pb (LA-MC-ICP-MS) analyses were performed on zircon crystals recovered from ten (10) samples of the Jaupaci Belt in order to obtain igneous crystallization and inheritance ages. The location of each sample is shown in Fig. 3 and individual analyses are listed in Supplementary table 3.A

Type 1 Suite - Metatonalite (GD-12)

Sample GD-12 presents one homogenous zircon population with zircon grains transparent/semi-transparent, light beige/brown with well-defined crystal faces, and show oscillatory zoning in CL imaging (Fig. 3.6). Sixteen zircon grains were analyzed. Eleven spots are discordant and were not used in the calculations. However, 5 crystals yielded a concordia age of 770 ± 8 Ma (MSWD = 1.6), which is interpreted as the crystallization age of the plutonic rock. Sm–Nd isotopic analyses indicate a T_{DM} model age of 0.86 Ga and a positive ε_{Nd} (T) of +5.41 (Table 3.3).

Type 2 Suite - Metatrondhjemite (GD-08)

Sample GD-08 present two types of zircon populations: one comprises pink, short prismatic zircon grains with well-defined faces and oscillatory zoning pattern; the other population is formed by colorless, usually fragmented and rounded zircon crystals showing no oscillatory zoning in CL images (Fig. 3.6). Ten analyses were performed revealing a complex age pattern with three age intervals: i) the first population with oscillatory zoning zircon crystals yielded a concordant age of 753 ± 12 Ma; ii) additionally two zircons provided slightly older ages of 873 ± 4 Ma and 792 ± 4 Ma (2σ) attributed to inherited component. The zircon grains from this population display Th/U ratio vary from 0.27 to 0.21 pointing to a magmatic origin (Belousova et al., 2002); iii) the second population of unzoned zircon (with low U/Th ratio <0.01) yielded younger ages close to the concordia line showing values between 665± 5 Ma to 657± 5 Ma (2σ). This young age may represent recrystallization related to regional metamorphism (Williams and Claesson, 1987). The concordant age of 753 ± 12 Ma (MSWD = 10.3) is interpreted here to be the best estimate for the crystallization age of the original plutonic rock. Furthermore this age is supported by petrological (and also

geochemistry) similarities between this sample and the basal metarhyolite (GD-19), which showed similar age (see below). The Sm–Nd isotopic analyses from the same sample give T_{DM} model ages of 1.26 Ga and positive $\varepsilon_{Nd}(T)$ of +4.61 (Table 3.3).

Jaupaci Sequence – Basal metarhyolite (GD-19)

Zircon grains from the basal metarhyolite are homogenous, light brown transparent euhedral to subhedral crystals. Most grains selected for analysis have approximately 100 µm. In CL images, grains appear as well-defined crystals with oscillatory zoning (Fig. 3.6). Th/U ratios vary from 0.20 to 0.30, which is consistent with a magmatic origin, crystallized from felsic to intermediate magmas. Fifteen analyses were carried out with eight zircon grains yielded a concordia age of 748 ± 10 Ma (MSWD = 3.1) which is interpreted as the crystallization age of the volcanic rock. The Sm–Nd isotopic analyses give T_{DM} model ages of 1.1 Ga and positive ε_{Nd} (T) of +1.19 (Table 3.3).

Jaupaci Sequence – felsic metavolcanic (GD-07)

This felsic metavolcanic sample was collected in the western part of Jaupaci Sequence interlayered with metabasalts. The 50-250 µm long zircon crystals are subhedral, elongated/sub-elongated crystals, some of them showing well-developed oscillatory zoning (Fig. 3.6). Nineteen analyses were carried out on eighteen zircon grains from sample GD-07. Six spot analyses yielded a concordia age of 598 ± 10 Ma (MSWD = 0.61), which is interpreted as the crystallization age of the original volcanic rock. The remaining six analyses yielded a concordia age of 828 ± 6 Ma (MSWD = 0.51), which are interpreted as an inheritance age. Sm–Nd isotopic analysis from the same sample gives a T_{DM} model age of 0.9 Ga with positive ε_{Nd} (T) of +3.79 (Table 3.3).

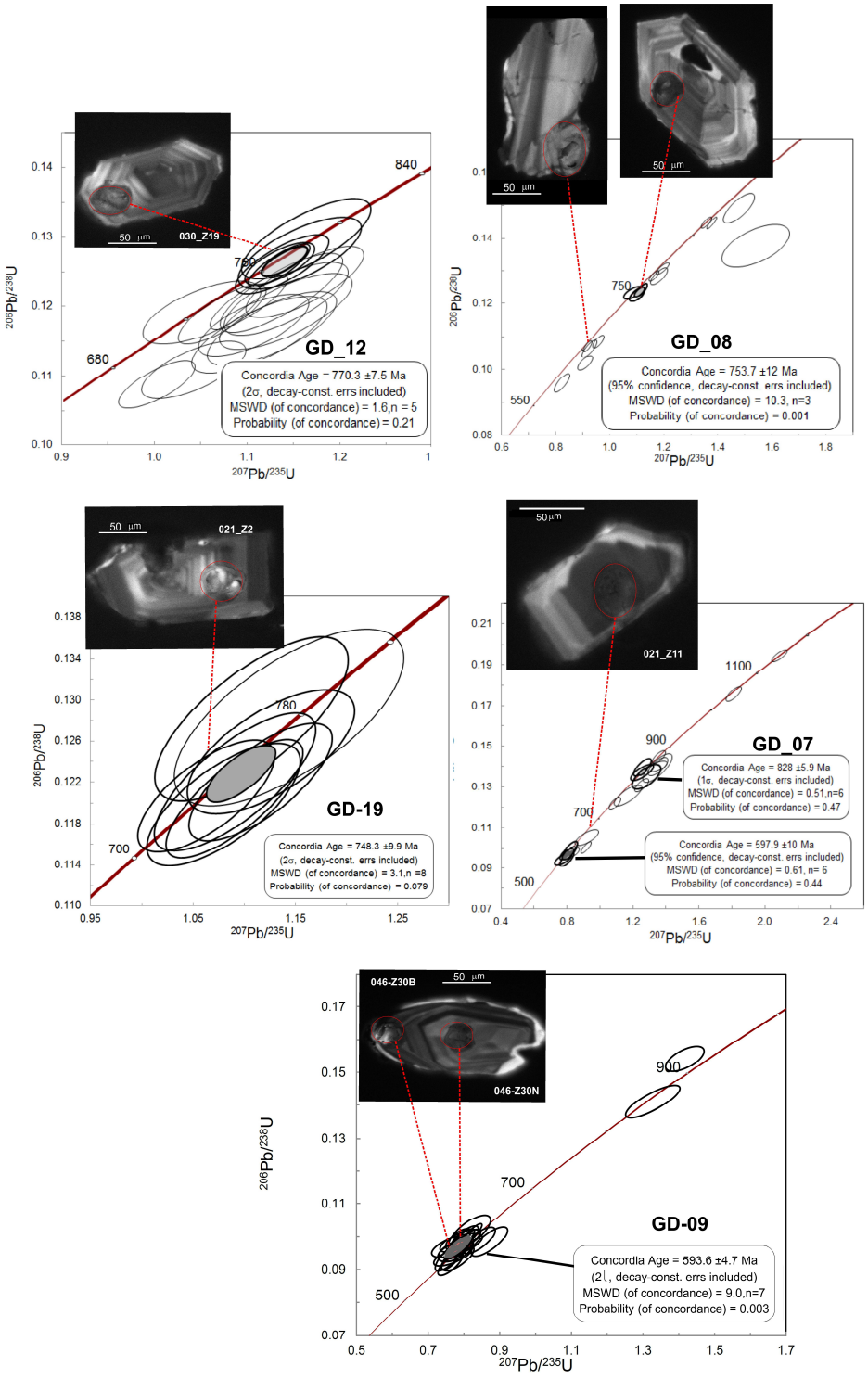

Figure 3.6 –Concordia diagram for zircon grains of orthogneiss: metatonalite (sample GD-12) and metatrondhjemite (sample GD-08); Jaupaci Sequence: metarhyolite (sample GD-19), and felsic metavolcanics (sample GD-07); and Serra Negra Suite gabbro (GD-09). Showing the CL images with analyzed spots in the representative zircon grains (the specific age of each zircon is shown in attached table). Laser spots (30µm) on the zircon rims are indicated by red open circles

Jaupaci Sequence – Amphibole schist (GD-32)

One sample of amphibole schist did not have zircon grains. We collected three samples for Sm–Nd isotopic analyses (GD-17,GD-32 and GD-37) which indicated T_{DM} model ages between 0.8 and 0.82 Ga and positive $\varepsilon_{Nd}(T)$ values of +5.17 to +6.72 (table 3).

Serra Negra Suite - Gabbro (GD-09).

Zircon crystals from this gabbro are generally light brown to yellow with ovoid shapes. Most zircon crystals show well developed sector zoning and grains vary in size from 100 to 150 µm (Fig. 3.6) characteristic of igneous zircon. Th/U ratios range from 0.24to 0.48. Twenty-five analyses on different zircon grains were performed and seven spots yielded a concordia age of 594 ± 5 Ma (MSWD = 9.0), which is interpreted as the crystallization age of the gabbro. One spot yielded concordant older age of 851 ± 6 Ma (2σ) that is attributed to inherited components. Sm–Nd isotopic analysis of the same sample gives a T_{DM} model age of 0.88 Ga and positive ε_{Nd} (T) of +3.97 (Table 3).

Serra Negra Suite –Bastos granite (GD-22).

Zircon grains from the Bastos granite are mostly colorless and clear. They show well-defined crystal faces with zircon core-overgrowths and similar size (~250 µm). Most are strongly luminescent grains with oscillatory zoning (Fig3.7). Th/U ratios range from 0.18 to 0.48. Twenty-two analyses were carried out on twenty different zircon grains. A concordia age of 577 ± 4 (MSWD = 1.4) was defined by seven concordant analyses and reflects the age of magmatic crystallization

Serra Negra Suite- Impertinente Granite Equigranular facies (GD-21).

Zircon grains from this equigranular granite form a homogenous population with beige to brown colour, euhedral and well-defined crystal faces. In general the dimension of zircons vary from 100 to 200 µm and in CL images, grains are mostly luminescent showing oscillatory zoning. Th/U ratios range from 0.26 to 0.40. Thirteen analyses were

performed and seven analyses yielded a concordia age of 561 ± 4 Ma (MSWD = 1.3), interpreted as age of magmatic crystallization (Fig 3.7).

Serra Negra Suite – Iporá Granite (GD-16).

Zircon grains from the Iporá granite are colorless to brown, with well-defined crystal faces and range in size from 100 to 150 µm . In CL images, most of them are luminescent with growth zoning as well as oscillatory or sector zoning (Fig.3.7). Sixteen analyses were carried out and four analytical points yielded a concordia age of 511 ± 7 (MSWD = 0.7), interpreted as the age of intrusion of the granite. One analysis is also concordant and yielded 568 Ma ± 7 (2σ), interpreted as an inherited zircon grain.

Serra Negra Suite - Impertinente Granite Porphyritic facies (GD-20).

Zircons grains from the porphyritic granite are subhedral to euhedral, translucent and colourless, with dimensions ranging from 100 to 150 µm. In the CL images most are luminescent grains with fine growth zoning as well as oscillatory or sector zoning (Fig. 3.7). Eighteen analyses were carried out from which eight analytical points yielded a concordia age of 506 ± 4 (MSWD = 1.1), interpreted as the age of crystallization of the granite. One concordant analysis yielded an Archean age of 2680 Ma ± 20 (2σ), interpreted as an inherited component.

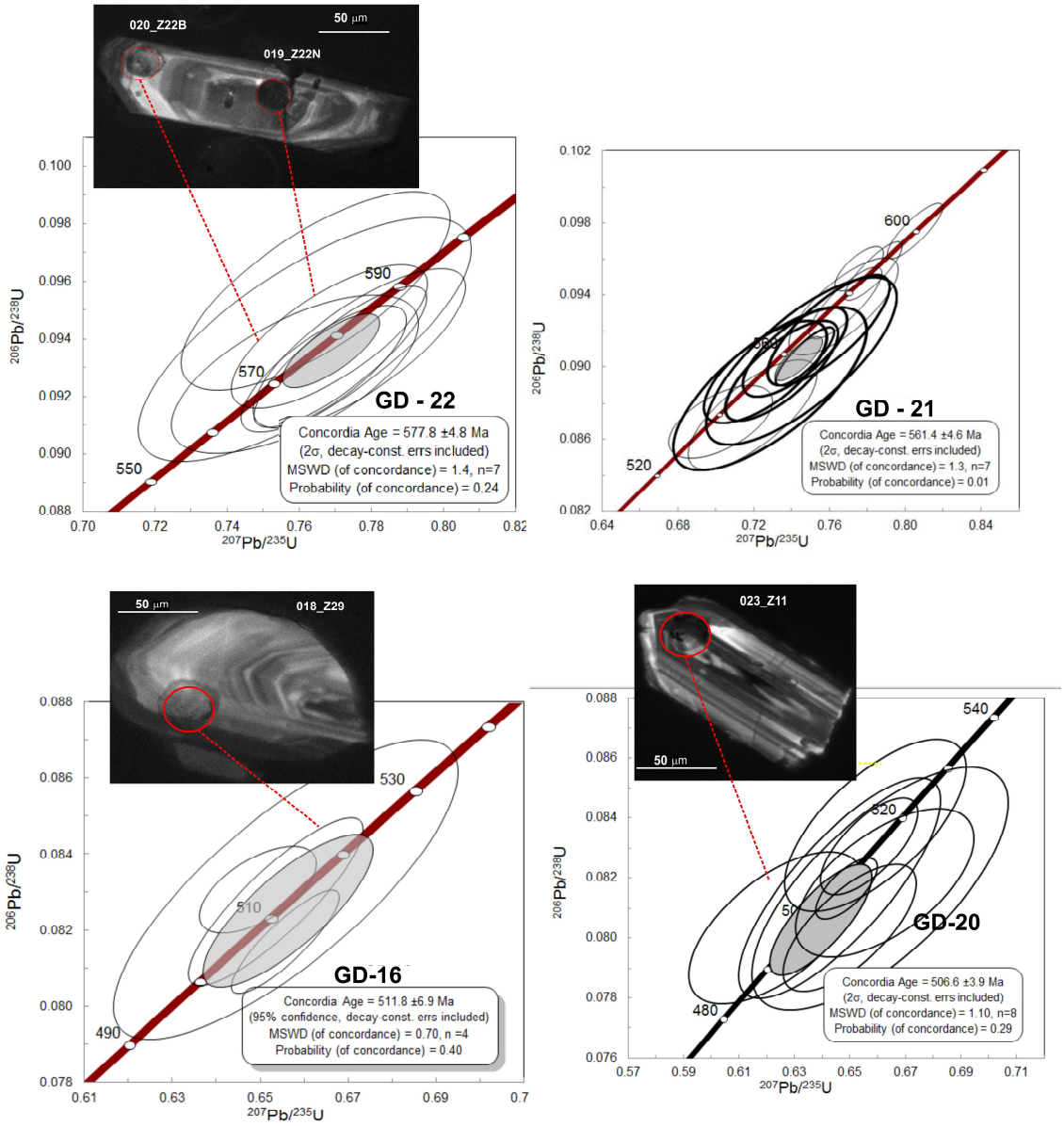

Figure 3.7 – Concordia diagram for zircon grains of Serra Negra Suite: Bastos Granite (sample GD-22), Impertinente Granite equigranular facies (GD-21), Iporá Granite (sample GD-22), Impertinente Granite porphyritic facies (sample GD-20). Also showing the CL and BSE images with analyzed spots in the zircon grains (the specific age of each zircon is shown in attached table). Laser spots (30µm) on the zircon are indicated by red open circles.

Table 3.3 - Sm–Nd isotopic data for Jaupaci Belt rocks

Sample	Rock	Unit	Sm(ppm)	Nd(ppm)	$^{147}Sm/^{144}Nd$	$^{143}Nd/^{144}Nd \pm 2SE$	$\varepsilon_{Nd\,(0)}$	$T_{DM\,(Ga)}$	$\varepsilon_{Nd\,(T)}$
GD-29	Metagranodiorite	Type 1 Suite	8.671	43.274	0.1213	0.512493+/-9	-2.83	0.91	4.61
GD-12	Metatonalite	Type 1 Suite	7.879	32.947	0.1446	0.512652+/-19	0.27	0.86	5.41
GD_08	Metatrondhjemite	Type 2 Suite	0.638	2.999	0.1286	0.512539+/-10	-1.92	0.9	4.61
GD-30	Metagranite	Type 2 Suite	0.312	1.222	0.1545	0.512537+/-21	-1.96	1.29	2.08
GD_19	Basal Metarhyolite	Jaupaci Sequence	2.606	15.412	0.1022	0.512234+/-15	-7.88	1.1	1.19
GD_17	Chlorite schist	Jaupaci Sequence	5.26	20.03	0.1588	0.512756+/-9	2.3	0.8	5.17
GD-32	Amphibole schist	Jaupaci Sequence	4.091	15.368	0.1609	0.512770+/-9	2.57	0.8	5.28
GD-33	Clhorite schist	Jaupaci Sequence	5.031	16.339	0.1861	0.512941+/-6	5.91	-	6.72
GD_34	Felsic metavolcanics	Jaupaci Sequence	6.237	25.679	0.1468	0.512667+/-17	0.56	0.86	4.21
GD_27	Felsic metavolcanics	Jaupaci Sequence	27.012	88.129	0.1853	0.512934+/-20	5.77		6.64
GD_28	Felsic metavolcanics	Jaupaci Sequence	8.351	34.421	0.1467	0.512690+/-5	1.02	0.81	4.79
GD-34	Felsic metavolcanics	Jaupaci Sequence	5.131	25.264	0.1228	0.512559+/-20	-1.55	0.82	4.04
GD_07	Felsic metavolcanics	Jaupaci Sequence	7.57	32.428	0.1411	0.512617+/-17	-0.48	0.9	3.79
GD-31	Felsic metavolcanics	Jaupaci Sequence	5.899	27.184	0.1312	0.512592+/-13	-0.9	0.84	4.89
GD_09	Gabbro	Serra Negra Suite	2.41	10.234	0.1423	0.512631+/-22	-0.13	0.88	3.97

3.7. Geochemistry results

Forty seven samples were collected for whole rock major and trace element analyses. Drill core and outcrop samples from selected rock types of the Jaupaci Belt rocks were investigated. Fourteen samples are from arc granitoids/orthogneisses, twenty five samples are from the supracrustal rocks of the Jaupaci Sequence, and nine samples from the Serra Negra Suite (Supplementary table 3.B).

3.7.1 Orthogneisses (Arc granitoids)

The two tonalite groups, Type 1 (770 ± 8 Ma tonalite-granodiorite) and Type 2 (754± 12 Ma trondhjemite-granite) are calc-alkaline rocks (Fig. 3.8A). The average major oxide compositions of Type 1 rocks are SiO_2 72 wt.%, CaO_2 1.65 wt.%, Na2O 3.37 wt.%, K_2O 3.03 wt.%, whereas type 2 are SiO_2 69 wt.%, CaO_2 2.16 wt.%, Na_2O 6.35 wt.%, K_2O 2.11 wt.%. The type 1 is peraluminous and calc-alkaline, whereas type 2 is metaluminous to weakly peraluminous with adakitic affinities (Fig. 3.8B and 3.8C). MORB-normalized plots for Type 1 rocks show marked depletion in Ti, Sr and P and enrichment in Zr, whereas Type 2 orthogneisses show depletion in Th, Y and Yb and enrichment in Sr in some samples (Fig. 3.9A). Chondrite-normalized rare earth element patterns clearly distinguish the two types of tonalitic orthogneisses: Type 1 rocks have $[La/Lu]_N$ ratios around 5 whereas in Type 2 rocks these values are approximately 20. LREE patterns in type 1 rocks are fairly horizontal when compared with the Type 2 patterns which show depleted HREE compared to LREE. (Fig. 3.9B).

In the Rb versus Y+Nb diagram (Fig. 3.8D), Type 1 samples fall within the post-collisional granite field. Type 2 compositions are similar to the volcanic arc granite field (VAG).

3.7.2 Jaupaci Sequence

Volcanism in the Jaupaci Sequence is bimodal, with highly evolved calc-alkaline to high-K metavolcanic acid rocks and tholeitic MORB metabasalts.

The felsic rocks of Jaupaci Sequence are divided into two geochemical groups: the basal metarhyolites and upper felsic metavolcanics represented by metadacite (biotite feldspar quartz schist) and metarhyolites (muscovite-feldspar quartz schist).

The metarhyolites show high SiO_2 (average of 72 wt.%), calk-alkaline affinity and are metaluminous to weakly peraluminous (Fig. 3.8B and 3.8E). They are strongly fractionated and chondrite-normalized plots show marked depletions of Ti, Y and Yb, while several samples also show enrichment in Sr and Th (Fig 3.9C). The high Sr/Y and La/Yb ratios point to adakitic affinity (Fig. 3.8C). They are strongly depleted in HREE and have fractionated REE profiles with $[La/Lu]_n$ ratio around 50, which is typical of arc magmas (Fig. 3.9D). In the Rb versus Y+Nb diagram (Fig. 3.8D), most samples fall within the volcanic arc granite field (VAG). In Th/Ta versus Yb diagram, most sample fall in the active continental margin field (Fig. 3.8E).

The upper felsic metavolcanic rocks are chemically equivalent to metadacites and metarhyolites (Fig. 3.8E). Metarhyolites show 72 wt.% SiO_2, whereas metadacites show 68 wt.% SiO_2. They are slightly peraluminous and belong to the calc-alkaline series (Fig. 3.8A and 3.8B). In chondrite-normalized plots they show Ti, Sr and P depletions and several samples also show Zr enrichment (Fig. 3.9C). They are strongly enriched in LREE (>100 times chondrite), with marked negative Eu anomalies ($Eu/Eu* < 0.7$) and generally have flat HREE with $[La/Lu]_n$ ratio around 10 (Fig. 3.9D). Metarhyolites show pronounced Eu anomalies and negative Sr anomalies in the multi-elementar diagram. The metadacite are slightly enriched in LILE (Sr and Ba) compared to metarhyolites. In the Rb vs Y+Nb diagram (Fig. 3.8D), most samples fall within the volcanic post-collisional field. In Th/Ta versus Yb, most samples are similar to within plate rocks (Fig. 3.8F).

The chlorite schist and amphibole-schist are chemically equivalent to tholeiitic basalts with average SiO_2 content of 48 wt.% (Fig. 3.8A). The REE profiles are sub-

parallel showing slightly LREE-enriched ([La/Lu]*n* (2.3–2.8) and small positive Eu anomalies. All REE profiles are convex upwards, displaying variable depletion of La and Ce (Fig. 3.9E). Primitive mantle normalized plots are characterized by relatively flat profiles, showing negative Nb anomalies, enrichment in Rb, Ba and K and variable Sr anomalies (Fig. 3.9F). The scatter in Rb, Ba and K should reflect mobility during metamorphism/alteration. Although alteration has caused some scatter in Sr contents, the general inverse relationship between Sr and MgO suggests that some of the original relationships are still preserved.

3.7.3 Serra Negra Suite

The Iporá, Israelândia, Impertinente, Bastos and Piloândia granites share chemical affinities with high-K granitic rocks (Fig. 3.10A and Fig. 3.10B). They are metaluminous to weakly peraluminous (Fig. 3.10C), and their normalized rare earth elements show $[La/Lu]_N$ ratio between 5 and 15, point0,3 to strong LREE enrichment. The pronounced Eu and Sr negative anomalies indicate plagioclase fractionation in late magmatic stages (Fig. 3.10D). Primitive mantle-normalized plots show marked depletions in Sr, Ti and P and several samples also show enrichment in Rb and Th (Fig. 3.10E). In the Rb versus Y+Nb diagram (Fig. 3.10F) sample compositions fall within the post-collisional granite field.

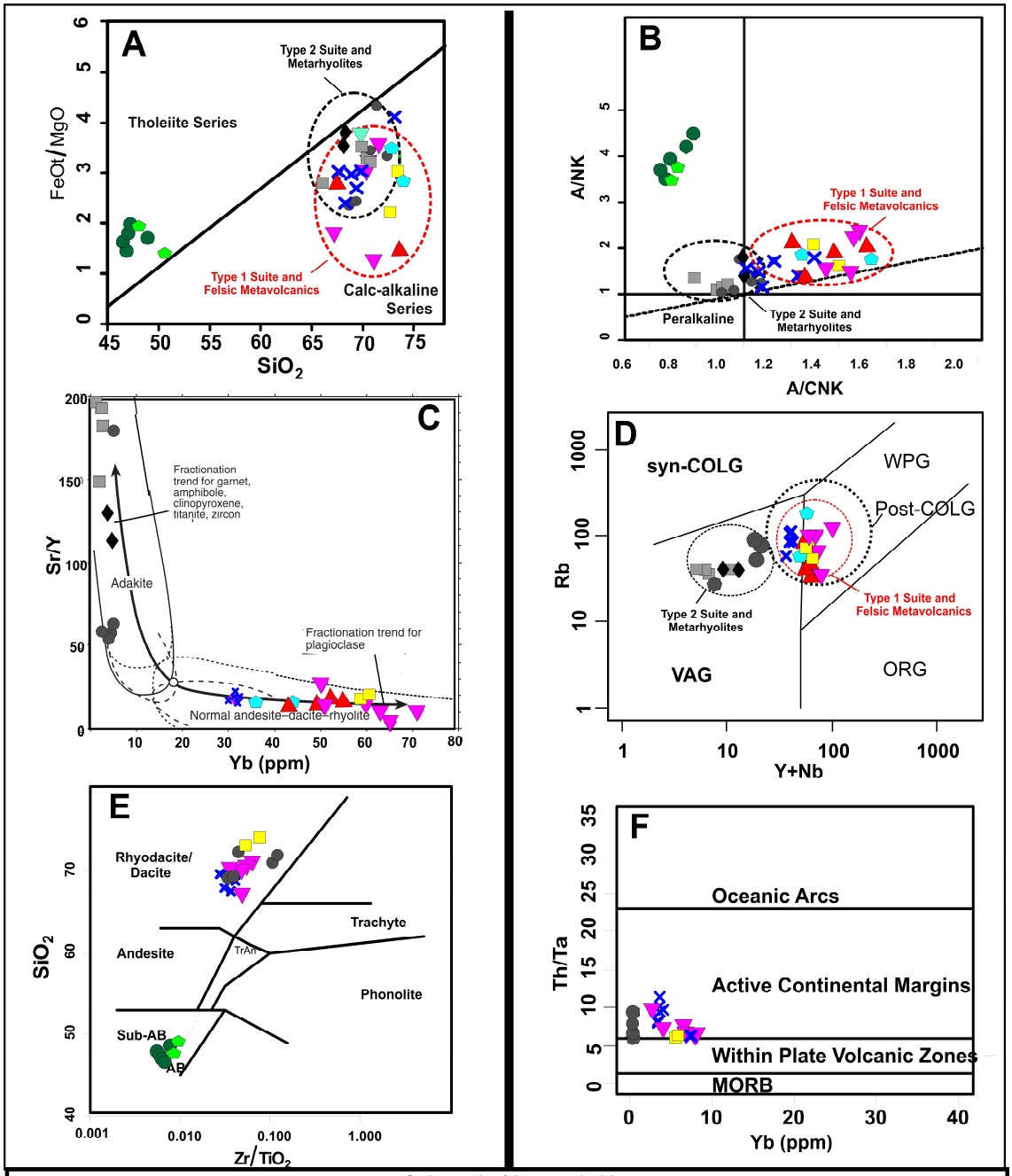

Figure 3.8 - Plots for orthogneiss and Jaupaci Sequence:A) SiO_2 vs. FeOt/MgO diagram (Miyashiro, 1974); B) A/NK versus A/CKN diagram plot (Shand 1943);C) Plots of (a) Sr/Y vs. Y (Defant and Drummond, 1993);D) Rb versus Y+Nb plot of (Pearce et al., 1996); E) Zr/TiO2–Nb/Y diagram after Winchester and Floyd (1977); F) Geotectonic diagram for felsic rocks after Schandl and Gorton (2002).

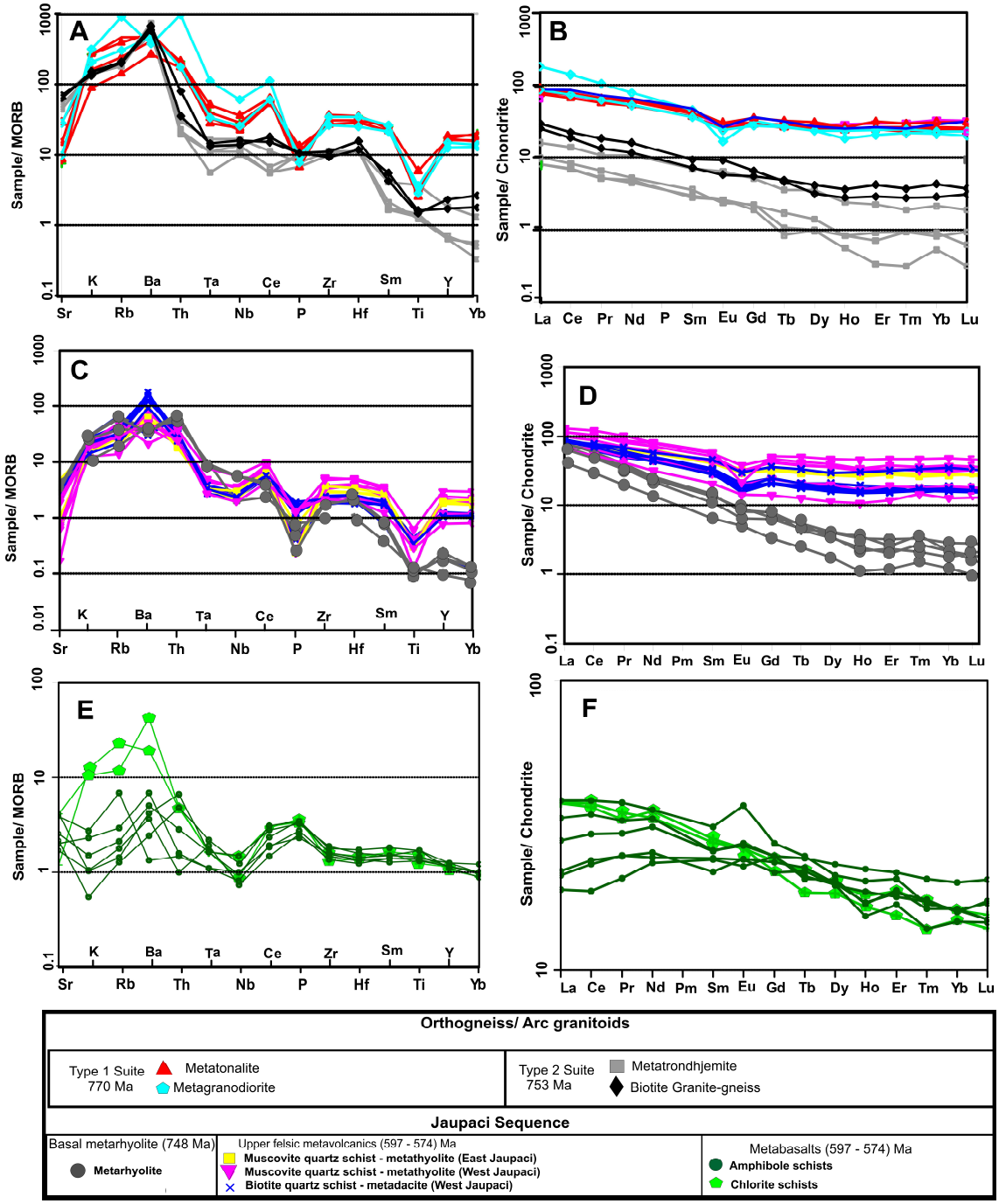

Figure 3.9 – MORB-normalized spider diagrams and chondrite-normalized REE patterns for the metagranitoids and orthogneisses (A and B respectively), metavolcanic felsic rocks of Jaupaci Belt (C and D) and the metabasalts (E and F). MORB and chondrite normalization values after Pearce (1983) and chondrite values according Sun and McDonough (1989).

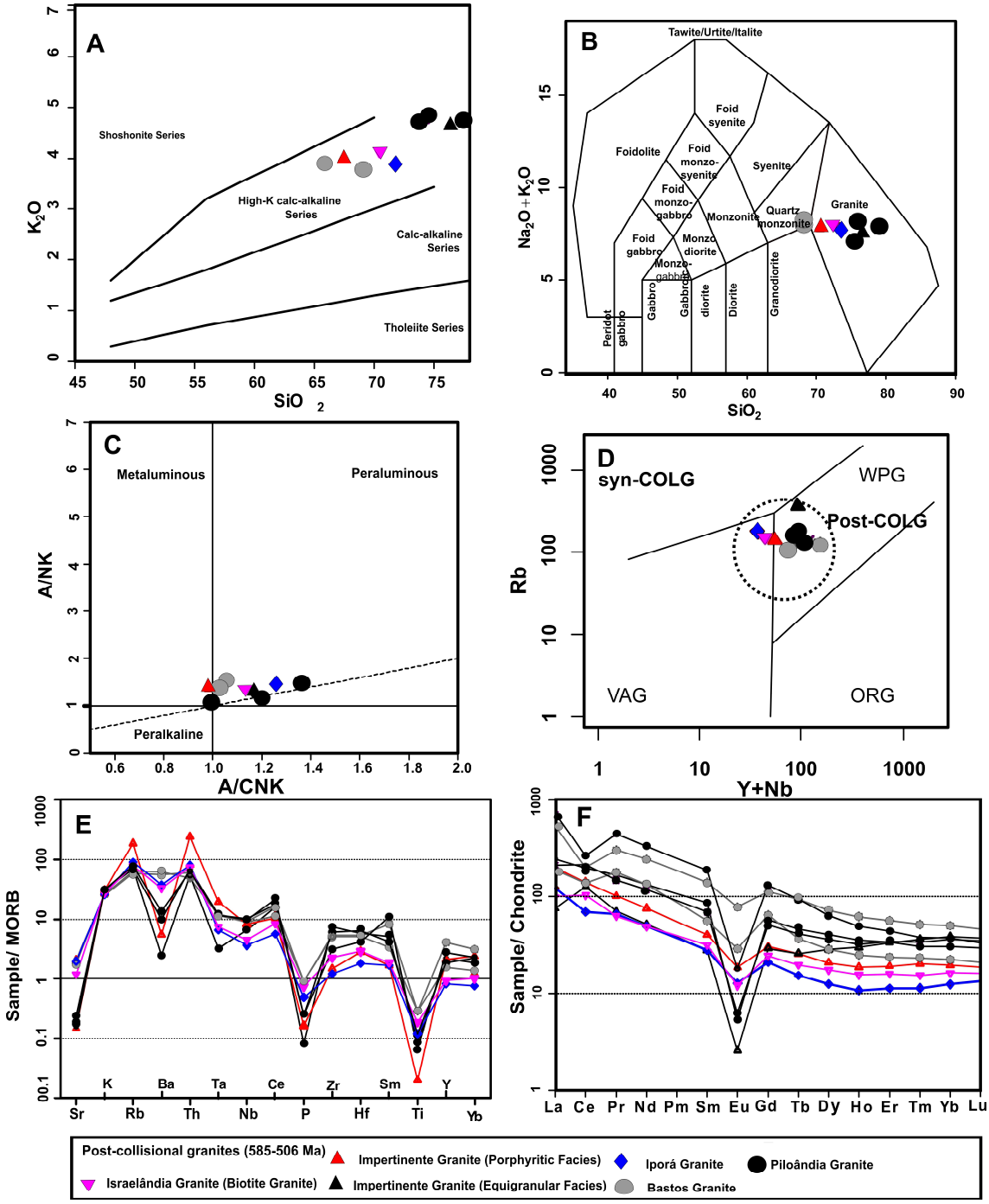

Figure 3.10 – Plots of Serra Negra granites: A) SiO_2 versus K_2O plot from Pecerillo and Taylor (2001); B) SiO_2 versus K_2O+N_2O plot for granitoid classification (Middlemost 1985); C) A/NK versus A/CKN diagram plot (Shand 1943); D) Rb versus Y+Nb plot of Pearce et al., (1996); E) REE patterns normalized by chondrite after Pearce (1983);F) spider diagrams with Primitive Mantle-normalization after Sun and McDonough (1989)

3.8. Discussion

3.8.1. Age and source of magmatic events

The integration of isotopic and whole rock geochemistry data for the Jaupaci belt presented in this study define two main magmatic events: i) Neoproterozoic event that took place at 770-750 Ma in an arc setting; ii) Late-Neoproterozoic/Cambrian event that comprise three post-tectonic magmatic phases: ~597-585 Ma, ~577-539 Ma and ~511-506 Ma, which mark the cessation of continental accretion.

Arc setting magmatism

A defining characteristic of the Goiás Magmatic Arc is the continuous accretion with two magmatic peaks related to consumption of Goiás-Pharusian Ocean: an early event that occurred in an intra-oceanic arc setting at ca. 920 -800 Ma and a later developed in a continental arc setting at ca. 660-630 Ma (Pimentel et al., 2000, Kroner and Cordani 2003, Laux et al., 2005, Brito Neves et al., 2014). Previous geochronological studies have already indicated the existence of a magmatic event between ~790-750 Ma (Pimentel et al., 1991; Laux et al., 2005; Guimarães et al., 2012), however, the authors have pointed out that it has only generated scattered magmatic rocks in the Arenópolis Arc. However, our data indicate that it represent a much broader juvenile crustal growth episode, defined at two specific time intervals (~770 Ma and ~753-748 Ma) and displaying remarkable geochemical and petrological differences.

The first magmatic event is represented by ilmenite-bearing, calc-alkaline, peraluminous tonalite and granodiorite of Type 1 Suite. These granitoids have higher K_2O (2.02–5.24 wt%), Rb (42–179 ppm), Zr (mostly 242–1114 ppm) and are strongly peraluminous (A/CNK >1.2) compared with the Type 2 granitoids. They are notably enriched in LILE and most of HFSE compared to N-MORB (Fig. 3.9A), have HREE enriched patterns with negative Eu anomalies (Fig. 3.9B) and are similar to post-collision granites (Fig.3.8D). The higher fractionated HREE patterns of the Type-1 granitoids may reflect small amount of garnet in their source. These parental magmas were evolved through fractional crystallization of apatite and Fe–Ti oxides (rutile) and/or hornblende as indicated by P and Ti troughs in the MORB-normalized patterns.

The negative Eu anomaly in REE patterns reflects plagioclase fractionation or/and residual plagioclase. These trace elements patterns could be generated by amphibolite melting at depths of ca. 8–10 kbar, where garnet and plagioclase become stable (Beard, 1995; Rapp and Watson, 1995; Moyen and Stevens, 2006). Consequently, the parental magmas of the Type-1 granitoids were generated at least 20-25 km thick crust. The parental magmas involved melting or contamination with sedimentary rocks in order to produce ilmenite-bearing peraluminous magmas. However the reservoir is predominantly from juvenile material as suggested by T_{DM} model ages of 0.86 to 0.91 Ga and positive ε_{Nd} (T) values range +4.6 to 5.4. The peraluminous nature and positive εNd (T) isotopic compositions of these granitoids do not match those of the melts generated solely from sedimentary crustal rocks. This discrepancy argues for the presence of juvenile mantle material that must have been incorporated at the time of generation of the granitoid. According to Sylvester (1998 and reference therein) high ratio values of CaO/Na_2O (>0.3) are indicative of peramulinous magma that have been produced through mixing of basaltic with sedimentary-derived melts. The type 1 granitoids display CaO/Na_2O average ratio of 0.56. Therefore, the geochemical characteristics of post-collision granitoids coupled with high SiO_2 contents (70–73 wt%), are consistent with derivation of their parental magmas by low-degree partial melting of arc juvenile lower crust of basaltic and sedimentary rocks composition at greater depth due to increased island arc crust thickness as a consequence of arc maturation. Such process of arc maturation with significantly thickened arc crust is widely recognized in other oceanic arcs resulted by fractional crystallization and/or anatexis of infracrustal juvenile rocks (Boutelier et al., 2003; DeBari and Greene 2011).

The second magmatic event (753-748 Ma) encompasses magnetite-bearing, metaluminous intrusions (Type 2 orthogneisses) and the basal metarhyolites of the Jaupaci Sequence. Both share the same geochemical and isotopic signature with higher Na_2O (5.55-6.79 wt%) , Sr (528-830 ppm) and lower Y (1.9-7.5 ppm) and Yb (0.11-0.9 ppm) than Type-1 granitoids. Strong enrichment in LILE (Ba, Sr) as well as negative anomalies in P and HFSE is usually assumed to be a signature of arc-derived magmas (Taylor and McLennan, 1995); iii) high Sr/Y ratios, enrichment in LREE, depletation in HREE and inconspicuous Eu anomalies are consistent with with adakitic affinity , which origin is related to partial melting of hydrated mafic source rocks in the form of eclogite or garnet amphibolite (Rapp et al., 1991; Drummond et al., 1996; Martin, 1998). Adakitc rocks have different petrogenesis origin, such as: (1) assimilation-

fractional crystallization (AFC) processes (Castillo et al., 1999; Macpherson et al., 2006); (2) melting of mantle peridotite under hydrous conditions (Stern and Hanson, 1991); or (3) delaminated mafic lower crust (Kay and Kay, 1993; Defant et al., 2002); or (4) partial melting of thickened lower crust (Johnson et al.,1997; Guo et al., 2006; Liu et al., 2008). AFC process to originate the Type-2 granitoids and metarhyolites adakitic rocks seems unlikely. Likewise, these adakitc rocks cannot have been produced by direct melting of mantle peridotite, due low concentrations of MgO, Ni and high content of SiO_2 (68-73 wt%). Therefore the geochemical features (Fig 3.11 A and B) coupled with positive ε_{Nd} (T) values varying from +1.1 to +2.08 is more likely to have evolved from low partial melting of thick juvenile lower crust. Experimental studies that have shown that mafic materials can melt to produce an adakitic melt at pressures equivalent to a crustal thickness above 40 km (Rapp and Watson, 1995; Rapp et al., 1999). Such thickness is generally developed in continental active margin, whereas in intra-oceanic setting the arcs are built in thin (less than 35 km) mafic crust. Consequently magmas generated intra-oceanic arc are more mafic and less contaminated than magmas generated in active continental margin (Stern 2010). The T_{DM} model ages are slightly older than those of Type-1 granitoids with 1.1–1.29 Ga indicate some crustal contamination.Thus, a continental active margin is most likely scenario to generation of adakitic Type-2 granitoids and equivalent volcanic rocks at ~753-748 Ma. This setting is also supported by e geotectonic diagram of Th/Ta x Yb (Fig 3.8F). On the other hand, the isotope and the ε_{Nd} (t) values do not support the involvement of pre-Neoproterozoic crust in the genesis of these rocks. Consequently, the only way of active continental margin to present positive ε_{Nd} (t) values is the subduction occurring under older juvenile continental crust. The age of this older crust is provided by xenocrystic zircon grains crystallized between 880 and 790 Ma obtained in Type-2 trondjhemite sample (GD-08).

Post-collisional magmatism

The post-collisional event is marked by transition of the plutonic/volcanic rocks from calc-alkaline to alkaline dominated assemblages of Suite Serra Negra and bimodal volcanics rocks (felsic metavolcanics and metabasalts) of Jaupaci Sequence. The emplacement of these granitoids took place in protracted magmatic event (~597-506

Ma) and has been accompanied with development of the Moiporá-Novo Brasil strike-slip shear zone (MNBSZ). The data presented in this work combined with previous study have shown that granitoids of Serra Negra display distinct isotopic, geochemical and deformation features. Thus, the simple classification of Suite or even Supersuite (Picher, 1983) is inappropriate for these granitoids. In this work we divided post-collisional granioids in three distinct groups that followed the evolution of MNBSZ history: pre-, syn- and post-kinematics events:

The **pre-kinematics** event started with bimodal magmatism consisting of peraluminous rhyolitic-dacitic magmas dated at 598 ± 10 Ma (sample GD-07) and N-MORB basaltic magmas, represented by amphibole and chlorite schist. This volcanic event was followed by emplacement of granitoids displaying A-type signature (Israelândia intrusion with 585 ± 20 Ma) and small plugs of gabbros (GD-09 with 593± 4 Ma). Nd isotopic data of pre-kinematic plutonic/volcanic rocks display T_{DM} model age of 0.80 – 0.92 Ga and positive ε_{Nd} (T) with values range from +2.3 to +6.6. The **syn-kinematic** event is related to A-type granites emplaced along the MNBSZ. The A-type granites from this event are strongly deformed with ages between 577 and 539 Ma The syn-kinematic intrusions are represented by Bastos (577± 4 Ma), Impertinente (561 Ma± 4), Moiporá (556 ± 4 Ma), Ivolândia (550 Ma), Messianopólis (542± 4 Ma) and Piloândia granites (539± 6 Ma). Nd isotopic data shows TDM model age of 1.27 – 2.25 Ga and negative ε_{Nd} (T) with values range from -1.0 to -19.0 (Table 3.2). The last event consists of **post-kinematic** A-type intrusions, represented by undeformed granitiods as Iporá Granite (511 Ma ± 7) and porphyritic facies of the Impertinente Granite (506± 3 Ma). This event present Nd isotopic data with T_{DM} model age of 0.9 – 1.2 Ga and negative to slightly positive ε_{Nd} (T) with values range from -4.6 to +1.1. In the section below we detailed the petrogenesis of each event:

Pre-kinematic event (ca. 597-585 Ma): the basaltic magmas show silica contents between 46.4–50.3 wt. %, relatively high MgO concentrations (6.1–8.0 wt.%) and Fe_2O_3 (8.7 – 10.5%) and high Cr contents (175–295 ppm) coupled with positive values of ε_{Nd}(T) between +5.2 and +6.7 suggesting derivation from a asthenospheric mantle source (Saunders et al., 1992).However, the trace element compositions of the pre-kinematics mafic rocks indicate their mantle source is more complex. The Nb negative anomalies and high abundances of incompatible trace element indicate some degree of metasomatism of the mantle due to the introduction of subduction-derived material. This geochemical signature constitutes one of the prevailing characteristics of

post-collisional magmatism, they are generally attributed to metasomatism induced by slab-derived fluids or silicate melts prior to collision (Pearce et al., 1990; Turner et al., 1992; Turner et al., 1996).The low La/Yb ratios (3.5 to 1.9) reflect a melting regime dominated by relatively large melt fraction with spinel as the predominant residual phase (Kelemen et al,. 1993), which coupled with relatively flat MREE and HREE patterns, suggests that the original magmas may have been formed by relatively high degree of partial melting of mantle source at shallow conditions. All of these features are consistent with N-MORB basaltic magmas derived from high degrees of partial melting of a metasomatized asthenospheric mantle under an extensional setting of post-collisional tectonics.

The granite and felsic metavolcanic rocks present similar geochemical features with: high silica and alkalis contents (68.06-78.06 wt.% and 5.85-8.55wt.% respectively); low MgO and CaO (0.1-0.9 wt. % and 0.88-2.22 wt.%); enrichement in REE with marked negative Eu anomalies; low abundance in P, Ti and Sr; high concentrations of Ga, Zr, Nb, Ce and Y (Fig.3.11C). All these feature are typical of A-type granites (Whalen et al., 1987; Bonin 2007; Frost and Frost 2011). Furthermore, the 10,000×Ga/Al ratio values range from 3.2 to 5.6, whereas the volcanic rocks show lower values with ratios range from 3.2 to 2.5. On the discrimination diagrams of Whalen et al., (1987), all granites samples plot into the A-type granite field, whereas felsic metavolcanics present A and I-type affinities (Fig. 3.11D and 3.11E). The samples fall into the A2-type granite field (Fig. 3.11F), according to the classification of Eby (1990), representing, therefore, rocks formed by crustal melting in post-collisional settings, with melts being derived straight from the sialic crust or underplated material that has been through a cycle of island arc magmatism.

Several petrogenetic models for A-type magmas have been proposed: (1) direct fractionation products of mantle-derived alkaline basalts (e.g., Turner et al., 1992; Litvinovsky et al., 2002; Mushkin et al., 2003); (2) partial melting of specific crustal protoliths (Whalen et al., 1987; Creaser et al., 1991); (3) combination of crustally-derived felsic magma with mantle-derived mafic magma (Kerr and Fryer 1993; Mingram et al., 2000). The A-type granites and felsic metavolcanics have positive εNd(T) range from +2.3 to +6.6 that are similar of metabasalts of Jaupaci Sequence. Additionally, marked depletions in Sr, Ti and P indicate process of fractional crystallization of apatite and Fe–Ti oxides in the sources. This evidence combined point to extensive fractional crystallization model from coeval mafic magmas. However, an

extreme differentiation of coeval tholeiitic parent magmas is untenable, since the volumes of felsic magmas are large compared to mafic magmas. Alternative model of pure crustal origin seems to be possible to generate A-type magmas of Jaupaci belt. This model is supported by the peraluminous nature coupled with inherited zircons in the granitoids and felsic metavolcanic rocks (ages mainly within the interval between 778 and 828 Ma). Nevertheless, this model might not be fully applicable to type-A granite and felsic metavolcanic, since some granite samples are slightly metaluminous, present mafic enclaves and have high positive ε_{Nd} (T). Thus, the occurrence of MMEs in the granites coupled with isotope pattern, indicate that the A-type granites and felsic metavolcanics petrogenesis may have involved hybridization of mantle-derived magma with partial melting of crustal 778–828 Ma arc material, followed by fractional crystallization.

Therefore, pre-kinematic events are related to mantle upwelling in extensional post-collisional environment that caused partial melting of a thinned and metasomatised lithosphere, resulting in mafic and felsic alkaline magmatic products. The continuous input of heat through lithospheric structures leads to a weakened lithosphere that enhances extension promoting the delamination of sub-continental listhopheric mantle (SCLM). This is evidenced by deep seismic and gravimetric surveys that showed that the GMA is the thinnest crust of the central sector of the Brasilia Belt with thickness varying from 34 km to 44 km (Berrocal et al., 2004; Soares et al., 2006; Curto et al., 2015). In this setting, the tholeiitic metabasalts represent the asthenospheric melts, after delamination of the lower crust. The asthenosphere acts, therefore, as heat engine to promote low degrees of partial melting of the newly underplated lower crust which have interacted with older felsic crust (778–828 Ma) producing felsic magmas, with I and A-type features.

Sin-kinematic event (577-539 Ma): the felsic magmas of this event are similar to the pre-kinematic granitoids, presenting A-type signature (Fig.3.11C), high incompatible trace elements concentrations (Ga, Zr, Nb, Ce and Y), depletion in Eu, Ti and P and enrichment in the LREE. However, this magmatic event have older T_{DM} model (1.0 to 2.7 Ga) with slightly positive to negative ε_{Nd} (T) values, varying from +1.1 to -19 (Table 3.2), showing some involvement Archean/Paleoproterozoic crust (Fig. 3.12). In this event, the strike–slip shearing was associated with compressional strain that also developed regional folding and imprinted greenschist metamorphic assemblage in the Jaupaci Belt rocks. The most prominent structure developed in this event is the

MNBSZ with more than 200 km wide and probably may extend to the south under Phanerozoic cover.The age of the granites hosted in MNBSZ, their orientation at a high angle to the shear zone main strike, as well as structural analysis are evidence of dextral-lateral movements and MNBSZ developed between ~577 to 539 Ma. Strike-slip movements continued after the granite intrusion, resulting in their sheared granite and to mylonites textures. Such movement causes displacement of lithotectonic assemblages and former neighbouring terranes and units, sorting out the Arenópolis Arc in two domains generically named in this work as western and eastern domains (Fig. 3.2). According to Storti (2003) sub-vertical strike-slip shear zones with strike-lengths and offsets greater than 300 km and 30 km, respectively, are very likely to be of a size sufficient to cut much, if not all, of the lithosphere. Gravimetric and magnetic data support this interpretation where the main major fault zones in this region represent limits of tectonic domains characterized by different types of crust and mantle (Curto et al., 2015)

Thus, the MNBSZ represent a translithospheric suture, defining continental deformation with significant lateral displacement. In this scenario, the MNBSZ allowed the juxtaposition of two distinct lithospheric blocks: in the west the juvenile Arc of the Jaupaci Belt, and to the east, the Archean block of Goiás Massif in the west (Fig 3.2). Moreover, translithospheric sutures are deep enough to act as conduits for mantle material allowing interaction with base of the lithosphere and providing heat to re-melt it generating A-type granites (Schaltegger and Brack 2007; Pirajno 2007, Curto et al., 2015). Pirajno (2010) proposed a model, in which the lateral migration of mantle material is drawn towards regions of lower pressure, probably enhanced by translithospheric–discontinuities. The mantle material migrates laterally into these discontinuities, interacts with different sectors of the heterogeneous sub-continental lithospheric mantle (SCLM), resulting in the formation of alkali-rich intrusions. The interaction of heterogeneous SCLM source is supported by Nd isotope signatures of syn-kinematics A-type granites. They present T_{DM} model age of 1.27 – 2.25 Ga and negative ε_{Nd} (T) with values range from -1.0 to -20, therefore these rocks clearly showing an important component of Paleoproterozoic (Góias Massif) crust with mixing either of juvenile crust (Fig.3.12).

Post-kinematic event (511-506 Ma): this event is represented by undeformed granites that took place at 511 to 506 Ma. They present similar geochemical signature of the previous A-type granites events; however they are exclusively peraluminous

magmas. The presence of MME in the Iporá granite point to similar petrogenesis of pre-kinemtics A-type granites. Nd isotopic data display T_{DM} model age of 0.9 – 1.2 Ga and negative to slightly positive ε_{Nd} (T) with values range from -4.6 to +1.1, showing a predominance of juvenile component mantle source compared with source of syn-kinamtics granites. Based on this data is possible to inferred that final stages of evolution of Jaupaci Belt is related to a late extension event , where the generation of A-type granites involved a new hybridization of mantle-derived magma with partial melting of crustal.

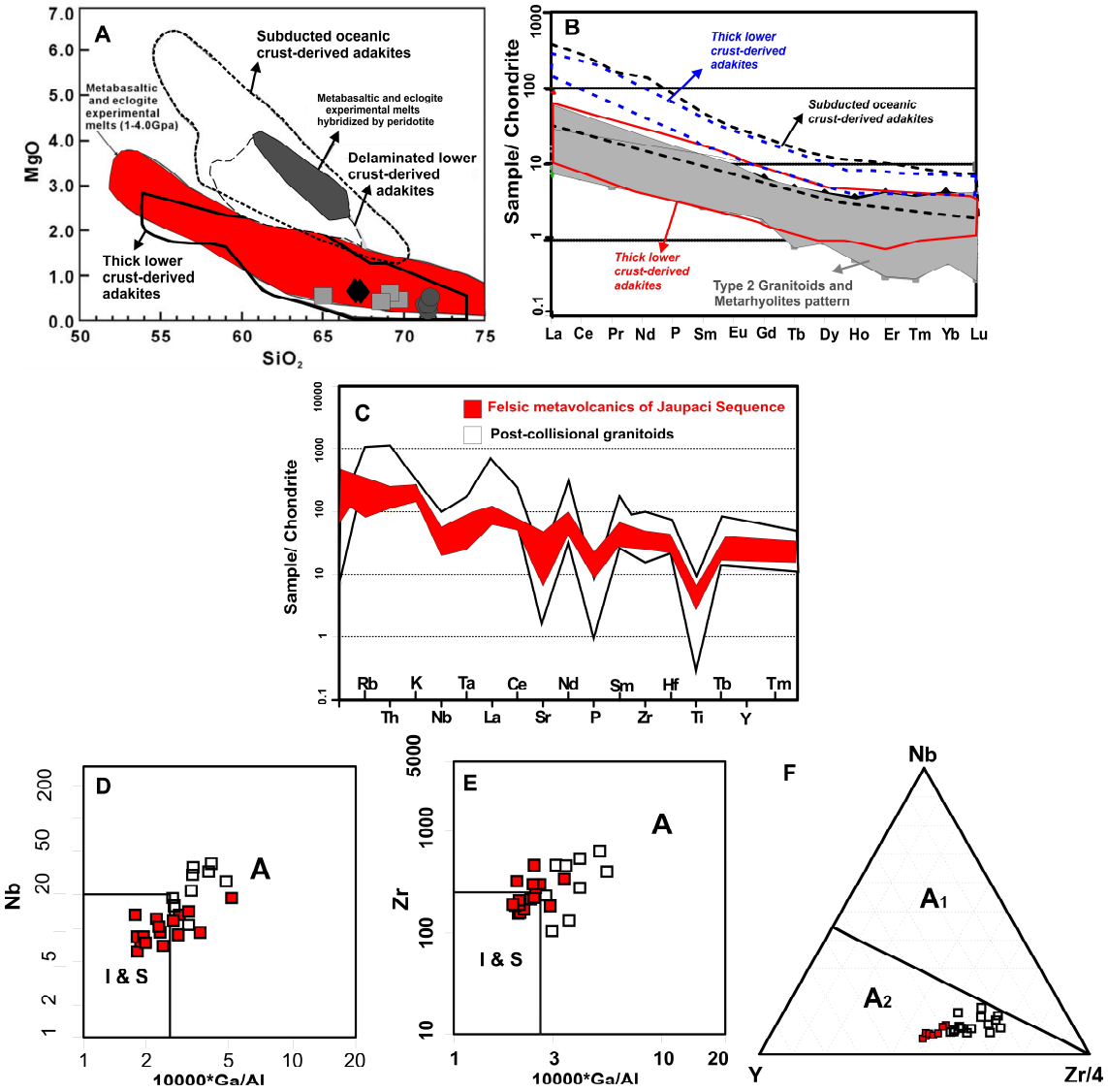

Figure 3.11 - A) MgO wt.% vs. SiO2 (wt.%) diagrams for the ~750 Ma adakitic rocks (Type-2 granitiods and metarhyolites, symbols same from Fig.3.8). The field of delaminated lower crust-derived adakitic rocks are from Wang et al., (2004); Liu et al., (2009). The field of subducted oceanic crust-derived adakites is constructed using data from Defant and Drummond (1993), Kay et al., (2002), Defant et al., (2002) and Martin et

al., (2005). Data for thick lower crust-derived adakitic rocks are from Petford and Atherton (1996), Johnson et al., (1997). The field of metabasaltic and eclogite experimental melts (1–4.0 GPa) is from Rapp et al., (1999, 2002), Rapp and Watson (1995), and references therein. The field of metabasaltic and eclogite experimental melts hybridized with peridotite is after Rapp et al., (1999); B) Chondrite-normalized REE diagram of adakitic type-2 granitoids and volcanic rocks of Jaupaci Belt, normalized after Sun and McDonough (1989). The REE and trace element data for delaminated lower crust-derived adakitic rocks, subducted oceanic crust-derived adakites, and thick lower crust-derived adakites are d from the same data sources as those in 11A; C) Spider diagrams comparing felsic metavolcanics with Serra Negra Suite granitoids, chondrite normalization after Sun and McDonough (1989); D) and E) Discrimination diagram of Whalen et al., (1987), showing the I and A-type nature of the Serra Negra Suite and felsic metavolcanics of Jaupaci Sequence; F) Plots of the Serra Negra granitoids and Jaupaci felsic metavolcanics on the Nb–Y–Zr/4 discrimination diagrams for the subdivision of the A-type granites into A1 and A2 sub-types (Eby, 1992).

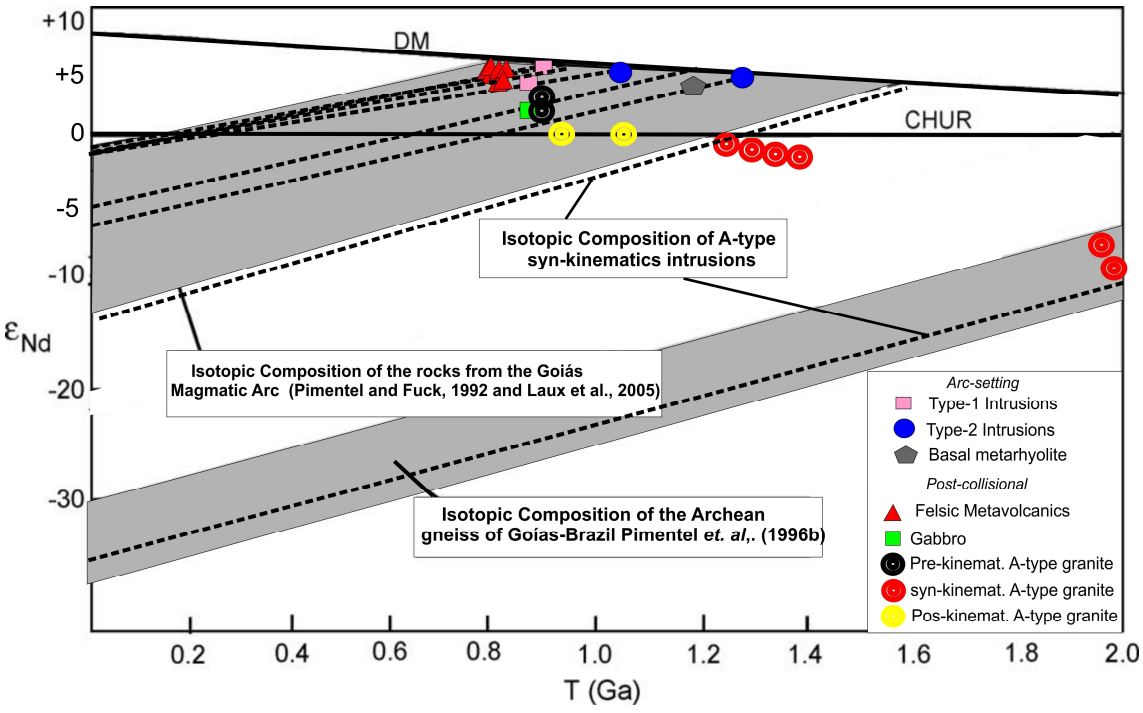

Figure 3.12 - ε_{Nd} (T) versus Time (Ga) diagram showing Nd isotopic composition of the Jaupaci Belt rocks. Nd isotopic composition of the Goiás magmatic arc is from Pimentel and Fuck (1992) and Laux et al., 2005; Archean gneisses is from Pimentel et al., (1996). The Nd isotopic from Post-collisional granitoids intruded in the Archean gneiss (Motta-Araujo, 2012) show a mixture of Archean and juvenile material. The isotopic data and references from A-type granites are listed in the table 3.2

3.8.2. The Jaupaci Belt in the evolution of Arenópolis Magmatic Arc

The age of the substratum of the Jaupaci Belt is given by the ages of inherited zircon grains (880, 830 and 790 Ma) in the younger magmatic units of the belt. The sources of these zircon grains may be correlated with orthogneisses dated in neighboring terranes: to the west of the Jaupaci Belt, U-Pb ages of 899 ± 7 Ma and 890 ± 6 have been reported for the Arenópolis gneiss and Morro do Baú gabbro, respectively (Pimentel and Fuck 1994; Pimentel et al., 2003) to the east ages ranging from 886 ± 6 to 790 ± 10 Ma have been reported to amphibolites and granitoids (Laux et al., 2005). The isotopic and geochemical signatures of these plutonic rocks have been compared with primitive M-type granitoids of intra-oceanic island arcs formed due to consumption of Goiás-Pharusian oceanic lithosphere (Pimentel et al,. 2000 ; Laux et al., 2005, Cordani et al., 2013a). Therefore, based on previous works (Laux et al., 2004; Laux et al.,2005, Motta-Araujo 2012) and in our data is possible define three episodes of intra-oceanic arc magmatism in Arenópolis Magmatic Arc: early granitoids at 899-886 Ma, succeeded by 828-820 Ma and finally an episode of arc maturation with peraluminous magmatism produced by re-melting of overthickened island arc at 790-770 Ma (Fig. 3.13A).

The metarhyolites and Type 2 intrusions dated between ca. 753-749 Ma have similar U-Pb ages of those of the crystal tuffs of the Bom Jardim Sequence (749 ± 6 Ma). Both are composed mainly by felsic rocks and Th/Ta ratio values varying from 6 to 10 and indicate origin in an active continental margin (Schandl and Gordon 2002). This is also supported by Paleoproterozoic and Archean (1.85-2.6 Ga) inherited zircons in the crystal tuff combined with negative ε_{Nd} (t) values (Guimarães et al., 2012). Therefore, the continuous consumption of oceanic lithosphere led to the docking of the previously consolidated island arc into an allochthonous sliver of Archean/Paleoproterozoic crust (probably represented by the Ribeirão gneisses, Fig 3.2) producing the continental-type magmatic arcs (Fig. 3.13B). The contrast of ε_{Nd} (t) values between the Jaupaci and Bom Jardim rocks is possibly explained by different paleo-positions in this continental arc setting. The 750 Ma Jaupaci felsic volcanics showed solely juvenile sources (+1.1 to +4.6), whereas the Bom Jardim volcanics involved the contribution of older crustal material in their petrogenesis (-5.9 to +4.6).

The younger arc-related igneous event in the Arenopolis Arc is mainly represented by a large landmass formed by the Firminópolis-Turvânia-Paminópolis

orthogneisses that took place at 637-630 Ma (Laux et al., 2005). The petrogenesis of the igneous protholiths of these gneisses involved contamination with older sialic crust during ascent and crystallization, which may indicate proximity and participation of, the edge of the São Francisco continental plate (Laux et al., 2005). The magmatism along the active margin of the Arenópolis Arc spanned from ca. 660 to 630 Ma and is geographically concentrated on its eastern segment, indicating consumption of oceanic lithosphere along east-dipping subduction during convergence between the Paranapanema and São Francisco continents (Fig. 3.13C). This subduction is further supported by igneous and metamorphic overgrowths age in UHT Anapolis-Itauçu granulites dated at ca. 650 to 640 Ma (Piuzana et al., 2003, Baldwin and Brown 2008). Furthermore, petrological data of Laux et al., (2005) indicate that regional amphibolite metamorphic assemblage was imprited in the Arenópolis Arc in peak of metamorphic event. The final stage Paranapanema and São Francisco continents collision (Fig 3.14D) is marked by post-peak cooling age in zircon and emplacement of synorogenic mafic ultramafic complex at 627 Ma (Laux et al., 2005; Della Giustina 2010; ,Mota e Silva et al., 2011)

Post-collisional A-type granitoids are widespread in the western part of the Arenópolis Arc (fig.3.2). The Rio Caiapó and Serra do Iran granites show similar isotopic patterns to the pre-kinematic granitoids within the Jaupaci Belt. This is evidenced by their crystallization ages of ca. 588 Ma, slightly positive ε_{Nd} (T) values and Neoproterozoic T_{DM} model ages. On the other hand the Serra da Negra granite was dated at 538 ± 14 Ma (U-Pb zircon age),with ε_{Nd}(t) value of -4.0 and 1.5 Ga T_{DM} model ages. These isotopic features are similar to those of post-kinematic granitoids. The post-collisional volcanics in other sequences of the Arenópolis Arc may be represented by metarhyolites of the Iporá Sequence with U-Pb ages of 636 ± 3 Ma (Rodrigues et al., 1996). However, this sample also show a younger concordant zircon at ~597 Ma that is considered in this work more adequate to represent the crystallization age of this felsic volcanic rock. Based on this it is suggested that the metavolcanic rocks of the Iporá Sequence may represent a lateral equivalent of the upper metavolcanics of the Jaupaci Sequence, whereas the metapelites and conglomerates reported in the Iporá Sequence may represent sediments formed in this post-collisional basin.

As demonstrated above the post-collisional granitoids and coeval bimodal volcanic magmatism (~600-506 Ma) are restricted to the western segment of the Arenópolis Arc (Fig.3.2). The differences observed between these two segments may be

explained by the involvement of the western segment in crustal-scale strike-slip shear zones partitioning into two major structures: the Transbrasiliano Lineament in the west and the Moiporá-Novo Brasil Shear Zone in the east (Based on regional analytical signal amplitude image the MNBSZ may represent a NNW display of the NE dextral Transbrasiliano Strike-Slip System). Consequently, alternating periods of transtensional and transpressional stresses are expected (Fig.3.13E and 3.13F). Cordani et al., (2013a) suggested that this is probably related to the Pampean orogeny, in the southwestern margin of Gondwana, which was tectonically active during most of the Cambrian, until at least 540 Ma (Rapela et al., 1998, Ramos et al., 2015). Hence, during the transpressional strain a greenschit metamorphic assemblage was developed in the western segment of Arenopolis Magmatic Arc (Fig.3.13F).

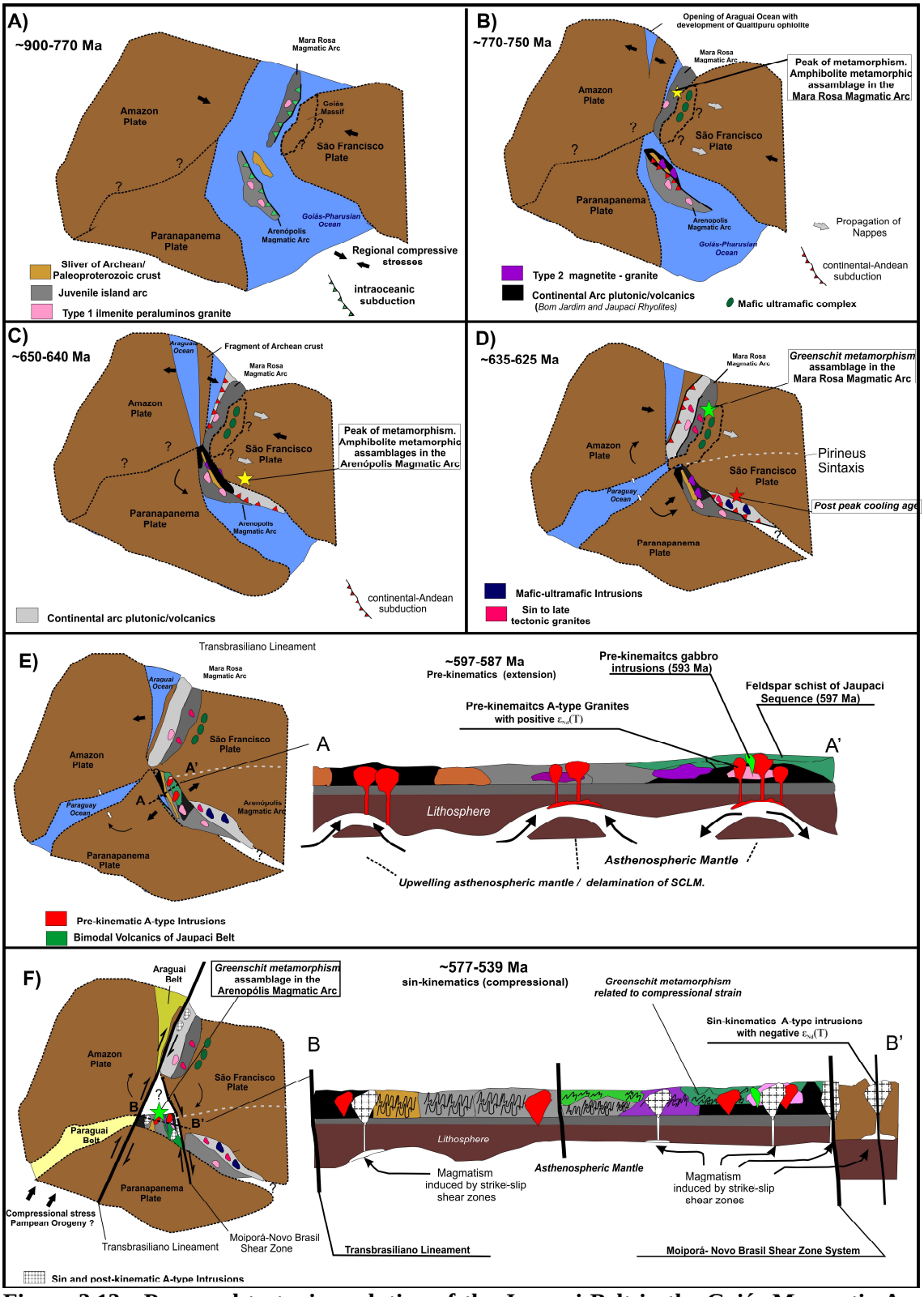

Figure 3.13 - Proposed tectonic evolution of the Jaupaci Belt in the Goiás Magmatic Arc with cratonic arrangement throughout time, based on model of Pimentel et al., (2000) and De´l Rey Silva et al., (2011): (A) the consumption of Goiás-Pharusian Ocean with development of early island arc assemblages and emplacement of peraluminous granites (ca. 900 to 770 Ma) in the GMA. Paleocontinents arrangement illustrates the Goiás Massif

as epicratonic western margin of the São Francisco plate proposed by Cordeiro (2014) and Amazonian and Paranapanema blocks initially conjoined as proposed by D'el Rey Silva et al,. 2011.The subduction with westward vergence is based on deep seismic data from Soares et al., (2005); (B) the continuous subductions of the oceanic lithosphere lead to docking of island arc into an allochthonous sliver of archean/Paleoproterozoic crust producing the continental-type magmatic arcs in the Arenópolis Arc. Whereas the Mara Rosa Arc collided against the Goiás Massif generating mafic ultramafic complex in back-arc setting at 770 Ma and metamorphic peak dated at 757-750 Ma, that resulted in the nappes propagation of passive margin sedimentary rocks towards ESE (Junges et al., 2002; Giustina et al., 2011; D'el Rey Silva et al., 2011 Giovarnadi et al., 2017). At the same time started the diachronous opening of the Araguaia Ocean represented by crystallization age of Quaitipuru ophiolite at ca. 757 Ma (Paixão et al., 2008); (C) Anticlockwise rotation of Amazon paleocontinent controlled by collision with irregular margim of São Francisco plate resulting in the utter opening of Araguaia Ocean. Coevally are recorded ca. 650 to 640 Ma peak metamorphic overgrowths age in UHT Anapolis-Itauçu granulites and (Piuzana et al., 2003; Baldwin and Brown 2008); (D) Rifting of Paraguai Ocean with Paranapanema block drifted-apart from Amazonia paleocontinent and followed to SW-NE collision against São Francisco paleomargem, this collision resulted in NE shortening and resulting in the development of high strain zone called Pireneus Sintaxis (Araujo Filho 2000, D'el Rey Silva et al., 2011).Furthermore are recorded in this stage post-peak cooling zircon ages, emplacement of syn to late-orogenic diorite/tonalite and mafic ultramafic complex at 635-627 Ma (Junges et al., 2002; Laux et al,. 2005 , Moreira et al,. 2007, Mota e Silva et al., 2011). (E) Mantle upwelling in extensional post-collisional environment that caused partial melting of a thinned and metasomatised lithosphere, resulting pre-kinematics A-type granitoids and bimodal volcanics in the western segment of Arenópolis Arc. (F) Compressional stage probably related to the Pampean orogeny resulting in: development of dextral Transbrasiliano Lineament and MNBSZ shear zones; emplacement of sin to post-kinematic A-type granitoids and greenschist metamorphic assemblages in the western segment of Arenópolis Arc. At the same time obduction of the Quitipuru ophiolite with closing of Araguaia Ocean and deformation-metamorphism of the Paraguai Belt (Paixão et al 2008 , Cordani et al 2013a).

3.8.3. Tectonic implication for the evolution of the Goiás Magmatic Arc and Gondwana

The integration of detailed geological mapping, whole rock geochemistry, U–Pb zircon ages, Sm–Nd isotopic characteristics provide new and valuable insights to understand the tectonic and magmatic evolution of the Arenópolis Arc. In this section we compare the evolution of Jaupaci Belt with other specific Neoproterozoic juvenile arcs (North segment of GMA, Borborema Province, Dom Feliciano Belt, Hoggar Shield, Anti-Atlas Belt and Arabian Nubian Shield) with those discussed here, trying to fit a worldwide picture of magmatic arcs associated with the assembly of Gondwana (Fig. 3.14). We correlate the data presented here with four tectonic events spanning ca. 400 My:

Island Arc event -. The break-up of Rodínia resulted in the development of new subduction zones in intraoceanic settings marking the initial phase of closure of the Goiás-Pharusian and Mozambique oceans. Juvenile crustal formation is constrained roughly between 900-820 Ma, which was followed by less abundant peraluminous melts at ca. 790-770 Ma. Examples throughout Godwana are observed: in the northern segment of the GMA, represented by the Mara Rosa Volcano-Sedimentary Sequence and arc granitoids with equivalent ages of 900-860 Ma (Pimentel et al., 2000; Oliveira et al., 2015, Frasca 2015); in the southern segment of West Gondwana represented by metadiorites and orthogneisses (Vila Nova Arc) crystallized at ca. 879–850 Ma in the São Gabriel Terrane (Lena et al., 2014, Saalmann et al., 2011); in the northern part of West Godwana oceanic terranes have been identified in two main events: early represented by plutonic rocks dated by Caby (2003 and references therein) at ca. 868–848 in the Hoggar Shield (Iskel Terrrane) and younger intra-oceanic event (797-714 Ma) that encompasses: gabbros in the Amalaoulaou Complex dated at ca. 797 Ma (Berger et al., 2011); volcanic and plutonic rocks dated at ca 767-720 Ma in the Anti-Atlas Belt (Hefferan et al,. 2014; Blein et al,. 2014,. Triantafyllou et al., 2015); and plutonic rock in the Timlesi arc with ages crystallization ca.730-714 in the western segment of Dahomeyan belt (Caby et al., 1989; Bosch et al., 2015).

In East Gondwana island arc granitoids are dated at 870-850 Ma in the Arabian Shield (Midyan, Hijaz and Asir Terranes) and 870± 11 Ma mafic rocks from ophiolites in the Nubian Shield (Stern and Johnson 2004, Johnson 2006, Johnson et al., 2011, Robinson et al., 2014).

Continental Arc event : The two stages of ocean basin closure between ~770–630 Ma indicated in this paper, appear to be consistent with the study of Meert (2003) who recorded ~750–650Ma igneous activity in continental arcs, suggesting a shift in global tectonics of Gondwana, when Andean type magmatism prevailed, with the consumption of the Goiás-Pharusian and Mozambique oceans. Examples are recognized in the northern segment of the GMA, as peraluminous gneiss crystallized between ca. at 790 Ma with continental arcs signature (Matteini et al., 2010). In this continental arc setting Goivanardi et al., (2017) defined that emplacement of three mafic ultramafic complexes (Fig 3.1) were developed in a back-arc setting during a subduction event at c.a. 790-770 Ma.Additionally, 750 Ma metamorphic events likely related to the accretion of the magmatic arc to a Paleoproterozoic continental block (Junges et al., 2002, Della Giustina et al., 2011). Also, 663 to 654 Ma metavolcanic rocks with continental signatures are recorded in the Santa Terezinha Sequence (Dantas et al,. 2001, Frasca 2015). In southwest Gondwana, igneous activity took place between ca.760 and 690 Ma represented by volcano-sedimentary sequences and gneisses. This is called the São Gabriel Event (Saalmann et al., 2011, Hartmann et al., 2011). In northern West Gondwana the stage of ocean-continent subduction was dated at plutonic rocks ca. 690-630 Ma in the Iforas region represented by Kindal and Tessandjanet terranes (Bruguier et al., 2008; Bosch et al., 2015) and in the Benino-Nigerian Shield at ~670-610 Ma (Kalsbeek et al., 2012; Ganade de Araujo et al., 2016). In the Anti-Atlas Belt plutonic and volcanics rocks are generated with continental arc signature in two stages: a first event at ~700 Ma and younger at ca. 660-640 Ma (El Hadi et al 2010; Blein et al., 2014,. Triantafyllou et al., 2015).

In East Gondwana the same setting is reported in the Hyjaz and Ar Ryan terranes, with the age of 710-640 Ma (Doebrich et al., 2007; Jonhson et al,. 2014).

Collisional event –. The closure of the Goiás-Pharusian ocean was followed by continent-continent collision (Himalayan-type orogen) which is recorded by the abundant metamorphic ages at ca. 630-625 Ma, throughout the GMA (Junges et al,. 2002, Moraes et al., 2007). In the Borborema Province (NE Brazil) the collisional event is constrained by the age of metamorphic zircons grains in eclogite-facies (HP/UHP) metamorphic rocks indicating the age of 616-626 Ma (Ganade de Araújo et al., 2014a), similar to those reported by Berger et al.,(2014) and Ganade de Araújo (2014) ca. 623-609 Ma, in the region of Amalaoulou and Gourma (Togo and Mali). These are the earliest evidence of large-scale deep-continental subduction and consequent uplift of

Himalayan-scale Mountains in the geological record (Affaton et al., 2000, Janh et al., 2001 Ganade de Araújo et al., 2014a). The overlap between ages of late stage continental arc rocks and of the collisional suggests that these two events are at least almost coeval with subduction shortly followed by continental collision extending throughout West Gondwana. The precise timing and spatial distribution of the change from subduction- to collision-dominated tectonics is not clear.

Post-collisional event – After crustal thickening and orogenesis a series of post-collisional granitoids, extension basins and intracontinental strike-slip shear zones were developed over the older basement other recently created Neoproterozoic crust. Examples are recognized in the and Borborema Province, where post-collisional A-type (ca.540-523 Ma) and felsic volcanic in Jaibaras Basin are related do development of Transbrasiliano Lineament (Garcia et al., 2010; Santos et al., 2013). In the southern segment of western Gondwana, in the Dom Feliciano Belt A-types post-kinematic granites are associated with the development of the Major Gercino Shear Zone at ~590 to 580 Ma (Chemale et al., 2012). In northern segment, the generation of post-collisional granitoids is recorded in central segments of Tuareg Shield with age range from ca. 599 to 523 Ma (Paquette et al., 1998; Caby 2003; Bosch et al., 2015). Likewise, in Benino-Nigerian Shield with granitoids dated at ca. 564-543 Ma (Kalsbeek et al., 2012; Ganade de Araújo et al., 2016).

In East Gondwana, Robinson et al., (2014) described several post-collisional intrusions dated between ca. 615–585 Ma in the Mydian, Afif, Asir and Ar-Ryan terranes. The role of shear zones to induce magmatism is document in the Hijaz Terrane, where ~525Ma A-type magmatism is a product of extension induced by stress transfer along the Najd Fault, which possibly marks the final stages of Gondwana assembly in central Arabia (Robinson et al., 2014).

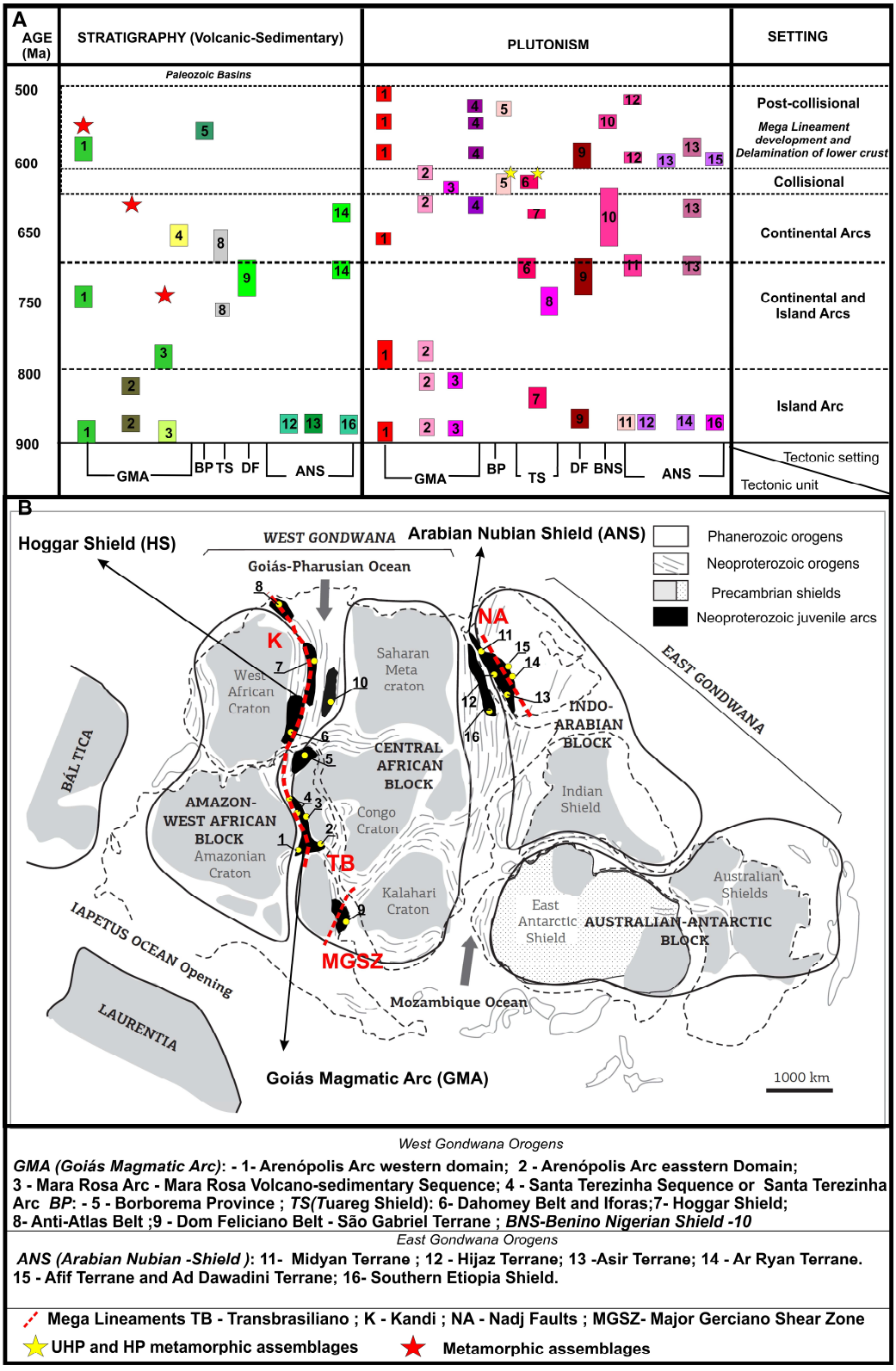

Figure 3.14 – A) Comparative chart of Neoproterozoic arcs separated by ages of deposition of volcano-sedimentary sequence and events of plutonism and tectonic setting. B) blocks of Gondwana with the location of each arc and the mega-lineaments (red line), after the closing of the Goiás-Pharusian and Mozambique oceans (adapted from Cordani et al., 2013).

3.8. Conclusions

The integration of regional data coupled U-with isotopic Sm-Nd and Whole rocks geochemistry presented in this studied allow the following conclusions:

- The main magmatic activity of Jaupaci Belt is temporally defined by two main magmatic events:i) an early Neoproterozoic that took place at 770 -750 Ma, developed in an arc setting, where granitoids/volcanics were developed with positive εNd (t) sourced from 880-820 Ma pre-existing juvenile arc-derived reservoir; ii) late Neoproterozoic-Cambrian event of magmatism evolved from 597 to 506 Ma related to a post-collisional setting. The post-collisional magmas is protracted event divided as pre, sin and post-kinematic with distinct sources, thus the former definition of Serra Negra Suite is inappropriate. To explain such protracted period of post-collisional intrusions (~90Ma) we invoke three distinct events of magma generation: the ca. 597-587 Ma pre-kinematics bimodal magmas evolved from extension setting, where the mafic asthenospheric melts are sources from high degrees of partial melting of the metasomatised asthenospheric mantle; and felsic magmas derived from hybridization of mantle-derived magma with partial melting of crustal 778–828 Ma arc material, followed by fractional crystallization. These rocks display positive εNd (t) and Neoproterozoic T_{DM} ages; the ca.577-539 Ma syn-kinematic event with concurrent development of MNBSZ and A-type granitoids. The translithospheric MNBSZ structure allowed interaction of heterogeneous SCLM with signature of Paleoproterozoic and either juvenile crust (Jaupaci Belt). Hence, the syn-kinematics A-type granites present T_{DM} model age of 1.27 – 2.25 Ga and negative ε_{Nd} (T) with values range from -1.0 to -20; a late extension event at 511-506 Ma with generation of A-type granites involved a new hybridization of mantle-derived magma . The Nd isotopes present T_{DM} model age of 0.9 – 1.2 Ga and negative to slightly positive ε_{Nd} (T), point to a predominance of juvenile component source compared with source of syn-kinematic granites.

- The Arenópolis Arc may be sub-divided into two domains showing distinct geological evolution, separated by the Moíporá-Novo Brasil Shear zone system, which may be generically called the Western Domain and Eastern domains; both

domains initiated their evolution with intra-oceanic arc magmatism originated due to long-lived (ca. 899 to 770 Ma) with subduction of the Goiás-Pharusian oceanic lithosphere; the continuous convergence of the São Francisco and Amazon paleocontinents allowed the docking of this juvenile arc along the allochthonous sliver of Archean/Paleoproterozoic crust (ca. 750 Ma), generating melts with continental arc affinity in the western domain. Subsequently, the convergence between the Parapanema and São Francisco continents took place with east-dipping subduction in the São Francisco margin, generating the ca. 660-627 Ma continental arc magmatism in the Eastern Domain. The last magmatic event (ca. 597 to 587 Ma) is only recorded in the Western Domain that firstly occurred in an extensional setting, most probably related to the post-collisional delamination of SCLM. Rock units of the Western Domain were later involved in the MNBSZ and Transbrasiliano deformation. These translithospheric sutures are deep enough to act as conduits for mantle material allowing interaction with base of the lithosphere and providing heat to re-melt it generating A-type granitoids (ca. 577 -539 Ma).

- Based on aeromagnetic data (ASA) MNBSZ is it likely to be a crustal-scale shear zone that branch out of the major Transbrasiliano shear system along the NNW direction (Fig. 3.1). This argument is sustained by emplacement and deformation of syn-kinematic intrusion at ~577-539 Ma defined in this work is the same age of K-Ar and emplacement of A-type intrusion along the Transbrasiliano Lineament in NE of Brazil (Santos et al., 2013). This implies that activity of Transbrasiliano Lineament was much more longer than previous reported by Ganade de Araujo et al., (2016) with first nucleation of shear zone system during collision in the WGO (ca. 610 Ma) to its movement cessation after the São Francisco craton collision (ca. 590 Ma). The reactivation of Transbrasiliano is probably related to distal compressional strain of the Pampean orogeny that took place at ca. 540 Ma.

- Despite the distinct geographic distribution of juvenile arcs in the Gondwana, they may be correlated with coeval tectonic events throughout the Neoproterozoic and early Cambrian.

Acknowledgements

The University of Brasília is gratefully acknowledged for fieldwork support and access to laboratory facilities. We thank the Yamana Gold Inc. and the Brazilian Council for Research and Technological Development (CNPQ) for providing, respectively, logistical and financial support for this study. The authors also thank the geologists Juliano Souza and Iris Godoy, for their fieldwork and mine assistance. Finally, we are indebted to anonymous reviewers for their helpful reviews of the original manuscript.

3.9. References

Affaton P., Kröner A., Seddoh K.F. 2000. Pan-African granulite formation in the Kabye Massif of northern Togo (West Africa): Pb–Pb zircon ages. International Journal of Earth Sciences, v.88: p.778-790.

Agbossoumondé, Y., Guillot, S., Ménot, R.P., 2004. Pan-African subduction-collisionevent evidenced by high-pressure granulites from the Agou Massif, southernTogo. Precambrian Res. v.135, p. 1–21

Albarède, F., Telouk, P., Blichert-Toft, J., Boyet, M., Agranier, A. Nelson, B., 2004. Precise and accurate isotopic measurements using multiple collector ICPMS. 823 Geochim. Cosmochim. Acta 68, p.2725–2744.

Araújo Filho, J.O., 2000. The Pirineus syntaxis: an example of intersection of two Brasiliano fold thrust belts in Central Brazil, and its implications for the tectonic evolution of Western Gondwana. Rev. Bras. Geosci. 30, 144–148.

Assumpção, M. M., Schimmel, C., Escalante, J.R., Barbosa, M. Rocha; 2004. Intraplate seismicity in SE Brazil: stress concentration in lithospheric thin spots. Geophysical Journal International 159 (1), 390-399

Babinski, M., Chemale Jr., F., Hartamann, L.A., Van Schmus, W.R., Silva, L.C., 1997. U-Pb and Sm-Nd geochronology of the Neoproterozoic Granitic-Gneissic Dom Feliciano belt, Southern Brazil. J. South Am. Earth Sci. v.10, p. 263–274.

Baldwin, J.A & Brown., 2008. Age and duration of ultrahigh-temperature metamorphism in the Anápolis-Itauçu Complex, Southern Brasília Belt, central Brazil – constraints from U-Pb geochronology, mineral rare earth element chemistry and trace element thermometry. Journal of Metamorphic Geology, v.26 p. 213-233.

Beard, J.S., 1995. Experimental, geological and geochemical constraints on the origins of low-K silicic magmas in oceanic arcs. Journal of Geophysical Research 100 (B8), 15593–15600.

Belousova, E.A., Griffin, W.L., Suzanna, Y.O., Fisher, N.I., 2002. Igneous zircon: trace element composition as an indicator of source rock type. Contribution Mineralogy Petrology .v.143, p.602–622.

Berger J., Caby R., Liégois J.P., Mercier J.C., Demaiffe D. 2011. Deep inside a Neoproterozoic intra-oceanic arc: growth, differentiation and exhumation of the Amalaoulaou complex (Gourma, Mali). Contributions to Mineralogy and Petrology, v.162, p.773-796.

Berger J., Ouzegane K., Bendaoud Abderrahmane , Liégeois J.P , Kiénast J.R., Bruguier O., Caby R 2014. Continental subduction recorded by Neoproterozoic eclogite and garnet amphibolites from Western Hoggar (Tassendjanet terrane, Tuareg Shield, Algeria). Precambrian Research. v. 247, p. 139–158.

Berrocal J., Marangoni Y., Côgo de Sá N., Fuck R.A., Soares J.E.P, Dantas E., Perosi F., Fernandes C. 2004. Deep seismic refraction and gravity crustal model and tectonic deformation in Tocantins Province, Central Brazil. Tectonophysics, v.388:p:187-199

Blein, O., Baudin, T., Chevremont, P., Soulaimani, A., Admou, H., Gasquet, P.,Cocherie, A., Egal, E., Youbi, N., Razin, P., Bouabdelli, M., Gombert, P., 2014.Geochronological constraints on the polycyclic magmatism in the Bou Azzer-ElGraara inlier (Central Anti-Atlas Morocco). J. Afr. Earth Sci. v.99, p. 287–306

Bosch D., Bruguier O., Caby R., Buscail F., Hammor D., 2015. Orogenic development of the Adrar des Iforas (Tuareg Shield, NE Mali): New geochemical and geochronological data and geodynamic implications. Journal of Geodynamics v. 96 p.104–130.

Bonin, B., 2007. A-type granites and related rocks: evolution of a concept, problems and prospects. Lithos v.97, p.1–29..

Brito Neves B.B., Fuck, R.A., Pimentel, M.M 2014. The Brasiliano collage in South America: a review. Brazilian Journal of Geology, v. 44(3), p. 493-518.

Bruguier O., Bosch D., Caby R., Galland B., Hammor D. 2008. Sampling an active continental paleo-margin: a LA-ICP-MS U-Pb zircon study from the Adrar des Iforas (Mali). Geochimica et Cosmochimica Acta, v.72(12):A118.

Buhn, B., Pimentel, M.M., Matteini, M., Dantas, E.L., 2009. High spatial resolution analysis of Pb and U isotopes for geochronology by laser ablation multi-collector inductively coupled plasma mass spectrometry (LA-MC-ICP-MS). Anais da Academia Brasileira de Ciências v.81, p.1–16.

Caby, R., 1989. Precambrian terranes of Benin Nigeria and Northeast Brazil and LateProterozoic South Atlantic fit. Geol. Soc. Am. Spec. Pap. v.230, p.145–158.

Caby, R., 2003. Terrane assembly and geodynamic evolution of central western Hoggar: a synthesis. Journal Afrincan Earth Science,v. 37, p.133–159.

Castillo, P.R., Janney, P.E., Solidum, R.U., 1999. Petrology and geochemistry of Camiguin Island, southern Philippines: insights to the source of adakites and other lavas in a complex arc setting. Contributions to Mineralogy and Petrology v.34, p. 33–51.

Chemale F., Mallman G., Bitencourt M.F, Kawashita K., 2012. Time constraints on magmatism along the Major Gercino Shear Zone, southern Brazil: Implications for West Gondwana reconstruction. Gondwana Research , v. 22 p. 184-199.

Cordani, U,G. Pimentel, M,M. Araújo C,E,G. Basei, M,A,S Fuck R.A and Girardi, V,A,V, 2013a. Was there an Ediacaran Clymene Ocean in Central of South America ? American Journal of Science, v.313, p.517-539.

Cordani, U,G. Pimentel, M,M. Araújo C,E,G. Basei, M,A,S Fuck R.A 2013b. The significance of the Transbrasiliano-Kandi tectonic corridor for the amalgamation of West Gondwana. Brazilian Journal of Geology, v. 43, p. 583-597.

Cordeiro, P.O. F., 2014. Compartimentação geológica e geocronológica do embasamento norte da Faixa Brasília. PhD Thesis unpublished, 157 p. Universidade de Brasília.

Cox, G.M., Lewis, C.J., Collins, A.S., Halverson, G.P., Jourdan, F., Foden, J., Nettle, D., Kattan, F., 2012. Ediacaran terrane accretion within the Arabian–Nubian Shield. Gondwana Research. v.21, p. 341–352.

Creaser, R.A., Price, R.C., Wormald, R.J., 1991. A-type granites revisited: assessment of a residual-source model. Geology 19 (2), 163–166.

Curto J.B., Vidotti R.M., Fuck R.A., Blakely R.J., Alvarenga C.J.S., Dantas E.L.2014. The tectonic evolution of the Transbrasiliano Lineament in northern Paraná Basin, Brazil, as inferred from aeromagnetic data. Journal of Geophysical Research. v. 119 (3), p. 1544-1562**.**

Curto, J.B., Vodotti, R.M., Blakely, R.J., Fuck, R.A., 2015. Crustal framework of the northwest Paraná Basin, Brazil: Insights from joint modeling of magnetic and gravity data. *Tectonophysics*. v.655, p. 58-72.

Dantas, E.L., Jost, H., Fuck, R.A., Brod, J.A., Pimentel, M.M., Menezes, P.R., 2001. Proveniência e idade deposicional de sequências metavulcano-sedimentares da Região de Santa Terezinha de Goiás baseada em dados isotópicos Sm–Nd e U–Pb em monocristal de zircão. Revista Brasileira de Geociências v.31 (3),p. 329–334.

Dardene, M.A. 2000. The Brasília Fold Belt. In: Cordani, U.G., Milani, E.J., Thomaz Filho, Campos, D.A. (eds), Tectonic Evolution of South America p.231-263.

Defant, M.J., and Drummond, M.S., 1993, Mount St. Helens: Potential example of the partial melting of the subducted lithosphere in a volcanic arc: Geology, v. 21, p. 547–550.

Defant, M.J., Kepezhinskas, P., Defant, M.J., Xu, J.F., Kepezhinskas, P., Wang, Q., Zhang, Q., Xiao, L., 2002. Adakites: some variations on a theme. Acta Petrologica Sinica v.18, p.129–142.

Della Giustina, M.E.S., Oliveira, C.G., Pimentel, M.M., Melo, L.V., Fuck, R.A., Dantas, E.L., Buhn, B., 2009. U–Pb and Sm–Nd constraints on the nature of the Campinorte Sequence and related Paleoproterozoic juvenile orthogneisses, Tocantins Province, Central Brazil. Geological Society of London Special Publication, v.323, p.255-269.

Della Giustina, M.E.S., 2010. Geocronologia e significado tectônico de rochas máficas de alto grau metamórfico da Faixa Brasília. Unpublished PhD thesis, 101, University of Brasília, p. 121.

Della Giustina, M.E.S., Pimentel, M.M., Ferreira Filho, C. F.,., Fuck, R.A., Andrade S., 2011.U–Pb–Hf-trace element systematics and geochronology of zircon from a granulite-facies metamorphosed mafic–ultramafic layered complex in Central Brazil.. Precambrian Research, v. 247 p.126–138.

D'el-Rey Silva, L.J.H., Oliveira I.L., Pohren, C.B., Tanikazi M.L.N., Carneiro R.C., Fernandes G. L. F., Aragão P. E. 2011. Coeval perpendicular shortenings in the Brasília belt: Collision of irregular plate margins leading to oroclinal bending in the Neoproterozoic of central Brazil. Journal of South American Earth Sciences v.32 p.1-13.

DePaolo D.J., 1981. A neodymium and strontium isotopic study of the Mesozoic calc-856 alkaline granitic batholiths of the Sierra Nevada and Peninsular Ranges. California 857 Journal Geophysical Research v.86, p.10470–10488.

Doebrich J. L. , Al-Jehani A. M. , Alim A. Siddiqui A.A., Hayes T. S., Wooden J. L , Johnson P. R. 2007. Geology and metallogeny of the Ar Rayn terrane, eastern Arabian shield: Evolution of a Neoproterozoic continental-margin arc during assembly of Gondwana within the East African orogeny. Precambrian Research v.158 p. 17–50.

Dostal J., Dupuy C., Caby R. 1994. Geochemistry of the neoproterozoic Tilemsi belt of Iforas (Mali, Sahara) - a crustal section of an oceanic island-arc. Precambrian Research, v.65(1-4), p.55-69.

Drummond, M.S., Defant, M.J., and Kepezhinskas, P.K., 1996, Petrogenesis of slab-derived trondhjemite-tonalite-dacite/adakite magmas: Geological Society of America, Special Paper v.315, p. 205–215.

Eby, G.N., 1992. Chemical subdivision of the A-type granitoids: petrogenetic and tectonic implications. Geology, v.20, p. 641–644.

El Hadi, H., Simancas, J.F., Martínez-Poyatos, D., Azor, A., Tahiri, A., Montero, P.,Fanning, C.M., Bea, F., González-Lodeiro, F., 2010. Structural andgeochronological constraints on the evolution of the Bou Azzer Neoproterozoicophiolite (Anti-Atlas, Morocco). Precambrian Res. v.182 (1), p.1–14.

Feng, M., Van Der Lee, S. & Assumpcao, M., 2007. Upper mantle structure of South America from joint inversion of wave-forms and fundamental mode group velocities of Rayleigh waves, J. geophys. Res. ,112 (B04312), 16 pp

Fritz, H., Abdelsalam, M., Ali, K.A., Bingen, B., Collins, A., Fowler, A.R., Ghebreab, W., Hauzenberger, C.A., Johnson, P., Kusky, T., Macey, P., Muhongo, S., Stern, R.J., Viola, G., 2013. Orogen styles of the East African Orogens: A review of the Neoproterozoic to Cambrian tectonic evolution. Journal Africa. Earth Science v.86,p. 65–106.

Fuck, R.A., Pimentel, M.M. and Silva, L.J.H.D. 1994. Compartimentação tectônica da porção oriental da Província Tocantins. Actas, 38 Congresso Brasileiro de Geologia, Balneário Camboriú-SC, 1, pp. 215-216.

Fuck, R. A. ; Dantas, E.L.; Vidotti, R.M. ; Roig, H. L. ; Almeida, T. 2013. Deformação intracontinental em sistemas transcorrentes: o caso do Lineamento Transbrasiliano, geometria, idade e significado, In: 140° Simpósio Nacional de Estudos Tectônicos. Chapada dos Guimarães. Sociedade Brasileira de Geologia. p. 1-3.

Fuck, R.A., Dantas, E.L., Pimentel, M.M., Botelho, N.F., Armstrong, R., Laux, J.H., Junges, S.L., Soares, J.E., Praxedes, I.F., 2014. Paleoproterozoic crust-formation and reworking events in the Tocantins Province, central Brazil: A contribution for Atlantica supercontinent reconstruction. Precambrian Research v.244 ,p.53-74.

Frasca, A.A.S., 2015. Amálgamas do W-Gondwana na província do Tocantins. Unpublished Phd thesis, Universidade de Brasília, 105 pp.

Frost, C.D., Frost, B.R., 2011. On ferroan (A-type) granitoids: their compositional variability and modes of origin. J. Petrol. v. 52, p.39–53.

Ganade de Araújo C.E.., Rubatto D., Hermann J., Cordani U.G., Caby R., Basey M.S. 2014a. Ediacaran 2,500-km-long synchronous deep continental subduction in the West Gondwana Orogen. Letter for nature p.8.

Ganade de Araújo, C.E., Weinberg, R.F., Cordani, U.G., 2014b. Extruding the Borborema Province (NE Brazil): a two-stage Neoproterozoic collision process. Terra Nova v.26, p.157–168.

Ganade de Araújo C.E., Cordani U.G., Agbossoumoundé Y., Caby R., Basey M.S. Weinberg R.F, Sato K., 2016. Tightening-up NE Brazil and NW Africa connections: NewU–Pb/Lu–Hf zircon data of a complete plate tectonic cycle in the Dahomey belt of the West Gondwana Orogen in Togo and Benin. Precambrian Research v. 276 p.24–42.

Garcia, M.G.M., Parente, C.V., Silva Filho, W.F., Almeida, A.R., 2010. Idade do vul-canismo ácido da Formacão Parapuí: implicacões na estratigrafia da Bacia Eopaleozóica Jaibaras-CE. In: XLV Congresso Brasileiro de Geologia, Belém-PA.

Gioia, S.M.G.1997. Preparação da metodologia Sm/Nd para datação de amostras geológicas e sua aplicação em rochas das áreas de Firminóplis, Fazenda Nova e Americano do Brasil. Unpublished Msc thesis, Universidade de Brasília, 121 p.

Gioia S.M.C.L., Pimentel M.M., 2000. The Sm-Nd isotopic method in the 876 geochronology laboratory of the University of Brasília. Anais da Academia 877 Brasileira de Ciências, v. 72(2) ,p. 219-245.

Giovanardi T., Girardi V. A.V., Correia C.T., Tassinari C.olombo C.G., Sato K., Cipriani A., Mazzucchelli M. New U-Pb SHRIMP-II zircon intrusion ages of the Cana Brava and Barro Alto layered complexes, central Brazil: constraints on the genesis andevolution of the Tonian Goias Stratiform Complex. Lithos, v.282-283, p.339-357.

Gorayeb, P.S.S., Chaves, C.L., Moura, C.A.V., da Silva, L.L.R., 2013. Neoproterozoic granites of the Lajeado intrusive suite, north-center Brazil: a late Ediacaran remelting of a Paleoproterozoic crust. Journal of South American Earth Sciences, v.45, p. 278–292.

Guimarães, S,B. Moura, M, A. Dantas, E . L., 2012. Petrology and geochronology of Bom Jardim copper deposit. Brazilian Journal of Geology, v.42, n.4, 2012, p.841-862.

Guo, F., Fan, W.M., Li, C.W., 2006. Geochemistry of late Mesozoic adakites from the Sulu belt, eastern China: magma genesis and implications for crustal recycling beneath continental collisional orogens. Geological Magazine v.143,p.1–13.

Jahn, B., Caby, R. and Monie, P., 2001. The oldest UHP eclogites of the World: age of UHP metamorphism, nature of protoliths and tectonic implications. Chemical Geology, v. 178, p. 143–158.

Hasui, Y.; Carneiro, C. D. R.; Almeida, F. F. M.; Bartorelli, A., 2012. Geologia do Brasil, Ed. Beca. pag 118.

Hartmann, L.A., Philipp, R.P., Santos, J.O.S., McNaughton, N.J., 2011. Time frame of the 753–680 Ma juvenile accretion during the São Gabriel orogeny, Southern Brazilian shield. Gondwana Res. v.19, p.84–99.

Hefferan, K., Soulaimani, A., Samson, S.D., Admou, H., Inglis, J., Saquaque, A., Chaib,L., Heywood, N., 2014. A reconsideration of Pan African orogenic cycle in theAnti-Atlas Mountains, Morocco. J. Afr. Earth Sci. v.98, p. 34–46.

Henry, B., Derder, M.E.M., Bayou, B., Guemache, M.A., Nouar, O., Ouabadi, A., Djellit, H., Amenna, M., Hemmi, A., 2008. Inhomogeneous shearing related with rocks composition: evidence from a major late-Panafrican shear zone in the Tuareg shield (Algeria). Swiss Journal Geology, v. 101,p 453–464.

Irvine, T.N., Baragar, W.R.A., 1971. A guide to the chemical classification of then common volcanic rocks. Canada Journal of Earth Science 8, 523–548.

Jackson S.E., Pearson N.J., Griffin W.L., Belousova, E.A., 2004. The application of laser ablation-inductively coupled plasma-mass spectrometry. Chemical Geology, v.211,p 47–69.

Johnson, K., Barnes, C.G., Miller, C.A., 1997. Petrology, geochemistry, and genesis of high-Al tonalite and trondhjemites of the Cornucopia stock, Blue Mountains, Northeastern Oregon. Journal of Petrology v.38, p.1585–1611.

Johnson, P.R., 2006. Explanatory notes to the map of Proterozoic geology of western Saudi Arabia. Technical Report, Saudi Geological Survey, SGS-TR-2006-4/1427H 2006 G.

Johnson, P.R., Andersen, A., Collins, A.S., Fowler, A.R., Fritz, H., Ghebreab, W., Kusky, T., Stern, R.J., 2011. Late Cryogenian–Ediacaran history of the Arabian–Nubian Shield: A review of depositional, plutonic, structural, and tectonic events in the closing stages of the northern East African Orogen. Journal of Africa Earth Science, v.10,p. 1–179.

Jost, H., Chemale, F., Dussin, I.A., Tassinari, C.C.G., Martins, R., 2010. A U-Pb zircon Paleoproterozoic age for the metasedimentary host rocks and gold mineralization of the Crixás greenstone belt, Goiás, central Brazil. Ore Geology Reviews, v. 37, p.127-139.

Junges, S.L.; Pimentel, M.M.; Moraes, R., 2002 Nd isotopic study of the Neoproterozoic Mara Rosa Arc, central Brazil: implications for the evolution of the Brasília Belt. Precambrian Research, v.117, n.1-2, p.101-108.

Laux, J.H., Pimentel, M.M., Dantas, E.L. Armstrong, R., Armele, A., Nilson, A.A., 2004 . Mafic magmatism associated with the Goiás Magmatic Arc in the Anicuns region, Goiás, central Brazil: Sm-Nd isotopes and ID-TIMS and SHRIMP U-Pb data. Journal of South American Earth Sciences, v.16(7), p.599-614.

Laux, J.H., Pimentel, M.M., Dantas, E.L. Armstrong, R., Junges, S.L., 2005. Two Neoproterozoic crustal events in the Brasília Belt, central Brazil. Journal of South American Earth Sciences, v.18 p.183-198.

Lena L.O.F., Pimentel M. M., Philipp R.P., Amrstrong R., Sato K., 2014. Evolution of the Neoproterozoic São Gabriel juvenile Terrane, southern Brazil based on high spatial resolution U-Pb ages from detrital zircons Precambrian Research, v. 247 p.126–138

Liégeois, J.P., Benhallou, A., Azzouni-Sekkal, A., Yahiaoui, R., Bonin, B., 2005. The Hoggar swell and volcanism: reactivation of the Precambrian Tuareg shield during Alpine convergence and West African Cenozoic volcanism. In: Foulger, G.R., Natland, J.H., Presnall, D.C., Anderson, D.L. (Eds.), Plates, Plumes and Paradigms. Geological Society of America Special Paper, v. 388, p. 379–400.

Litvinovsky, B.A., Jahn, B.M., Zanvilevich, A.N., Saunders, A., Poulain, S., Kuzmin, .V., Reichow, M.K., Titov, A.V., 2002. Petrogenesis of syenite–granite suites from the Bryansky Complex

(Transbaikalia, Russia): implications for the origin of A-type granitoid magmas. Chemical Geology v.189 (1–2), p.105–133.

Liu, S., Hu, R.Z., Feng, C.X., Zou, H.B., Li, C., Chi, X.G., Peng, J.T., Zhong, H., Qi, L., Qi,Y.Q., Wang, T., 2008. Cenozoic high Sr/Y volcanic rocks in the Qiangtangterrane, northern Tibet: geochemical and isotopic evidence for the origin of delaminated lower continental melts. Geological Magazine v.145 (4), p.463–474.

Liu, S., Hu, R.Z., Gao S., Feng, C., Yu B., Qi., Wang T., Feng G., Coulson I.M., 2009. Zircon U–Pb age, geochemistry and Sr–Nd–Pb isotopic compositions of adakitic volcanic rocks from Jiaodong, Shandong Province, Eastern China: Constraints on petrogenesis and implications. Journal of Asian Earth Sciences, v. 35 p.445-458.

Ludwig, K.R., 2003. Isoplot 3.00: A geochronological toolkit for Microsoft Excel. Berkeley Geochronological Center, Special Publication 4, 70 pp

Macpherson, C.G., Dreher, S.T., Thirlwall, M.F., 2006. Adakites without slab melting: high pressure differentiation of island arc magma, Mindanao, the Philippines. Earth and Planetary Science Letters v.243, p.581–593.

Kalsbeek, F., Affaton, P., Ekwueme, B., Freid, R., Thranea, K., 2012. Geochronology of granitoid and metasedimentary rocks from Togo and Benin, West Africa: comparisons with NE Brazil. Precambrian Res. v.196–197, p. 218–233.

Kay, R.W., Kay, S.M., 2002. Andean adakites: three ways to make them. Acta Petrology Sinica v.18, p.303–311.

Keleman P. B, Shimizu N., Dunn T. 1993. Relative depletion of niobium in some arc magmas and the continental crust: partitioning of K, Nb, La and Ce during melt/rock reaction in the upper mantle. Earth Planet Sci Lett v.120, p. 111–134.

Kerr, A., Fryer, B.J., 1993. Nd isotope evidence for crust-mantle interaction in the generation of A-type granitoid suites in Labrador, Canada. Chemical Geology v.104 (1–4), p.39–60.

Kroner, A.Cordani, U,G.,2003. African, southern Indian and South American Craton were not part of Rodinia continent: evidence from field relationship and geochronology: Tectonophysics, v.375, n.1-4, p.325-352.

Maurice A.E., Bakhit B.R., Basta F.F., Khiami A.A. 2013 Geochemistry of gabbros and granitoids (M- and I-types) from the Nubian Shield of Egypt: Roots of Neoproterozoic intra-oceanic island arc. Precambrian Research v. 224, p.397– 411

Matteini M., Junges S.L., Dantas E.L., Pimentel M.M., Buhn B. 2010. In Situ Zircon U-Pb and Lu-Hf isotope systematic on magmatic rocks: insight on the crustal evolution Neoproterizoic Goiás Magmatic Arc, Brasília belt, Central Brazil. Gondwana Research, v.17: p.1-12.

Martin, H., Smithies, R.H., Rapp, R., Moyen, J.F., Champion, D., 2005. An overview of adakite, tonalite–trondhjemite–granodiorite (TTG), and sanukitoid: relationships and some implications for crustal evolution. Lithos v.79, p.1–24

Meert, J.G., 2003. A synopsis of events related to the assembly of eastern Gondwana. Tectonophysics ,v.362, p.1–40.

Meschede, M., 1986. A method of discriminating between different types of mid-ocean ridge basalts and continental tholeiites with the Nb–Zr–Y diagram. Chemical Geology v.56, p. 207–218.

Mingram, B., Trumbull, R.B., Littman, S., Gerstenberger, H., 2000. A petrogenetic study of anorogenic felsic magmatism in the Cretaceous Paresis ring complex, Namibia: evidence for mixing of crust and mantle-derived components. Lithos v.54 (1–2), p.1–22.

Moraes, R., Fuck R.A., Brown, M. Piccoli, P., Balwin, J., Dantas E.L., Laux, J.H, Junges, S.2007. Wollastonite-scapolite-clinopyroxene marble of the Anápolis-Itauçu Complex, Goiás: more evidence of ultrahigh- temperature metamorphism. Revista Brasiliera de Geociências, v.37(4), p. 11-17.

Mota e Silva, J., Ferreira Filho C. F., Bunh B., Dantas E.L., 2011. Geology, petrology and geochemistry of the "Americano do Brasil" layered intrusion, central Brazil, and its Ni–Cu sulfide deposits. Mineralium Deposita, v. 46 p. 57-90.

Motta-Araújo, J.G., 2013. Eventos Ígneos e metamórficos Neoproterozoicos/Eopaleozoicos no arco magmático de Arenópolis, Goiás. Unpublished Phd thesis, Universidade de Brasília, 73 pp.

Moyen, J.-F., Stevens, G., 2006. Experimental constraints on TTG petrogenesis: implications for Archean geodynamics. In: Benn, K., Mareschal, J.-C., Condie, K.C. (Eds.), Archean Geodynamics and Environments. AGU, pp. 149–178.

Mushkin, A., Navon, O., Halicz, L., Hartmann, G., Stein, M., 2003. The petrogenesis of Atype magmas from the Amram Massif, Southern Israel. Journal of Petrology v.44 (5), p.815–832.

Miyashiro, A., 1974. Volcanic rock series in island arcs and active continental margins.American Journal of Science 274, 321–355.

Nagel, T.J., Hoffmann, J.E., Münker, C., 2012. Generation of Eoarchean tonalite–trondhjemite–granodiorite series from thickened mafic arc crust. Geology 40 (4), 375–378.

Oliveira C.G., Bedran de Oliveira F., Della Giustina M.E.S,, Marques G.C., Dantas E.L., Pimentel M.M., Bunh B. M. 2015. The Chapada Cu-Au deposit, Mara Rosa Magmatic Arc, Central Brazil: Constraints on the Metalogenesis of a Neoproterozoic large porphyry-type deposit. 2015, Ore Geology Reviews, v. 72, p. 1-21.

Paixão, M.A.P., Nilson, A.A., Dantas, E.L., 2008. The Neoproterozoic Quatipuru Ophiolite and the Araguaia fold belt, central-northern Brazil, compared with correlatives in NW Africa. Geological Society London Special Publications, v. 294, p.297-318.

Paquette, J.L., Caby, R., Djouadi, M.T., Bouchez, J.L., 1998. U–Pb dating of thePan-African orogeny in the Tuareg shield: the post-collisional syn-shearTioueine pluton (western Hoggar Algeria). Lithos v.45, p. 245–253.

Pearce, J.A., Cann, J.R., 1973. Tectonic setting of basic volcanic rocks determined using trace element analyses. Earth Planet Science. Letter. v.19,p.290–300.

Pearce, J.A., 1983. Role of the subcontinental lithosphere in magma genesis at active continental margins. In: Hawkesworth, C.I., Norry, M.J. (Eds.), Continental Basalts and Mantle Xenoliths. Shiva, Nantwich, pp. 230–249.

Pearce, J.A., Harris, N.B.W., and Tindle, A.G., 1984. Trace element discrimination diagrams for the tectonic interpretation of granitic rocks. Journal of Petrology v.25, p.956-983.

Pearce, J.A., Bender, J.F., De Long, S.E., Kidd, W.S.F., Low, P.J., Güner, Y., Saroglu, F., Yilmaz, Y., Moorbath, S., Mitchell, J.G., 1990. Genesis of collision volcanism in Eastern Anatolia, Turkey. J. Volcanol. Geotherm. Res. 44, 189–229.

Pearce, J.A., Peate, D.W., 1995. Tectonic implications of the composition of volcanic arc magmas. Annual. Reviews of Earth Science. v.23, p. 251–285.

Pearce, J.A., 1996. Sources and settings of granitic rocks. Episodes v.19, p.120–125.

Pirajno, F., 2007. Mantle plumes, associated intraplate tectono-magmatic processes and ore systems. Episodes v.30, p. 6-19.

Pirajno, F., 2010. Intracontinental strike-slip faults, associated magmatism, mineral systems and mantle dynamics: examples from NW China and Altay-Sayan (Siberia). Journal of Geodynamics v.50, p.325-346.

Pena, G.S. and Figueiredo, M.J. 1972. Projeto Alcalinas. Goiânia, DNPM-CPRM. (Relatório Inédito), 143 p.

Petford, N., Atherton, M., 1996. Na-rich partial melts from newly underplated basaltic crust: the Cordillera Blanca Batholith, Peru. Journal of Petrology 37, 1491–1521.

Pitcher, W.S., 1983. Granite type and tectonic environment. In: Hsu, K. _Ed.., Mountain 1331 Building Processes, Vol. 19–40, Academic Press, London.

Pimentel, M.M. and Fuck, R.A. 1987. Origem e evolução das rochas metavulcânicas e metaplutônicas da região de Arenópolis (GO). Revista Brasileira de Geociências v.17(1), p. 2-14.

Pimentel M.M., Heaman L., Fuck R.A. 1991. U-Pb zircon and sphenc geochronology of late Proterozoic volcanic arc rock units from southwestern Goiás, Central Brazil. Journal of South American Earth Sciences, v.4, p.329-339.

Pimentel, M.M. and Fuck, R.A. 1992. Neoproterozoic crustal accretion in central Brazil. Geology, v.20, p.375-379.

Pimentel, M.M. and Fuck, R.A. 1994. Geocronologia Rb-Sr da porção sudeste do maciço de Goiás. Revista Brasileira de Geociências, v.24(2), p. 104-111.

Pimentel,M.M., Fuck,R.A. and Alvarenga,C.J.S. 1996. Post-Brasiliano (Pan-African) high-K granitic magmatism in central Brazil: late Precambrian/early Paleozoic extension. Precambrian Research, 80:p.217-238

Pimentel, M.M., Fuck, R.A., Silva, L.J.H.D., 1996 b. Dados Rb–Sr e Sm–Nd da região de Jussara-Goiás-Mossâmedes (GO), e o limite entre terrenos antigos do Maciço de Goiás e o Arco Magmático de Goiás. Revista Brasileira de Geociências v.26 (2), p.61–70.

Pimentel, M.M., Whitehouse, M.J., Viana, M.G., Fuck, R.A. and Machado, N. 1997. The Mara Rosa Arc in the Tocantins Province: further evidence for Neoproterozoic crustal accretion in central Brazil. Precambrian Research, v.81, p.299-310.

Pimentel, M.M., Fuck, R.A., Botelho, N.F.1999a. Granites and the geodynamic history of the Neoproterozoic Brasília Belt, Central Brazil: review.Lithos, v.46(3), p. 463-483.

Pimentel, M.M., Fuck, R.A., Ferreira Filho, C.F., Araújo, S.M., 2000. The basement of the Brasília Belt and the Goiás Magmatic Arc. In: Cordani, U.G., Milani, E.J., Thomaz Filho, A., Campos, D.A. (eds)

Tectonic Evolution of South America. 31st International Geological Congress, Rio de Janeiro, 195–229.

Pimentel, M.M; Hollanda, M H ; Armstrong, R ., 2003. U-Pb SHRIMP age and Sm-Nd isotopic characteristics of the Morro do Baú gabbro: implications for the evolution of the Arenópolis volcano-sedimentary sequence, Goiás Magmatic Arc., Anais da Academia Brasileira de Ciências, Rio de Janeiro, v. 75, n.3, p. 331-339,

Pimentel, M.M., Ferreira Filho, C.F., Armstrong, R.A., 2004. SHRIMP U-Pb and Sm-Nd ages of the Niquelândia layered complex: Meso- (1.25 Ga) and Neoproterozoic (0.79 Ga) extensional events in central Brazil. Precambrian Research v.132, p.133-153.

Pitcher, W.S., 1983. Granite type and tectonic environment. In: Hsu, K. _Ed.., Mountain Building Processes, Vol. 19–40, Academic Press, London

Piuzana D., Pimentel MM, Fuck R.A., Armstrong R.A., 2003. Neoproterozoic granulite facies metamorphism and contemporaneous granite magmatism in the Brasília Belt, Central Brazil: regional implications of new SHRIMP U–Pb and Sm–Nd data. Precambrian Research v.125, p. 245–273

Ramos V., Escayola M., Leal P., Pimentel M.M., Santos J.O.S., The late stages of the Pampean Orogeny, Córdoba (Argentina): Evidence of post-collisional Early Cambrian slab break-off magmatism. Journal of South America v. 64, p. 351-364.

Rapela C.W., Pankhurst R.J., Casquet C., Baldo E., Saavedra J., Galindo C., Fanning C.M. 1998. The Pampean Orogeny of the southern proto-Andes: Cambrian continental collision in the Sierras de Cordoba. In: Pankhurst R.J., Rapela C.W., (eds.). The proto-Andean Margin of Gondwana. Geological Society of London Special Publication, v.142, p. 181-217.

Rapp, R.P., Watson, E.B., 1995. Dehydratation melting of metabasalt at 8–32 kbar: implications for continental growth and crust–mantle recycling. Journal of Petrology v.36, p.891–931.

Rapp, R.P., Shimizu, N., Norman, M.D., Applegate, G.S., 1999. Reaction between slabderived melts and peridotite in the mantle wedge: experimental constraints at 38 GPa. Chemical Geology v.160, p.335–356.

Rapp, R.P., Xiao, L., Shimizu, N., 2002. Experimental constraints on the origin of potassium-rich adakite in east China. Acta Petrologica Sinica v.18, p.293–311

Robinson F.A., Foden J.D., Collins A.S., Payne J.L., 2014 , Arabian Shield magmatic cycles and their relationship with Gondwana assembly: Insights from zircon U–Pb and Hf isotopes. Earth and Planetary Science Letters v.408 p.207–225.

Rodrigues, J.B., Gioia, S.M.L.C., Pimentel, M.M. 1999. Geocronologia e geoquímica de ortognaisses da região entre Iporá e Firminópolis: Implicações para a evolução do Arco Magmático de Goiás. Revista Brasileira de Geociências, v.29(2), p. 207-216.

Saalmann, K., Remus, M.V.D., Hartmann, L.A., 2005. Geochemistry and crustal evolution of volcano-sedimentary successions and orthogneisses in the São Gabriel belt, southernmost Brazil – relics of Neoproterozoic magmatic arcs. Gondwana Research. v.8, p.143–162.

Saalmann, K., Gerdes, A., Lahaye, Y., Hartmann, L.A., Remus, M.V.D., Läufer, A., 2011.Multiple accretions at the eastern margin of the Rio de la Plata craton: the prolonged Brasiliano orogeny in southernmost Brazil. International Journal of Earth Sciences v.100, p.355–378.

Santos, R.V., Oliveira C. G., Parente C.V., Garcia, M.M., Dantas E. 2013. L., Hydrothermal alteration related to a deep mantle source controlled by a Cambrian intracontinental strike-slip fault: Evidence for the Meruoca felsic intrusion associated with the Transbrasiliano Lineament, Northeastern Brazil. Journal of South American Earth Sciences v.43, p.33-41.

Shand, S.J., 1943. Eruptive rocks, their genesis, composition, classification, and their relation to ore-deposits with a chapter on meteorite. John Wiley and Sons, New York.

Schandl, E.S., Gorton, M.P., 2002. Application of high field strength elements to discriminate tectonic settings in VMS environments. Economic Geology v.97, p. 629.

Schaltegger, U., Brack, P., 2007. Crustal-scale magmatic systems during intracontinental strike-slip tectonics: U, Pb and Hf isotopic constraints from Permian magmatic rocks of the Southern Alps. International Journal of Earth Sciences (Geol Rundschau)v. 96, p. 1131-1151.

Soares, j. E. P.; Berrocal, J.; Fuck, R. A.; Mooney, W.D.; Ventura, D.B.R. 2006. Seismic characteristics of central brazil crust and upper mantle: a deep seismic refraction study. Journal of geophysical research, USA, v. 111, p. 1029-1060.

Stern, R.A., Hanson, G.N., 1991. Archean high-Mg granodiorite: a derivative of light rare earth element enriched monzodiorite of mantle origin. Journal of Petrology v.32, p.201–238.

Stern, R.J., Johnson, P.R., Kröner, A., Yibas, B., 2004. Neoproterozoic ophiolites of the Arabian–Nubian Shield. In: Kusky, T.M. (Ed.), Precambrian Ophiolites and Related Rocks. Developments in Precambrian Geology, v. 13, p.95–128.

Stern, R.J., 2010. The anatomy and ontogeny of modern intra-oceanic arc systems.Geol. Soc. London 338 (1), 7–34, Special Publications.

Stern, R.J., Johnson, P., 2010. Continental lithosphere of the Arabian Plate: A geologic, petrologic, and geophysical synthesis. Earth-Science. Reviews v.101, p.29–67.

Stern R.J., Kamal A. Ali , Abdelsalam M. G. , Wilded S. A., Zhoue Q. 2012. U–Pb zircon geochronology of the eastern part of the Southern Ethiopian Shield. Precambrian Research v. 206-207, p.159-167.

Storti, F., Holdsworth, R.E., Salvini, F., 2003. Intraplate strike-slip deformation belts. Geological Society, London, Special Publication v.210, p. 1–14.

Sun, S.S., and McDonough, W.F., 1989, Chemical and isotopic systematics of oceanic basalts: Implications for mantle compositions and processes: Geological Society of London Special Publication v.42, p. 313−345

Sylverter P.J. 1998 Post-collisional strongly peraluminous granites. Lithos v.45 p., 29-44.

Taylor, S.R., McLennan, S.M., 1995. The geochemical evolution of the continental crust. Rev. Geophys. v.33, p.241–265.

Turner, S., Sandiford, M., Foden, J., 1992. Some geodynamic and compositional constraints on “postorogenic” magmatism. Geology v.20, p. 931–934.

Turner, S., Arnaud, N., Liu, J., Rogers, N., Hawkesworth, C., Harris, N., Kelly, S., van Calsteren, P., Deng, W., 1996. Post-collision, shoshonitic volcanism on the Tibetan Plateau: implications for convective thinning of the lithosphere and the source of ocean island basalts. J. Petrol. 27, 45–71.

Triantafyllou A., Berger J., Baele J., Diot H, Ennih N., Plissart G, Monnier C., Watlet A., Bruguier O., Spagna P., Vandycke S., 2015.The Tachakoucht–Iriri–Tourtit arc complex (Moroccan Anti-Atlas): Neoproterozoic records of polyphased subduction-accretion dynamics during the Pan-African orogeny. Journal of Geodynamics, v. 96, p. 81-103.

Valeriano, C.M., Pimentel, M.M., Heilbron, M., Almeida, J.C.H., Trouw, R.A.J.,2008. Tectonic evolution of the Brasilia Belt, central Brazil, and early assembly of Gondwana. Geological Society, London Special Publication 294,p.197–p.210.

Wang, Q., Xu, J.F., Zhao, Z.H., Bao, Z.W., Xu, W., Xiong, X.L., 2004. Cretaceous highpotassium intrusive rocks in the Yueshan–Hongzhen area of east China: adakites in an extensional tectonic regime within a continent. Geochemical Journal v.38, p.417–434.

Whalen, J.B., Currie, K.L., Chappell, B.W., 1987. A-type granites: geochemical characteristics, discrimination and petrogenesis. Contributions to Mineralogy and Petrology v.95 (4), p.407–419.

Winchester, J.A., Floyd, P.A., 1977. Geochemical discrimination of different magma series and their differentiation products using immobile elements. Chemical. Geolog, v.20, p.323–343.

Wood, D.A., 1980. The application of a Th-Hf-Ta diagram to problems of ectonomagmatic classification and to establishing the nature of crustal contamination of basaltic lavas of the British Tertiary volcanic province. Earth Planet Science Letter.v. 50, p.11–30.

Supplementary Table.3.A-summary of ICP-MS U–Pb zircon data.

Sample	f(206)%	Th/U	6/4 ratio	7/6 ratio	1s(%)	7/5 ratio	1s(%)	6/8 ratio	1s(%)	Rho	7/6 age	1s(Ma)	7/5 age	1s(Ma)	6/8 age	1s(Ma)	Conc (%) 6/8 - 7/5
GD 12																	
004-Z1	0.446	0.256	3938	0.069	1.855	1.111	2.689	0.116	1.946	0.735	854	38	759	14	708	13	93
005-Z2	0.155	0.159	11466	0.065	1.293	0.865	2.317	0.096	1.922	0.826	727	28	633	11	590	11	93
007-Z4	0.092	0.243	19139	0.068	1.560	1.105	2.201	0.117	1.553	0.698	818	34	756	12	715	11	95
008-Z5	0.081	0.236	21746	0.065	1.071	1.071	1.807	0.119	1.456	0.799	725	23	739	9	724	10	98
010-Z7	0.133	0.277	13223	0.067	1.092	1.001	1.679	0.109	1.275	0.750	767	24	704	9	666	8	95
013-Z8	0.045	0.278	39259	0.068	1.599	1.040	2.216	0.111	1.535	0.685	809	34	724	11	678	10	94
015-Z10	0.088	0.559	19866	0.069	1.751	1.140	2.561	0.119	1.870	0.725	848	37	773	14	727	13	94
018-Z12	0.073	0.304	23980	0.070	1.732	1.125	2.540	0.117	1.857	0.726	864	37	765	14	712	13	93
020-Z14	0.071	0.326	24585	0.068	1.611	1.140	2.388	0.121	1.763	0.733	817	35	773	13	737	12	95
026-Z15	0.088	0.193	19787	0.065	1.640	1.162	2.457	0.130	1.829	0.740	712	36	783	13	786	14	100
028-Z17	0.081	0.259	21518	0.066	0.828	1.100	1.566	0.121	1.330	0.842	749	18	753	8	735	9	98
029-Z18	0.029	0.562	59352	0.065	0.921	1.133	1.352	0.126	0.990	0.714	719	20	769	7	766	7	100
030-Z19	0.113	0.293	15466	0.066	1.660	1.155	2.355	0.128	1.670	0.703	734	36	780	13	775	12	99
031-Z20	0.038	0.259	46213	0.065	0.663	1.133	1.207	0.126	1.009	0.823	722	14	769	7	765	7	99
032-Z21	0.072	0.616	21634	0.127	0.763	5.737	1.377	0.328	1.146	0.822	2004	14	1937	12	1829	18	94
036-Z23	0.042	0.229	41558	0.068	1.432	1.161	2.241	0.124	1.723	0.764	813	31	782	12	751	12	96
037-Z24	0.127	0.297	13819	0.067	1.413	1.135	2.377	0.122	1.911	0.800	792	31	770	13	743	13	96
040-Z27	0.995	0.355	1762	0.064	1.942	1.049	2.479	0.119	1.541	0.658	676	41	728	13	726	11	100
041-Z29	0.053	0.385	33108	0.065	1.161	1.136	1.818	0.126	1.400	0.762	725	25	771	10	766	10	99

Sample	f(206)%	Th/U	6/4 ratio	7/6 ratio	1s(%)	7/5 ratio	1s(%)	6/8 ratio	1s(%)	Rho	7/6 age	1s(Ma)	7/5 age	1s(Ma)	6/8 age	1s(Ma)	Conc (%) 6/8 - 7/5
GD 08																	
003-Z1	0.032	0.126	53113	0.072	1.029	1.478	1.606	0.149	1.232	0.757	981	21	922	10	897	10	97
011-Z5	0.024	0.341	71999	0.067	0.682	1.181	1.089	0.128	0.850	0.758	829	14	792	6	779	6	98
013-Z7	0.117	0.015	15089	0.063	0.723	0.925	1.246	0.107	1.015	0.801	706	15	665	6	653	6	98
017-Z9	0.089	0.116	19752	0.064	0.589	0.957	0.937	0.109	0.729	0.746	738	12	682	5	665	5	98
018-Z10	0.015	0.272	116753	0.065	0.419	1.120	0.741	0.124	0.611	0.782	787	9	763	4	755	4	99
019-Z11	0.008	0.005	232310	0.062	0.395	0.918	0.706	0.107	0.585	0.782	677	8	662	3	657	4	99
025-Z15	0.017	0.097	105356	0.062	0.860	0.822	1.461	0.096	1.182	0.799	675	18	609	7	592	7	97
032-Z20	0.035	0.214	50642	0.064	1.147	1.087	1.308	0.123	0.628	0.682	740	24	747	7	749	4	100
035-Z21	0.028	0.356	62402	0.066	0.327	1.164	0.621	0.129	0.529	0.795	796	7	784	3	780	4	99
036-Z22	0.013	0.379	135042	0.068	0.278	1.358	0.570	0.145	0.498	0.815	867	6	871	3	873	4	100
037-Z23	0.003	0.380	548555	0.069	0.189	1.378	0.534	0.145	0.499	0.903	899	4	879	3	872	4	99
041-Z25	0.067	0.016	26589	0.065	0.825	0.909	1.205	0.102	0.878	0.706	758	17	657	6	627	5	96
044-Z28	0.011	0.686	156698	0.066	0.569	1.196	0.783	0.131	0.538	0.821	816	12	799	4	792	4	99

Sample	f(206)%	Th/U	6/4 ratio	7/6 ratio	1s(%)	7/5 ratio	1s(%)	6/8 ratio	1s(%)	Rho	7/6 age	1s(Ma)	7/5 age	1s(Ma)	6/8 age	1s(Ma)	Conc (%) 6/8 - 7/5
GD 19																	
010-Z22	0.018	0.415	79318	0.157	0.534	9.200	0.959	0.424	0.797	0.809	2380	9	2358	9	2277	15	97
011-Z24	0.016	0.366	103735	0.094	0.563	2.855	1.071	0.219	0.911	0.836	1461	11	1370	8	1279	11	93
012-Z5N	0.082	0.211	21285	0.065	1.999	1.080	2.838	0.120	2.014	0.705	724	44	743	15	730	14	98
014-Z4	0.066	0.234	26383	0.063	2.403	1.107	3.488	0.128	2.528	0.722	635	53	757	19	778	19	103
015-Z23	0.025	0.174	65014	0.092	0.326	3.116	1.028	0.245	0.975	0.944	1414	6	1437	8	1415	12	99
020-Z3	0.060	0.225	29379	0.066	1.573	1.090	2.503	0.120	1.948	0.774	735	34	749	13	733	13	98
021-Z2	0.061	0.233	28684	0.065	2.221	1.126	2.967	0.125	1.967	0.658	725	48	766	16	759	14	99
022-Z14	0.052	0.222	33377	0.065	2.942	1.144	4.007	0.128	2.721	0.677	702	64	774	22	778	20	101
025-Z22	0.088	0.024	19293	0.075	0.432	1.845	0.834	0.178	0.714	0.831	1019	9	1061	5	1054	7	99
027-Z28	0.047	0.296	37287	0.072	3.102	1.155	4.641	0.117	3.453	0.743	920	66	780	25	712	23	91
030-Z15	0.051	0.246	34322	0.066	1.724	1.116	2.568	0.122	1.904	0.737	756	37	761	14	743	13	98
031-Z26	0.005	0.307	343129	0.060	0.654	0.701	1.104	0.085	0.889	0.786	547	15	540	5	523	4	97
032-Z25	0.077	0.203	22741	0.064	1.796	1.063	2.566	0.121	1.833	0.709	676	40	735	13	735	13	100
033-Z6	0.012	0.145	136657	0.097	0.427	3.496	0.734	0.262	0.596	0.766	1506	8	1526	6	1502	8	98
034-Z17	0.091	0.225	19237	0.065	1.936	1.091	2.956	0.122	2.234	0.753	707	42	749	16	742	16	99

Sample	f(206)%	Th/U	6/4 ratio	7/6 ratio	1s(%)	7/5 ratio	1s(%)	6/8 ratio	1s(%)	Rho	7/6 age	1s(Ma)	7/5 age	1s(Ma)	6/8 age	1s(Ma)	Conc (%) 6/8 - 7/5
GD 07																	
003-Z1	0.049	0.337	36060	0.065	0.903	1.092	1.321	0.122	0.964	0.711	768	19	749	7	743	7	99
005-Z3N	0.079	0.344	21912	0.069	2.044	1.280	2.755	0.135	1.847	0.665	893	42	837	16	816	14	97
006-Z3B	0.067	0.454	25916	0.070	1.636	1.348	1.808	0.140	0.770	0.638	922	34	867	11	845	6	98
011-Z5B	0.070	0.276	24857	0.070	1.256	1.352	1.809	0.140	1.302	0.710	928	26	868	11	845	10	97
012-Z6	0.070	0.495	25032	0.067	2.492	1.170	2.950	0.126	1.579	0.775	849	52	787	16	765	11	97
015-Z7	0.049	0.480	36395	0.060	1.341	0.822	2.003	0.100	1.487	0.735	596	29	609	9	612	9	101
016-Z8	0.106	0.625	16295	0.070	1.711	1.350	2.715	0.139	2.107	0.773	936	35	867	16	841	17	97
018-Z10	0.048	0.421	36863	0.059	2.435	0.777	2.747	0.095	1.272	0.707	582	53	584	12	584	7	100
021-Z11	0.071	0.316	25083	0.061	1.401	0.800	2.120	0.095	1.591	0.744	650	30	597	10	583	9	98
022-Z12	0.031	0.353	57615	0.059	1.014	0.785	1.418	0.097	0.991	0.680	559	22	588	6	596	6	101
024-Z14	0.045	0.465	38327	0.067	1.890	1.257	2.226	0.137	1.175	0.758	825	39	826	13	827	9	100
033-Z19	0.061	0.617	28456	0.068	0.792	1.358	1.203	0.145	0.906	0.732	870	16	871	7	871	7	100
034-Z20	0.090	0.487	19437	0.069	0.974	1.254	1.421	0.131	1.035	0.712	913	20	825	8	793	8	96
035-Z21	0.963	0.735	1799	0.065	1.115	1.257	1.731	0.139	1.311	0.752	786	23	827	10	842	10	102
040-Z24B	0.252	0.241	7026	0.066	0.755	0.915	1.355	0.100	1.125	0.820	809	16	660	7	617	7	94
041-Z25	0.009	0.089	177168	0.078	0.664	2.088	0.905	0.195	0.616	0.801	1140	13	1145	6	1147	6	100
044-Z26	0.011	0.323	154684	0.075	0.645	1.812	1.048	0.176	0.826	0.765	1058	13	1050	7	1045	8	100
045-Z27	0.044	0.322	40264	0.061	1.043	0.830	1.374	0.099	0.894	0.626	643	22	614	6	606	5	99
046-Z28	0.023	0.439	76328	0.062	0.942	0.850	1.236	0.099	0.799	0.615	686	20	624	6	608	5	97
047-Z29	0.045	0.333	39399	0.063	2.751	0.921	3.123	0.105	1.478	0.718	719	58	663	15	646	9	98

Sample	f(206)%	Th/U	6/4 ratio	7/6 ratio	1s(%)	7/5 ratio	1s(%)	6/8 ratio	1s(%)	Rho	7/6 age	1s(Ma)	7/5 age	1s(Ma)	6/8 age	1s(Ma)	Conc (%) 6/8 - 7/5
GD 09																	
003-Z01	0.074	0.254	24149	0.061	1.683	0.784	2.362	0.094	1.657	0.695	632	36	588	11	576	9	98
004-Z02	0.046	0.287	38590	0.059	1.143	0.781	1.709	0.096	1.271	0.733	566	25	586	8	591	7	101
005-Z03	0.066	0.367	26986	0.059	1.075	0.781	1.621	0.095	1.214	0.737	585	23	586	7	586	7	100
006-Z04	0.080	0.335	21536	0.068	1.887	1.330	2.333	0.141	1.372	0.813	878	39	859	14	851	11	99
009-Z05	0.046	0.340	38420	0.059	2.117	0.777	2.554	0.096	1.429	0.550	564	46	584	11	589	8	101
010-Z06	0.142	0.356	12466	0.057	1.267	0.786	1.819	0.099	1.305	0.707	508	28	589	8	610	8	104
011-Z07	0.031	0.481	56899	0.059	0.638	0.826	1.273	0.101	1.101	0.856	576	14	611	6	621	7	102
012-Z08	0.055	0.332	32091	0.059	2.471	0.769	2.760	0.094	1.229	0.688	582	54	579	12	579	7	100
015-Z09	0.056	0.254	31735	0.060	1.183	0.764	1.869	0.092	1.447	0.767	619	26	576	8	566	8	98
016-Z10	0.074	0.347	24031	0.058	0.940	0.802	1.476	0.100	1.138	0.759	546	21	598	7	612	7	102
017-Z11	0.075	0.332	23575	0.059	0.909	0.792	1.392	0.097	1.054	0.742	568	20	592	6	599	6	101
018-Z12	0.066	0.340	27091	0.059	2.291	0.780	2.530	0.096	1.074	0.659	559	50	585	11	592	6	101
021-Z13	0.030	0.258	58422	0.060	1.025	0.820	1.422	0.100	0.986	0.674	589	22	608	7	613	6	101
027-Z17	0.114	0.259	15532	0.059	2.018	0.818	2.928	0.101	2.123	0.721	550	44	607	13	622	13	103
028-Z18	0.163	0.240	10913	0.064	1.523	0.873	2.381	0.098	1.830	0.764	751	32	637	11	606	11	95
029-Z19	0.023	0.730	76267	0.067	1.189	1.419	1.550	0.154	0.995	0.622	831	25	897	9	924	9	103
033-Z21	0.051	0.334	34923	0.059	1.306	0.794	1.714	0.097	1.109	0.632	580	28	593	8	597	6	101
035-Z23	0.057	0.351	31050	0.060	0.835	0.765	1.431	0.093	1.162	0.802	601	18	577	6	571	6	99
036-Z24	0.098	0.261	18088	0.060	1.745	0.813	2.057	0.098	1.089	0.748	616	38	604	9	601	6	99
039-Z25	0.045	0.270	39689	0.062	1.466	0.844	2.208	0.099	1.651	0.742	671	31	621	10	608	10	98
040-Z26	0.098	0.267	18118	0.059	1.449	0.771	2.626	0.095	2.190	0.831	568	32	580	12	583	12	101
041-Z27	0.191	0.340	9298	0.059	1.270	0.803	1.987	0.100	1.528	0.762	549	28	598	9	612	9	102
042-Z28	0.069	0.279	25718	0.058	2.523	0.791	2.887	0.099	1.403	0.723	533	55	592	13	607	8	103
045-Z29	0.048	0.249	36755	0.058	1.080	0.784	1.573	0.097	1.144	0.714	542	24	588	7	600	7	102
046-Z30B	0.040	0.367	44071	0.059	0.729	0.785	1.293	0.097	1.068	0.814	557	16	588	6	596	6	101
048-Z30N	0.071	0.267	25046	0.058	3.382	0.782	3.707	0.097	1.518	0.655	540	74	587	17	599	9	102

Sample	f(206)%	Th/U	6/4 ratio	7/6 ratio	1s(%)	7/5 ratio	1s(%)	6/8 ratio	1s(%)	Rho	7/6 age	1s(Ma)	7/5 age	1s(Ma)	6/8 age	1s(Ma)	Conc (%) 6/8 - 7/5
GD 22																	
004-Z1	0.035	0.184	51299	0.060	1.152	0.750	1.786	0.090	1.365	0.756	547	26	568	8	558	7	98
005-Z2	0.027	0.183	65049	0.060	0.967	0.777	1.549	0.094	1.210	0.771	546	22	584	7	577	7	99
006-Z3	0.024	0.187	73680	0.059	0.963	0.768	1.449	0.094	1.082	0.733	512	22	579	6	580	6	100
008-Z6	0.063	0.201	28324	0.059	1.657	0.761	2.481	0.094	1.846	0.739	495	38	575	11	579	10	101
009-Z7	0.046	0.051	38579	0.061	0.741	0.821	1.723	0.097	1.556	0.900	589	17	609	8	597	9	98
010-Z9	0.039	0.268	45650	0.060	0.976	0.800	1.732	0.097	1.431	0.820	542	22	597	8	595	8	100
013-Z10	0.022	0.190	79606	0.059	0.707	0.814	1.342	0.100	1.140	0.841	508	16	605	6	614	7	102
014-Z11	0.034	0.217	51996	0.059	1.153	0.790	1.625	0.097	1.146	0.691	517	26	591	7	594	7	101
016-Z13	0.027	0.199	65725	0.060	0.733	0.824	1.272	0.100	1.040	0.805	534	17	610	6	614	6	101
017-Z14	0.028	0.168	63384	0.060	0.846	0.796	1.329	0.096	1.025	0.756	539	19	595	6	593	6	100
018-Z15	0.025	0.173	70170	0.060	1.214	0.797	1.768	0.097	1.285	0.716	524	27	595	8	598	7	100
019-Z22N	0.024	0.252	72770	0.059	1.395	0.759	1.847	0.093	1.210	0.642	516	32	573	8	572	7	100
020-Z22B	0.012	0.181	151346	0.060	0.757	0.767	1.227	0.093	0.966	0.770	534	17	578	5	573	5	99
024-Z17	0.026	0.176	69348	0.059	0.582	0.787	1.034	0.096	0.854	0.807	512	13	589	5	593	5	101
026-Z19	0.027	0.181	65406	0.060	0.768	0.781	1.150	0.095	0.856	0.720	527	17	586	5	585	5	100
027-Z20	1.120	0.161	1607	0.063	1.147	0.614	1.670	0.071	1.214	0.764	648	24	486	6	440	5	91
028-Z21N	2.249	0.173	793	0.056	1.601	0.687	2.510	0.089	1.934	0.844	399	35	531	10	547	10	103
029-Z21B	0.053	0.183	33704	0.060	1.080	0.764	1.851	0.092	1.503	0.806	554	24	577	8	566	8	98
030-Z16	0.051	0.215	34742	0.060	0.936	0.798	1.343	0.096	0.964	0.698	545	21	596	6	593	5	99
033-Z23	0.045	0.184	39513	0.058	1.353	0.764	1.999	0.096	1.472	0.729	464	31	577	9	589	8	102
034-Z24	0.014	0.223	124518	0.057	0.568	0.688	1.167	0.087	1.019	0.863	445	13	532	5	537	5	101
035-Z25	0.050	0.256	36094	0.057	0.928	0.666	1.456	0.085	1.121	0.758	417	21	518	6	527	6	102
038-Z27N	0.050	0.202	35362	0.062	0.771	0.816	1.259	0.096	0.995	0.775	606	17	606	6	589	6	97
039-Z28	0.010	0.308	169719	0.060	0.684	0.771	1.273	0.093	1.073	0.833	538	15	581	6	576	6	99

Sample	f(206)%	Th/U	6/4 ratio	7/6 ratio	1s(%)	7/5 ratio	1s(%)	6/8 ratio	1s(%)	Rho	7/6 age	1s(Ma)	7/5 age	1s(Ma)	6/8 age	1s(Ma)	Conc (%) 6/8 - 7/5
GD 21																	
004-Z1	0.037	0.268	47989	0.060	1.068	0.759	1.734	0.092	1.366	0.780	534	24	574	8	568	7	99
012 Z5	0.088	0.282	20216	0.060	1.786	0.745	2.758	0.090	2.102	0.759	534	40	565	12	558	11	99
017-Z8	0.024	0.328	74098	0.059	0.419	0.776	0.676	0.095	0.530	0.716	502	9	583	3	588	3	101
018-Z9	0.009	0.305	200616	0.060	0.379	0.783	0.789	0.095	0.692	0.853	525	9	587	4	587	4	100
023-Z12N	0.009	0.474	199851	0.060	0.354	0.805	0.739	0.098	0.649	0.850	535	8	600	3	600	4	100
032-Z17	0.038	0.300	47400	0.059	1.296	0.726	1.831	0.090	1.293	0.695	492	29	554	8	554	7	100
037-Z19	0.062	0.403	28705	0.060	1.300	0.719	1.926	0.087	1.421	0.729	530	29	550	8	540	7	98
038-Z20	0.039	0.312	45419	0.059	1.065	0.735	1.658	0.090	1.270	0.756	516	24	559	7	555	7	99
040-Z22	0.103	0.398	17273	0.059	1.971	0.728	2.857	0.089	2.068	0.720	522	44	556	12	549	11	99
041-Z23	0.036	0.290	49427	0.059	1.021	0.742	1.513	0.091	1.117	0.724	512	23	563	7	561	6	100
042-Z24	0.022	0.396	81297	0.060	0.541	0.768	1.024	0.094	0.869	0.832	525	12	579	5	577	5	100
045-Z25	0.037	0.322	48022	0.060	0.978	0.767	1.536	0.093	1.185	0.760	527	22	578	7	576	7	100
046-Z26	0.005	0.315	368848	0.060	0.421	0.747	0.839	0.091	0.725	0.842	533	9	566	4	559	4	99
047-Z27	0.026	0.402	67829	0.059	1.290	0.702	1.602	0.087	0.951	0.571	488	29	540	7	538	5	100

Sample	f(206)%	Th/U	6/4 ratio	7/6 ratio	1s(%)	7/5 ratio	1s(%)	6/8 ratio	1s(%)	Rho	7/6 age	1s(Ma)	7/5 age	1s(Ma)	6/8 age	1s(Ma)	Conc (%) 6/8 - 7/5
GD 16																	
004_Z1	1.745	0.180	1030	0.054	1.587	0.555	2.282	0.074	1.640	0.786	316	36	448	8	461	7	103
007_Z3B	0.392	0.254	4554	0.060	0.517	0.712	0.820	0.086	0.637	0.751	539	11	546	3	533	3	98
009_Z7B	0.967	0.195	1864	0.056	1.395	0.540	1.831	0.070	1.186	0.683	392	31	439	6	435	5	99
013_Z8	0.011	0.141	164874	0.057	0.609	0.653	1.247	0.083	1.088	0.864	438	14	511	5	513	5	100
014_Z9	0.012	0.269	149892	0.058	0.952	0.643	1.478	0.080	1.130	0.752	476	22	504	6	497	5	98
015_Z10	0.046	0.286	38762	0.057	1.496	0.656	2.449	0.083	1.939	0.788	438	34	512	10	515	10	100
017_Z12	1.101	0.267	1646	0.062	0.955	0.509	3.532	0.059	3.401	0.972	622	20	418	12	372	12	89
018_Z13	0.172	0.274	10436	0.060	0.795	0.653	1.222	0.080	0.928	0.740	524	18	510	5	493	4	97
019_Z14	0.339	0.129	5305	0.061	0.438	0.636	1.942	0.076	1.892	0.974	569	10	500	8	472	9	94
023_Z15B	2.709	0.242	667	0.057	1.597	0.492	2.018	0.062	1.234	0.719	446	35	406	7	389	5	96
026_Z17	0.172	0.206	10451	0.060	0.659	0.653	0.945	0.078	0.677	0.673	557	15	511	4	487	3	95
028_Z19	0.006	0.220	324885	0.057	0.620	0.649	0.838	0.083	0.563	0.603	416	14	508	3	515	3	101
032_Z21N	1.081	0.400	1646	0.058	1.193	0.741	1.719	0.092	1.238	0.758	481	26	563	7	568	7	101
033_Z22B	0.511	0.209	3522	0.059	1.138	0.572	3.223	0.071	3.016	0.943	487	25	459	12	442	13	96
034_Z23	0.093	0.202	19232	0.063	0.764	0.687	1.699	0.079	1.517	0.889	638	17	531	7	492	7	93
036_Z25	0.502	0.172	3589	0.058	0.541	0.568	0.976	0.072	0.812	0.831	451	12	457	4	446	3	98
037_Z26	0.085	0.161	21109	0.058	0.351	0.656	0.769	0.082	0.684	0.868	474	8	512	3	506	3	99

Sample	f(206)%	Th/U	6/4 ratio	7/6 ratio	1s(%)	7/5 ratio	1s(%)	6/8 ratio	1s(%)	Rho	7/6 age	1s(Ma)	7/5 age	1s(Ma)	6/8 age	1s(Ma)	Conc (%) 6/8 - 7/5
GD 20																	
009-Z3N	0.091	0.284	19663	0.059	2.022	0.661	2.862	0.082	2.025	0.703	493	46	515	12	506	10	98
010-Z3B	0.088	0.238	20366	0.061	0.724	0.713	1.325	0.085	1.110	0.827	574	16	547	6	526	6	96
011-Z4N	0.100	0.330	17790	0.060	1.466	0.706	2.123	0.086	1.536	0.716	527	33	543	9	531	8	98
016-Z6	0.112	0.475	16011	0.057	1.386	0.646	2.304	0.082	1.840	0.795	443	32	506	9	506	9	100
018-Z8	0.034	0.314	53022	0.058	0.719	0.639	1.178	0.081	0.934	0.775	449	16	502	5	500	4	100
023-Z11	0.035	0.366	51131	0.059	1.567	0.663	1.992	0.082	1.229	0.605	494	36	516	8	507	6	98
024-Z12	0.054	0.224	33484	0.059	1.047	0.650	1.505	0.080	1.080	0.703	492	24	508	6	498	5	98
027-Z13	0.069	0.359	25913	0.056	1.597	0.623	2.054	0.080	1.292	0.618	399	37	492	8	498	6	101
028-Z14	0.034	0.178	52880	0.057	1.474	0.659	2.028	0.084	1.393	0.677	431	34	514	8	519	7	101
029-Z15	0.032	0.667	42112	0.184	0.794	13.060	1.198	0.516	0.898	0.728	2640	14	2684	11	2680	20	100
033-Z16	0.010	0.304	186717	0.057	0.745	0.657	1.089	0.083	0.793	0.700	443	17	513	4	514	4	100
035-Z18	0.012	0.576	147366	0.060	0.683	0.682	1.114	0.083	0.880	0.770	535	15	528	5	512	4	97
036-Z19	0.027	0.393	66955	0.059	0.921	0.613	1.241	0.075	0.832	0.642	521	21	486	5	465	4	96
041-Z22	0.820	0.202	2201	0.056	1.677	0.512	2.079	0.066	1.229	0.620	398	37	420	7	412	5	98

Supplementary Table 3.B - Major and trace element data for representative Jaupaci Sequence Arc granitoids, Jaupaci Sequence and post-collisional granitoids samples from the Jaupaci belt.

Rock	Metarhyolite	Metarhyolite	Metarhyolite	Metarhyolite	Metarhyolite	Felsic Metavolcanics	Felsic Metavolcanics
Jaupaci Sequence	**Sample (GD-19)**	**Sample (GD-35)**	**Sample (GD-38)**	**Sample (GD-40)**	**Sample (GD-41)**	**Sample (GD-07)**	**Sample (GD-44)**
SiO2 (wt%)	73.08	72.89	72.42	71.83	71.36	67.73	69.83
TiO2	0.15	0.17	0.20	0.13	0.14	0.66	0.55
Al2O3	15.41	15.29	16.75	15.74	15.94	16.87	15.57
Fe2O3	1.49	1.62	1.91	1.52	1.68	4.79	4.38
MnO	0.03	0.04	0.03	0.04	0.04	0.17	0.17
MgO	0.17	0.23	0.51	0.14	0.35	1.43	1.30
CaO	0.62	1.08	1.19	1.05	1.41	2.91	2.66
Na2O	5.11	4.55	5.88	6.01	6.53	4.08	3.45
K2O	4.46	4.48	1.56	4.27	3.94	2.76	3.15
P2O5	0.05	0.06	0.09	0.06	0.03	0.21	0.16
LOI	0.52	1.25	2.50	1.11	1.07	2.92	2.04
Total	100.69	100.53	100.73	100.92	101.53	102.06	101.71
Na2O + K2O (wt %)	9.57	9.02	7.44	10.28	10.47	6.84	6.60
Sr/Y	58.8	66.4	185.2	58.0	65.7	7.6	7.9
La/Yb	51.4	65.8	50.4	44.3	48.9	7.0	7.0
Th/Ta	8.4	8.3	7.7	7.7	9.2	9.7	10.1
$(La/Lu)_N$	77.1	89.3	109.2	102.0	93.8	12.7	10.7
V (ppm)	8.00	10.00	27.00	15.00	18.00	85	71
Cr	20.00	20.00	30.00	20.00	40.00	50	50
Co	0.00	0.00	0.00	0.00	0.00	8.6	8.8
Ni	0.00	0.00	0.00	0.00	0.00	46	35
cu	0.00	0.00	0.00	0.00	0.00	38	44
Zn	0.00	0.00	0.00	0.00	0.00	78	77
Ga	24.40	25.90	19.10	27.60	25.70	18.5	18.1
Rb	131.50	129.50	39.80	118.00	75.90	65.2	66.3
Sr	341.00	372.00	537.00	435.00	394.00	282	271
Y	5.80	5.60	2.90	7.50	6.00	37.2	34.1
Zr	154.00	168.00	87.00	153.00	160.00	202	174
Nb	19.70	19.20	7.10	20.10	19.60	8.9	8
Mo	0.00	0.00	0.00	0.00	0.00	2	3
Sn	5.00	4.00	1.00	4.00	4.00	2	2
Cs	0.90	1.46	2.60	2.07	0.64	2.8	1.96
Ba	596.00	751.00	866.00	684.00	759.00	3150	3590
La	21.60	25.00	13.10	20.40	22.50	28.4	24.9
Ce	41.70	48.40	24.00	39.40	42.50	60	52.3
Nd	14.30	15.80	8.30	14.10	14.60	30.3	26.6
Sm	2.59	2.93	1.28	2.68	2.78	6.63	5.52
Eu	0.56	0.60	0.37	0.68	0.63	1.56	1.27
Gd	1.99	2.04	0.88	1.73	2.04	6.54	5.46
Tb	0.22	0.25	0.12	0.26	0.21	0.99	0.93
Dy	1.25	1.15	0.58	1.34	1.10	6.79	5.99
Ho	0.20	0.16	0.08	0.26	0.18	1.42	1.24
Er	0.50	0.50	0.25	0.55	0.43	4	3.96
Tm	0.07	0.07	0.05	0.12	0.09	0.6	0.51
Yb	0.42	0.38	0.26	0.46	0.46	4.04	3.57
Lu	0.07	0.07	0.03	0.05	0.06	0.56	0.58
Hf	4.90	5.40	2.40	5.20	5.00	5.9	4.8
Ta	1.60	1.70	1.40	1.70	1.50	0.7	0.5
W	2.00	2.00	3.00	1.00	1.00	5	4
Pb	0.00	0.00	0.00	0.00	0.00	9	11
Th	13.50	14.05	10.79	13.15	13.80	6.82	5.07
U	9.37	10.30	0.54	9.87	9.58	2.22	1.7
Ag	0	0	0	0	0	1	1
Pr	4.22	4.83	2.43	4.09	4.48	7.01	6.28
Tl	0.5	0.5	0.5	0.5	0.5	0.5	0.5

Rock	Felsic Metavolcanics	Felsic Metavolcanics	Felsic Metavolcanics	Felsic Metavolcanics	Felsic Metavolcanics	Felsic Metavolcanics	Felsic Metavolcanics
Jaupaci Sequence	**Sample (GD-45)**	**Sample (GD-46)**	**Sample (GD-48)**	**Sample (GD-50)**	**Sample (GD-51)**	**Sample (GD-52)**	**Sample (GD-53)**
SiO2 (wt%)	68.90	67.42	69.33	68.29	67.13	72.59	71.19
TiO2	0.58	0.65	0.52	0.53	0.93	0.56	0.48
Al2O3	15.84	15.39	16.48	16.38	16.26	15.59	17.02
Fe2O3	4.35	4.26	4.67	3.80	6.42	2.78	3.69
MnO	0.15	0.10	0.11	0.16	0.12	0.08	0.10
MgO	1.32	1.35	1.56	1.43	3.14	1.11	2.65
CaO	3.06	2.25	1.95	3.47	2.17	2.45	2.18
Na2O	3.48	3.68	3.38	5.12	1.65	2.91	2.41
K2O	3.30	4.10	3.34	2.12	3.43	2.55	3.20
P2O5	0.19	0.14	0.15	0.24	0.15	0.09	0.15
LOI	2.38	2.47	4.07	2.66	4.51	2.59	3.39
Total	101.6	99.69	101.78	101.78	101.50	101.0	103.19
Na2O + K2O (wt %)	6.78	7.78	6.71	7.24	5.08	5.46	5.61
Sr/Y	11.1	9.0	10.0	11.9	0.9	9.8	1.4
La/Yb	7.5	7.4	7.7	7.7	4.0	4.5	4.5
Th/Ta	8.0	11.5	9.4	8.1	5.4	6.2	6.3
$(La/Lu)_N$	12.4	11.8	13.6	12.4	6.9	7.8	7.4
V (ppm)	77	73.00	59.00	64.00	152.00	24	33.00
Cr	50	50.00	30.00	30.00	140.00	40	40.00
Co	10.4	7.60	0.00	0.00	0.00	2.1	0.00
Ni	36	32.00	0.00	0.00	0.00	19	0.00
cu	33	26.00	0.00	0.00	0.00	13	0.00
Zn	78	84.00	0.00	0.00	0.00	112	0.00
Ga	18.1	20.10	21.10	17.00	46.50	20.8	23.20
Rb	83.5	88.80	64.60	45.00	97.70	58.3	79.70
Sr	374	312.00	316.00	372.00	83.80	574	91.20
Y	33.8	34.50	31.70	31.20	91.10	58.5	64.80
Zr	165	224.00	222.00	196.00	434.00	260	301.00
Nb	8.1	9.60	10.50	8.40	19.80	7.6	11.90
Mo	2	2.00	0.00	0.00	0.00	2	0.00
Sn	2	2.00	3.00	1.00	6.00	2	4.00
Cs	2.49	2.34	1.53	1.74	2.98	1.52	2.77
Ba	3150	2580.00	2440.00	1840.00	429.00	1635	1005.00
La	25.3	27.40	28.30	26.30	40.80	27.2	30.90
Ce	51	56.50	62.20	57.10	99.70	60.5	72.60
Nd	26.2	29.30	29.40	25.90	50.00	38.7	38.10
Sm	5.8	6.25	6.53	5.70	11.95	8.5	8.25
Eu	1.14	1.32	1.35	1.49	1.60	2.44	2.32
Gd	5.49	5.54	6.40	5.38	13.35	8.88	10.80
Tb	0.85	0.91	1.00	0.87	2.41	1.45	1.79
Dy	5.42	5.71	5.78	5.19	15.25	9.82	11.55
Ho	1.18	1.25	1.17	1.11	3.31	2.04	2.29
Er	3.33	3.71	3.42	3.26	9.87	6.22	7.02
Tm	0.53	0.53	0.56	0.57	1.53	0.93	1.09
Yb	3.39	3.69	3.67	3.43	10.15	6.08	6.88
Lu	0.51	0.58	0.52	0.53	1.47	0.87	1.04
Hf	4.3	6.20	6.20	4.90	12.30	7	9.10
Ta	0.6	0.60	0.70	0.60	1.40	0.6	0.90
W	6	6.00	3.00	2.00	7.00	5	2.00
Pb	12	13.00	0.00	0.00	0.00	30	0.00
Th	4.8	6.88	6.58	4.87	7.57	3.7	5.66
U	1.79	2.37	1.94	1.70	3.00	1.68	1.84
Ag	1	1	0	0	0	1	0
Pr	6.02	6.64	7.59	6.7	12.5	7.86	8.82
Tl	0.5	0.5	0.5	0.5	0.5	0.5	0.5

Rock	Felsic Metavolcanics	Felsic Metavolcanics	Felsic Metavolcanics	Felsic Metavolcanics	Felsic Metavolcanics	Felsic Metavolcanics
Jaupaci Sequence	**Sample (GD-54)**	**Sample (GD-55)**	**Sample (GD-56)**	**Sample (GD-57)**	**Sample (GD-58)**	**Sample (GD-59)**
SiO2 (wt%)	70.22	78.06	78.09	73.17	69.89	75.62
TiO2	0.63	0.19	0.19	0.46	0.44	0.46
Al2O3	16.36	15.35	15.48	15.32	16.25	15.22
Fe2O3	3.36	2.35	2.38	2.44	3.28	2.41
MnO	0.11	0.04	0.03	0.14	0.08	0.11
MgO	0.98	0.23	0.10	0.53	0.78	0.71
CaO	2.96	0.88	0.27	0.71	2.34	0.74
Na2O	4.65	4.73	3.20	5.20	5.67	4.24
K2O	2.46	1.88	4.25	2.39	2.88	2.38
P2O5	0.16	0.03	0.03	0.03	0.17	0.03
LOI	3.44	0.74	0.90	1.24	2.69	1.40
Total	102.02	103.87	104.22	100.55	101.91	102.09
Na2O + K2O (wt %)	7.11	6.60	7.46	7.59	8.55	6.61
Sr/Y	6.4	1.0	0.3	1.9	11.3	2.2
La/Yb	5.8	4.6	5.5	3.7	7.5	4.5
Th/Ta	7.3	6.1	7.5	6.3	9.8	6.1
$(La/Lu)_N$	9.9	7.9	8.5	6.5	11.7	7.0
V (ppm)	45.00	24.00	22.00	22.00	63.00	33.00
Cr	20.00	20.00	20.00	20.00	20.00	50.00
Co	0.00	0.00	0.00	0.00	0.00	1.70
Ni	0.00	0.00	0.00	0.00	0.00	22.00
cu	0.00	0.00	0.00	0.00	0.00	8.00
Zn	0.00	0.00	0.00	0.00	0.00	92.00
Ga	17.90	19.80	16.30	27.90	16.70	20.50
Rb	60.10	27.60	50.80	43.40	57.80	53.70
Sr	229.00	75.30	20.80	115.50	260.00	120.50
Y	36.00	72.80	65.90	60.10	23.10	54.70
Zr	223.00	469.00	337.00	338.00	198.00	273.00
Nb	8.50	12.50	12.90	10.70	6.90	7.70
Mo	0.00	0.00	0.00	0.00	0.00	3.00
Sn	2.00	3.00	3.00	3.00	3.00	3.00
Cs	2.26	1.52	0.62	2.27	2.02	3.06
Ba	812.00	1090.00	1495.00	1240.00	1010.00	1305.00
La	23.00	36.50	36.00	27.10	20.20	25.50
Ce	53.10	86.10	82.50	64.50	43.40	57.70
Nd	27.30	48.50	44.20	35.20	19.00	34.60
Sm	5.68	11.15	10.20	9.03	4.06	7.99
Eu	1.49	2.80	2.27	2.22	1.06	2.17
Gd	6.37	12.25	11.10	9.38	3.68	8.27
Tb	1.00	2.01	1.82	1.59	0.61	1.40
Dy	6.54	12.90	11.75	9.57	3.69	8.90
Ho	1.22	2.45	2.38	2.20	0.78	1.90
Er	4.10	8.04	7.02	6.69	2.49	5.86
Tm	0.59	1.18	1.04	1.09	0.48	0.86
Yb	3.94	7.85	6.55	7.32	2.71	5.73
Lu	0.58	1.16	1.06	1.04	0.43	0.91
Hf	5.60	11.70	9.80	8.30	4.90	6.90
Ta	0.60	0.90	0.80	0.60	0.50	0.60
W	8.00	1.00	24.00	5.00	5.00	5.00
Pb	0.00	0.00	0.00	0.00	0.00	13.00
Th	4.39	5.45	6.01	3.80	4.88	3.63
U	1.86	1.75	1.53	1.48	2.13	1.78
Ag	0	0	0	0	0	1
Pr	6.27	10.75	10.15	8.52	5.07	7.53
Tl	0.5	0.5	0.5	0.5	0.5	0.5

Rock	Amphibole schist	Amphibole schist	Amphibole schist	Amphibole schist	Amphibole schist	Amphibole schist	Clhorite schist	Clhorite schist
Jaupaci Sequence	**Sample GD-43**	**Sample GD-32**	**Sample GD-47**	**Sample GD-49**	**Sample GD-60**	**Sample GD-61**	**Sample GD-17**	**Sample GD-33**
SiO2 (wt%)	47.02	47.62	48.90	46.66	47.45	46.36	48.8	47.63
TiO2	2.59	2.16	2.23	2.01	2.58	2.07	1.87	2.33
Al2O3	16.58	11.3	16.65	16.11	16.58	17.08	15.2	16.50
Fe2O3	14.08	16.47	13.01	13.41	13.66	13.23	11.95	13.52
MnO	0.24	0.26	0.21	0.23	0.22	0.22	0.18	0.19
MgO	7.01	8.09	6.88	8.12	6.13	7.42	7.69	6.19
CaO	9.75	11.91	10.14	10.48	10.84	12.33	8.53	7.82
Na2O	2.27	1.67	2.32	2.49	2.65	1.02	1.88	1.96
K2O	0.08	0.16	0.23	0.35	0.16	0.41	1.85	1.58
P2O5	0.43	0.31	0.40	0.29	0.43	0.34	0.41	0.45
LOI	5.07	0.54	4.34	4.36	3.54	5.18	5.12	4.85
Total	100.1	100.18	101.0	100.2	100.8	100.58	101.55	103.2
Na2O + K2O (wt %)	2.4	1.8	2.5	2.8	2.8	1.4	3.7	3.5
$(La/Lu)_N$	3.1	1.3	3.1	1.7	2.6	2.0	3.4	3.7
V (ppm)	326	438	295	335	314	328	214	311
Cr	170	0	180	210	150	250	210	230
Co	0	52.7	0	0	0	0	0	50.9
Ni	0	64	0	0	0	0	0	123
Cu	0	96	0	0	0	0	0	90
Zn	0	125	0	0	0	0	0	125
Ga	23.5	19.5	19.9	19.8	21	21.7	21.8	21.7
Rb	2.6	3.6	4.3	5.9	2.9	14	46.3	23.6
Sr	264	208	311	243	505	468	146	508
Y	38.4	38.38	35.4	34.9	33.7	34.8	34.8	31.6
Zr	164	124	171	142	147	135	146	121
Nb	5	5.27	5.4	2.9	4.2	3.5	5.2	3.1
Mo	0	2	0	0	0	0	0	2
Sn	1	1.3	2	1	1	1	1	1
Cs	0.27	0.44	0.5	0.53	0.37	0.75	3.9	2.37
Ba	49	74	103.5	138	85.2	27.3	389	852
La	12	5.9	10.4	6.8	8.7	6.6	11.8	11.7
Ce	31.2	15.2	27.9	19.4	23.9	18.8	30.6	29.7
Nd	21.6	14.1	20.1	15.3	18.7	14.7	20.2	21.3
Sm	6.11	4.7	5.06	4.27	5.05	4.77	5.39	5.55
Eu	2.74	1.68	1.99	1.79	2.02	1.78	1.94	1.94
Gd	7.11	6.43	6.42	6.13	6.45	5.64	6.2	5.69
Tb	1.18	1.16	0.98	1.07	1	1.04	1.04	0.88
Dy	6.84	7.46	6.6	6.42	6.35	6.32	6.42	5.93
Ho	1.46	1.6	1.22	1.23	1.1	1.34	1.3	1.19
Er	4.34	4.55	3.96	3.88	3.54	3.78	3.95	3.24
Tm	0.55	0.67	0.53	0.57	0.45	0.56	0.56	0.45
Yb	3.38	4.2	3.42	3.32	3.07	3.37	3.38	3.11
Lu	0.55	0.66	0.48	0.56	0.47	0.48	0.5	0.45
Hf	4.2	3.03	3.9	3.3	3.5	3.2	3.6	3.4
Ta	0.4	0.35	0.3	0.2	0.3	0.2	0.3	0.3
W	1	1.4	40	13	1	1	1	3
Pb	0	0	0	0	0	0	0	6
Th	0.97	0.2	0.57	0.32	1.34	0.3	0.96	1
U	0.45	0.08	0.26	0.18	0.18	0.11	0.39	0.48
Ag	0	0	0	0	0	0	0	1
Pr	4.64	2.53	4.02	3.03	3.62	3.05	4.28	4.06
Tl	<0,5	0.5	0.5	0.5	0.5	<0,5	0.5	0.5

Rock	Metatonalite - Type 1 Suite	Metatonalite - Type 1 Suite	Metatonalite - Type 1 Suite	Metatonalite - Type 1 Suite	Granodiorite - Type 1 Suite	Granodiorite - Type 1 Suite
Orthogneisses/ Arc Granitoids	**Sample GD-29**	**Sample GD-12**	**Sample GD-14**	**Sample GD-60**	**Sample GD-61**	**Sample GD-62**
SiO2 (wt%)	73.65	67.42	75.81	70.16	72.83	72.30
TiO2	0.47	0.88	0.38	0.35	0.54	0.42
Al2O3	16.09	16.56	15.54	14.33	15.52	16.32
Fe2O3	3.36	5.34	2.03	2.94	3.40	3.50
MnO	0.11	0.18	0.07	0.11	0.10	0.05
MgO	2.09	1.72	0.14	0.38	0.88	0.51
CaO	1.72	3.31	0.86	1.25	2.03	0.76
Na2O	1.18	3.62	5.74	4.23	3.22	2.64
K2O	3.97	2.42	1.33	2.06	3.09	4.75
P2O5	0.16	0.14	0.08	0.06	0.12	0.09
LOI	3.65	2.74	1.05	0.91	2.77	2.68
Total	103.0	101.7	102.1	96.78	101.9	104.1
Na2O + K2O (wt %)	5.1	6.0	7.1	6.3	6.3	7.4
CaO/Na2O	1.5	0.9	0.1	0.3	0.6	0.3
Sr/Y	3.7	6.9	1.8	2.7	7.6	3.1
La/Yb	4.2	5.3	3.7	4.7	5.6	12.6
$(La/Lu)_N$	6.9	8.9	6.1	7.8	9.1	21.4
V (ppm)	31	79	12	5	64	25
Cr	40	40	20	0	20	20
Co	3	10.3	0	1.3	0	0
Ni	18	26	0	8	0	0
Cu	6	11	0	14	0	0
Zn	90	123	0	65	0	0
Ga	20	22.1	21.5	20.5	21.3	24.8
Rb	78	47.7	28.5	42.1	60.5	179.5
Sr	178.5	345	102.5	143	338	117.5
Y	48.8	49.8	55.6	52.72	44.4	37.9
Zr	242	274	328	281	237	309
Nb	7.8	12.5	8.4	9.61	8.9	21.1
Mo	2	3	0	2	0	0
Sn	3	3	2	1.2	2	8
Cs	3.33	1.49	0.64	0.54	2.53	6.2
Ba	1080	822	525	1187	957	744
La	23	28.1	24	29.1	26.5	55.7
Ce	52.5	62.6	58.9	67	59.4	112
Nd	30.9	36.4	34.8	38	31.1	46.5
Sm	7.13	8.46	7.75	9	7.03	8.7
Eu	1.82	2.21	2.2	2.49	1.74	1.22
Gd	7.35	7.82	9.02	9.4	7.05	8.37
Tb	1.22	1.33	1.5	1.54	1.25	1.27
Dy	8.3	8.91	9.78	9.69	7.49	7.51
Ho	1.72	1.84	1.88	2.07	1.68	1.32
Er	5.51	5.33	6.52	6.31	4.97	4.26
Tm	0.84	0.81	0.94	0.95	0.79	0.7
Yb	5.47	5.27	6.44	6.2	4.77	4.42
Lu	0.83	0.79	0.98	0.93	0.73	0.65
Hf	6.8	7.4	8.4	8.5	6	8.2
Ta	0.6	0.9	0.5	0.61	0.6	2
W	12	9	5	0.8	2	1
Pb	13	10	0	0	0	0
Th	3.91	4.21	3.46	4.6	3.51	19.3
U	1.4	1.67	1.34	2	1.33	7.53
Ag	1	1	0	0	0	0
Pr	6.85	7.95	7.6	8.57	7.43	12.8
Tl	0.5	0.5	0.5	0.5	0.5	0.5

Rock	Trondhjemite - Type 2 Suite	Trondhjemite - Type 2 Suite	Trondhjemite - Type 2 Suite	Trondhjemite - Type 2 Suite	Biotite Granite Gneiss - Type 2 Suite	Biotite Granite Gneiss - Type 2 Suite
Orthogneisses/ Arc Granitoids	**Sample GD-08**	**Sample GD-67**	**Sample GD-70**	**Sample GD-71**	**Sample GD-30**	**Sample GD-72**
SiO2 (wt%)	70.52	65.46	69.92	70.78	68.01	68.22
TiO2	0.21	0.56	0.20	0.18	0.24	0.22
Al2O3	15.88	16.31	16.08	15.46	16.84	16.76
Fe2O3	1.90	3.46	1.78	1.70	2.62	2.73
MnO	0.03	0.05	0.03	0.03	0.01	0.01
MgO	0.52	0.72	0.45	0.47	0.66	0.65
CaO	1.71	3.72	1.76	1.45	2.37	2.02
Na2O	6.39	6.65	6.64	6.74	5.55	5.77
K2O	2.05	2.22	2.08	2.08	2.26	2
P2O5	0.08	0.09	0.12	0.12	0.13	0.13
LOI	1.91	3.8	2.06	1.87	0.34	0.47
Total	99.5	99.5	99.3	99.3	99.02	98.97
Na2O + K2O (wt %)	8.4	8.9	8.7	8.8	7.8	7.8
CaO/Na2O	0.3	0.6	0.3	0.2	0.4	0.4
Sr/Y	277.9	153.7	292.9	436.3	147.9	120.3
La/Yb	22.7	11.4	14.7	16.3	15.2	8.7
$(La/Lu)_N$	62.5	20.8	20.8	38.8	22.8	16.3
V (ppm)	33	59	18	23	15	19
Cr	40	90	20	20	0	0
Co	2.6	10.7	0	0	3.2	3.4
Ni	26	33	0	0	9	10
Cu	8	10	0	0	6	5
Zn	78	56	0	0	20	62
Ga	21.9	24	26	24	23	25.7
Rb	40.1	40.7	40.1	36.1	41	39.8
Sr	528	830	615	829	753	834
Y	1.9	5.4	2.1	1.9	5.09	6.93
Zr	88	100	93	102	83	100
Nb	3.5	5.8	3.9	4.8	4.84	5.65
Mo	3	3	0	0	2	2
Sn	1	1	1	1	0.4	0.8
Cs	0.71	0.9	0.88	0.67	0.45	0.4
Ba	1025	1095	1460	1280	1350	1173
La	2.5	5	2.5	3.1	9.1	7.8
Ce	5.6	11.3	5.5	6.6	17.9	15.2
Nd	2.7	6.4	2.9	3.1	9.6	7
Sm	0.58	1.35	0.54	0.7	1.8	1.4
Eu	0.19	0.47	0.19	0.17	0.67	0.42
Gd	0.48	1.33	0.55	0.58	1.68	1.42
Tb	0.04	0.17	0.08	0.05	0.22	0.23
Dy	0.31	1.14	0.45	0.32	1.02	1.34
Ho	0.04	0.17	0.06	0.06	0.2	0.26
Er	0.07	0.47	0.15	0.19	0.61	0.88
Tm	0.01	0.06	0.03	0.03	0.09	0.12
Yb	0.11	0.44	0.17	0.19	0.6	0.9
Lu	0.01	0.06	0.03	0.02	0.1	0.12
Hf	2.7	2.7	2.7	2.7	2.85	3.75
Ta	0.1	0.3	0.2	0.2	0.24	0.26
W	4	5	1	3	0.5	1.1
Pb	8	11	0	0	0	0
Th	0.45	0.6	0.44	0.39	1.6	0.7
U	0.34	0.72	0.33	0.38	0.8	0.42
Ag	1	1	0	0	0	0
Pr	0.64	1.29	0.62	0.8	2.25	1.64
Tl	0.5	0.5	0.5	0.5	0.5	0.5

Rock	Israêlandia Granite	Israêlandia Granite	Bastos Granite	Impertinente Granite (equigranular facies)	Piloândia Granite	Piloândia Granite	Iporá Granite	Impertinente Granite (porphyritic facies)
Post-collisional Granitoids	**pre-kinematic Sample GD-01**	**pre-kinematic Sample GD-02**	**syn-kinematic Sample GD-22**	**syn-kinematic Sample GD-21**	**syn-kinematic Sample GD-03**	**syn-kinematic Sample GD-04**	**post-kynematic Sample GD-16**	**post-kynematic Sample GD-20**
SiO2 (wt%)	70.51	77.53	65.74	67.46	74.3	73.88	71.79	78.48
TiO2	0.28	0.13	0.43	0.5	0.18	0.1	0.18	0.03
Al2O3	14.06	10.4	14.76	13.68	13.12	12.42	14.88	13.24
Fe2O3	2.95	2.35	5.27	3.59	3.14	2.32	2.11	2.12
MnO	0.01	0.01	0.05	0.01	0.01	0.01	0.01	0.01
MgO	0.52	0.01	0.62	0.9	0.25	0.17	0.39	0.19
CaO	1.12	0.19	2.04	1.84	0.25	0.13	0.82	0.4
Na2O	3.61	3.11	3.95	3.48	2.29	3.08	3.73	3.38
K2O	4.12	4.66	3.92	3.98	4.77	4.73	3.89	4.59
P2O5	0.09	0.01	0.11	0.19	0.03	0.03	0.06	0.02
LOI	0.21	0.34	0.43	0.11	0.63	0.37	0.66	0.23
Cr2O3	0.01	0.01	0.01	0.01	0.01	0.01	0.01	0.01
SrO	0	0	0	0	0	0	0	0
BaO	0	0	0	0	0	0	0	0
Total	97.48	98.54	97.33	95.73	98.94	97.2	98.48	102.67
Na2O + K2O (wt%	7.73	7.77	7.87	7.46	7.06	7.81	7.62	7.97
$(La/Lu)_N$	9.9	13.4	15.5	14.5	8.3	13.8	14.8	4.8
V (ppm)	5	8	5	16	5	5	5	5
Cr	0	0	0	0	0	0	0	0
Co	3.4	0.5	4.7	6.5	0.8	0.6	2.5	0.7
Ni	5	5	7	10	6	5	6	5
Cu	8	7	10	31	5	6	5	5
Zn	24	209	85	23	106	69	17	30
Ga	21.2	28	27.1	19.8	27.5	26.9	23.3	25.2
Rb	153.2	140.2	127.1	142.8	154.3	136.1	180	371.5
Sr	142	29	220	249	19	21	238	18
Y	27.97	65.36	120.69	37.29	55.94	82.91	24.7	63.22
Zr	204	673	475	220	553	278	108	134
Nb	15.64	23.08	32.16	17.61	35.13	33.92	12.56	28.8
Mo	2	2	2	2	2	2	2	2
Sn	5.5	3.1	4.1	5.1	5	4.8	3.3	11.2
Cs	5.13	1.07	2.83	3.1	4.75	1.58	6.4	8.59
Ba	657	49	1223	945	270	200	751	110
La	31	76.4	163.1	60.7	65.2	220.7	38.3	23.3
Ce	83.9	158	162.1	114.3	172.8	215.5	56.4	102.8
Nd	29.6	80.4	146.3	45.3	71.3	199.8	29.8	31.2
Sm	6.2	16.8	27.3	7.9	13.5	36.5	5.5	5.5
Eu	0.89	0.4	5.71	1.37	0.46	1.33	0.94	0.19
Gd	6.37	14.93	29.21	7.88	13.3	33.94	5.5	7.56
Tb	0.94	2.22	4.45	1.22	1.96	4.49	0.73	1.23
Dy	5.62	13.11	23.28	6.72	11.55	20.52	4.03	9.21
Ho	1.12	2.53	4.47	1.35	2.3	3.56	0.78	2.15
Er	3.34	7.11	11.91	4.03	7.23	9.25	2.37	7.01
Tm	0.5	0.99	1.68	0.66	1.1	1.23	0.37	1.17
Yb	3.4	6.4	10.5	4.1	7.5	7.8	2.6	8.1
Lu	0.52	0.95	1.5	0.6	1.12	1.07	0.43	1.21
Hf	6.87	13.99	12.94	7.02	15.19	9.93	4.34	6.77
Ta	1.35	0.57	2.07	1.7	2.05	2.11	1.17	3.48
W	1.2	1.5	0.8	0.6	4.7	1.5	1.6	1.7
Pb	0	0	0	0	0	0	0	0
Th	14.6	10.7	9.8	16	12.5	13.7	16	47.9
U	4.63	3.43	3.94	5.13	3.21	3.9	5.44	5.16
Ag	0	0	0	0	0	0	0	0
Pr	7.71	20.28	37.08	12.44	18.03	53.91	8.07	8.6
Tl	0.5	0.5	0.5	0.5	0.5	0.5	0.5	0.9

4. THE FAZENDA NOVA GOLD DEPOSIT, GOIÁS MAGMATIC ARC: LATE NEOPRETOROZOIC INTRUSION RELATED AURIFEROUS MINERALZATION CONTROLLED BY INTRACONTINENTAL STRIKE-SLIP FAULTING.

Abstract

The Fazenda Nova gold deposit (650 koz with 4.0 g/t Au of inferred resource, cut-off of 2.0 g/t Au) consists of stock-work Au-As mineralization hosted in late-Neoproterozoic dikes located in the Goiás Magmatic Arc, central Brazil. The dikes consist of a set of post-collisional ilmenite-bearing dolerites, diorite porphyries, trachyte, syenite porphyry (named as Bacilândia Intrusions). U-Pb dating indicates at least two pulses of dike intrusions: the earliet comprise small volume dikes with ages varying from 593 ± 5 to 590 ± 5 Ma and a second pulse, comprises a large volume of dikes with age between 574 ± 7 to 572 ± 5 Ma. Three hydrothermal alteration stages were identified in Fazenda Nova deposit: i) the early or main stage comprise a pervasive sericitization of feldspar and biotitization of mafic minerals with stock-work of quartz associated with disseminated sulfide assemblage of arsenopyrite-pyrrhotite-stibnite in addition to hydrothermal siderite, scheelite, rutile and apatite. The most common sulfide in this stage is fine-grained needle arsenopyrite that hostes inclusion of gold, galena and pyrite grains. The temperature estimated for crystallization of acicular arsenopyrite and pyrrhotite along with gold was of 340°C based on arsenopyrite geothermometry; ii) the intermediate stage is represented by stockworks of calcite-quartz veins associated with hydrothermal chlorite, tourmaline, epidote, titanite and disseminated sulfide assemblage of pyrrhotite-arsenopyrite-pyrite. The arsenopyrite at this stage display tabular texture with no sulfides or gold inclusions. The crystallization temperature of tabular arsenopyrite-pyrite was estimated at 305°C. C-O isotopes data from calcite veins provide $\delta^{13}C$ values ranging from -9.68 to -11.57‰ and $\delta^{18}O$ values from 12.87 to 13.84‰, these values are equivalent to those of hydrothermal mantle-juvenile/magmatic carbonates iii) the late stage is veining and brecciation infilled by monotonous calcite-ankerite with no gold mineralization or hydrothermal alteration

The dikes and gold mineralization present strong relationship with the crustal-scale strike-slip Bacilândia Fault. The Bacilândia Fault is a second order crustal-scale fault that branch out of the major crustal-scale Moiporá-Novo Brasil Shear Zone (MNBSZ) along the NNW direction. The Bacilândia fault played important role to channelize melts to uppercrust and mineralized hydrothermal fluids. The major activity of this fault took place at ~572 Ma with emplacement of second pulse of dikes and most likely development of hydrothermal stages in Fazenda Nova deposit. The Fazenda Nova deposit is classified as epizonal Reduced Intrusion Related based on the follow evidence: i) mineralization developed during post-collisional tectonic setting above previously metasomatized subcontinental lithosphere mantle; ii) the dikes crystallized from metaluminous magmas with primary oxidation state that form ilmenite-series intrusions iii) high geothermal gradients indicate by ore deposition at temperatures of 340° to 300°C and vein textures formed only at shallow depths (<4 km); iv) metal association of Au-As-W-Sb; v) volatile saturation induced by magmatic processes such as fractional crystallization or magma mixing; vi) CO_2 hydrothermal veins with C-O isotopes displaying magmatic/mantle fluids affinities

Key words: Goiás Magmatic Arc, post-collisional magmatism, Reduced Intrusion Related gold deposit, intracontinental strike-slip.

4.1. Introduction

The mineral deposits identified, so far, in the Goiás Magmatic Arc are part of a convergent accretionary orogen with tectonic evolution between 900 and 600 Ma. This evolving convergent plate margin scenario started with the 890-860 Ma old Cu-Au porphyry Chapada deposit related to intra-oceanic magmatic arcs (Oliveira et al., 2015) and finished with Ni-Cu mafic–ultramafic synorogenic intrusions emplaced at 626 Ma during the Brasiliano/Pan-African Orogenic Cycle in Brazil (Laux et al., 2004, Mota e Silva et al., 2011). Following this orogenic cycle post-collisional A-type magmatism took place at 600 to 500 Ma associated with intracontinental strikes-slip faulting (Marques, 2017). In this last event, there is no record of occurrence of mineral deposits.

Two tectonic processes are widely recognized to generated ore deposit in post-collisional settings: large-scale lithosphere thinning and intracontinental strike-slip shear zones. The lithosphere thinning and gold metallogeny is very well documented in the North China Craton by Guo et al.,(2013); Li and Santosh (2013); and Yang et al., (2014). In these articles the authors concluded that the gold mineralization resulted from multiple tectonic processes including, delamination of lower crust, mantle upwelling and mobilization and concentration of the ore metals largely associated with crust–mantle interaction processes. The source of gold includes the basement rocks and the metasomatized and enriched mantle developed during older tectonic cycles associated with the Precambrian and Phanerozoic evolution of the North China Craton. Intracontinental strike-slip faulting define continental deformation zones and lithospheric blocks, which may reach the deep crustal level and are able to act as conduits for mantle flow and upwelling that generate magmatism and circulation of hydrothermal fluids (Storti et al., 2003). The magma-fluid generation is caused by upwelling of asthenospheric material inducing partial melting of thickened juvenile mafic lower crust or delaminated mafic lower crust. These melts are channeled to the upper crust by trans-lithospheric strike-slip faults. In both tectonic process the thermal source for circulation of hydrothermal fluids may be derived from mafic underplating, alkaline magmas and A-type granitic intrusions, generating mineral deposits unrelated to convergent plate margins (Vauchez and Tommasi 2003, Schaltegger and Brack, 2007; Pirajno et al., 2008 , Pirajno 2010).

Several mineral deposits are documented in the literature related to lithosphere thinning and intracontinental strike-slip faults, including: magmatic Ni-Cu-PGE and Fe-Ti-V in northwest China (Pirajno et al., 2008); Cu-Au porphyry-skarn in eastern China (Pirajno and Zhou, 2015); Fe-Cu-Au-(ETR-U), Cu-Au veins in the Iberian Pyrite Belt (Tornos et al., 2005); polymetallic mineralization (Ag-Sb-Pb) related to alkaline mafic intrusions in northwest Mongolia (Borisenko et al., 2006); orogenic-Au deposits, low-sulphidation epithermal Au-Ag, granitoid-related greisen, rare earth pegmatites, intrusion related Au in central Asia (Pirajno et al., 2009; Yakubchuk et al., 2005); and some of the granitoid hosted Au deposits in the Jiandong peninsula, north china craton (Wang et al.,1998; Zhao et al., 2012; Li and Santosh., 2014).

The Fazenda Nova gold deposit has recently been defined in the Neoproterozoic Goiás Magmatic Arc in the central portion of Brazil (Fig. 4.1).The inferred resource has been estimated at 650 koz at a 4.0 g/t Au (cut-off grade of 2.5 Au g/t, Yamana press release, 2013). The resource is open at depth and along strike. Fazenda Nova was mined during 2005-2007 for the oxide ore (73 koz of Au), but the refractory nature of the sulfide ore and the complex structural control have collectively hindered development of the underlying sulfide resource. An earlier article classified the deposit as orogenic gold (Oliveira et al., 2014) but advanced drilling has revealed the relationship of Au mineralization with post-collisional alkaline intrusive rocks.

This paper documents the petrographic, geochemical and geochronological signatures of the Fazenda Nova gold deposit related to lithosphere thinning and strike-slip intracontinental shear zones during the late Neoproterozoic/Cambrian. We focus our study in the magmatic process that led from gold extraction in the mantle to gold precipitation in the shallow epizonal environment. Additionally, a characterization of fluids and hydrothermal alteration is also proposed, using stable isotope and sulfide geothermometry. These results provide a model describing the hydrothermal evolution and gold formation at the Fazenda Nova deposit

4.2.Regional Setting

The Tocantins Province is comprised of three orogenic belts formed during the Neoproterozoic Brasiliano cycle: the Paraguay, the Araguaia, and the Brasília belts. They were developed as a result of the convergence and collision of three continental blocks: Amazon, São Francisco/Congo, and Paranapanema (or Paraná) (Pimentel et al., 2001). The crustal growth started with the break-up of Rodinia, followed by a prolonged period of island and continental arc magmatism, between 930 – 635 Ma that was terminated by the collision related ~630 Ma Brasiliano orogeny (Pimentel and Fuck, 1997, Pimentel et al., 2000) with closure of the Goiás-Pharusian Ocean. (Kroner and Cordani 2003, Cordani et al., 2013).

The Fazenda Nova Au deposit is within the Brasilia Fold Belt (Fig. 4.1), which is made up of external and internal tectonic zones. The eastern external zone is a craton-verging fold-and-thrust belt, comprising thick passive margin sedimentary deposits, deformed and metamorphosed under greenschist facies or lower P-T conditions. The internal, western zone of the belt comprises: (i) the metamorphic core of the belt including the Neoproterozoic Anápolis-Itauçu granulites (locally UHT granulites) separated by faults from the mainly turbiditic lower grade metasedimentary rocks of the Araxá Group which include small ophiolite remnants; (ii) the Goiás Massif made of Archean granite-greenstone terrains, Paleoproterozoic orthogneisses largely covered by folded metasedimentary sequences, recently interpreted as the São Francisco pericratonic western margin; (iii) and the Goiás Magmatic Arc in the western part which hosts the Fazenda Nova Au deposit (Pimentel and Fuck 1992; Fuck et al., 1994; Pimentel et al., 2000; Pimentel et al., 2004; Valeriano et al., 2008, Della Giustina et al., 2009, Jost et al., 2010 Fuck et al., 2014).

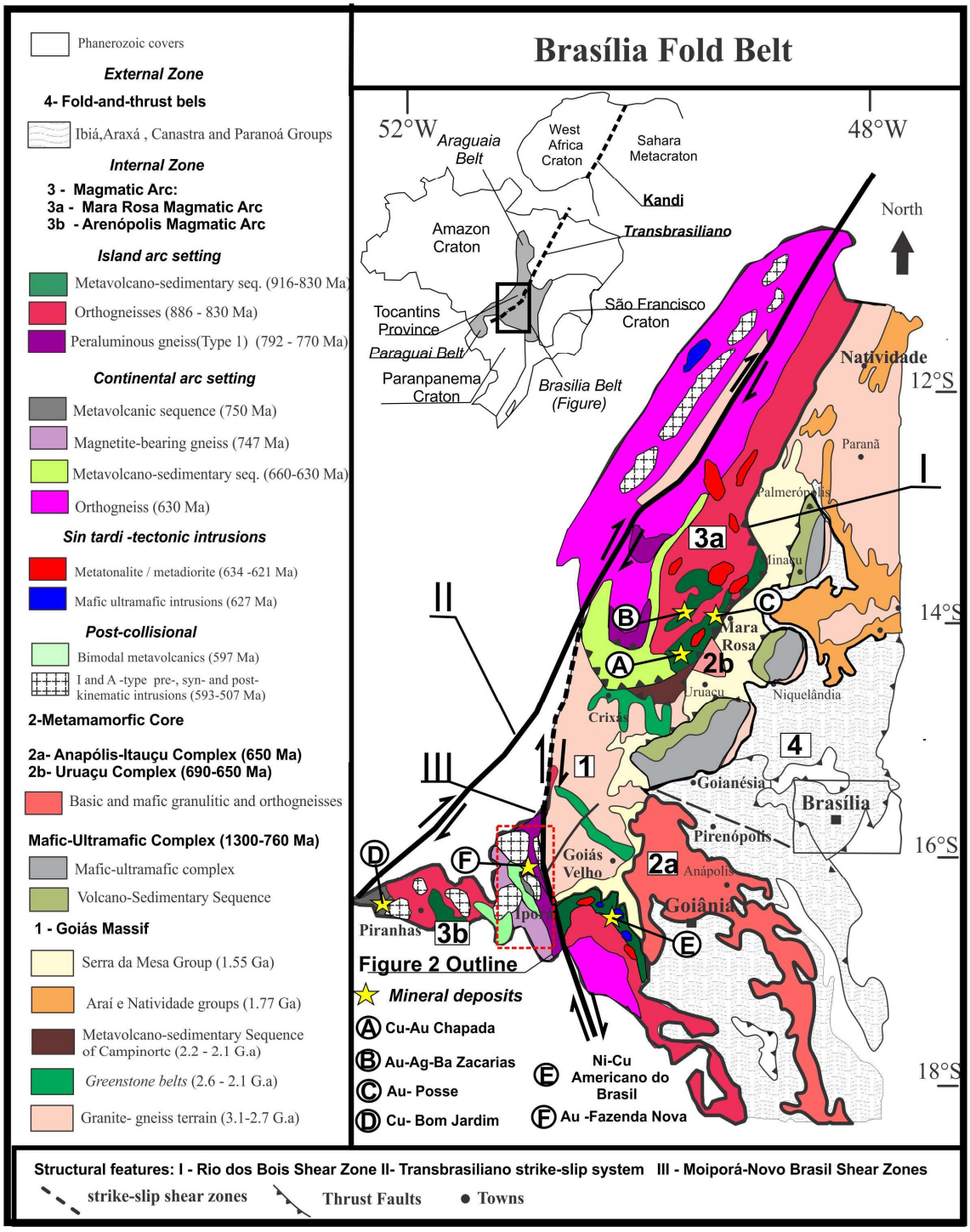

Figure 4.1 – Geological sketch map of the Brasilia Fold Belt with the main mineral deposits of the Goiás Magmatic Arc (modified from Fuck et al. 1994, Dardenne 2000).

4.2.1 -The Goiás Magmatic Arc

The Goiás Magmatic Arc is one the largest Neoproterozoic juvenile terrains exposed in the world, with a minimal NNE strike length of 1000 km, which may be longer since the southern and northern portion are covered by Paleozoic–Mesozoic sedimentary rocks. The Goiás Magmatic Arc is exposed in two areas separated by the Archean rocks of the Goiás Massif: the northern segment named the Mara Rosa Magmatic Arc and the southern segment known as the Arenópolis Magmatic Arc (Fig. 4.1).

Available geochronological data reveal a complex evolution of the arc system, with four main episodes of magmatism and genesis of mineral deposits (table 4.1): (i) the earliest event took place between ca. 900 and 770 Ma, comprising tonalitic/dioritic/dacitic rocks formed in an intra-oceanic setting that hosts Cu-Au porphyry and Au-Ag-Ba volcanogenic deposits (Poll, 1994;Pimentel et al., 2000, Laux et al., 2005, Oliveira et al., 2015); (ii) the second episode is represented by continental arc volcanism at ca. 750 Ma associated with volcanogenic disseminated Cu deposits such as the Bom Jardim deposit (Guimarães et al., 2012); (iii) the third episode, dominated by felsic volcanic and granitic rocks dated at ca. 660-630 Ma displays geochemical and isotopic affinities with continental arc settings. This event was followed by emplacement of syn-orogenic tonalitic, dioritic and mafic-ultramafic intrusions associated with Ni-Cu mineralization (Laux et al,. 2004; Mota e Silva 2011) ; iv) and the post-collisional magmatism that took place during protracted period ca. 597 to 504 Ma, representing the transition from calc-alkaline to alkaline, high-K and A-type dominated assemblages. (Pimentel et al., 1996; Marques, 2017) Despite the coeval tectonic events, the Mara Rosa and the Arenópolis arcs display remarkable differences. The former is dominated by regional amphibolite grade metamorphism and low angle foliation related to the development of isoclinal folding and thrust to reverse faults whereas metamorphism in the latter is greenschist facies and foliation is of high angle and related to the development of strike-slip faults.

The Fazenda Nova Au deposit is located in the Jaupaci Belt in the central part of Arenópolis Magmatic Arc, which comprises orthogneisses and granitoid intrusions exposed between NNW trending metavolcanic rocks of the Jaupaci Sequence (Fig. 4.2). Marques (2017) defined five main periods of magmatism in this Belt:

i) The 770 Ma magmatic event is represented by ilmenite-bearing, calc-alkaline, metatonalite and granodiorite of Type 1 Suite, generated in an island arc setting. The reservoir for this event is predominantly from juvenile material suggested by the T_{DM} model ages of 0.86 to 0.91 Ga and +5.41 εNd (T) values.

ii) The 750 Ma magmatic event took place in a continental arc-back arc setting comprising adakitic, magnetite-bearing granites, trondhjemite and equivalent volcanic rocks represented by metarhyolites of the base of the Jaupaci Sequence. These plutonic/volcanic rocks are mainly sourced from a juvenile arc-derived reservoir suggested by T_{DM} model ages 1.1 to 1.26 Ga and ε_{Nd} (T) values between +1.1 to +4.6.

iii) The 597-585 Ma event comprising I and A-type pre-kinematic granitoid intrusions, mafic dikes and bimodal volcanism of the upper part of the Jaupaci Sequence, including N-MORB basalts and ilmenite-bearing A-type felsic volcanics. Neoproterozoic T_{DM} model ages and positive ε_{Nd} (T) of +2.3 to +4.21 of these rocks are consistent with an origin involving partial melting of Neoproterozoic juvenile sources.

iv) The 577-539 Ma development of crustal-scale intracontinental translithospheric strike-slip faults followed by the emplacement of A-type syn-kynematic granitoids.

v) The 511-506 Ma post-kynematic A-type granite intrusions. The syn-kinematic and post-kinematic granitoids show slightly positive to negative ε_{Nd} (T) values, varying from +1.1 to -19.

.

Table 4.1 - Summary of isotopic data for the Arenópolis Arc and related deposits. Quoted references (1) Pimentel and Fuck 1992; (2) Pimentel and Fuck (1994); (3) Pimentel et al., (1996); (4) Pimentel et al., (1997); (5) Dantas et al., (2001); (6) Pimentel et al., (2003); (7) Laux et al., (2004); (8) Laux et al., (2005); (9) Matteini et al., (2010); (10) Guimarães et al., (2012) ; (11) Motta Araujo (2013); (12) Oliveira et al., (2015); (13) Frasca (2015); (14) Marques, (2017); * Oliveira (2017) unpublished data.

GOÍAS MAGMATIC ARC MINERALIZATIONS AND ISOTOPIC DATA SUMMARY							
Segment	Setting	Volcano-sedimentary Sequence	**Age: U-Pb Zircon (Ma)**	**ε_{Nd} (*T*)**	Plutonics	**Age: U-Pb Zircon (Ma)**	**ε_{Nd} (*T*)**
North Segment Mara Rosa Magmatic Arc	Island Arc	Mara Rosa Sequence felsic metavolcanoclastic rock	916 ± 5 (9)		Porphyry to equigranular metadiorite (Cu-Au porphyry)	884 ± 14 864 ± 8 (12)	
		Mara Rosa Sequence metavolcanoclastic rock	908 ± 8 (12)		Metatonalite	856± 7 (2)	+3.7
		Mara Rosa Sequence felsic Metavolcanic (volcanogenic Au-Ag-Ba)	906 (*)		Granite gneiss	811 ±7 / 792 ±8 (9)	-9.3 /-7.2
		Mara Rosa Sequence felsic Metavolcanic (Orogenic Au)	862± 7 (4)	+4.6			
	Continental Arc	Santa Terezinha Sequence felsic Metavolcanic	661 ± 7 (5)				
	Syn-tectonic				Metadiorite	638 ± 3 (9)	+0.8
					Metadiorite	634 ± 3 (9)	
	Post-collisional				A-Type Granites	540± 5 / 528± 5(13)	-2.26/ -2.02
Southern Segment Arenopolis Magmatic Arc	Island Arc	Arenópolis Sequence Metarhyolite	900 ± 8 (2)	+4.6	Arenópolis Granite Gneiss	899 ± 7 (1)	+3.2
		Côrrego da Boa Esperança amphibole schist	886 ± 5 (7)	+6.0	Gabbro (Morro do Baú)	890 ± 6 (6)	+6.9
		Anicuns-Itaberaí amphibolite	830 ± 8 (7)	+5.0	Sanclerlândia Gneiss	820 ± 7 (8)	+4.0
					Iporá Granito Gneiss	804 ± 6 (8)	+1.8
					Granito Creoulos	782± 12 (8)	+3.8
					Suite- 1 Metatonalites	770± 7 (14)	+4.1
	Continental Arc	Bom Jardim felsic volcanoclastic (Cu volcanogenic)	749 ± 6 (10)	+1.0	Suite- 2 Granite gneiss	748± 9 (14)	+4.6
		Jaupaci metarhyolite	748± 9 (14)	+1.2	Matrinxã granite gneiss	699± 9 (8)	+1.2
					Palminópolis gneiss	637 ± 2 (8)	-6.4
					Firminópolis/Turvânia granite-gniess	634± 5 / 630± 5(8)	-4.6
	Sin-tectonic				Americano do Brasil mafic ultramafic complex (Ni-Cu)	626 ± 8 (7)	+3.0
					Anicuns Santa-Barbara Suíte	622 ± 6 (7)	+2.6
	Post-collisional A-type pre-kinematic volcanic/intrusion	Jaupaci felsic metavolcanics	597± 10 (14)	+4.7	Gabbro	593 ± 4 (14)	+6.9
					Israêlandia Granite	587± 20 (3)	+2.3
	A-type syn-kinematic intrusion				Basto Granite	577± 5 (14)	
					Impertinente Granite (equigranular)	561± 5 (14)	
					Messianópolis Granite	542 ± 4 (12)	-20
					Piloândia Granite	539± 9 (12)	-2.2
	A-type post-kinematic intrusion				Iporá Granite	511 ± 8 (14)	+0.7
					Impertinente Granite (porphyry)	506 ± 4 (14)	-4.6

4.2.2 -Regional Structures

The Fazenda Nova deposit lies between two major dextral strike-slip faults (Fig. 4.1), the Transbrasiliano Lineament in the west and Moiporá-Novo Brasil shear zones (MNBZ) in the east. The Transbrasiliano is a continental scale discontinuity running from Argentina to northeast Brazil, also extending into the African continent under the name of Kandi Lineament with more than 4000 km in length. The Transbrasiliano Lineament is defined by a series of deep ductile shear zones probably reaching the base of the lithosphere, utilizing weak lithospheric zones and/or block boundaries formed during continental collisions (Cordani et al., 2013). The nature of the Transbrasiliano is ambiguous being interpreted either as a collisional suture, or as a first order strike-slip zone generated by the lateral escape along the collision zone between the Amazonian and São Francisco cratons (Hasui et al., 2012). The most accepted model in the literature was put forward by Fuck et al., (2013) and interprets the lineament as an intracontinental strike slip deformational system with dextral motion or, according to Ganade de Araújo et al., (2014), the Transbrasiliano Lineament is a transform plate boundary also with dextral motion. In the Arenópolis Arc the Transbrasiliano Lineament includes strong N30°E-trending gravity and magnetic gradients, those structures and weakness zones may have facilitated the action of magmatic and hydrothermal processes (Curto et al., 2015).

The Moiporá-Novo Brasil is a dextral crustal-scale N-S shear zone that branches out of the major Transbrasiliano shear system and separates the Neoproterozoic rocks of the Jaupaci Belt from the Goiás Massif Archean block (Fig 4.2). The peak of strain was estimated by Marques (2017) at ~577-539 Ma based on the syn-kinematic granitoids ages that were emplaced into this shear zone. The Fazenda Nova gold deposit is located along a NNW splay (named in this study as the Bacilândia Fault) of the main branch of the MNBSZ. Smaller gold occurrences are also recognized along the Bacilândia Fault (Fig 4.2).

4.3. Geology of the Fazenda Nova gold deposit

4.3.1. Local Geology

The defined gold resources of the Fazenda Nova deposit are distributed in the N-S and E-W trending Lavrinha and the Vital orebodies, respectively, which lie within and adjacent to a 1.2 km long, north-northwest trending swarm of dolerite ,trachyte and syenite porphyry dikes (Fig 4.3). The country rocks of the dikes encompass the following units: i) The oldest comprise Type-1 ilmenite-bearing metatonalite exposed as tectonic slices within the Jaupaci Sequence, a rock yielding a U-Pb zircon age of 770 ± 7 Ma (Marques 2017); ii) the metatonalites are intruded by a small pluton of Type-2 adakitic trondhjemite, the east border of which is limited by the Bacilândia Fault where a zone of deformed breccias with clasts of metatonalite and trondhjemite in a matrix of sericite, pyrite and ilmenite was developed. The trondhjemite was dated at 753 ± 12 Ma by U-Pb on zircon (Marques 2017); iii) the volcanic rocks are represented by post-collisional bimodal rocks from the upper part of the Jaupaci Sequence. The rock types comprise epidote-chlorite schist representing N-MORB basalts, whereas biotite-feldspar schist and muscovite-feldspar schist represent A-type metadacite and metarhyolite, respectively. The metarhyolite was dated by U-Pb zircon at 598 ± 10 Ma (Marques 2017). The metamorphic assemblage of epidote-chlorite in mafic volcanics indicates that these rocks were submitted to greenschist-facies metamorphism.

The swarm of mineralized alkaline mafic, intermediate and felsic intrusions was emplaced as dikes, sills, plugs or small bodies (Fig. 4.4A) with NNW main direction. Individual dikes and sill range from 2 to 35 m in width, and plugs and small stocks up to 50 meters. The contacts get indurated and foliation is blurred adjacent to the dyke walls. It is not clear whether this texture destruction results uniquely from thermal re-crystallization at the contact of the dykes. In this work we defined the set of dikes at the Fazenda Nova deposit as the Bacilândia Intrusions. The field relationships indicate that all intrusive phases were emplaced in at least two pulses, where the oldest exhibit a penetrative foliation while the youngest are undeformed, therefore showing that the Bacilândia Intrusions represent a long-lived magmatic event (Fig. 4.4B). The petrographic characteristics of the six intrusive phases are discussed below in their relative order of emplacement.

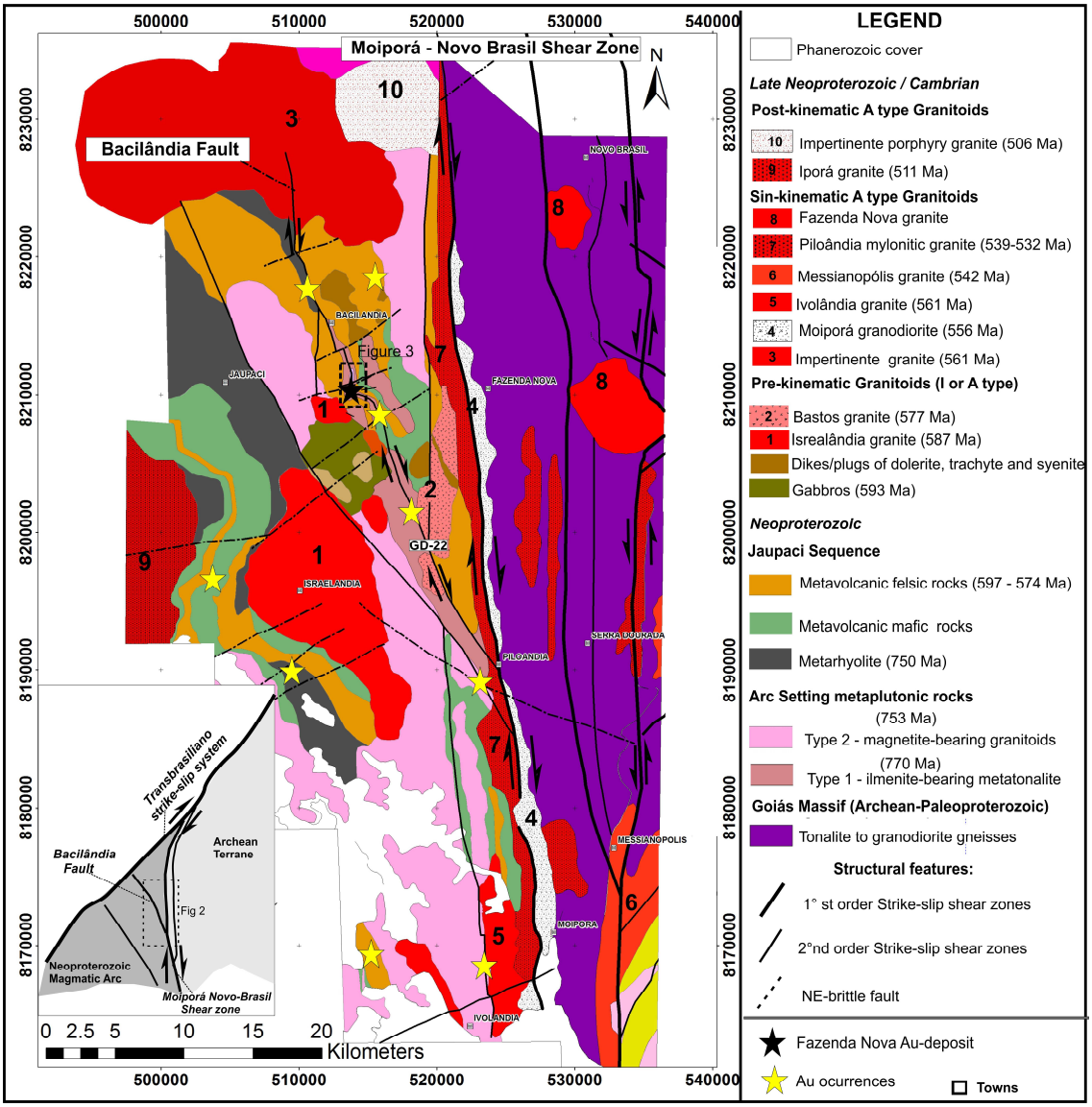

Figure 4.2 – The Geological map of the Jaupaci Belt showing the main structural features and location of Fazenda Nova gold deposit and gold occurrence.

Gabbro is a coarse-grained intrusion with phaneritic texture containing euhedral pyroxene, plagioclase, hornblende and large amounts of coarse ilmenite. These rocks usually show strong hydrothermal alteration and deformation, in which pyroxene is altered to chlorite, plagioclase to sericite and ilmenite to rutile/leucoxene. Accessory phases include igneous titanite, zircon and magmatic sulfides (pyrrhotite and chalcopyrite). A small plug of gabbro was dated by Marques (2017), southwest of the Fazenda Nova property on U-Pb zircon age that yielding 593 ± 4.7 Ma. Sm–Nd isotopic analysis of the same sample gives a T_{DM} model age of 0.88 Ga and positive ε_{Nd} (T) of +3.97

Dolerite represents the largest volume of dikes of the Bacilândia intrusions. It is a fine-grained, blackish rock with aphanitic to porphyritic texture containing 20 to 25 vol.% of plagioclase phenocrysts with occasional mafic phenocrysts of hornblende, set in a groundmass of fine-grained biotite and plagioclase. The biotite is the main component of the aphanitic groundmass with dark-brown pleochroism usually associated with ilmenite. Amphibole shows dark to pale-green pleochroism and occurs as disseminated elongated grains. The accessory phases are ilmenite (altered to rutile), and magmatic sulfides (pyrrhotite and chalcopyrite). The dolerite intrusions appear to have been emplaced at shallow subvolcanic levels as they often contain primary vesicles/amygdales and, locally, breccias formed at the margins of the dikes (Fig. 4.4 C).

Trachyte is a sub-volcanic porphyry intrusion which contains aligned large (5mm to 1 mm) K-feldspar phenocrysts (Fig. 4.4D), within an aphanitic groundmass with biotite, plagioclase, amphibole and locally quartz. Sanidine presents typical Carlsbad twinning and is locally altered to fine-grained sericite. The biotite shows brown pleochroism and is usually associated with ilmenite/rutile. The amphiboles are usually altered to fine-grained brown biotite. The accessory phase includes ilmenite (commoly altered to rutile), zircon, apatite and trace of magmatic sulfides (pyrrhotite and chalcopyrite).

Diorite porphyry is a stock-like intrusion containing plagioclase, biotite and hornblende phenocrysts in an aphanitic biotite-feldspar-quartz matrix (Fig 4.4 E). The plagioclase phenocrysts are rarely preserved, showing alteration into fine-grained sericite and lesser clay minerals. The biotite occurs in the aphanitic matrix or as phenocrysts with up to 0.5 mm-sized lamellae with brown pleochroism. The hornblende is scarce and is commonly altered to fine-grained brown biotite. Accessory phases include ilmenite, rutile, zircon, apatite and trace of magmatic sulfides (pyrrhotite and chalcopyrite).

Syenite porphyry contains K-feldspar and biotite phenocrysts in aphanitic biotitic, quartz-feldspar matrix. The K-feldpar phenocrysts are locally altered to fine grained sericite, carbonate-rutile alteration. The biotite occurs in the aphanitic matrix or as phenocrysts with up to 0.3 mm-sized lamellae disseminated in the rock. Accessory phases include ilmenite, rutile, zircon and magmatic sulfides (pyrrhotite and chalcopyrite). Syenite commonly displays mafic microgranular enclaves (MMEs) with centimeter to decimeter size (Fig. 4.4F). The mineralogy of mafic enclaves is identical

to that of host syenite, but mafic enclaves contain higher amounts of mafic minerals (~20 vol.% of biotite and ~10 vol.% of hornblende). K-feldspar and plagioclase crystals inside the enclaves and in the host syenite are similar in size in some places and feldspar crystals commonly crosscut the enclaves/host boundary.

Lamprophyre occurs as small dikes composed of olivine phenocrysts within a dark fine grained groundmass composed of biotite (phlogopite), plagioclase, apatite, and less ilmenite. The lamprophyre dikes are clearly later than other dikes as they lack hydrothermal alteration or deformation.

Several measures of magnetic susceptibility were taken in dikes from drill core samples. The values showed low to very low magnetic susceptibility (0.26 to 0.56 SI x 10^{-3}) also supporting that dikes belongs to ilmenite series.

.

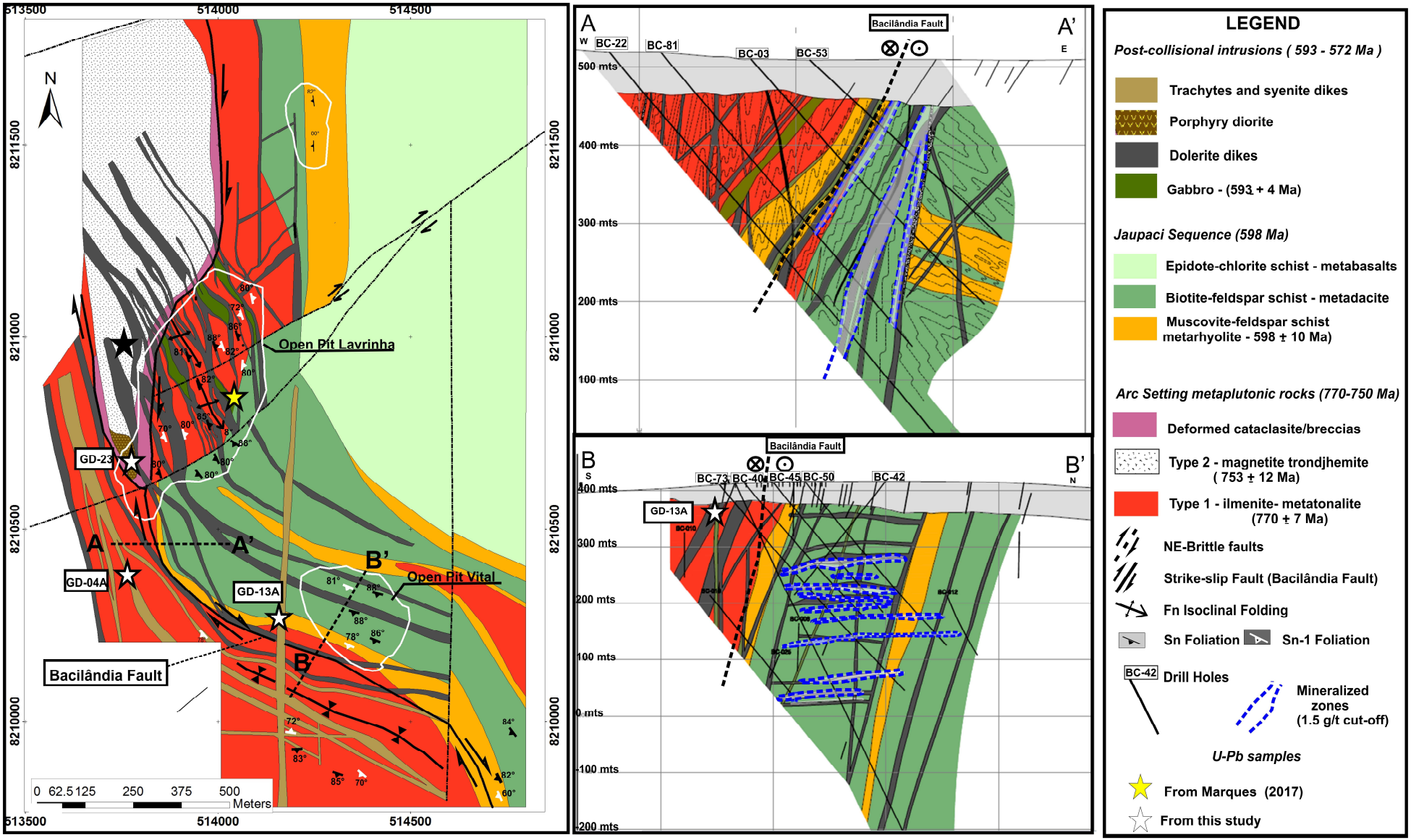

Figure 4.3 - Geology map and cross-sections of the Fazenda Nova property showing the location of the U-Pb samples of Marques (2017) and samples collected in this study. Cross sections at A-A´ and B-B' showing the slight to strong discordance between ore zones (>2.0 g/t Au) and the dike/sill complex.

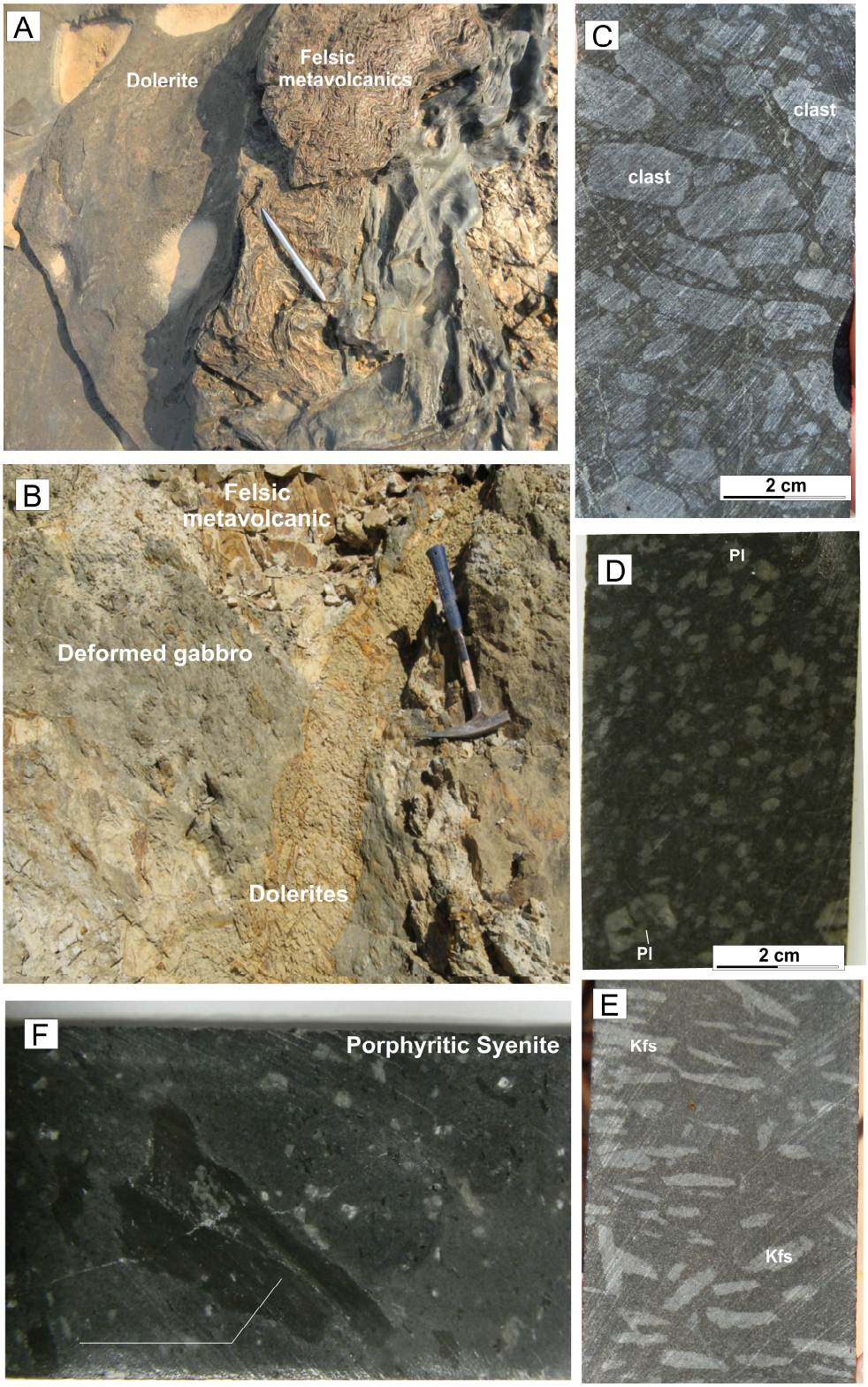

Figure 4.4 - Main textural features of dikes and sills of the Fazenda Nova deposit: A) Outcrop showing metric undeformed dykes of dolerites intruded into folded felsic metavolcanics of the Jaupaci Sequence; B) Outcrop in the Fazenda Nova open pit showing two events of dike intrusion, felsic metavolcanics are intruded by deformed gabbros, which in turn are crosscut by undeformed dolerites; C) Intrusion breccias formed at the margins of the dolerite dykes which contain clasts of the wall rock in a fine-grained

magmatic cement of mafic composition; D) sample of porphyry diorite with phenocrysts of plagioclase (Pl) sample collected for U-Pb zircon analyses); E) drill core sample of trachyte showing oriented phenocrysts of K-feldspar (Kfs) and fine biotite rich groundmass; F) drill core sample of porphyritic syenite with centimetric mafic enclave and microgranular enclaves.

4.3.2.Local Structures and stages of deformation

The structural geology of the Fazenda Nova deposit has been mapped mainly through study of core samples and limited surface exposures. The deformation took place during three main phases (D_{n-1}, D_n, D_{n+1}) with involvement of the Jaupaci Belt rocks in the development of the Bacilândia fault.

Dn-1 phase produced essentially S_{n-1} penetrative schistosity marked by the orientation of micaceous minerals. This foliation is parallel to the compositional banding (S_0) defined by alternate micaceous and quartz-feldspar layers. The strike of the Sn-1 schistosity varies from NNW-SSE in the north to WNW-ESE in the south and the dip changes from sub-vertical to steeply west- or east-dipping, thus delineating a possible post-D_{n-1} macrofold affecting the S_{n-1} foliation. This deformation affected Type-1 tonalite, Type-2 trondhjemite and volcanic rocks of the Jaupaci Sequence, whereas dikes and sills do not show S_{n-1} fabrics. Therefore, such dikes/sills must post-date D_{n-1} ductile deformation

D_n structures record ENE-WSW shortening that generated folds (F_n) with NNW striking axial planar foliation (S_n) and strike-slip faults (Moiporá-Novo Brasil Shear Zone, Bacilândia fault and other secondary faults). The F_n folds are asymmetric, up-right, tight to isoclinal with NNW-ESE striking axial planes and fold axes gently plunging to the SSE. These folds are typically centimetric to a few meters in wave length, although some may reach up to regional scale. The S_n foliation is a penetrative axial-planar schistosity with a NNW strike and sub-vertical to steep dip to the west. In the south of the deposit the Sn foliation is rotated into a WNW direction and a steep dip to the south. The interference of S_n with S_{n-1} produced a strong intersection lineation (L_n) parallel to the F_n fold axes as well as L-tectonites in the hinge zones of such folds (Fig. 4.5A). Additionally in the Dn event is developed the Bacilândia Fault, which comprises N-S to NNW strike-slip fault. Such important fault reworked the S_{n-1} foliation generated a variety of fault rocks, such as cataclasites, deformed breccias and mylonites.

The cataclasites/breccias are mainly observed in the metaplutonic rocks, commonly the contact between the trondhjemite (Type-2) and metatonalite (Type-1) is marked by a broad corridor (~ 25 meters) of progressive foliation and comminution of both rocks. The mylonites are represented by fine-grained rocks (as volcanic rocks and dolerites dykes) with S-C foliation (Fig. 4.5 B). This foliation is better developed in fine-grained rocks such as volcanic rocks and dolerites dikes (Fig. 4.5 B). Quartz segregations and directional stretching lineations are commonly observed in felsic volcanic rocks. Most kinematic indicators along the Bacilândia fault indicate dextral slip. The D_n deformation affected some dikes along the Bacilândia fault showing that the emplacement of early, small volumes of dikes is pre to syn-D_n ductile deformation. However, the bulk of the dikes are not affected by the S_n foliation.

A large volume of northwest dikes/sills were emplaced after the Dn deformation. These dikes are folded and deformed by a later D_{n+1} deformation that rotated the S_{n-1}/S_n fabrics and the Bacilândia Fault from the northerly trend to an east-west trend. The rotation of foliation is related to box folding (F_{n+1}) with an NE-SW and NW-SE pair of axial planes (S_{n+1}) with steep plunging fold axes to NNE (Fig. 4.5 C and D). The S_{n+1} foliation is a discrete spaced cleavage or fracture cleavage with NE direction mainly observed in fine-grained rocks as the dikes and metavolcanics. NE and N-S conjugate brittle faults with dextral kinematics displaced dikes and older foliations and are interpreted as the late stage of deformation in the Fazenda Nova Deposit.

.

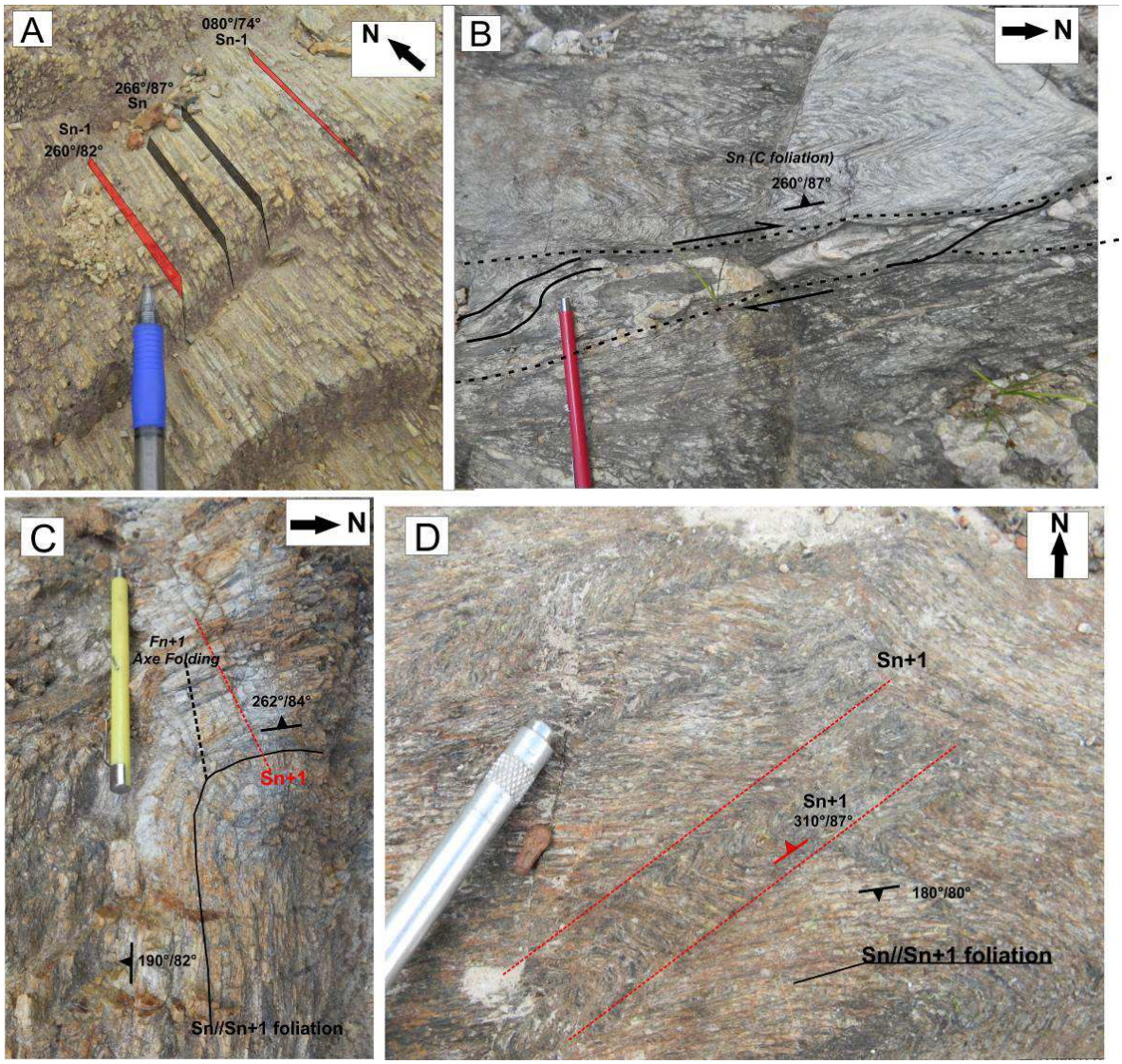

Figure 4.5 - Deformational structures of the Fazenda Nova deposit. All photos are from open pit exposures. A) Outcrop of type-1 metatonalite in the Lavrinha open pit showing strong intersection lineation between the Sn-1 and the Sn foliations in the Fn fold hinge; B) Felsic metavolcanic rocks (muscovite-feldspar schist) with S-C milonitic foliation with dextral offset produced by the Bacilândia fault (NNW striking); C) Rotation of the S_n//S_{n-1} foliations related to box folding (F_{n+1}) with steep NNE-plunging fold axes; D) S_{n+1} spaced cleavage with NE-SW direction in felsic metavolcanics.

4.4. Analytical procedures

4.4.1. U–Pb and Sm-Nd isotopic analyses

Zircon concentrates were extracted from ca. 10 kg rock samples using conventional gravimetric and magnetic techniques. Mineral fractions were hand-picked under a binocular microscope to obtain fractions of similar size, shape and color. For in situ U-Pb analyses, hand-picked zircon grains were mounted in epoxy mounts and polished to obtain a smooth surface. Before analyses, mounts were cleaned with dilute (ca. 2%) HNO_3. Backscattered electron images or cathodoluminescence images were obtained using a FEI-QUANTA 450 working at 10 kV at the University of Brasília.The U-Pb LA-ICPMS analyses followed the analytical procedure described by Buhn et al., (2009). In this LA-ICPMS U-Pb analyses samples were placed in an especially adapted laser cell. A New Wave UP213 Nd: YAG laser (λ = 213 nm), linked to a Thermo Finnigan Neptune Multi-collector ICPMS was used. Helium was used as the carrier gas and mixed with argon before entering the ICPMS. The laser was run at a frequency of 10 Hz and energy of ~100 mJ/cm2 with a spot diameter of 30μm.

For the U-Pb LA-ICPMS zircon analyses, a fragment of zircon standard GJ-1 (Jackson et al., 2004) was used as the primary reference material in a standard-sample bracketing method, accounting for mass bias and drift correction. The resulting correction factor for each sample analysis considers the relative position of each 199 analysis within the sequence of 4 samples bracketed by two standard and two blank analyses (Albarède et al., 2004). An internal standard was run at the start and at the end of each analytical session, yielding accuracy around 2% and precision in the range of 1% (1σ). Uncertainties in sample analyses were propagated by quadratic addition of the external uncertainty observed for the standards to the reproducibility and within-run precision of each unknown analysis. Zircon grains with $^{206}Pb/^{204}Pb$ lower than 1000 were rejected. U–Pb age data were calculated and plotted using ISOPLOT v.3 (Ludwig, 2003) and errors for isotopic ratios are presented at the 1σ level.

Seven drill core samples were selected for isotopic analyses of Sm-Nd, comprising two samples from dolerite, two samples of syenite porphyry, one sample of trachyte ,one sample of diorite porphyry and one sample of lamprophyrie. Sm-Nd isotopic analyses followed the method described by Gioia and Pimentel (2000) and were carried out at the Geochronology Laboratory of the University of Brasília. Whole

rock powders (ca. 50 mg) were mixed with ^{149}Sm-^{150}Nd spike solution and dissolved in Savillex capsules. Sm and Nd extraction of whole-rock samples followed conventional cation exchange techniques. Sm and Nd samples were loaded on Re evaporation filaments of double filament assemblies and the isotopic measurements were carried out on a multi-collector Finnigan MAT 262 mass spectrometer in static mode. Uncertainties for Sm/Nd and $^{143}Nd/^{144}Nd$ ratios are better than ±0.5% (2σ) and ±0.005% (2σ), respectively, based on repeated analyses of international rock standards BHVO-1 and BCR-1. The $^{143}Nd/^{144}Nd$ ratios were normalized to $^{146}Nd/^{144}Nd$ of 0.7219 and the decay constant used was 6.54×10^{-12} a^{-1}. The T_{DM} values were calculated using the model of DePaolo (1981). Nd procedure blanks were better than 100 pg.

4.4.2. Whole-rock chemical analyses

Twenty six samples from the Bacilandia Intrusions were collected for whole rock analyses after preliminary petrographic examination. These samples were analyzed for major, minor, and trace components, which included rare earth element (REE). Whole rock analyses were performed at ALS Chemex, Peru. Major oxides and minor elements were obtained by ICP-AES spectrometry following a lithium metaborate/tetraborate fusion and dilute nitric digestion of a sample aliquot of 0.1 g. Rare earth and refractory elements were determined by ICPMS following a lithium metaborate / tetraborate fusion and nitric acid digestion of 0.1 g samples. The loss on ignition (LOI) was measured after ignition at 1000°C. All rocks analyzed were affected by regional metamorphism, and some also by hydrothermal alteration. The volcanic rocks were metamorphosed to the greenschist facies conditions and thus the primary geochemical compositions are liable to subsequent modifications. Large ion lithophile elements (e.g. Rb, Ba, K, Sr) are generally considered mobile under metamorphic conditions whereas rare earth elements and high field strength elements (e.g. Th, Nb, Ti, Zr, Y) are considered the least mobile or immobile (Rollinson, 1993). Given these considerations, only those elements generally considered to be immobile are used in the geochemical diagrams. To minimize some effects of alteration, all samples were carefully selected to exclude veining and recent weathering. Samples with LOI greater than 5.0 were discarded. Exceptionally, we used Gabbro samples with elevated LOI values only in trace element classification.

4.4.3. Mineral chemical analyses

Twelve thin sections were selected for determining the composition of silicates, sulfides and carbonates via the JEOL JXA-8230 electron microprobe at the Electron Microprobe Laboratory in the University of Brasília. WDS (wavelength dispersive X-ray spectrometer) beam operating conditions were 20 kV and 20 nA, with a 10s counting time. Thin sections were polished and metalized with a 250 Å thick carbon film.

4.4.4. Carbon-Oxygen isotope samples

Eight drill core samples were collected from hydrothermal carbonate veins for carbon-oxygen isotopes analyses, after an examination of polished thin sections. We selected these carbonate rich alterations with the goal of evaluating the origin of the hydrothermal fluids. Approximately 300 mg of carbonate was extracted from each sample using a hand-micro drill, and these carbonate samples were analyzed for carbon and oxygen isotopes by IRMS (Delta Plus Advantage) at the Geochronos Lab of the University of Brasília. Analyses of NBS 18 during the period of this study yield an average value of -5.1‰ for $\delta\ ^{13}C_{VPDB}$ and 23.1‰ for $\delta\ ^{18}O_{VSMOW}$

4.5. Age of Bacilândia Intrusions

Three samples from Bacilândia Intrusions were selected for isotopic U-Pb LA-ICP-MS analysis representing de different stage of intrusions, one from the diorite porphyry (GD-23), one from trachyte (GD-04A) and one from syenite porphyry (GD-13A), being the two latters intrusions samples with no tectonic fabrics. Results are given in the supplementary table 4.A.

The **diorite porphyry** sample (GD-23) was collected from drill core sample that was representative of the central portion from diorite porphyry stock. Zircon grains in this rock are colorless or light-brown, transparent to semi-transparent and subhedral with a few euhedral crystals. Their length varies from 50 to 200 μm. The grains display clear oscillatory zoning and Th/U ratios with a range from 0.25 to 0.73 indicating a magmatic origin. Ten spots were analyzed on 10 zircons, where six spots analyses yielded the concordia age of 590 ± 5 Ma (MSWD = 1.9, Fig. 4.6A), which is interpreted as the crystallization age of the original diorite porphyry.

The **trachyte sample** (GD-04A) was also collected in vicinities of the open pit of Fazenda Nova deposit. This trachyte outcrop as dike (with few meters wide) emplaced into Type-1 metatonalite. Zircon grains from this sample may be divided into two main populations based on their morphologies and internal structures: (i) the most abundant population (approximately 90 % of the grains) consist of subhedral elongated crystals with rounded edges and occasional oscillatory zoning and (ii) a less abundant (10 %) formed of euhedral, elongated crystals, with well-developed zoning. The grains selected for analyses are in the size range between 50 and 300 μm. Twenty two analyses on twenty two zircon grains were carried out, and ten grains of the first population yielded a concordia age of 772 ± 6 Ma (MSWD = 4.8 ,Fig. 4.6B). According to their characteristics they are most likely represent inherited zircons. The large amount of inherited zircon crystals is probably due to the proximity to Type-1 samples with ca. 770 Ma old metatonalite country rocks. Two zircon grains of the second population yielded the younger concordia age of 574 ± 10 Ma (MSWD = 0.09, Fig. 4.6B), which is interpreted as the crystallization age of the original trachyte dike.

The **syenite porphyry** sample (GD-13A) was collected in outcrop close of the Fazenda Nova open pit as dike emplaced in felsic metavolcanics. Most of the zircon grains in this rock are colorless or light-brown, transparent to semi-transparent and euhedral to subhedral prisms, length varying from 100 to 300 μm and oscillatory zoning, indicating their igneous origin. Th/U ratios vary from 0.11 to 0.31. A total of 31 spots were analyzed on 31 zircons. Four spot analyses yielded the concordia age of 572 ± 5 Ma (MSWD = 1.9, Fig. 4.6C), which is interpreted as the crystallization age of the original syenite dyke. Other six analyses yielded a concordia age of 598 ± 3 Ma (MSWD = 0.17, Fig. 4.6C) which is interpreted as an inherited componente. The large amount of inherited zircon crystals is probably due to the proximity of this sample to felsic metavolcanics with similar age of 597 ± 5 Ma.

Sm-Nd analyses in dikes present $^{147}Sm/^{144}Nd$ values from 0.13 to 0.14 and T_{DM} model ages are between 0.75 to 0.88 Ga. ε_{Nd} values at T = 572 Ma, range from +1.88 to +4.5 (table 4.2).

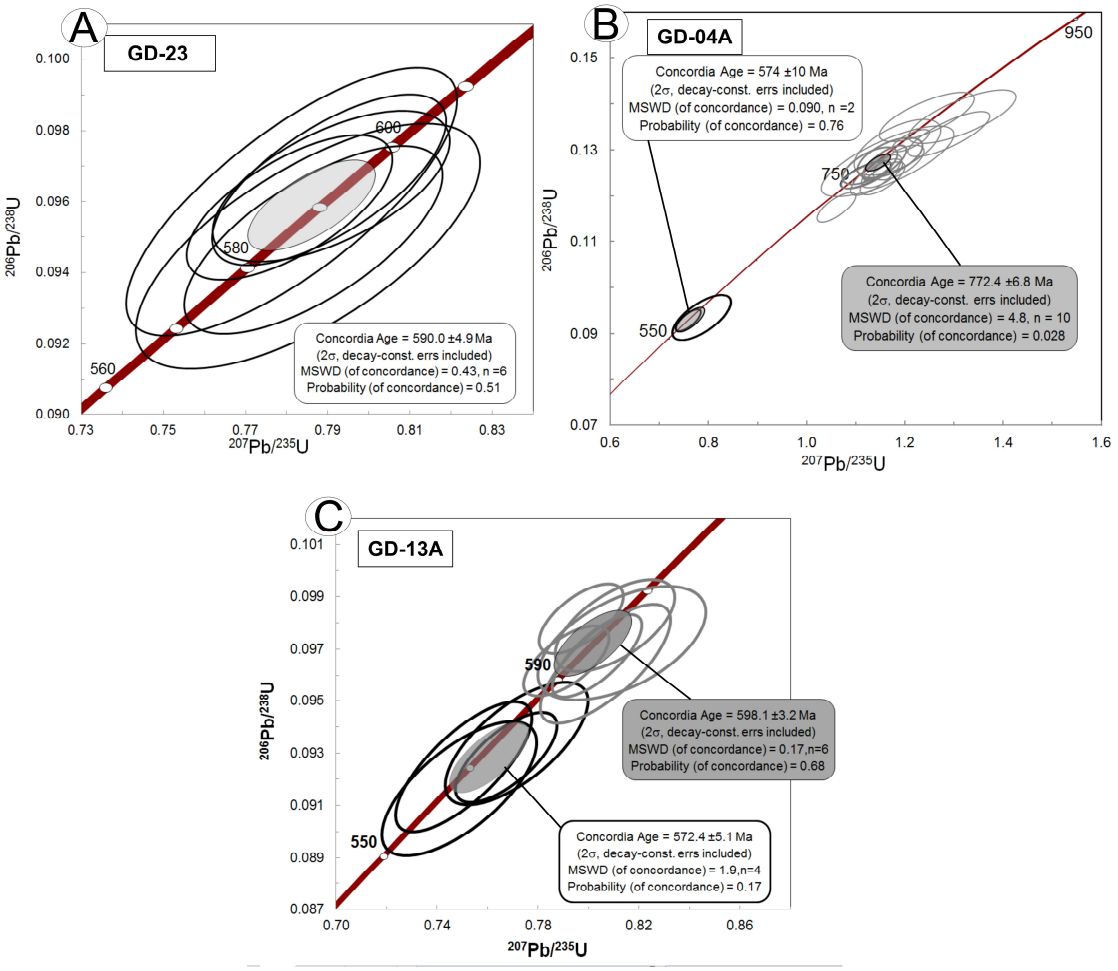

Figure 4.6 - Concordia diagram for zircon grains of: A) diorite porphyry (sample GD-23); B) trachyte (GD-04A) and C) syenite porphyry (sample GD-13A).

Table 4.2 Sm–Nd isotopic data for the Bacilândia Intrusions

Sample	Rock	Sm(ppm)	Nd(ppm)	$^{147}Sm/^{144}Nd$	$^{143}Nd/^{144}Nd \pm 2SE$	$\varepsilon_{Nd\,(0)}$	$T_{DM\,(Ga)}$	$\varepsilon_{Nd\,(T)}$
GD-05A	Dolerite	5.376	23.272	0.1396	0.512635+/-14	-0.05	0.84	3.81
GD-11	Dolerite	4.636	19.669	0.1425	0.512632+/-6	-0.12	0.88	3.56
GD_09	Gabbro	2.41	10.234	0.1423	0.512631+/-22	-0.13	0.88	3.97
GD_23	Diorite porphyry	2.41	10.234	0.1423	0.512633+/-22	-0.11	0.86	3.87
GD-04A	Trachyte	8.244	37.097	0.1343	0.512601+/-8	-0.72	0.85	3.51
GD-13A	Syenite porphyry	6.82	31.477	0.131	0.512640+/-14	0.03	0.75	4.5
GD_25	Lamprophyre	9.884	59.641	0.1002	0.512418+/-6	-4.29	0.84	1.88

4.6. Geochemistry of major and trace elements of Bacilândia Intrusions

Gabbros, dolerites, trachytes, diorite porphyry, syenite porphyry and lamprophyres are high-K calc-alkaline to shoshonitic and have a clear alkaline affinity with composition varying from basalts and alkali-basalts to more evolved trachytes (Fig. 4.7A). Aluminum saturation increases with increased silica content, and the rocks can be considered metaluminous to slightly peraluminous (Fig. 4.7B). Harker variation diagrams (Fig. 4.8) indicate that CaO, Fe_2O_3, TiO_2 and MgO systematically decrease with increasing SiO2, forming relatively smooth trends. The Na_2O and K_2O show a positive correlation with SiO_2. The less evolved rocks generally feature higher P_2O_5 contents. The variation of major elements of each type of Bacilândia Intrusions is shown in the Table 4.3.

Table 4.3 Major elements data for Bacilâdia Intrusions. The gabbro was not included in table due the high values of LOI.

Major elements	Dolerite	Diorite porphyry	Trachyte	Syenite porphyry	Lamprophyre
SiO_2 wt%	46.8-52.6	55.2–63.7	52.1–62.27	64.71-71.07	45.2
Fe_2O_3 wt%	9.6-14.7	7.47-10.37	8.25-11.6	3.48-6.45	14.54
MgO wt%	8.8-3.1	1.31-3.54	1.33-4.66	0.47-0.96	7.11
TiO_2 wt%	1.9-3.2	1.04-1.93	2.35-0.78	0.39-0.72	3.38
CaO wt%	6.8-9.9	2.59-6.64	3.98-6.7	1.62- 2.94	10.72
$Na_2O + K_2O$ wt%	3.21-6.58	5.66-5.89	5.68-6.62	7.74-8.69	8.79

All Bacilândia intrusives are strongly enriched in LILEs (consistent with the high K contents) and some HFSE, such as Nb and Ta. Negative P and Ti anomalies are present in the syenite porphyry, trachyte and diorite porphyry (Fig. 4.9A and C). Chondrite-normalized REE plots show that light REE are strongly enriched in all rocks, with the highest absolute values in syenite porphyry. The diorite porphyry is slightly more enriched in middle and LREE (Fig. 4.9B and D). The Eu depletion in syenite porphyry indicates some plagioclase fractionation in later magmatic stages. The syenite porphyry, trachyte and diorite porphyry plot in the post-tectonic granites field in the Rb versus Y+Nb diagram (Fig. 4.7C). The gabbro and dolerite intrusions plot as E-MORB, whereas lamprophyre dikes plot as alkaline within-plate basalts (Fig.4.7 D). All results are given in the supplementary table 4.B

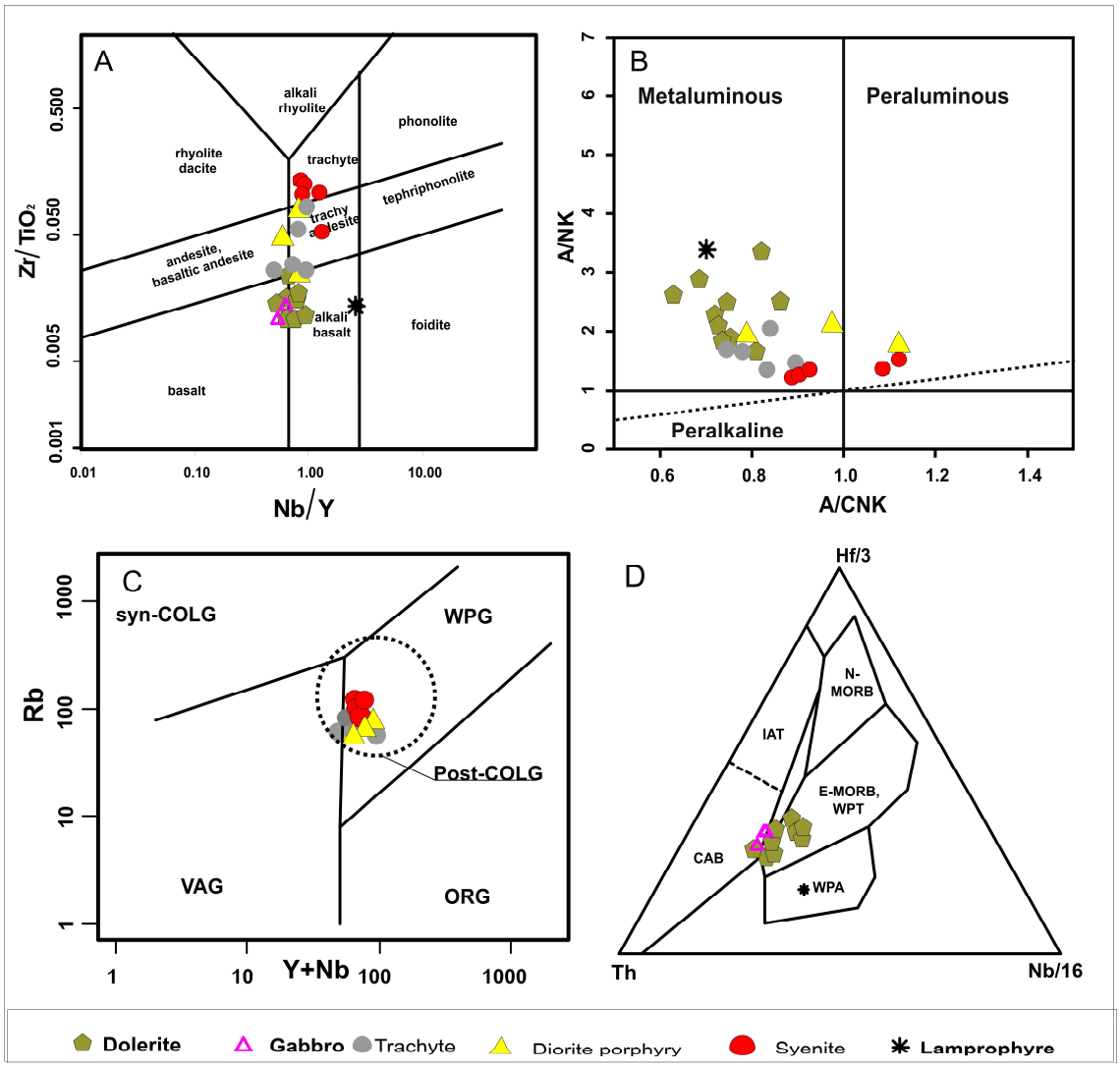

Figure 4.7 –Plot for Bacilândia intrusions A) Zr/TiO_2 versus Nb/Y composition diagram after Pearce (1996); B) A/NK versus A/CKN (Shand, 1943);. (C) Rb versus Y+Nb tectonic classification plot after Pearce et al., (1984) for felsic components of Bacilândia Intrusions ; (D) Th-Hf-Nb diagram (after Wood, 1980);WPT - within-plate tholeiites, WPA - alkaline within-plate basalts and; CAB volcanic-arc basalts; IAT – Island Arcs tholeiites. Note the negative Eu anomaly in syenite

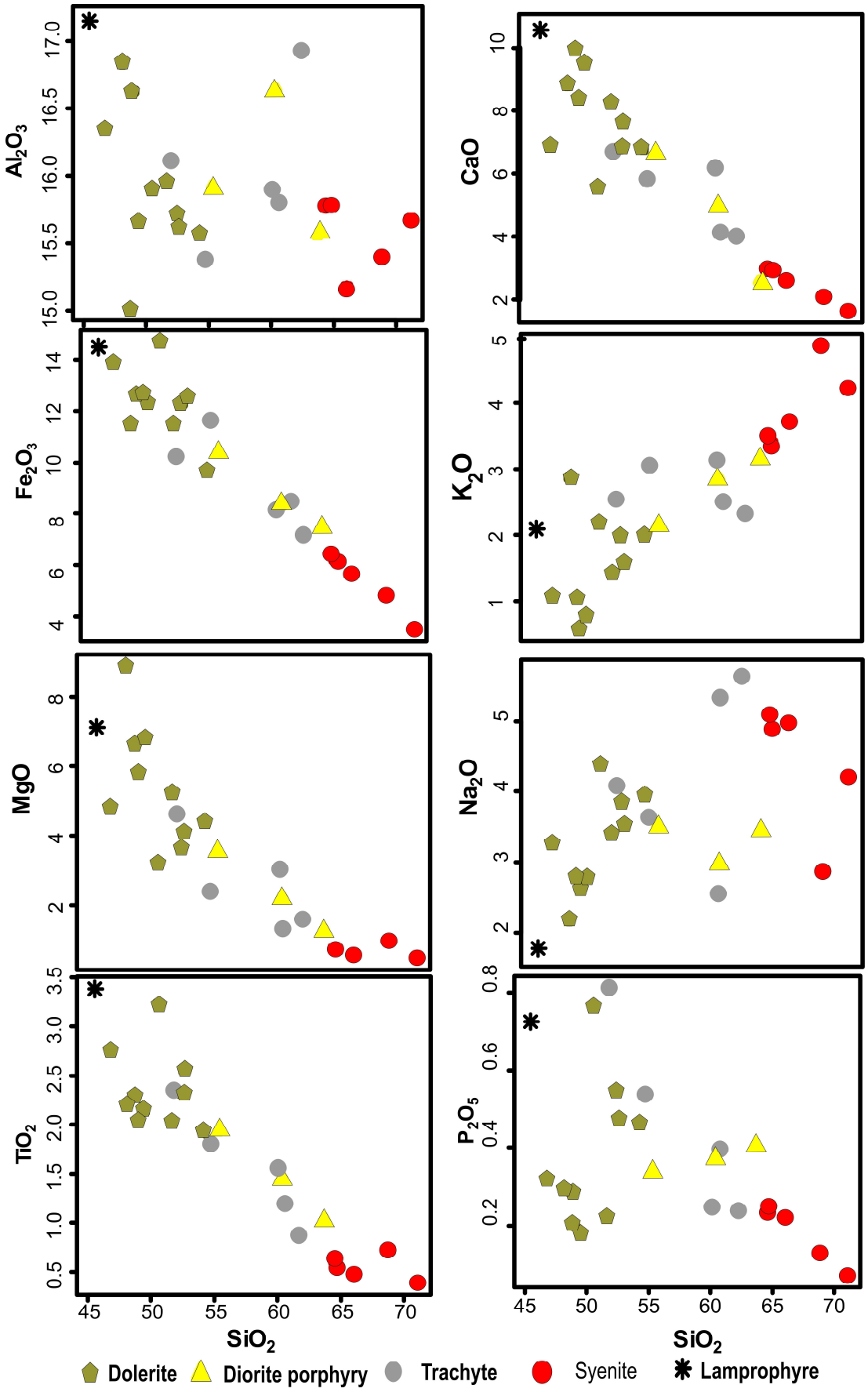

Figure 4.8 - Major element Harker variation diagrams for intrusive rocks at the Fazenda Nova Deposit. Major element compositions are normalized to volatile free values.

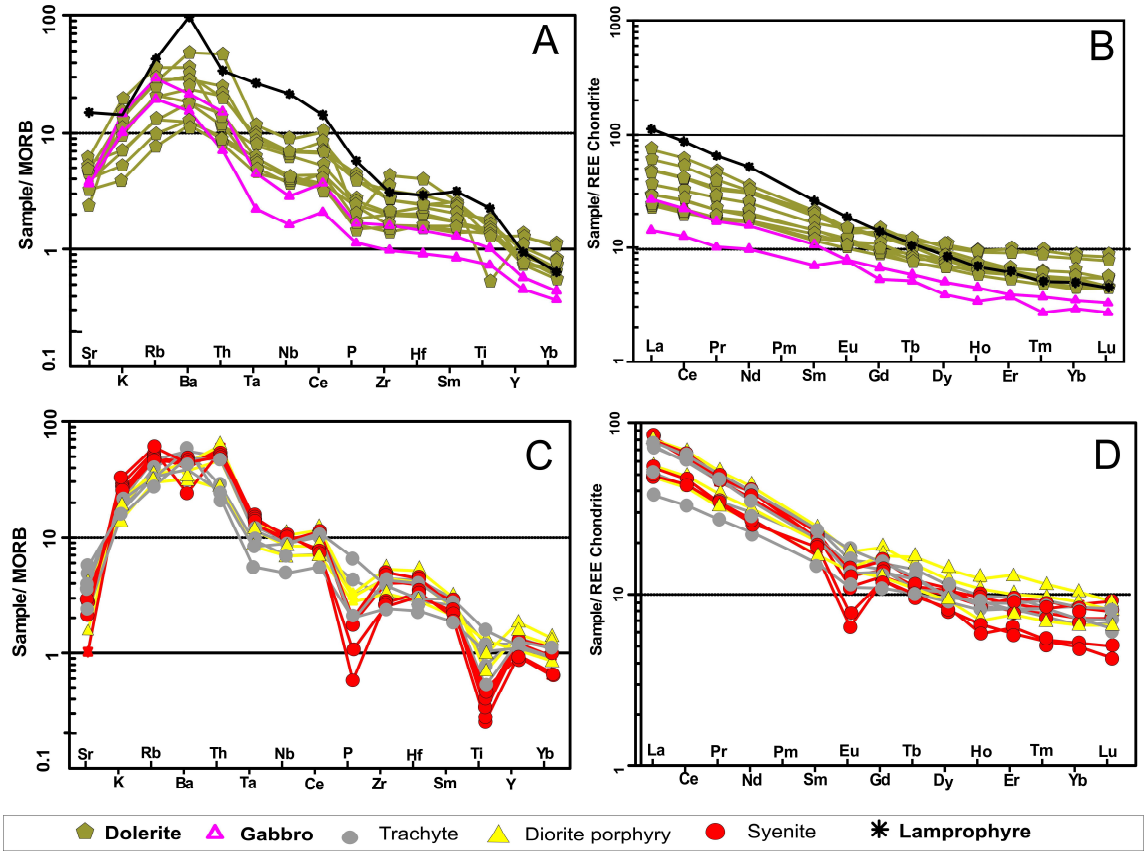

Figure 4.9 - MORB-normalized spider diagrams and chondrite-normalized REE patterns for the dolerite, gabbro and lamprophyre (A and B); porphyry diorite, trachyte and syenite (C and D). MORB and chondrite normalization values after Pearce (1983) and Sun and McDonough (1989), respectively. Trace element characteristics across the compositional range of intrusions are remarkably uniform. All samples are strongly enriched in incompatible elements, particularly LILE and light REE, and feature high LILE/HSFE ratios.

4.7. The Fazenda Nova Gold Mineralization

The gold resource at the Fazenda Nova deposit occurs in NNW–SSE striking, steeply west dipping mineralized bodies (Lavrinha open Pit), which are sub-parallel to the dikes. This NNW trending dyke swarm was rotated by F_{n+1} folding into the WNW-striking steeply south-dipping attitude seen at the Vital open pit to the South. The flat to shallow dipping mineralized zones at Vital are spatially related to sills (Fig 4.3).

The gold mineralization at the Fazenda Nova deposit is characterized by a strong gold-arsenopyrite association, which occurs as irregular veinlets/veins, and lesser crackle breccias, filled by quartz ± carbonate ± arsenopyrite ± pyrrhotite ± pyrite. There is no correlation between the density of veining and gold grade, but good correlation is seen between gold and arsenic. The presence of arsenopyrite in veinlets/veins and as fine acicular disseminations is the most obvious control on gold grades, so much that some intervals with dense veining carry no gold if arsenopyrite is not present. A consistent and general sequence of paragenetic relationships is observed between primary igneous and hydrothermal minerals in three different stages, classified in chronological order as: early, intermediate and late stage, as explained below (Table 4.4). The three stages of alteration affected all Bacilândia intrusives and wall rocks, except for the lamprophyres, which show no hydrothermal alteration.

The **early stage (main stage)** may be divided into subtypes: i) the first is hosted preferably in, or near, the contacts of intrusions. The pervasive sericitization (fine-grained sericite) of feldspar and biotitization of mafic minerals are the most obvious alteration features (Fig. 4.10A and B). The intrusions, (eg dolerites and trachytes), typically contain igneous ilmenite partially altered to rutile/titanite and widely disseminated hydrothermal apatite grains in the matrix (Fig. 4.10C). The hydrothermal assemblage of biotite-rutile-apatite and locally carbonate (siderite) is frequently observed with fine-grained acicular arsenopyrite, pyrrhotite and less scheelite and stibinite. (Fig4.10D). ii) the second subtype of early alteration is represented by mineralized quartz veins/veinlets and crackle breccias filled in by quartz + arsenopyrite ± pyrrhotite. Alteration consists of a fine-grained mass of biotite selvages with arsenopyrite and pyrrhotite in the quartz veins (Fig. 4.10E and F). In the metamorphic country rocks (metatonalite, felsic metavolcanics) early mineralization is represented by quartz stockwork with massive veinlets and veins of fine acicular arsenopyrite with sericitic alteration (Fig4.11A). Hydrothermal crackle breccias consist of a grayish to brownish-colored breccia of angular to subangular fragments of intensely altered dikes, or felsic host rocks, cemented by an abundant silicified groundmass of acicular arsenopyrite ± pyrrhotite Fig4.11B). These two subtypes exhibit mutual cross-cutting relationships suggesting they are essentially synchronous.

Early stage mineralization generally grades from 3.0 to 30 g/t Au with an average value of about 6.0 g/t Au (Yamana reports). The sulfide concentration is about 8% to 15%, with the gold grades proportional to the content of arsenopyrite in the

groundmass of the dikes or in the veins/veinlets. The early mineralization is hosted in dikes that usually are not deformed, moreover, when hosted in the wall rocks; truncate the ductile S_n tectonic fabrics. However, some of the arsenopyrite bearing-veins from this early event are still deformed by the S_{n+1} foliation. Thus, a post-D_n and partially pre- to syn-D_{n+1} age for the early stage alteration is inferred based on above relationships.

The **intermediate stage** is represented by stockworks of carbonate (calcite) ± quartz veins with pyrrhotite and less fine-grained arsenopyrite-pyrite (Fig.4.11C). Alteration in the wall rocks depends on host composition, showing chloritization (Fe-chlorite) of mafic minerals, hydrothermal epidote, titanite (leucoxene) and tourmaline rich alteration in the mafic intrusions, and carbonate-quartz veins in the felsic metamorphic rocks. In this stage the arsenopyrite grains are predominantly tabular and occur in equilibrium with pyrite and rarely with pyrrhotite (Fig4.11D).

The intermediate stage grades vary from 0.3 to 3 g/t Au with an average value of ca.1.5 g/t Au (Table 4.4) and sulfide concentrations of ca.5% to 8%. This style of mineralization represents barren to low grade material with some mineralized zones continuous over 30 meters. The early quartz-arsenopyrite veins are frequently cut by quartz-chlorite-carbonate intermediate veins (Fig 4.11E), although the opposite relationship has also been found locally. This suggests that the two events are partially overlapped in time and may even reflect a spatial proximal to distal alteration zoning.

The **late stage** of alteration is represented by veining/brecciation that occurs only in the dikes as barren veinlets and crackle breccias infilled by monotonous calcite-ankerite occasionally with comb/cockade texture (Fig.4.11F and G). These veins are barren and lack alteration selvages and sulfides. The late stage veins consistently cut across early stage alteration and intermediate carbonate-quartz veins and are not affected by any deformation and are , therefore, inferred to be post-D_{n+1} in age.

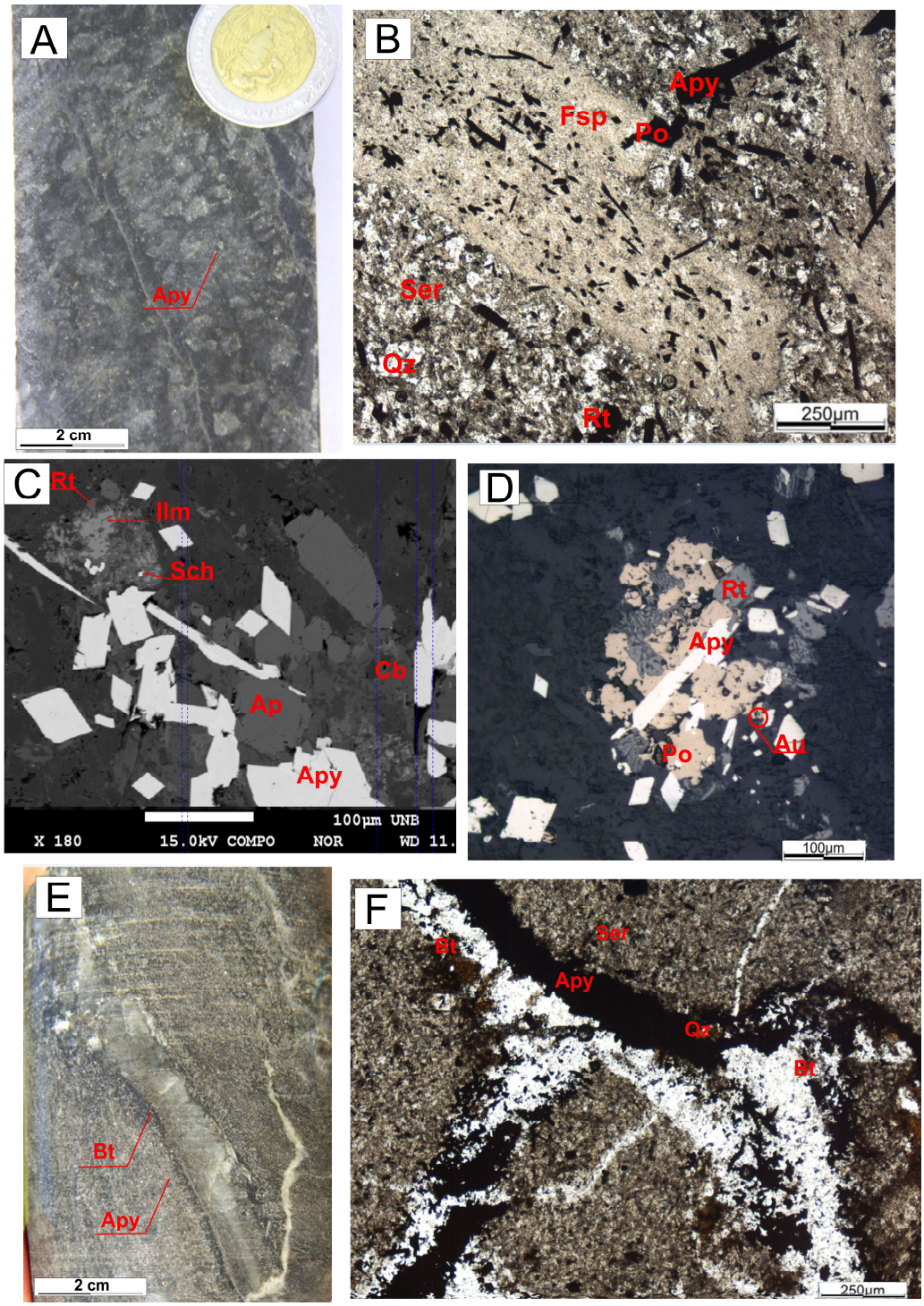

Figure 4.10 – Photographs of drill core samples (A and E), thin section photomicrography (B,D and F) and scanning electron microscope (SEM) backscattered electron images (C) of early stage alteration styles in the Fazenda Nova deposit. A) Diorite porphyry displaying pervasive early alteration characterized by dissemination of fine-grained arsenopyrite, sericitization of feldspar and fine-grained biotite; B) Diorite porphyry with disseminated acicular arsenopyrite, sericitization (Ser) of feldspar phenocrysts and minerals in the groundmass; acicular arsenopyrite (Apy) is particularly abundant in the relict of feldspar phenocryst; (C) Typical alteration in mafic dikes showing hydrothermal

assemblage of apatite (Ap), disseminated carbonate (Cb), acicular arsenopyrite (Ap), scheelite (Sch) and ilmenite (Ilm) partially altered to rutile (Rt); D) Acicular arsenopyrite-rutile-pyrrhotite hydrothermal assemblage with gold (Au) in the contact between arsenopyrite (Apy) and pyrrhotite (Po); E) Dolerite with typical alteration associated with high grade gold intervals comprising pervasive biotite-arsenopyrite-pyrrhotite hydrothermal association and quartz veins with fine-grained biotite-arsenopyrite selvages; F) Dolerite crosscut by quartz veins with arsenopyrite and fine-grained dark-brown biotite selvages (TL,N//).

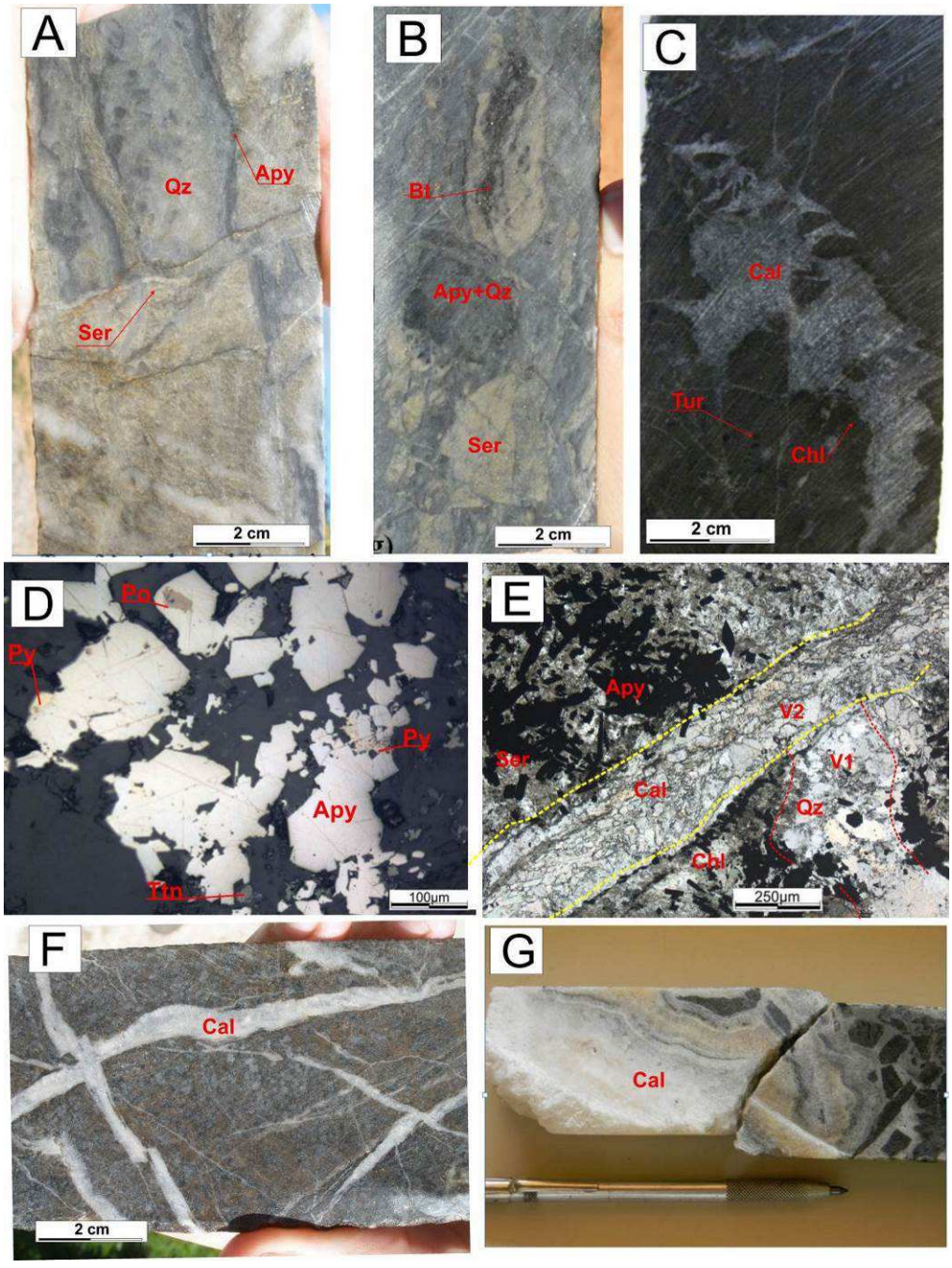

Figure 4.11 Photographs of drill core samples (A,B,C,F and G), thin section photomicrography (D and E) of early stage , intermediate and late stages of alteration in the Fazenda Nova deposit. A) Early alteration in Type-1 metatonalite with sericite (Ser) arsenopyrite (Apy) selvages in the quartz veins; B) Early-stage hydrothermal breccia with sericitized felsic metavolcanic clasts and silicified matrix with acicular arsenopyrite (apy) rich-alteration; C) Dolerite with calcite (Cal) veins/veinlets with fine-grained chlorite-pyrrhotite-tourmaline (Tur) selvages representing the Intermediate alteration stage; D) Acicular and tabular arsenopyrite (Apy) with pyrrhotite-pyrite-titanite hydrothermal assemblage in the intermediate alteration stage; E) Thin section photomicrography (TL,N//) showing dolerite with two sets of veins, early alteration vein (V1) represented by quartz-arsenopyrite-rich vein and carbonate ± quartz vein (V2) with chlorite (Chl) and fine-grained tabular arsenopyrite (Apy) selvages of the intermediate stage; F) Late stage alteration with barren calcite veins in gabbros; G) Late stage hydrothermal breccia with calcite (Cal) veins displaying cockade texture.

Table 4.4 – Table with main characteristics of the three stages of alteration in the Fazenda Nova Deposit (the grades were extracted from Yamana reports)

Main Features	Early Stage	Intermediate Stage	Late Stage
Texture of alteration	Pervavise, stock-work and crackle breccias	Mainly carbonate stock-works	Carbonate stock-work (comb and cocade
Dike Alteration	Pervasive alteration with dissemanited sulfides, biotitization and sericitization and replacement of ilminite by rutile/leucoxene , disseminated apatite; quartz stock-work with biotite sulfides selvages; crackle-breccias cemented by silicified groundmass with sulfides	Vein, veinlets and stock-work of calcite with Fe-chlorite, sulfides and toumaline selvages	Veinlets and stock-work of milky calcite and less ankerite
Wall-Rock Alteration	Sericitization with fine-grained sulfides filling micro-fractures; quartz stockwork with sericite and sulfide selvage	Veins and veinltes compsed by sericite, carbonate and turmaline veins	No alteration
Main Metallic Mineralogy	Needle arsenopyrite + pyrrhotite + rutile+ leucoxene	Tabular arsenopyrite + pyrrhotite +pyrite + titanite	None
Seconday Metallic Mineralogy	Pyrite + Galena +Scheelite +tabular arsenopyrite + stibinite	needle arsenopyrite	None
Elemental Association	Au + As +Sb + W (Pb)	As + Au.	None
Sulfide Contents	10 % to 25 %	3% to 5 %	None
Au Grades	>3.0 gpt to avarage of 6.0 gpt Au	< 3.0 gpt avarage of 1.5 gpt /Au	None
Gold Occurence	In lattice of arsenopyrite, invisible gold and less free state	In lattice of arsenopyrite, invisible gold and free state	None
Deformation event	pre to sin-D_{n+1}	pre to sin-D_{n+1}	Post D_{n+1}

4.8. Ore mineralogy

In the **early-stage alteration**, gold occurs mostly conctact or as inclusion in the arsenopyrite and lesser pyrrhotite (Fig. 4.10D and Fig 4.12A). Two morphologic varieties of arsenopyrite are recognized in the early stage: a more common acicular-prismatic type and a less frequent tabular type. Electron microprobe analysis indicate (table 4.5) that both arsenopyrite types have low arsenic contents of 41.31–46.16 wt % As (average of 31.83 at % As) in the acicular type and 38.73 – 41.15 wt % As (average of 29.5 at % As) in the tabular one. The tabular type contains more sulphur (19.9–24.3 wt %) and Fe ranging from 34.2 to 36.85 wt %. The acicular grains are fine-grained (10 to 300 μm) with high gold contents ranging from 150 to 2200 ppm. The Au concentrations in acicular arsenopyrite indicate an equal distribution of elemental gold as nanoparticles (Fig. 4.12B). Acicular arsenopyrite may exhibit poykilitic texture (Fig. 4.12C) and high porosity with microinclusions of galena, pyrite and high contents of Cu, Pb, Bi and Ag (4.12 D). The tabular arsenopyrite type occurs as fine-grained, flattened, isometric, often rhombic pyramidal crystals with no gold contents.

Pyrrhotite contains S varying from 39.4 to 51.54 wt % and Fe from 45.55 to 60.16 wt %. When Gold is visible, present rounded to sub-rounded edges with size ranging from 5 to 20 μm, locally were observed very fine-grained with 0.5 μm in size. The gold occurs mainly incorporated by arsenopyrite, or fills microfractures in the arsenopyrite or pyrrhotite. Due the majority of gold is incorporated in the crystal structure of the arsenopyrite the Fazenda Nova gold mineralization is metallurgically refractory.

When present, gold in the **Intermediate stage** occurs as free particles in contact with tabular arsenopyrite (Fig.4.11 E) and locally with pyrite, or associated with preserved early-stage acicular arsenopyrite. In some cases, free gold is associated with tabular arsenopyrite (Fig.4.12 E), pyrrhotite and silicates. Electron microprobe analyses indicate that the compositions of tabular and acicular arsenopyrite are similar that of the early hydrothermal stage (Table 4.5). Pyrite is S deficient (50–53 wt %) with Fe contents ranging from 45.55 to 48.21 wt %, locally containing elevated As and Pb.

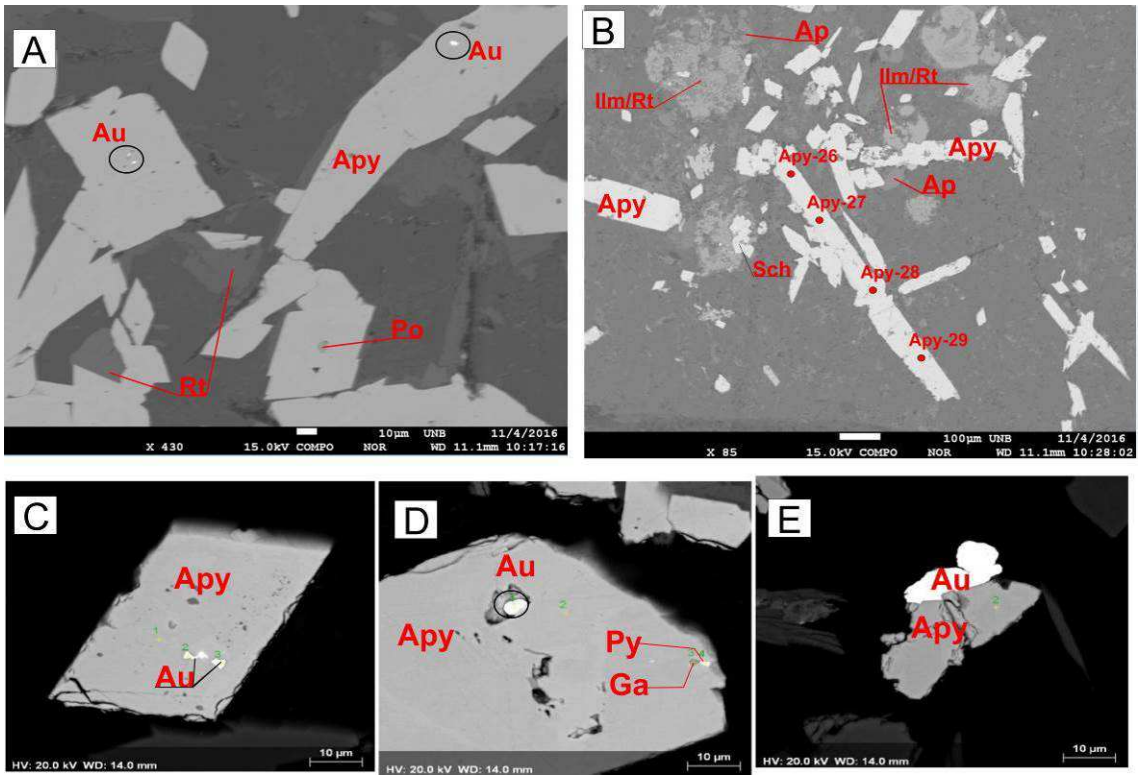

Fig 4.12 - Scanning electron microscope (SEM) backscattered electron images. A) Acicular arsenopyrite and hydrothermal rutile assemblage with gold enclosed by arsenopyrite. B) Acicular arsenopyrite-rutile-apatite hydrothermal assemblage with arsenopyrite havinghomogeneous gold values (apy-26 with 740 ppm Au, apy-27 with 790 ppm Au, apy-28 with 540 ppm and apy-29 with 640 ppm Au). C). Typical acicular arsenopyrite (Apy-14 with 1400 ppm Au and 30.27 wt % As with gold inclusion. D) Porosity acicular arsenopyrite (Apy-12 with 1920 ppm Au and 30.87 wt % As with gold microinclusion, galena and pyrite inclusions. E) Tabular arsenopyrite (Apy-26 with no Au contents and 29.36 % As) in contact with gold.

Table 4.5 - Electron Microprobe Data (wt %) for the early and intermediate stage of alteration of Fazenda Nova deposit. Abbreviations Apy = Arsenopyrite, Po= pyrrhotite, Py=Pyrite, Au = Gold and b.d.l = below detection limit.

Sample -ID	At % As	As %	S %	Bi %	Ag %	Sb %	Pb %	Au %	Fe %	Cu %	Total %	Morphology
Early Stage of Alteration												
Apy_02	30.16	41.31	22.48	0.02	0.03	0.01	0.10	0.06	36.28	b.d.l	100.44	Needle
Apy_03	30.21	41.38	22.37	b.d.l	0.00	b.d.l	0.09	0.07	35.75	0.05	99.91	Needle
Apy_04	31.16	42.69	22.33	0.07	b.d.l	b.d.l	0.08	0.12	36.02	0.03	101.46	Needle
Apy_05	31.70	43.42	20.60	0.01	b.d.l	b.d.l	0.00	0.07	35.45	b.d.l	99.66	Needle
Apy_07	31.74	43.52	20.73	0.12	0.01	b.d.l	0.05	0.21	35.94	0.04	101.10	Needle
Apy_08	30.55	41.85	22.98	0.04	b.d.l	0.01	0.07	0.05	35.98	b.d.l	100.75	Needle
Apy_09	30.75	42.13	22.56	0.05	b.d.l	b.d.l	b.d.l	0.15	36.16	0.01	101.22	Needle
Apy_10	33.18	45.45	20.20	b.d.l	b.d.l	b.d.l	0.07	0.18	35.50	b.d.l	101.54	Needle
Apy_12	30.86	42.27	22.53	0.02	0.03	b.d.l	0.05	0.19	36.11	b.d.l	101.44	Needle
Apy_13	30.31	41.53	22.31	b.d.l	0.01	0.00	0.01	0.07	36.25	0.03	100.36	Needle
Apy_14	30.26	41.45	22.53	0.05	0.02	b.d.l	0.07	0.14	36.38	0.02	100.84	Needle
Apy_16	30.47	41.74	22.73	b.d.l	0.01	b.d.l	0.15	0.15	36.11	b.d.l	101.05	Needle
Apy_17	33.84	45.36	19.47	0.06	0.02	b.d.l	b.d.l	0.5	35.13	0.02	100.31	Needle
Apy_20	31.37	42.97	21.42	0.05	0.03	b.d.l	0.02	0.02	35.10	0.03	99.70	Needle
Apy_21	33.32	45.64	22.42	b.d.l	b.d.l	b.d.l	0.03	0.03	34.93	b.d.l	103.06	Needle
Apy_22	34.36	47.07	19.42	b.d.l	b.d.l	b.d.l	0.09	b.d.l	34.76	b.d.l	101.41	Needle
Apy_23	33.70	46.16	20.06	b.d.l	0.03	b.d.l	0.08	b.d.l	34.44	0.00	100.79	Needle
Apy_24	32.02	43.86	21.81	b.d.l	b.d.l	b.d.l	0.02	b.d.l	35.21	b.d.l	100.98	Needle
Apy_25	32.56	44.60	22.18	b.d.l	b.d.l	b.d.l	b.d.l	0.03	35.83	0.03	101.76	Needle
Apy_26	32.78	44.91	21.75	b.d.l	b.d.l	b.d.l	0.20	0.07	35.72	b.d.l	101.72	Needle
Apy_27	31.70	43.43	22.59	0.08	b.d.l	b.d.l	0.10	0.08	36.13	b.d.l	101.33	Needle
Apy_28	31.65	43.36	22.25	b.d.l	b.d.l	b.d.l	0.16	0.05	35.80	b.d.l	101.71	Needle
Apy_29	31.78	43.54	22.74	0.05	b.d.l	b.d.l	0.06	0.06	35.69	b.d.l	101.17	Needle
Apy_18	29.66	40.63	23.80	0.00	0.00	0.00	0.04	0.020	36.55	b.d.l	101.22	Tabular
Apy_19	29.84	40.87	23.14	0.05	0.02	0.07	0.02	b.d.l	36.43	b.d.l	100.74	Tabular
Apy_21	30.01	41.10	23.38	0.11	0.01	0.03	0.16	b.d.l	36.46	b.d.l	101.38	Tabular
Apy_22	28.56	39.13	24.37	0.07	b.d.l	0.25	0.19	b.d.l	36.86	0.02	101.23	Tabular
Apy_23	30.04	41.15	23.29	0.01	0.03	0.09	b.d.l	b.d.l	36.94	b.d.l	101.11	Tabular
Apy_26	29.36	40.21	23.22	0.11	0.01	0.16	0.06	b.d.l	36.66	0.01	100.59	Tabular
Po_01	b.d.l	b.d.l	39.31	0.11	b.d.l	b.d.l	0.06	b.d.l	59.94	0.02	99.59	
Po_02	b.d.l	b.d.l	39.89	0.16	0.01	b.d.l	0.11	b.d.l	60.16	0.02	100.58	
Po_03	b.d.l	b.d.l	40.08	0.02	0.00	0.000	0.16	0.000	59.92	0.015	100.44	
Au_01	b.d.l	b.d.l	b.d.l	b.d.l	13.1	b.d.l	b.d.l	86.9	b.d.l	b.d.l	100	Inclusion in Apy
Au_02	b.d.l	b.d.l	b.d.l	b.d.l	12.2	b.d.l	b.d.l	87.8	b.d.l	b.d.l	100	Inclusion in Apy
Au_03	b.d.l	b.d.l	b.d.l	b.d.l	15	b.d.l	b.d.l	85	b.d.l	b.d.l	100	Inclusion in Apy
Au_04 (Electrum)	b.d.l	b.d.l	b.d.l	b.d.l	22.6	b.d.l	b.d.l	77.4	b.d.l	b.d.l	100	Inclusion in Apy
Au_05	b.d.l	b.d.l	b.d.l	b.d.l	12	b.d.l	b.d.l	88	b.d.l	b.d.l	100	Free State
Au_06	b.d.l	b.d.l	b.d.l	b.d.l	14	b.d.l	b.d.l	86	b.d.l	b.d.l	100	Free State
Intermediate stage Alteration												
Apy_28	31.14	42.66	22.14	b.d.l	0.01	b.d.l	0.07	0	36.1270	0.01	101.13	Needle
Apy_29	33.18	45.46	19.47	0.056	0.02	b.d.l	b.d.l	0.03	35.13	0.021	100.31	Needle
Apy_30	31.63	43.33	22.60	0.03	0.03	b.d.l	0.11	0.02	36.25	b.d.l	102.53	Needle
Apy_31	30.90	42.33	22.16	0.09	b.d.l	b.d.l	0.00	0.08	35.61	b.d.l	100.39	Needle
Apy_33	30.65	41.99	21.30	b.d.l	b.d.l	0.024	b.d.l	0.04	36.05	0.011	99.53	Needle
Apy_34	29.83	40.86	23.40	b.d.l	0.05	0.19	0.10	b.d.l	36.74	b.d.l	101.44	Tabular
Apy_36	30.04	41.15	22.18	b.d.l	0.01	b.d.l	0.03	b.d.l	36.10	0.016	100.53	Tabular
Apy_37	28.27	38.73	21.80	0.03	0.01	b.d.l	0.06	b.d.l	35.25	b.d.l	96.18	Tabular
Py_01	b.d.l	b.d.l	51.54	0.04	b.d.l	b.d.l	0.11	b.d.l	46.34	0.013	98.25	
Py_02	b.d.l	0.039	51.35	0.21	b.d.l	0.041	0.15	b.d.l	45.55	0.034	98.62	
Py_03	b.d.l	b.d.l	53.62	b.d.l	b.d.l	b.d.l	0.18	b.d.l	47.514	0.015	98.61	
Py_04	b.d.l	b.d.l	53.12	b.d.l	b.d.l	b.d.l	0.30	b.d.l	46.954	0.007	99.51	
Py_05	b.d.l	0.044	50.09	b.d.l	b.d.l	0.038	0.30	b.d.l	48.215	0.028	98.15	

4.9. Carbon and oxygen isotopes of carbonate veins

The carbon and oxygen isotopic results from the analyses of calcite in carbonate veins from the intermediate stage are shown in Table 4.6. Most of the $\delta^{13}C$ and the $\delta^{18}O$ values of the carbonates are quite homogeneous with $\delta^{13}C$ ranging from -9.68 to -11.57‰ and $\delta^{18}O$ from 12.87 to 13.84‰. On the $\delta^{13}C_{VPDB}$ versus $\delta^{18}O_{SMOW}$ diagram (Fig. 4.13), the intermediate veins plot in the field of juvenile hydrothermal solutions derived from mantle sources (Swain et al., 2015).

Tabel 4.6- Carbon and oxygen isotopic data of carbonate (calcite) veins from intermediate alteration stage

Calcitc carbonate veins samples of intermediate stage	V-PDB	V-SMOW
	$d^{13}C‰$	$d^{18}O‰$
AM_01	-11.57	13.94
AM_02	-11.15	14.27
AM_03	-10.76	13.63
AM_04	-9.68	13.13
AM_05	-11.34	12.87
AM_06	-11.87	13.10
AM_07	-10.67	13.83
AM_08	-11.12	13.26

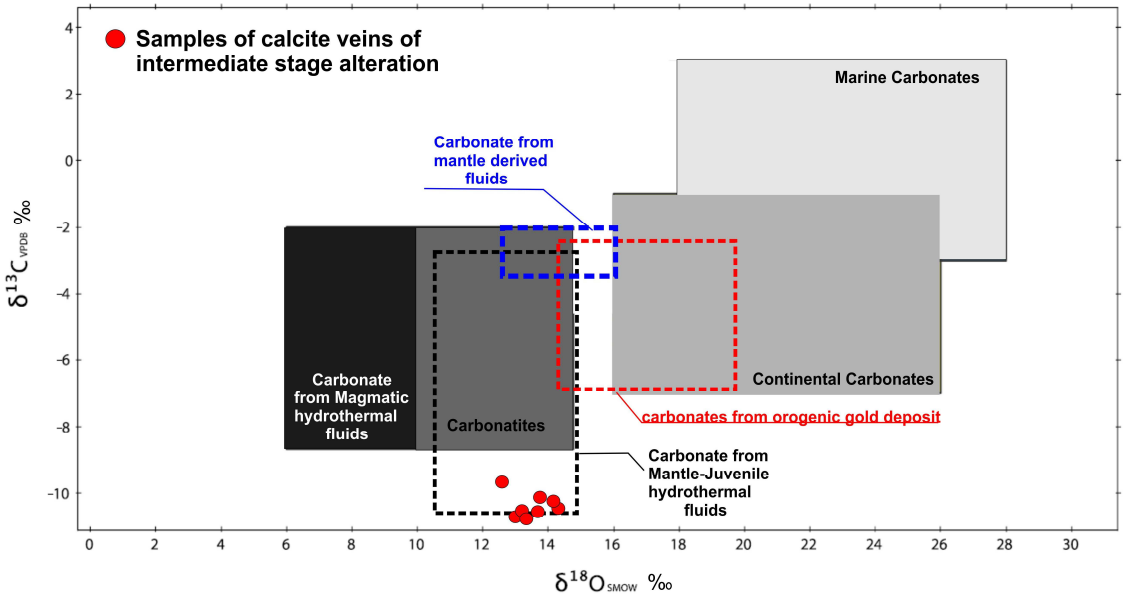

Figure 4.13 $\delta\ ^{13}C_{VDPB}$ ‰ versus $\delta^{18}O_{SMOW}$ ‰isotope diagram for the carbonate veins from the intermediate alteration stage. The fields are based on isotopic data from various studies defining a range for carbonates formed in different geological environments: continental and marine carbonates (Craig, 1953; Keith and Webber, 1964); carbonatites (Taylor et al., 1967); orogenic gold deposit fluids (Beaudoin and Pitre 2005; Craw et al., 2010); magmatic hydrothermal fluids (Ohmoto 1986, Sarangi et al., 2012); mantle hydrothermal fluids (Santos et al., 2013); and mantle-juvenile hydrothermal fluids Swain et al., 2015).

4.10 Discussion

4.10.1 – Magmatic processes and gold mineralization

The Bacilândia Intrusions were emplaced largely in the Jaupaci Sequence, with a close temporal and spatial association with gold mineralization, suggesting that magmatic process played a significant role in gold metallogeny. In order to establish the link between petrogenesis of the Bacilândia intrusions and gold fertility some assumptions are taken :i) the widely recognized association between alkalic magmas and gold mineralization (e.g. Rock et al. 1987; Jensen and Barton 2000; Muller 2002); ii) Loucks and Ballard (2003) reported that parental mafic magmas regionally and temporally associated with more evolved, gold-productive intrusives have higher contents of Nb, Th and other highly incompatible lithophile elements than average arc basalts. Furthermore, the authors concluded that parental magmas of gold-productive centers are related to either unusually low degrees of partial melting in the asthenospheric mantle wedge or to the melting of lithospheric mantle regions that were enriched in incompatible elements (i.e. fertilized) by the trapping of earlier low-degree partial melts of the deeper mantle; iii) Gold provinces in some parts of the world are linked to lithospheric instabilities following the lower crustal and lithospheric delamination (Leahy et al., 2005; Bierlein et al., 2006) as well as upwelling asthenosphere, which produce high-heat flow in the lithosphere coincident in time with the peak gold mineralization events(Goldfarb et al., 2005; Yang et al,. 2014).

The U-Pb geochronological data presented in this study indicates that the various intrusive phases of the alkaline Bacilândia Intrusives were emplaced during a protacted magmatic episode. The first intrusive event comprises gabbros and diorite porphyry dated at ~593-590 Ma overlapping with the ages of A-type pre-kinematic granitoids. The second pulse is represented by trachyte and syenite porphyry dated at ~574-572 Ma that took place concurrently with the emplacement of A-type syn-kinematic granitoids. The final intrusive pulse is represented by the late lamprophyre dikes. All rock-types have remarkably similar positive $\varepsilon_{Nd}(T)$ values, are enriched in LILE, in HFSE(Nb, Th and Zr) and light REEs, and all trace element signatures are relatively uniform and consistent with a cogenetic origin involving partial melting of slightly older metasomatized Neoproterozoic juvenile rocks. Constraints on the origin of the different

intrusive phases at the Fazenda Nova deposit and relationships with magmatic process are evaluated below.

4.10.2.1 – Significance of Dolerite and gabbro intrusion

The dolerites and gabbros display high contents of HFSE, LREE, LILE Nb, Ta, typical of E-MORB basalt, which are frequently originated from enriched mantle sources. The metasomatic origin for the E-MORB required an earlier episode of low-degree partial melting of an enriched mantle source to generate the elevated incompatible trace element abundances (Waters et al., 2011). Proposed low-degree melting mechanisms include metasomatism of overlying mantle by melting of eclogitized crust in subduction zones (Donnelly et al., 2004), metasomatism by melting of mantle within the low-velocity zone beneath oceanic lithosphere (Niu et al., 2002), and metasomatism of subcontinental lithosphere and subsequent delamination (Galer and O'Nions, 1986). Marques (2017) observed two tectonic events with mantle metasomatism in the Jaupaci Sequence: i) the first one, related to arc-back arc continental subduction with melting of pre-existing juvenile arc-derived crust (crystallized between 880 and 790 Ma), which originated ~750 Ma adakitic, magnetite-bearing type-2 trondhjemite and metarhyolites of the Jaupaci Sequence. This event is also regionally associated with Cu (and Au) mineralization represented by Cu-volcanogenic Bom Jardim deposit (Guimarães et al., 2012); the second event is related to extensional tectonism associated with the bimodal volcanics of the Jaupaci Sequence which erupted at 598 ± 10 Ma in a post-collisional setting. The volcanism of N-MORB metabasalts represents the asthenospheric melts, after mantle upwelling and delamination, while the A-type felsic magmas are generated by mixture of low degrees of partial melting of the newly underplated lower crust with older crustal source melting (778–828 Ma).

Thus, after the pulse of bimodal volcanics the continuous input of heat has led to a decompressional melting of asthenospheric mantle, consequently trigger the re-melting of lower crust that had been pre-enriched in incompatible elements to generate adakitic and/or A-type felsic magmas. The result of this melting is E-MORB mafic rocks of Bacilândia Intursions, represented by two events of intrusions: first emplaced at 593 ± 4 Ma (Marques 2017), represented by gabbros and dolerites displaying D_n foliation; and second event emplaced post-D_n represented by undeformed dolerites, probably with the same age of trachyte and syenite porphyry at ~574-572 Ma . The

change of astenospheric to lithospheric derived mafic magmas is supported by different REE pattern, which N-MORB metabasalt displaying low La/Yb (2.0 to 3.5, Marques 2017) and E-MORB dolerites/gabbros with high La/Yb (6.5 to 12.8, Fig. 4;14A). In general, low La/Yb ratios reflect a melting regime dominated by relatively large melt fraction and/or spinel as the predominant residual phase, whereas high La/Yb ratios are indicative of smaller melt fractions and/or garnet control (Kinzeler 1997, Hellebrand. et al., 2002). The parental magmas involved melting or contamination with crustal rocks in order to produce ilmenite-bearing mafic magmas and contain inherited zircon grains (gabbro sample dated by Marques 2017). However the reservoir is predominantly from juvenile material as suggested by metaluminous nature, T_{DM} model ages of 0.84 to 0.88 Ga and positive ε_{Nd} (T) values range +3.81 to +3.97. Thus, based on these isotopic and geochemical data the dolerite and gabbros were probably derived from low-degree (~8) of partial melting of a metasomatized juvenile lithospheric mantle in the garnet stability field (Fig. 4.14B). Low-percentage melts are especially enriched in highly incompatible chemical species, such as water, sulfate, chlorine, alkalis, LILE, and HFSE (such as U, Th, Nb, Ta,). According to Loucks and Ballard (2003) their link to exceptional Au ore-forming fertility arises gold must behave as an incompatible element during low percentages of partial melting of peridotite mantle or lithospheric mantle.

In summary, the subcontinental lithospheric mantle (SCLM) was initially metasomatized by subduction zone fluids at ~750 Ma, during which chalcophile (Cu) and siderophile (for instance Au and W) elements could be efficiently transported from the mantle source .The metasomatic assemblages then resided within the SCLM until melting occurred in response to lithospheric perturbations. Two major events of melting occurred after this continental collision: a major phase of extensional tectonics and delamination at 597-585 Ma followed by compresional event with development of crustal-scale strike-slip shear zone at ~577 Ma. In both tectonic environments the parental magmas where water-rich and low fO_2 due the presence of magmatic hornblende and ilmenita in gabbro and dolerite. During these melting events the extraction of metals from metassomatized mantle is mainly controlled by magma oxidatition state (Richards, 2009). Metal-solubility studies indicate that significant quantities of Au can be transported by magmatic fluids under either reducing or oxidizing conditions, whereas Cu transport is much more favored in the oxidizing environment (Rowins, 2000). Thus, the dolerites and gabbros have the potential to

transport and formed only-Au ore system and other metals as tungsten and antimony that are commonly transported in reduced conditions.

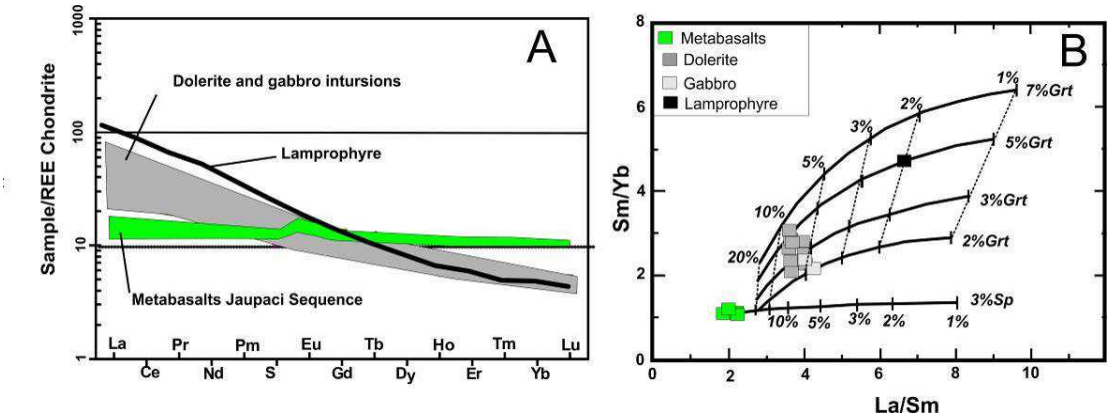

Figure 4.14 A) – Comparison of rare earth element spider diagrams pattern of metabasalts of Jaupaci Sequence and mafic menbers of Bacilândia Intrusions with normalized to the chondritic values of Sun and McDonough (1989); B) Variations in Sm/Yb vs. La/Sm (Ma et al., 2016) with melting curve of spinel-bearing peridotite / garnet-bearing peridotite source for metabasalts of Jaupaci Sequence , mafic dikes of Bacilândia Intrusions and lamprophyres.

4.10.2.2 – Significance of diorite porphyry, trachyte and syenite porphyry intrusions

Diorite porphyry, trachyte and syenite porphyry are likely to evolve from dolerites and gabbros by fractional crystallization, crustal assimilation and magma mixing rather than a dominantly crustal origin or partial melting of mafic lower crust. There are several evidences that support this interpretation: i) all felsic, intermediate and mafic rock types examined have positive $\varepsilon_{Nd}(T)$, similar trace element characteristics and similar mineralogy; ii) felsic and intermediate members display negative Eu anomalies coupled with marked depletions in Sr, Ti and P which point to fractional crystallization of plagioclase, apatite and Fe–Ti oxides in the source; iii) mafic components are volumetrically dominant supporting basic to felsic differentiation; iv) mafic enclaves in the syenite porphyry contain fine-grained K-feldspar crystals (contrasting with the porphyritic texture of the syenite) implying that the enclaves are hybrid; this observation is direct evidence that enclaves formed via magma mixing, instead of being restites or xenoliths (Didier and Barbarin 1991, Chappell and White 1991, Barbarin 2005). According to Patiño Douce (1995) and Castro et al., (1999) in order to generate felsic compositions, parental basic to intermediate magmas must have

evolved during ascent through crustal conduits after a residence period in chambers at the lower to middle crust. Processes that drive differentiation include fractionation of early phenocrysts, assimilation of crust and settling of resultant reaction assemblages. During continued flow through the conduit system, the parental magmas undergo contamination with reduced wall rocks (that where not mapped on surface) to produce ilmenite-bearing magmas and incorporate zircon xenocrystals (inherited zircons with 598 ± 3 Ma and 772 ± 6 Ma, in the syenite and trachyte sample, respectively). However, the magma reservoir is predominantly from juvenile material as suggested by T_{DM} model ages of 0.75 to 0.86 Ga and positive ε_{Nd} (T) varying from +3.8 to +4.5.

Gold behaviour during magmatic evolution is strongly controlled by the fO_2 of the melts. In more oxidized conditions, characterized by the presence of magnetite as the main Fe-Ti oxide, gold content in plutonic rocks decreases with increasing differentiation whereas the opposite occurs in more reduced conditions (Ishirara et al., 1985). According to Mccoy et al., (1997) gold behaves as an incompatible element under reducing conditions and tends to concentrate into the late fluids, possibly leading to gold mineralization related to highly evolved fluids. Therefore, the magmatic differentiation to originate felsic magmas of Bacilândia Intrusions enriched even more in Au, highly incompatible element and volatiles, whereas crustal contamination will potentially the source of As. However is not clear if the walls rocks will provide arsenic, since As-rich sedimentary rocks regionally are not recognized. An alternative model is proposed by Rowins (2000) and Mungall (2002), who suggested that W and As behave as incompatible element during the fractionation in reduced magmas and CO_2-rich hydrothermal fluids. Magma mixing process is likely responsible for volatile enrichment and fluid saturation by input of volatile-rich mafic magmas in more evolved syenite magmas.

Two events of differentiation from basic magmas occurred to generated felsic and intermediate magmas of Bacilândia intrusions: an early event represented by diorite porphyry dated at 590 ± 5 Ma and late event represented by trachyte and syenite porphyry dated at ~574-572 Ma.

4.10.2.3. Late lamprophyre intrusions

The lamprophyres are mafic alkaline dikes more enriched in LILE and HFSE. They plot in tectonic fields differs from dolerites and gabbros (Fig. 4.7), showing

alkaline within-plate basalts affinity. The high La/Yb ratios coupled with positive ε_{Nd} (T) are indicative of same juvenile mantle source of dolerites and gabbro, however the elevated Sm/Yb (4.74) and La/Sm (6.78) point to lower degree of melting (~2 %) with residual garnet to generate lamprophyries dikes (Fig. 4.16B). The lamprophyre post-date gold mineralization, hydrothermal alteration and other intrusion of Bacilândia Intrusions, for this reason is possible to infer the lamprophyre emplacement after 572 Ma (age of youngest mineralized syenite porphyry) in extensional tectonic setting. It is likely that those lamprophyres dikes are mantle-mafic derived magmas involved in the generation of post-kinematic A-type intrusion at 511 and 506 Ma (e.g Iporá granites).

4.10.2. Regional strike-slip faulting controlling alkaline intrusions and gold mineralization.

The spatial association of the Fazenda Nova deposit with a dense dyke swarm emplaced along the Bacilândia strike-slip fault suggests that this structure played a role in channeling of the fertile magmas and hydrothermal fluids to the upper crust. Field evidence coupled with the aeromagnetic survey indicates that the Bacilândia Fault is a second order crustal-scale shear zone that splays out of the major crustal-scale Moiporá-Novo Brasil shear system. Therefore, it is likely to act as a conduit for mantle material to reach the SCLM (sub-continental lithospheric mantle) and/or to provide enough heat to induce melting in the lithospheric mantle material as well as a channelway for the circulation of hydrothermal fluids (Storti 2003; Pirajno 2010). The Bacilândia Fault was probably active over long periods of time. It may have started in an extensional setting and subsequently reactivated during later compressional tectonic events. However, one single gold mineralization event is recorded indicating that a critical process may have occurred that transported the hydrothermal fluids and gold to the upper crust. A model of evolution for the Bacilândia Fault (Fig 4.15) may be envisaged based on the following evidence:

1-The spatial relationship between the Bacilândia Fault and the Jaupaci volcanics may suggest that this fault was active during the extensional environment that allowed the extrusion of this bimodal volcanism at 598 ± 10 Ma (Fig 4.15A) ;

2- Shortly after the onset of the volcanic basin, a shift to a compressional stress regime imprinted the D_{n-1} fabric in the type-1 and type-2 plutonic rocks and in the Jaupaci volcanics. The compressional event was followed by local extensional regime where the first pulse of dikes ascended. In this event were recorded small volume of

gabbros, dolerites, diorite porphyry and A-type granites (Israelândia granite), which took place roughly from 593 to 585 Ma (Fig 4.15B);

3-Subsequently, intense folding and shearing took place during the regional development of the D_n fabrics under greenschist metamorphic conditions. At the same time syn-kinematic mylonitic A-type granites were emplaced along the Moiporá-Nova Brasil shear zone at 577-539 Ma. In the Fazenda Nova deposit, the F_n folding and the Bacilândia Fault imprinted the S_n foliation indicating that reactivation and major activity of this fault were developed in this compressional setting and time span. Under this major compression environment, the hydrothermal conductivity of faults can increase by several orders of magnitude where high permeabilities are maintained even to considerable depths, promoting high heat flow and the arrival to epizonal depths of deep fluids with minor heat loss (Sanderson and Zhang, 1999).Therefore, a large volume of lower crust melting and hydrothermal fluids are generated in the D_n event, where local extensional zones (for instance the deflection of the Bacilândia fault in the south of the Lavrinha pit, Fig. 4.3) allowed magma emplacement and hydrothermal circulation. The geochronological data presented in this paper indicate that emplacement of the second pulse of trachytes and syenite porphyry (like other post-Dn dolerite intrusions) took place at ~574-572 Ma, so they occurred early in the evolution of the Bacilândia Fault. According to Selby et al., (2001) and Hart et al., (2004) reduced magmatic systems cool rapidly, implying that magmatic and hydrothermal processes must be essentially coeval. Thus, hydrothermal fluids should have migrated to upper crust soon after the emplacement of the younger syenite porphyry at 572 Ma, although the exact timing of gold mineralization cannot be determined by available data. When the hydrothermal fluids reached shallow levels the dikes may have acted as impermeable barriers, enabling the fluids to be trapped within the local extensional pathways with subsequent metal precipitation. The dikes are therefore stoppers that prevented the leakage and run-off of the ore-bearing fluids. The prolonged interaction of the Bacilândia Intrusions with the surrounding mineralizing fluids is also evidenced by the pervasive early alteration along the margins of the dikes. This would also explain the close association between the dikes and mineralization, as well as the absence of ore mineralization in structural channels (fault zones) which are devoid of these dikes (Fig 4.15C).

4-Continued deformation at shallow levels during the D_{n+1}event caused the bending of the Bacilândia fault which may also have acted as a deep conduit for

emplacement of the late lamprophyre dykes under extensional conditions. Late-stage barren hydrothermal fluids may relate to this final event (Fig 4.15D).

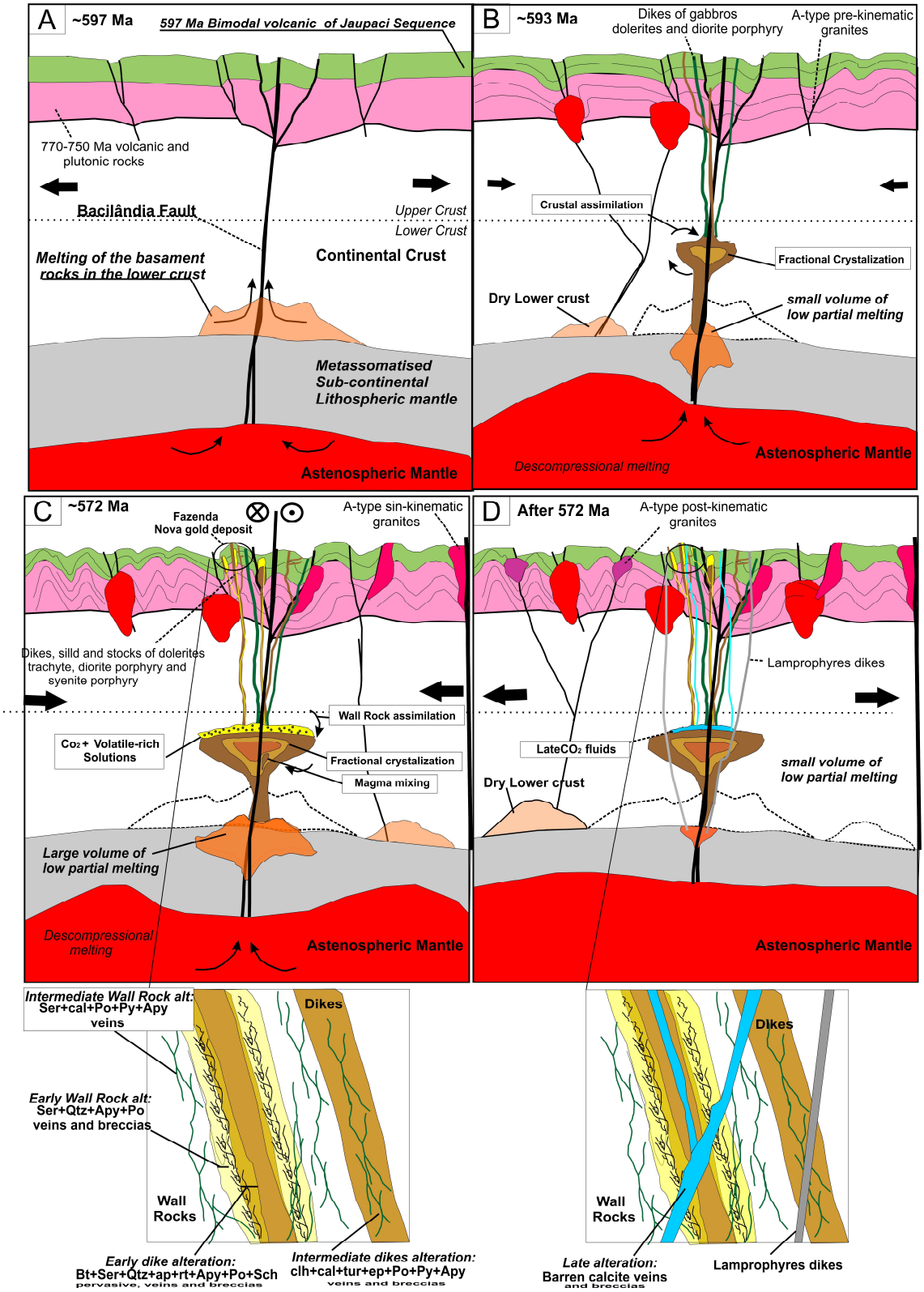

Figure 4.15 Schematic model based on the data presented here for the evolution of the Bacilândia Fault and progressive stages envisaged for the genesis of the Fazenda Nova

deposit. A) Bacilândia Fault acting as a deep conduit in an extensional setting that allowed the extrusion of volcanic rocks of the Jaupaci Sequence; B) Compressional setting (D_{n-1}) associated with the decompressional melting of the asthenosphere with partial melting of metassomatised mantle sub-continental lithospheric mantle to generate first pulse of Bacilândia Intrusions dikes. C) Major activity of Bacilândia Fault in the D_n compressional setting, where the large volume of dikes, sills and stocks of Bacilândia Intrusions were generated. In this stage the magma mixing, fractional crystallization and crustal assimilation play critical role in the generation of early and intermediate hydrothermal stages; D) Extensional setting with development of late hydrothermal fluids and emplacement of lamprophyres.

The A-type granites are temporally related to Bacilândia Intrusions, however show no Au mineralization. This is probably attributable to the H_2O-deficient and high temperature signatures of the parental magma typical of A-type granites (Loiselle and Wones, 1979; Collins et al., 1982). The source of A-type granites should be a "dry" lower crust possibly regions with no previous metasomatism (Fig 4.15).

4.10.3. Hydrothermal alteration and arsenopyrite geothermometry

4.10.3.1– Early stage alteration (main stage)

The early stage alteration occurred with paragenesis of arsenopyrite with pyrrhotite, apatite and rutile-leucoxene, evidencing the crucial role of deposition of these minerals with of gold-bearing acicular arsenopyrite. We use the arsenopyrite geothermometer (Barton, 1969; Sharp et al., 1985) and assume a maximum temperature of 340°C for crystallization of acicular arsenopyrite and pyrrhotite along with gold. (Fig.4.16A). The conditions to generation of such sulfide assemblage would have been low sulfur activity, with low pH environment and reduced (log $a_{\sum S}$ with –2.5 and log fO_2 ranging from –31.2 to –32.5, Fig.4.17B). At this temperature and ph, Flee et al., (1993); Stefansson and Seward (2004); Pokrovsky et al., (2014) suggested that the gold should be carried as bisulfide complexes in hydrothermal solutions ($AuHS^0$ and $Au(HS)_2$) ,or gold and arsenic can be transported together as thioarsenide complexes ($AuAsS_2$). Thus, Au solubility will be very sensitive to a decrease in the total activity of reduced sulfur species. Considering the gold is carry by bisulfide complex the deposition of gold may related to follow steps: i) the hydrothermal fluid cause the

oxidation of magmatic ilmenite to rutile and/or titanite that will release iron (Fe^{2+}) to hydrothermal solutions; ii) the interaction of iron-rich solutions with As-hydroxide complexes (As $(OH)_3$) and H_2S crystallized arsenopyrite and pyrrhotite that impoverishes the fluid in HS−, thereby destabilizing the dominant gold complexes $Au(HS)_2$ with gold precipitation. The excess of iron and titanium in solution form hydrothermal rutile and less siderite. The precipitation of gold with arsenic sulfides under reducing conditions is consistent with the study of Heinrich and Eadington (1986); Gilbert et al., (1998) Pokrovsky et al., (2002); who considered that reducing conditions are expected to decrease gold solubility of bisulfide complexes in the hydrothermal fluid favoring the gold precipitation.

The fine needle arsenopyrite is the main alteration feature of the early stage. According to Volkok et al., (2006) formation of this arsenopyrite texture enriched in gold seems to occur under considerable oversaturation of hydrothermal solutions with S-As-containing complex compounds of gold, whose decomposition results in a great number of sulfide seeds, which rapidly crystallize. The needle arsenopyrite is commonly characterized by high porosity with local presence of a significant number of metallic microinclusions as galena and pyrite, suggesting that the arsenopyrite precipitation was followed by trapping of gold and other metallic particles in the inclusion void spaces. The gold presents homogeneous distribution, which indicates a fast growth rate and short residence time for the Au+ ions (Becker et al., 2010). Thus, the growing of the arsenopyrite promotes the gold trapping and encapsulation. Fine-acicular high-Au arsenopyrites were found and studied at several large gold deposits localized in Hillgrove, Australia (Ashley et al., 2000), Suzdal and Zherek in the eastern of Kazakhstan (Kovalev et al., 2011), Dolin Creek in Alaska (Groves et al., 2004). At some of them gold is present in arsenopyrite in bound form, whereas at others, both in bound form and as metal nanoparticles (in Suzdal are reported 1000 to 2000 ppm of Au in acicular Arsenopyrite). One of the reasons for the Au enrichment of fine-acicular arsenopyrite is the high defectiveness of its structure, determined by the Fe:As:S proportion, as compared with well-crystallized arsenopyrite (Zhmodik, 2008). Cepedal et al., (2008) studied gold-bearing arsenopyrite in El Valle deposit proposed a mechanism in which gold is removed from ore fluids by chemisorption at As-rich, Fe-deficient surface sites and incorporated into the sulfides as solid solution.

4.10.3.2. Intermediate stage of alteration

After crystallization of acicular arsenopyrite with gold an intense carbonate-rich hydrothermal alteration of intermediate stage led to minor pyrite and tabular arsenopyrite crystallization, the acicular arsenopyrite found in this late episode is considered to be relict of the early sulfide stage. The arsenopyrite geothermometer assume a maximum temperature of 305°C for crystallization of tabular arsenopyrite and pyrite (Fig.4.16A), slightly high sulfur acitvity and lower reduced conditions of hydrothermal fluid compared with early stage (log $a_{\sum S}$ with 0.5, and log fO_2 ranging from –28.8 to –31 ,Fig.4.16B). The temperature and Eh conditions of intermediate and early alteration are quite similar evidenced by coexistence of both hydrothermal arsenopyrite stages (early acicular and late tabular arsenopyrite).

The tabular arsenopyrite present no gold contents showing that it might have been crystallized at late stage with any incorporation of Au in sulfide lattice. The deposition of gold associated with tabular arsenopyrite occurs in free-state, frequently associated with intermediate stage low-temperature hydrothermal assemblage (carbonates, sericite, and chlorite). The presence of intense carbonate alteration and crystallization of new minerals (e.g., chlorite and tourmaline) suggests the predominance of open-system processes with input of new elements and more oxidizing conditions, instead of closed system, involving only mineral transformations. It is not clear if intermediate event may have also resulted in addition of new gold, since most of this type of alteration is barren.

4.10.3.3. Late stage of alteration

Late-stage alteration is related to a barren CO_2- rich alteration possibly formed at shallow depth associated with boiling of fluids to originated cockcade and colloform vein texture (Moncada et al., 2012). However no alteration, sulfide or mineralization is associated to this phase showing that this late-boiling process did not play role on gold deposition in Fazenda Nova deposit.

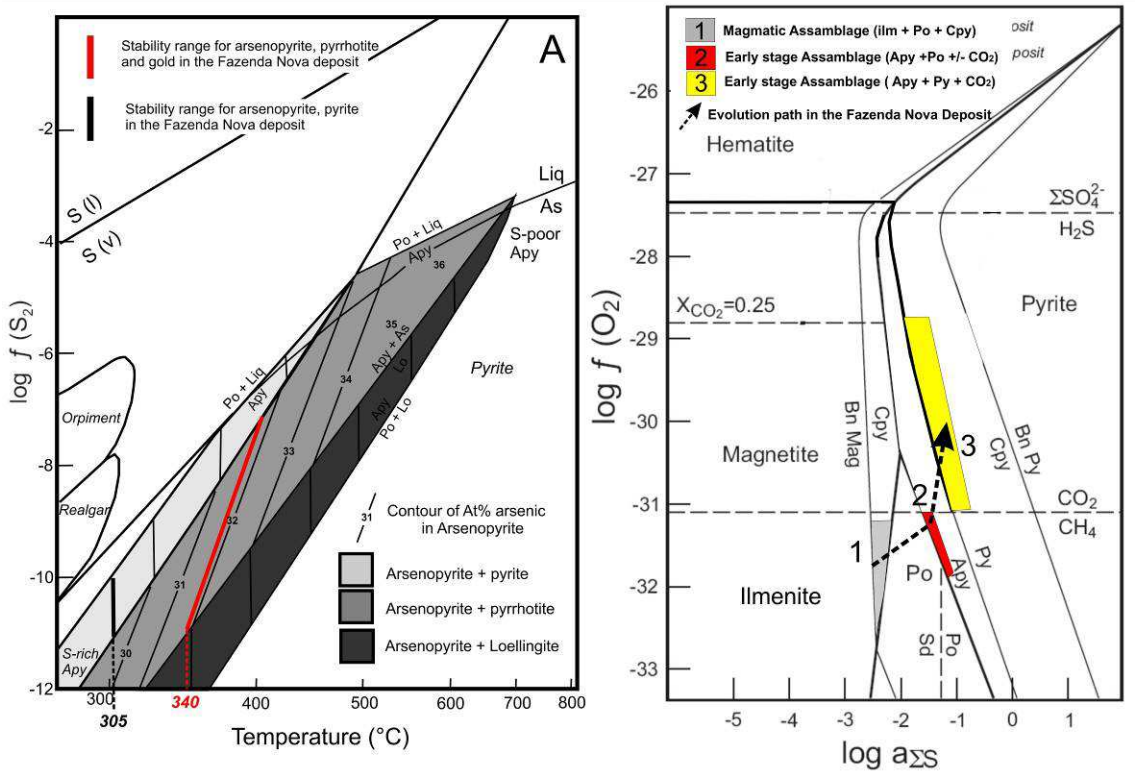

Figure 4.16 - A) The average composition of hydrothermal arsenopyrite of early sulfide stage is plotted. Temperature of crystallization of arsenopyrite and pyrrhotite along with gold is expected to be about 340°C. Phase diagram redrawn from Barton (1969), Kretschman and Scott (1976) and Sharp et al., (1985). Atomic proportions of arsenopyrite are indicated. Apy = arsenopyrite, Lo = loellingite, Po = pyrrhotite, Py = pyrite. B) Evolution of the chemical conditions at the Fazenda Nova deposit: log *f*O2 vs. log a∑S stability based on diagram Bigot and Jebrak diagram (2015); (1) Initiate with magmatic assamblages with pyrrhotite-chalcopyrite-ilmenite assemblage frequently observed in dykes ; evolved (2) to arsenopyrite-pyrrhotite-rutile (with less carbonate) assemblage of early stage ; finally (3) to pyrite-arsenopyrite- carbonate rich alteration of intemerdiate stage

4.10.4. Nature of the aqueous-carbonic ore fluid phase

The evolving fluids of the Fazenda Nova deposit show an increase in the CO_2 content with time, starting with mineralized quartz and carbonate-poor early stage alteration followed by carbonate-quartz intermediate stages and final barren CO_2-rich veining and alteration. Magmatic origin for carbon dioxide-rich aqueous fluids is not widely accepted in mineral deposit models. Firstly, most felsic intrusions do not contain carbon-bearing magmatic minerals and, therefore, it is commonly assumed that the magmas could not have produced carbon dioxide (e.g., Phillips and Zhou, 1999).

Secondly, low-salinity carbon dioxide-rich aqueous fluids associated with gold-only deposits are commonly interpreted to be metamorphic in origin (Phillips and Powell, 1993, Goldfarb et al., 2005). However, according to Lowenstern (2000, 2001) CO_2 contents are commonly associated with magmas that assimilated sedimentary crust. Additionally carbon dioxide has a low solubility in felsic melts and its solubility decreases with decreasing pressure and increase temperature (Giggenbach, 1997; Lowenstern, 2001). The low solubility of carbon dioxide will result in the early exsolution of volatiles from magma at much higher pressures than those predicted for magmas which contain only water. According to Baker (2002), deeper magmatic-hydrothermal systems are typically more CO_2 rich, and during progressive open-system degassing, early magmatic vapors will have greater concentrations of CO_2. Thus, early release of carbon dioxide from melts will increase the relative concentration of other volatiles in the melt, including potential metal-bearing bisulfide complexes. Phillips and Evans (2004) have suggested that CO_2 may have played a critical role in transporting Au by buffering the fluid in a pH range, where elevated Au concentration can be maintained by complexing with reduced sulphur.

The mineralized fluids from the Fazenda Nova deposit are derived from low-degree melting of metassomatized mantled (already enriched in volatiles) and crustal assimilation have played important role to generate Bacilândia magmas. The fractionation crystallization and magma mixing potentially increase saturation of fluids/volatiles in later stages of felsic to intermediate magmas and both magmatic process must have occurred in middle to lower crust, where magma are especially CO_2-rich. The increase of volatiles allows the melt reach fluid saturations when fluids exsolved from the melt, therefore metals and volatiles such as sulphur and halogens presumably preferentially partition from the melt into an exsolving aqueous-carbonic ore fluid phase (Hedenquist and Lowenstern, 1994). Furthermore the venulation and brecciation present in all alterations stages indicate that these hydrothermal fluid events, likely involved fluids under high pressure (hydrothermal or hydraulic breccias). Thus, is very likely that transport of aquo-carbonic fluids and metal-bearing bisulfide complexes is from magmatic source. This is supported by C-O isotopes indicating that carbonate are derived from magmatic/mantle hydrothermal solutions sources. Additionally the presence of apatite in hydrothermal early stage points towards the influence of magmatic volatiles (F, Cl) in hydrothermal solutions.

4.10.5. Deposit classification and metallogenic affiliation of mineralization

The Fazenda Nova deposit is characterized by a reduced/low-sulphidation sulphide assemblage (arsenopyrite-pyrite-pyrrhotite), Au-As-W-Sb metal association, significant CO_2 in the ore-forming fluid, and relatively low temperature biotite-sericite-chlorite-carbonate phyllic alteration along brittle stockwork/breccia structures clearly points to a low-sulphidation style of relatively shallow (epizonal) mineralization. These characteristics of the Fazenda Nova deposit most closely resemble those associated with both epizonal intrusion-related and epizonal orogenic gold deposits (Groves et al., 1998; Lang and Baker 2001; Groves et al., 2003; Goldfarb et al., 2005; Hart et al., 2002; Mair et al., 2011). According to Hart et al., (2004), reduced intrusion related gold deposits exhibit a predictable zonation of differing deposit styles from intrusion-hosted (Au-Bi-Te±W,Mo), proximal (Au-As±W,Sb) to pluton-distal (Au-As-Hg-Sb ±Pb,Zn) settings. There is also crustal-scale vertical zonation, with epizonal occurrences forming at shallower levels. The Fazenda Nova deposit metallic association and features are consistent with those of Reduced Intrusion Related gold deposits developed at proximal and shallow crustal settings. These features encompass: i) mineralization developed during post-collisional tectonic setting above previously metasomatized subcontinental lithosphere mantle; ii) dikes, sill and stocks systems reflecting some input from mantle-derived mafic alkaline magmas into the base of the crust; iii) metaluminous magmas with primary oxidation state that form ilmenite-series intrusions; iii) felsic magma mixed with volatile-rich mafic melts; iv) high geothermal gradients indicated by ore deposition at temperatures of 340° to 300°C assocated with veins textures exclusive of shallow formation depths (<4 km); v) volatile saturation induced by magmatic processes such as fractional crystallization, magma mixing, or crustal assimilation; vi) carbonate hydrothermal veins with C-O isotopes displaying magmatic/mantle fluids affinities. Alternatively, the temporal and spatial association of D_n event, development of Bacilândia fault, greenschist metamorphism and gold mineralization points to features of orogenic gold deposits.

We believe that the genetic model of Fazenda Nova deposit fit with IGRD, since magmatic process play important role in all stages of ore-formation. Firstly, low percentages of partial melting of lithospheric mantle melting concentrated gold as an incompatible element. Posteriorly, magmatic process as fractional crystallization, magma mixing and significant crustal contamination may be a critical factor for gold

concentration and fluid saturation in the melts. Furthermore, in the metamorphic devolatilization model for orogenic gold deposits, the auriferous fluid is considered to be derived from the breakdown of hydrous and carbonate minerals during prograde metamorphism (Kerrich and Fyfe, 1981). During these events, dissolution/decarbonation reactions produce CO_2 with $\delta^{13}C$ values similar to or more enriched than in the parent rocks (Ohmoto and Goldhaber, 1997). The $\delta^{13}C$ values obtained in this work present very low values range from -9.68 to -11.57‰, compared with orogenic gold deposit values with $\delta^{13}C$ range of -2.0 to -4.0‰, (Beaudoin and Pitre ,2005; Craw et al., 2010). Thus, the carbonate veins of Fazenda Nova deposit are derive from mantle-juvenile/magmatic volatiles rather than CO_2 from metamorphic devolatization. Nevertheless, if Fazenda Nova deposit is indeed an intrusion-related gold deposit, then the causative intrusion (or intrusion-hosted) system remains to be recognized. Thus, open entire new exploration potential for the deeper portion of Fazenda Nova deposit.

4.10.6. Deposits anologue to Fazenda Nova gold deposit

The Fazenda Nova gold deposit has a number of similarities to the Shotgun deposit located 150 km north of Dillingham, SW Alaska. As described by Rombach and Newberry (2001), auriferous quartz stockworks and breccia at Shotgun, resembling a porphyry-style system, cut a ca. 70 Ma felsic porphyry stock and Au-As mineralizing fluids are, for the most part, similar to those reported here for the Fazenda Nova deposit. These similarities encompasses: metaluminous ilmenite-bearing felsic intrusion that hosted the mineralization, degrees of magmatic fractionation to concentrate metal (Au,As, Bi and Te), proximal alteration of quartz stock-work veining with hydrothermal assemblage of sericite+biotite+rutile+feldspar+sulfides and distal alteration of tourmaline+carbonate+clhorite+albite; a dominant low-sulphidation arsenopyrite-pyrrhotite-pyrite sulfides assemblages; isotopes and fluid inclusions indicating temperature of late-mineralized hydrothermal fluids estimated at 380-360 °C. In contrast to Fazenda Nova, the Shotgun deposit is characterized by significant copper-bearing ore phases (chalcopyrite and bornite), important albite alteration, a high sodium (rather than Fe) concentration in the hydrothermal fluids, and Fazenda Nova has considerable resources hosted in mafic fine-grained dolerites, whereas at Shotgun the resources is mainly hosted in the porphyry stock. Also Shotgun recorded an early

hydrothermal sulfide stage with higher temperature represented by lollengite-arsenopyrite-pyrrhotite deposition temperatures of 470 to 630 °C. Thus, considering the features showed at Shotgun and Fazenda Nova deposit, it is possible to infer that they appear to be products of the same magmatic-hydrothermal system and only differ in depth of formation, with Fazenda Nova representing a shallow system (with temperature of hydrothermal fluids with 305 to 340°C), whereas Shotgun may represent a deeper portion of the magmatic-hydrothermal system that present a broader range of hydrothermal temperature varying of 630 to 350°C

4.11 – Conclusions

The main conclusions in the present study are listed below.

- The Fazenda Nova deposit mineralization is hosted in the Bacilândia Intrusions, a long-lived magmatic system of dikes, sills and stocks that were emplaced from ~593 to 572 Ma in the post-collisional tectonic setting of the Arenópolis Magmatic Arc. The stages of emplacement of the Bacilândia intrusions may correlate with three pulses of A-type granitoids: (1) the early event is represented by deformed gabbros, dolerites and syenites intruded at 593-590 Ma and is time-equivalent to the pre-kinematic A-type granitoids (585 Ma); (2) the 574-572 Ma trachyte and syenite porphyry are equivalent to early stages of syn-kinematic A-type intrusions (577-539 Ma); (3) and the late lamprophyres are likely related to post-kinematic A-type intrusions (after 572 Ma). The Bacilândia Intrusions have remarkably positive $\varepsilon_{Nd}(T)$ with values ranging from +1.88 to +4.5, similar T_{DM} model ages (0.75-0.88 Ga), are enriched in LILE, HFSE(Nb, Th and Zr) and light REE, and all trace element features are relatively uniform and consistent with a cogenetic origin and source involving partial melting of older metassomatized Neoproterozoic juvenile rocks (~770-598 Ma based on inherited zircon ages).
- Trace elements from dolerite and gabbros indicate mafic rocks derived from low-degree (~8%) partial melting of a fertile lithospheric mantle in the garnet stability field. This process specifically provides Au fertility, enrichment in incompatible elements and volatiles. The trachyte, diorite

porphyry and syenite porphyry evolved from dolerites by fractional crystallization, crustal assimilation and magma mixing rather than by a dominantly crustal origin or partial melting of mafic lower crust. These magmatic processes play a critical role in gold concentration and fluid saturation.

- The Bacilândia Fault is a NNW trending second order crustal-scale shear zone that branches out of the major crustal-scale N trending Moiporá-Novo Brasil shear system. The Bacilândia fault plays an important role in channelling the melts and the mineralized hydrothermal fluids to the upper crust. Main fault activity took place at ~572 Ma with the emplacement of a large volume of dikes and sills of the Bacilândia intrusion suite and development of hydrothermal alteration in the Fazenda Nova deposit.
- Three types of alteration are recognized in the Fazenda Nova deposit:
  - ✓ i) An early (main) alteration that comprises stockwork quartz veining and silicified breccias associated with pervasive sericite and biotite alteration (including a hydrothermal association of arsenopyrite, pyrrhotite, scheelite, stibnite, rutile, leucoxene, apatite and siderite). The most common sulfide in this stage is fine-grained acicular arsenopyrite that hosts invisible gold and inclusions of free native gold, galena and pyrite grains. The temperature estimated for acicular arsenopyrite, pyrrhotite and gold precipitation was estimated at 340°C. At such temperature, gold is transported as bisulfide complexes or thioarsenide complexes;
  - ✓ ii) An intermediate stage represented by calcite-quartz veining with a hydrothermal assemblage of chlorite-tourmaline-epidote-titanite-pyrrhotite-arsenopyrite-pyrite. The arsenopyrite exhibits a tabular habit with no gold inclusions, and the assemblage of tabular arsenopyrite-pyrite provides a temperature of 305°C;
  - ✓ iii) The late stage is comprised of barren veining/brecciation infilled by monotonous calcite-ankerite with comb/cockcade textures typical of very shallow brittle crustal levels

- The C-O isotopic data presented provided a $\delta^{13}C$ range from -9.68 to -11.57‰ and a $\delta^{18}O$ range from 12.87 to 13.84‰. These values are consistent with hydrothermal mantle-juvenile/magmatic carbonates.
- Such a magmatic isotopic signature coupled with a mineralized system that is: a) hosted in post-collisional reduced intrusives; b) characterized by shallow-level, open space-filling textures in veins and breccia textures; c) a metal association of Au with As-W-Sb ;d) a reduced low sulfidation assemblage of arsenopyrite-pyrrhotite-pyrite, and e) CO_2-rich hydrothermal fuids and related carbonate-rich hydrothermal alteration altogether strongly suggest that the Fazenda Nova deposit may be classified as an Epizonal Reduced Intrusion Related Gold System.

The Fazenda Nova deposit represents a significant new Intrusion Related gold resource in a region of central Brazil that has traditionally been known for orogenic gold deposits related to the Brasiliano Orogeny (630 Ma) or older Paleoproterozoic/Archean events . This classification opens up a new exploration frontier where the main prospective guide is the post-orogenic ,intracontinental, second order crustal-scale strike-slip shear zones that tapped deep fertile magmas and hydrothermal fluids distilled from previously metasomatized subcontinental lithospheric mantle.

4.12. References

Barbarin, B., 2005. Mafic magmatic enclaves and mafic rocks associated with some granitoids of the central Sierra Nevada batholith, California: nature, origin, and relations with the hosts. Lithos 80, 155–177.

Barton, Jr., P.B., 1969, Thermochemical study of the system Fe-As-S: Geochimica et Cosmochimica Acta, v. 33, p. 841–857

Beaudoin, G., Pitre, D., 2005. Stable isotope geochemistry of the Archaean Val-d'Or (Canada) orogenic gold vein field. Mineral. Deposita v.40, p.59–75.

Becker, U., Reich, M., and Biswas, S. (2010) Nanoparticle–host interactions in natural systems. In F. Brenker, and G. Jordan, Eds., Nanoscopic Approaches in Earth and Planetary Sciences: EMU Notes in Mineralogy, 8, 1–52

Bierlein, F.P., Groves, D.I., Goldfarb, R.J., Dubé, B., 2006. Lithospheric controls on the formation of provinces hosting giant orogenic gold deposits. Mineral. Deposita 40, 874–886.

Bigot L., Jébrak M., 2015. Gold Mineralization at the Syenite-Hosted Beattie Gold Deposit,Duparquet, Neoarchean Abitibi Belt, Canada . Econ. Geol. 110, 315–335.

Borisenko, A.S., Sotnikov, V.I., Izokh, A.E., Polyakov, G.V., Obolensky, A.A., 2006.Permo-Triassic mineralization in Asia and its relation to plume magmatism. Russian Geology and Geophysics 47, 166–182.

Castro, A., Patino Douce, A.E., Corretge, L.G., de la Rosa, J.D., El-Biad, M., and El-Hmidi, H., 1999, Origin of peraluminous granites and granodiorites, Iberian massif, Spain: An experimental test of granite petrogenesis: Contributions to Mineralogy and Petrology, v. 135, p. 255−276.

Chappell, B.W., White, A.J.R., 1991. Restite enclaves and the restite model. In: Barbarin, B., Didier, J. (Eds.), Enclaves and Granite Petrology. Elsevier, Amsterdam, pp. 375–381.

Craig, H., 1953. The geochemistry of the carbon isotopes. Geochimica et cosmochimica Acta 3, p53-92.

Craw, D., Upton, P., Yu, B., Horton, T., Chen, Y., 2010. Young orogenic gold mineralisation in active collisional mountains, Taiwan. Mineral. Deposita 45, 631–646.

Cepedal, A., Fuertes-Fuente, M., Martin-Izard, A., Gonzalez-Nistal, S., and Barrero, M., 2008, Gold-bearing As-rich pyrite and arsenopyrite from the El Valle gold deposit, Asturias, northwestern Spain: The Canadian Mineralogist,v. 46, p. 233–247.

Cordani, U,G. Pimentel, M,M. Araújo C,E,G. Basei, M,A,S Fuck R.A and Girardi, V,A,V, 2013a. Was there an Ediacaran Clymene Ocean in Central of South America ? *American Journal of Science*, v.313, p.517-539

Collins, W.J., Beams,S.D., White,A.J.R., Chappell,B.W.,1982. Nature and origin of A-type granites with particular reference to Southeastern Australia. *Contributions to Mineralogy and Petrology v.*80, p.189–200.

Curto, J.B., Vodotti, R.M., Blakely, R.J., Fuck, R.A., 2015. Crustal framework of the northwest Paraná Basin, Brazil: Insights from joint modeling of magnetic and gravity data. *Tectonophysics*. v.655, p. 58-72.

Dantas, E. L., Jost, H., Fuck, R. A., Brod, J. A., Pimentel, M. M. and Meneses, P. R., 2001. Proveniência e idade deposicional de sequências vulcano-sedimentares da região de Santa Terezinha de Goiás, baseada em dados isotópicos Sm-Nd e U-Pb em monocristal de zircão. *Revista Brasileira de Geociências* v.31(3): p. 329-33.

Della Giustina, M.E.S.D., Oliveira, C.G., Pimentel, M.M., Melo, L.V., Fuck, R.A., Dantas, E.L., Buhn, B., 2009. U–Pb and Sm–Nd constraints on the nature of the Campinorte Sequence and related Paleoproterozoic juvenile orthogneisses, Tocantins Province, Central Brazil. Geological Society of London Special Publication, v.323, p.255-269.

Didier, J., Barbarin, B., 1991a. The different types of enclaves in granites nomenclature. In: Didier, J., Barbarin, B. (Eds.), Enclaves and granite petrology. : Developments in Petrology. Elsevier, pp. 19–24.

Donnelly, K. E., Goldstein, S. L., Langmuir, C. H. & Spiegelman, M. (2004). Origin of enriched ocean ridge basalts and implications for mantle dynamics. Earth and Planetary Science Letters 226, 347-366.

Fleet, M.E., Chryssoulis, S.L., Davidson, R., Weisener, C.G., and Maclean, P.J., 1993, Arsenian pyrite from gold deposits: Au and As distribution investigated by SIMS and EMP, and color staining and surface oxidation by XPS and LIMS: The Canadian Mineralogist, v. 31, p. 1–17.

Frasca, A.A.S., 2015. Amálgamas do W-Gondwana na província do Tocantins. Unpublished Phd thesis, Universidade de Brasília, 105 pp.

Fuck, R.A., Pimentel, M.M. and Silva, L.J.H.D. 1994. Compartimentação tectônica da porção oriental da Província Tocantins. Actas, *38 Congresso Brasileiro de Geologia*, Balneário Camboriú-SC, 1, pp. 215-216.

Fuck, R. A. ; Dantas, E.L.; Vidotti, R.M. ; Roig, H. L. ; Almeida, T. 2013. Deformação intracontinental em sistemas transcorrentes: o caso do Lineamento Transbrasiliano, geometria, idade e significado, In: 140° Simpósio Nacional de Estudos Tectônicos. Chapada dos Guimarães. Sociedade Brasileira de Geologia. p. 1-3.

Fuck, R.A., Dantas, E.L., Pimentel, M.M., Botelho, N.F., Armstrong, R., Laux, J.H., Junges, S.L., Soares, J.E., Praxedes, I.F., 2014. Paleoproterozoic crust-formation and reworking events in the Tocantins Province, central Brazil: A contribution for Atlantica supercontinent reconstruction. *Precambrian Research, v.244* ,p.53-74.

Galer, S. J. G. & O'Nions, R. K. 1986. Magmagenesis and the mapping of chemical and isotopic variations in the mantle. *Chemical Geology*, v.56, p.45-61.

Ganade de Araújo, C.E., Weinberg, R.F., Cordani, U.G., 2014b. Extruding the Borborema Province (NE Brazil): a two-stage Neoproterozoic collision process. Terra Nova 26, 157–168.

Gibert F., Pascal M. L., and Pichavant M. (1998) Gold solubility and speciation in hydrothermal solutions: Experimental study of the stability of hydrosulfide complex of gold (AuHS0) at 350 to 450°C and 500 bars. Geochim. Cosmochim. Acta 62, 2931–2947

Genkin A. D., Bortnikov N. S., Cabri L. J., Wagner F. E., Stanley C. J., Safonov Y. G., McMahon G., Friedl J., Kerzin A. L., and Gamyanin G. N. (1998) A multidisciplinary study of invisible gold in

arsenopyrite from four mesothermal gold deposits in Siberia, Russian Federation. Econ. Geol. 93, 463–487.

Goldfarb, R.J., Baker, T., Dubé, B., Groves, D.I., Hart, C.J.R., Gosselin, P., 2005. Distribution, character and genesis of gold deposits in metamorphic terranes. Econ. Geol. 100th Anniv., p. 407–450.

Groves, D.I., Goldfarb, R.J., Robert, F., and Hart, C.J.R., 2003, Gold deposits in metamorphic belts: Overview of current understanding, outstanding problems, future research, and exploration significance: Economic Geology, v. 98, p. 1–29

Guimarães, S,B. Moura, M, A. Dantas, E . L., 2012. Petrology and geochronology of Bom Jardim copper deposit. *Brazilian Journal of Geology*, v.42, n.4, 2012, p.841-862.

Guo, P., Santosh, M., Li, S.R., 2013. Geodynamics of gold metallogeny in the Shandong Province, NE China: an integrated geological, geophysical and geochemical perspective. Gondwana Research, v.24,p. 1172-1202.

Groves, D.I., Golding, S.D., Rock, N.M.S., Barley, M.E., McNaughton, N.J., 1988. Archaean carbon reservoirs and their relevance to the fluid source for gold deposit. Nature 321, 254–257.

Hart, C.J.R., McCoy, D., Goldfarb, R.J., Smith, M., Roberts, P., Hulstein, R., Bakke, A.A., and Bundtzen, T.K., 2002, Geology, exploration and discovery in the Tintina gold province, Alaska and Yukon: Society of Economic Geologists, Special Publication 9, p. 241–274.

Hart, C.J.R., Mair, J.L., Goldfarb, R.J., and Groves, D.I., 2004, Source and redox controls on metallogenic variations in intrusion-related ore systems, Tombstone-Tungsten belt, Yukon Territory, Canada: Transactions of the Royal Society of Edinburgh, Earth Science, v. 95, p. 319−337.

Hasui, Y.; Carneiro, C. D. R.; Almeida, F. F. M.; Bartorelli, A., 2012. Geologia do Brasil, Ed. Beca. pag 118.

Hellebrand, E., Snow, J.E., Hoppe, P., Hofmann, A.W., 2002. Garnet-field melting and late-stage refertilization in “residual” abyssal peridotites from the Central IndianRidge. *J. Petrol*. 12, 2305–2338.

Heinrich C. A. and Eadington P. J., 1986. Thermodynamic predictions of the hydrothermal chemistry of arsenic and their significance for the paragenetic sequence of some cassiterite-arsenopyrite-base metal sulfide deposits. Econ. Geol. 81, 511–529

Ishirara, S. 1981. The Granitoid Series and Mineralization. *Economic Geology 75th Anniversary Volume*, pp.458-484.

Keith, M., Webber, J., 1964. Carbon and oxygen isotopic composition of selected limestones and fossils. *Geochimica et Cosmochimica* Acta 28, 1787-1816.

Kerrich, R., Fyfe, W.S., 1981. The gold-carbonate association: source of CO_2 and CO_2 fixation reactions in Archaean lode deposits. *Chem. Geol*. v.33,p. 265–293.

Krestchmar U. Scott S.D. (1976), Phase relations involving Arsenopyrite in the system Fe-As-S and their application. Canadian Mineralogist, v.14, p. 364-386.

Lang, J.R., and Baker, T., 2001, Intrusion-related gold systems: the present level of understanding: *Mineralium Deposita*, v. 36, p. 477–489

Laux, J.H., Pimentel, M.M., Dantas, E.L. Armstrong, R., Armele, A., Nilson, A.A., 2004. Mafic magmatism associated with the Goiás Magmatic Arc in the Anicuns region, Goiás, central Brazil:

Sm-Nd isotopes and ID-TIMS and SHRIMP U-Pb data. *Journal of South American Earth Sciences*, v.16(7), p.599-614.

Laux, J.H., Pimentel, M.M., Dantas, E.L. Armstrong, R., Junges, S.L., 2005. Two Neoproterozoic crustal events in the Brasília Belt, central Brazil. *Journal of South American Earth Sciences*, v.18 p.183-198.

Leahy, A., Barnicoat, A.C., Foster, R.P., Lawrence, S.R., Napier, R.W., 2005. Geodynamic processes that control the global distribution of gold deposits. In: McDonald, I., Boyce, I., Butler, I.B., Herrington, R.J., Polya, D.A. (Eds.), Mineral Deposits and Earth Evolution: *Geol. Soc. London, Spec. Publ.*, 248, pp. 119–132.

Li, S.R., Santosh, M., 2014. Metallogeny and craton destruction: records from the North China Craton. *Ore Geology Reviews* v. 56,p. 376-414

Loucks RR, Ballard JR (2003) Report 2C: Petrochemical characteristics, petrogenesis and tectonic habits of gold-ore-forming arc magmas. Unpublished report for industry-sponsored research project: *Predictive Guides to Copper and Gold Mineralization at Circum-Pacific Convergent Plate Margins*. 69p

Hedenquist, J.W., Lowenstern, J.B., 1994. The role of magmas in the formation of hydrothermal ore deposits. *Nature* 370, 519–527

Jost, H., Chemale, F., Dussin, I.A., Tassinari, C.C.G., Martins, R., 2010. A U-Pb zircon Paleoproterozoic age for the metasedimentary host rocks and gold mineralization of the Crixás greenstone belt, Goiás, central Brazil. *Ore Geology Reviews*, v. 37, p.127-139.

Ma L., Jiang S.Y., Hofmann A.W., Xu Y.G., Dai B.Z., Hou M.L. 2016. Rapid lithospheric thinning of the North China Craton: New evidence from cretaceous mafic dikes in the Jiaodong Peninsula.v. 432, p. 1-15.

Mair, J.L., Farmer, G.L., Groves, D.I., Hart, C.J.R., and Goldfarb, R.J., 2011, Petrogenesis of postcollisional magmatism at scheelite dome, Yukon, Canada: Evidence for a lithospheric mantle source for magmas associated with intrusion-related gold systems: *Economic Geology*, v. 106, p. 451–480

Matteini M., Junges S.L. , Dantas E.L.; Pimentel M.M., Bühn B., 2010. In situ zircon U–Pb and Lu–Hf isotope systematic on magmatic rocks: Insights on the crustal evolution of the Neoproterozoic Goiás Magmatic Arc, Brasília belt, Gondwana Researchv. 17 p.1-12.

Marques, G.C., 2017. Evolução Tectônica e metalogenética no contexto do depósito aurífero de Fazenda Nova, Arco Magmático de Goiás. Unpublished Phd thesis, Universidade de Brasília, 182 pp.

Moncada, D., Mutchler, S., Nieto, A., Reynolds, T.J., Rimstidt, J.D., and Bodnar, R.J., 2012, Mineral textures and fluid inclusions petrography of the epithermal Ag-Au deposits at Guanajuato, Mexico: Application to exploration: Journal of Geochemical Exploration, v. 114, p. 20–35

Motta-Araújo, J.G., 2013. Eventos Ígneos e metamórficos Neoproterozoicos/Eopaleozoicos no arco magmático de Arenópolis, Goiás. Unpublished Phd thesis, Universidade de Brasília, 73 pp.

Mota e Silva, J., Ferreira Filho C. F., Bunh B., Dantas E.L., 2011. Geology, petrology and geochemistry of the "Americano do Brasil" layered intrusion, central Brazil, and its Ni–Cu sulfide deposits. Mineralium Deposita, v. 46 p. 57-90.

Muller D (2002) Gold-copper mineralization in alkaline rocks. *Mineralium Deposita* v.37:1–3.

Mungall, J.E., 2002, Roasting the mantle: Slab melting and the genesis of major Au and Au-rich Cu deposits: Geology, v. 30, p. 915–918.

Niu,Y. L. & Batiza, R. (1997).Trace element evidence from seamounts for recycled oceanic crust in the eastern Pacific mantle. Earth and Planetary Science Letters 148, 471-483

Ohmoto, H., Goldhaber,M.B., 1997. Geochemistry of Hydrothermal Ore Deposits. third ed.John Willey and Sons, New York, pp. 517–611.

Oliveira C.G., Kuyumjian R.M., Bedran de Oliveira F., Marques G.C., Palermo N., Dantas E.L. 2014. Metalogênese do Arco Magmatico de Goiás, *in Metalogênese da Províncias Tectônicas Brasilieras*-CPRM, p.455-466.

Oliveira C.G., Bedran de Oliveira F., Della Giustina M.E.S,, Marques G.C., Dantas E.L., Pimentel M.M., Bunh B. M. 2015. The Chapada Cu-Au deposit, Mara Rosa Magmatic Arc, Central Brazil: Constraints on the Metalogenesis of a Neoproterozoic large porphyry-type deposit. 2015, *Ore Geology Reviews*, v. 72, p. 1-21.

Oreskes, N., Einaudi, M.T., 1992. Origin of hydrothermal fluids at Olympic Dam: preliminary results from fluid inclusions and stable isotopes. Economic Geology v.87 (1),p.64- 90.

Patino Douce, A.E., 1995,Experimental generation of hybrid silicic melts by reaction of high-Al basalts with metamorphic rocks: Journal of Geophysical Research, v. 100, p. 15623−15639.

Pearce, J.A., 1983. Role of the subcontinental lithosphere in magma genesis at active continental margins. In: Hawkesworth, C.I., Norry, M.J. (Eds.), Continental Basalts and Mantle Xenoliths. Shiva, Nantwich, pp. 230–249.

Pearce, J.A., Harris, N.B.W., and Tindle, A.G., 1984. Trace element discrimination diagrams for the tectonic interpretation of granitic rocks. *Journal of Petrology* v.25, p.956-983.

Pearce, J.A., 1996. Sources and settings of granitic rocks. Episodes v.19, p.120–125.

Pirajno, F., Mao, J.-W., Zhang, Z.-C., Zhang, Z.-H., Chai, F.-M., 2008. The association of mafic-ultramafic intrusions and A-type magmatism in the Tian Shan and Altay orogens, NW China: implications for geodynamic evolution and potential for the discovery of new ore deposits. Journal of Asian Earth Sciences v.32,p 165e183.

Pirajno, F., Ernst, R.E., Borisenko, A.S., Fedoseev, G., Naumov, E.A., 2009. Intraplate magmatism in central Asia and China and associated metallogeny. Ore Geology Reviews 35, 114–136.

Pirajno, F., 2010. Intracontinental strike-slip faults, associated magmatism, mineral systems and mantle dynamics: examples from NW China and Altay-Sayan (Siberia). *Journal of Geodynamics* v.50, p.325-346.

Pirajno, F., Zhou T., 2015. Intracontinental Porphyry and Porphyry-Skarn Mineral Systems in Eastern China:Scrutiny of a Special Case “Made-in-China”. Economic Geology, v. 110, p. 603–629.

Pimentel, M.M. and Fuck, R.A. 1992. Neoproterozoic crustal accretion in central Brazil. *Geology*, v.20, p.375-379.

Pimentel,M.M., Fuck,R.A. and Alvarenga,C.J.S. 1996. Post-Brasiliano (Pan-African) high-K granitic magmatism in central Brazil: late Precambrian/early Paleozoic extension. *Precambrian Research,v.* 80:p.217-238.

Pimentel, M.M., Whitehouse, M.J., Viana, M.G., Fuck, R.A., Machado, N., 1997. The Mara Rosa Arc in the Tocantins Province: further evidence for Neoproterozoic crustal accretion in central Brazil. Precambrian Res. 81, 299–310.

Pimentel, M.M., Fuck, R.A., Ferreira Filho, C.F., Araújo, S.M., 2000. The basement of the Brasília Belt and the Goiás Magmatic Arc. In: Cordani, U.G., Milani, E.J., Thomaz Filho, A., Campos, D.A. (eds) *Tectonic Evolution of South America*. 31st International Geological Congress, Rio de Janeiro, 195–229.

Pimentel, M.M., Ferreira Filho, C.F., Armstrong, R.A., 2004. SHRIMP U-Pb and Sm-Nd ages of the Niquelândia layered complex: Meso- (1.25 Ga) and Neoproterozoic (0.79 Ga) extensional events in central Brazil. *Precambrian Research* v.132, p.133-153.

Phillips, G.N., Evans, K.A., 2004. Role of CO_2 in the formation of gold deposits. Nature v.429,p.860–863.

Pokrovski, G., Kara, S., and Roux, J., 2002, Stability and solubility of arsenopyrite, FeAsS, in crustal fluids: Geochimica Cosmochimica Acta, v. 66, p. 2361–2378.

Pokrovski, G.S., Akinfiev, N.N., Borisova, A.Y., Zotov, A.V., and Kouzmanov, K., 2014, Gold speciation and transport in geological fluids: Insights from experiments and physical-chemical modelling: Geological Society, London, Special Publications, v. 402, 62 p.

Sanderson, D.J., Zhang, X., 1999. Critical stress localization of flow associated with deformation of well-fractured rock masses, with implications for mineral deposits. In: McCaffrey, K.J.W., Lonergan, L., Wilkinson, J.J. (Eds.), Fractures, Fluid Flow and Mineralization, Geological Society, London, Special Publications no. 155, pp. 69– 81.

Santos, R.V., Oliveira C. G., Parente C.V., Garcia, M.M., Dantas E. 2013. L., Hydrothermal alteration related to a deep mantle source controlled by a Cambrian intracontinental strike-slip fault: Evidence for the Meruoca felsic intrusion associated with the Transbrasiliano Lineament, Northeastern Brazil. *Journal of South American Earth Sciences* v.43, p.33-41.

Sarangi, S., Sarkar, A., Srinivasan, R., Patel, S.C., 2012. Carbon isotope studies of auriferous QCVs from two orogenic gold deposits from the Neoarchean Chitradurga schist belt, Dharwar craton, India: evidence for mantle/magmatic source of auriferous fluid. J. Asian Earth Sci. 52, 1–11.Sarma, D.S., Fletcher, I.R., Rasmus

Schaltegger, U., Brack, P., 2007. Crustal-scale magmatic systems during ntracontinental strike-slip tectonics: U, Pb and Hf isotopic constraints from Permian magmatic rocks of the Southern Alps. International Journal of Earth Sciences (Geol Rundschau) v.96, p.1131-1151.

Shand, S.J., 1943. Eruptive rocks, their genesis, composition, classification, and their relation to ore-deposits with a chapter on meteorite. John Wiley and Sons, New York.

Storti, F., Holdsworth, R.E., Salvini, F. (Eds.), 2003. Intraplate Strike-slip Deformation Belts, vol. 210. The Geological Society, London, Special Publication, p. 234

Stefansson A., and Seward T.M, 2004, Gold (I) complexing in aqueous solutions from 300 to 600°C and from 500 to 1800 bar: Geochimica et Cosmochimica Acta, v. 68, p.4121–4143.

Sharp, Z.D., Essene, E.J., and Kelly, W.C., 1985, A re-examination of the arsenopyrite geothermometer: Pressure considerations and applications to natural assemblages: Canadian Mineralogist, v. 23, p. 517–534

Sun, S.S., and McDonough, W.F., 1989, Chemical and isotopic systematics of oceanic basalts: Implications for mantle compositions and processes: Geological Society of London Special Publication 42, p. 313−345

Swain S.K., Sarangi S., Srinivasan R., Sarkar A, Bhattacharya S., Patel S.C., Pasayat R.M., Sawkar R.H., 2015. Isotope (C and O) composition of auriferous quartz carbonate veins, central lode system, Gadag Gold Field, Dharwar Craton, India: Implications to source of ore fluids.Ore Geology Reviews v.70 p. 305–320

Richards, J.P., 2009. Postsubduction porphyry Cu–Au and epithermal Au deposits: products of remelting of subduction-modified lithosphere. Geology 37, 247–250

Ridolfi, F.,Renzulli,A.,Puerini,M.,2010. Stability and chemical equilibrium of amphibole in calc-alkaline magmas: an overview, new thermobarometric formulations and application to subduction-related volcanoes. Contributions to Mineralogy and Petrology, v.160, p.45–66.

Rombach, C.S., and Newberry, R.J., 2001, Genesis and mineralization of the Shotgun deposit, southwestern Alaska: Mineralium Deposita, v. 36, p. 607–621

Rowins, S.M., 2000, Reduced porphyry copper-gold deposits: A new variation on an old theme: Geology, v. 28, p. 491–494.

Taylor Jr., H.P., Frechen, J., Degens, E.T., 1967. Oxygen and carbon isotope studies of carbonatites from the Laacher See District, West Germany, and Alno District, Sweden. Geochimica et Cosmochimica Acta 31, 407-430

Tornos, F., Casquet, C., Relvas, J.M.R.S., 2005. Transpressional tectonics, lower crust decoupling and intrusion of deep mafic sills: a model for the unusual metallogenesis of SW Iberia. Ore Geology Reviews v.27, p. 133-163.

Rock N.M.S., Duller P., Haszeldine R.S., Groves D.I., (1987). Lamprophyres as potential gold exploration targets: Some preliminary observations and speculations. In SE Ho, DI Groves (eds) Recent Advances in Understanding Precambrian Gold Deposits, Geology Dept. & University Extension, Univ WA Publ 11: 271–286

Rowins, S.M., 1999, Reduced porphyry copper-gold deposits: A newly recognized style of gold mineralization: Geological Society of America Abstracts with Programs, v. 31, no. 7, p. A-92.

Rowins, S.M., 2000, Reduced porphyry copper-gold deposits: A new variation on an old theme: Geology, v. 28, p. 491–494.

Valeriano, C.M., Pimentel, M.M., Heilbron, M., Almeida, J.C.H., Trouw, R.A.J.,2008. Tectonic evolution of the Brasilia Belt, central Brazil, and early assembly of Gondwana. Geological Society, London Special Publication 294,p.197–p.210.

Vauchez, A., Tommasi, A., 2003. Wrench Faults Down to the Asthenosphere: geological and Geophysical Evidence and Thermo-mechanical Effects. In: The Geological Society, London, Special Publication, vol. 210, pp. 15e34

Volkov, A.V., Genkin, A.D., Goncharov, V.I., 2006. Gold species in ores of the Natalkinskoe and Maiskoe deposits (northeastern Russia). Tikhookeanskaya Geologiya 25 (6), 18–29

Yang, J.H., Sun, J.F., Chen, F.K., Wilde, S.A., Wu, F.Y., 2007. Sources and petrogenesis of late Triassic dolerite dikes in the Liaodong Peninsula: implications for post-collisional lithosphere thinning of the eastern North China Craton. J. Petrol. 48, 1973–1997.

Yang, Q. Santosh M., Shen J., Li S.., 2014. Juvenile vs. recycled crust in NE China: Zircon U–Pb geochronology, Hfisotope and an integrated model for Mesozoic gold mineralization inthe Jiaodong Peninsula.Gondwana Research v. 25 p. 1445–1468.

Yakubchuk, A.S., Shatov, V.V., Kirwin, D., Edwards, A., Tomurtogoo, O., Badarch, G.,Buryak, V.A., 2005. Gold and base metal metallogeny of the Central Asian Orogenic Supercollage. In: Economic Geology, v. 100th Anniversary Volume, pp. 1035–1068.

Wang, L.G., Yiu, Y.M., McNaughton, N.J., Groves, D.I., Luo, Z.K.,Huang, J.Z., Miao, L.C., Liu, Y.K., 1998. Constraints on crustal evolution and gold metallogeny in the Northwestern Jiaodong Peninsula, China, from SHRIMP U–Pb zircon studies of granitoids. Ore Geology Reviews 13, 275–291.

Waters C.L., Sims K.K.W., Perfit M.R., Blitchert-Toft J., Blusztajn J., 2011. Perspective on the Genesis of E-MORB from Chemical and Isotopic heterogeneity at 9-10°N East Pacific Rise. Journal of petrology v.52, p.565-602.

Wood, D.A., 1980. The application of a Th-Hf-Ta diagram to problems of ectonomagmatic classification and to establishing the nature of crustal contamination of basaltic lavas of the British Tertiary volcanic province. *Earth Planet Science Letter*.v. 50, p.11–30.

Zhao, H.J., Ma, F.S., Li, G.Q., Zhang, Y.M., Guo, J., 2012. Study of the hydrogeological characteristics and permeability of the Xinli Seabed Gold Mine in Laizhou Bay, Jiaodong Peninsula, China. Environmental Earth Sciences 65, 2003e2014.

Zhmodik, S.M., 2008. Gold-Concentrating Systems of Ophiolite Belts (by the Example of the Sayan–Baikal–Muya Belt) [in Russian]. AkademicheskoeIzd. “Geo”, Novosibirsk

Supplementary Table.4.A-summary of ICP-MS U–Pb zircon data

Sample	f(206)%	Th/U	6/4 ratio	7/6 ratio	1s(%)	7/5 ratio	1s(%)	6/8 ratio	1s(%)	Rho	7/6 age	1s(Ma)	7/5 age	1s(Ma)	6/8 age	1s(Ma)	Conc (%) 6/8 - 7/5
GD 23																	
015-ZR09	0.023	0.616	68941	0.059	0.907	0.781	1.310	0.096	0.870	0.664	569	20	586	6	590	5	101
008-ZR05	0.020	0.693	77283	0.059	1.314	0.781	2.105	0.096	1.602	0.761	567	28	586	9	591	9	101
012-ZR06	0.049	0.279	31792	0.060	1.552	0.785	2.182	0.095	1.489	0.682	607	33	588	10	584	8	99
006-ZR03	0.036	0.497	43267	0.060	1.121	0.786	1.638	0.095	1.135	0.693	606	24	589	7	585	6	99
007-ZR04	0.034	0.595	45570	0.059	1.314	0.790	1.476	0.097	1.018	0.690	579	22	591	7	595	6	101
016-ZR10	0.041	0.732	38133	0.059	1.003	0.791	1.494	0.096	0.899	0.602	584	24	592	7	594	5	100
013-ZR07	0.041	0.396	37730	0.059	1.135	0.768	1.578	0.097	1.112	0.705	506	23	578	7	597	6	103
004-ZR01	0.018	0.249	84702	0.057	1.056	0.813	1.021	0.099	0.705	0.691	591	14	604	5	607	4	101
014-ZR08	0.037	0.506	41686	0.061	1.032	0.825	1.661	0.098	1.247	0.751	632	22	611	8	605	7	99
005-ZR02	0.006	0.349	254786	0.084	0.427	2.543	0.797	0.221	0.562	0.705	1282	8	1284	6	1286	7	100

Sample	f(206)%	Th/U	6/4 ratio	7/6 ratio	1s(%)	7/5 ratio	1s(%)	6/8 ratio	1s(%)	Rho	7/6 age	1s(Ma)	7/5 age	1s(Ma)	6/8 age	1s(Ma)	Conc (%) 6/8 - 7/5
GD 04A																	
005-Z3	0.037	0.429	47170	0.066	1.072	1.160	1.519	0.128	1.076	0.693	802	22	782	8	775	8	99
009-Z5	0.029	0.473	61528	0.065	0.992	1.061	1.524	0.118	1.158	0.747	789	21	734	8	717	8	98
010-Z6	0.051	0.331	34013	0.066	1.166	1.142	1.854	0.125	1.442	0.770	820	24	773	10	757	10	98
011-Z7	0.091	0.291	19142	0.067	1.097	1.154	1.500	0.125	1.023	0.664	835	23	779	8	759	7	97
012-Z8	0.038	0.287	46436	0.065	1.597	1.120	1.875	0.125	0.982	0.718	779	34	763	10	758	7	99
015-Z9	0.056	0.279	31382	0.066	1.052	1.158	1.602	0.127	1.208	0.743	803	22	781	9	773	9	99
016-Z10	0.045	0.273	39111	0.068	1.116	1.155	1.620	0.124	1.174	0.712	855	23	779	9	753	8	97
017-Z11	0.081	0.299	21470	0.066	1.474	1.170	2.014	0.128	1.372	0.672	810	31	787	11	778	10	99
018-Z12	0.075	0.260	23240	0.066	2.750	1.245	3.172	0.137	1.581	0.738	799	58	821	18	829	12	101
021-Z13	0.024	0.266	75506	0.059	0.899	0.758	1.385	0.093	1.054	0.746	572	20	573	6	573	6	100
023-Z15	0.045	0.296	38899	0.067	0.537	1.177	0.897	0.128	0.718	0.769	828	11	790	5	777	5	98
024-Z16	0.014	0.327	121166	0.067	1.064	1.212	1.293	0.132	0.735	0.736	823	22	806	7	800	6	99
027-Z17	0.056	0.291	30864	0.067	0.629	1.205	1.129	0.130	0.937	0.815	841	13	803	6	789	7	98
028-Z18	0.165	0.578	10600	0.065	1.546	1.128	2.019	0.127	1.299	0.632	759	33	767	11	769	9	100
029-Z19	0.059	0.637	29528	0.066	1.854	1.169	2.308	0.128	1.375	0.585	807	39	786	13	779	10	99
030-Z20	0.062	0.607	27999	0.066	4.077	1.165	4.753	0.128	2.444	0.762	813	85	785	26	774	18	99
035-Z23	0.050	0.477	34693	0.067	0.991	1.186	1.463	0.128	1.077	0.721	852	21	794	8	774	8	97
036-Z24	0.139	0.345	12500	0.070	2.173	1.290	2.642	0.134	1.502	0.795	930	45	841	15	808	11	96
039-Z25	0.057	0.346	30625	0.066	2.408	1.185	3.061	0.131	1.891	0.612	800	50	794	17	792	14	100
040-Z26	0.066	0.286	27113	0.061	2.255	0.785	3.108	0.094	2.139	0.684	632	49	588	14	577	12	98
041-Z27	0.044	0.549	39577	0.068	1.299	1.188	1.775	0.127	1.209	0.669	857	27	795	10	773	9	97
042-Z28	0.085	0.301	20382	0.070	2.943	1.317	3.405	0.137	1.712	0.746	916	61	853	20	830	13	97

Sample	f(206)%	Th/U	6/4 ratio	7/6 ratio	1s(%)	7/5 ratio	1s(%)	6/8 ratio	1s(%)	Rho	7/6 age	1s(Ma)	7/5 age	1s(Ma)	6/8 age	1s(Ma)	Conc (%) 6/8 - 7/5
GD 13A																	
010_Zr7	0.0017	0.128	144002	0.061	0.39	0.813	1.67	0.0972	0.92	0.55	627	58	604	15	598	10	87.29
041-ZR51N	0.0021	0.206	74859	0.060	0.511	0.807	1.31	0.0965	0.96	0.74	627	34	601	12	594	11	98.85
047-ZR53N	0.0047	0.19	384630	0.056	0.851	0.81	1.19	0.0979	0.73	0.61	604	37	603	11	602	8	99.92
039-ZR49	0.0092	0.112	184253	0.061	1.097	0.803	0.9	0.0968	0.67	0.75	611	20	599	8	595	8	99.46
011-ZR36N	0.0117	0.147	164366	0.063	1.277	0.791	0.87	0.0966	0.57	0.66	582	23	592	8	594	7	100.42
010-ZR35	0.0161	0.123	153752	0.057	1.11	0.797	0.86	0.0982	0.55	0.64	562	23	595	8	604	6	101.47
004_Zr1	0.0018	0.128	42141	0.060	1.17	0.749	1.67	0.0917	1.15	0.69	576	50	568	14	565	12	86.97
007_Zr4	0.0019	0.112	29412	0.064	1.328	0.771	1.5	0.0934	1.03	0.68	600	44	581	13	576	11	100.32
053-ZR56	0.0131	0.13	174273	0.060	1.277	0.751	1.47	0.0925	1.1	0.75	561	39	569	13	570	12	100.32
036_Zr21	0.0041	0.093	100439	0.061	1.209	0.767	1.07	0.0929	0.75	0.7	601	29	578	9	572	8	99.00
99	0.0064	0.149	7477	0.060	0.487	0.908	3.52	0.1067	2.17	0.62	664	116	656	34	654	27	99.42
036-ZR48	0.0056	0.281	9857	0.062	0.598	0.858	2.39	0.1048	1.99	0.83	582	55	629	22	642	24	102..21
006-ZR33	0.0062	0.236	49746	0.061	1.507	0.837	2.05	0.1048	1.73	0.84	527	46	618	19	643	21	104.58
042-ZR51BP	0.0027	0.286	27595	0.061	0.282	0.811	2.09	0.1025	1.5	0.72	507	61	603	19	629	18	104.11
021-ZR41	0.01	0.174	20780	0.060	0.38	0.847	1.76	0.1054	1.41	0.8	540	43	623	16	646	17	103.00
040-ZR50	0.0066	0.333	6132	0.060	0.407	0.782	1.06	0.0939	0.74	0.69	618	29	586	9	578	8	99.32
033_Zr18	0.0082	0.091	3318	0.058	0.579	0.784	1	0.094	0.68	0.68	619	27	588	9	579	8	98.60
027-ZR44N	0.0082	0.151	47626	0.057	0.808	0.789	0.9	0.0944	0.67	0.75	624	20	590	8	581	7	98.70
017_Zr10N	0.0007	0.138	24005	0.058	0.606	0.748	3.58	0.0883	2.59	0.72	655	104	567	31	545	27	96.20
005_Zr2	0.0018	0.144	33484	0.059	0.759	0.758	1.41	0.0891	0.95	0.68	662	41	573	12	550	10	96.10
029-ZR45N	0.0037	0.291	93494	0.062	1.695	0.733	1.35	0.089	1.01	0.75	594	35	558	12	550	11	98.40
018_Zr11	0.0012	0.213	34325	0.060	0.398	0.828	2.82	0.0983	1.97	0.7	641	84	612	26	605	23	98.70
020_Zr12N	0.0008	0.162	30843	0.059	0.53	0.787	2.87	0.0958	1.87	0.65	588	92	590	26	590	21	100.00
037_Zr22B	0.0012	0.195	14915	0.060	0.616	0.86	2.61	0.0981	1.51	0.58	726	87	630	24	604	17	95.80
013_Zr8	0.0009	0.2	15739	0.059	0.686	0.794	2.65	0.0958	1.76	0.66	608	83	594	24	590	20	99.40
016_Zr10B	0.0018	0.191	24289	0.059	0.317	0.756	2.32	0.0959	1.21	0.52	498	84	572	20	591	14	103.30
019_Zr12B	0.0011	0.162	23673	0.059	0.32	0.808	2.66	0.0933	1.68	0.63	701	85	601	24	575	18	95.40
038_Zr22N	0.0009	0.177	36238	0.060	0.285	0.771	2.65	0.0921	1.9	0.72	627	77	580	23	568	21	97.30
034_Zr19	0.004	0.115	55792	0.060	0.519	0.713	1.94	0.0915	1.17	0.6	471	66	546	16	564	13	103.30
029_Zr17B	0.0031	0.17	116492	0.061	0.486	0.752	1.27	0.0906	0.87	0.69	611	36	569	11	559	9	98.20
024-ZR43N	0.0056	0.226	96433	0.061	0.819	0.765	0.97	0.091	0.64	0.65	638	27	577	9	562	7	97.30

Supplementary Table 4.B Major and trace element data for representative Arc granitoids, Jaupaci Sequence, and post-collisional granitoids samples from the Jaupaci belt.

Rock	Dolerite	Dolerite	Dolerite	Dolerite	Dolerite	Dolerite	Dolerite	Dolerite	Dolerite
Bacilândia Intrusions	**Sample GD-05**	**Sample GD-06**	**Sample GD-07**	**Sample GD-09**	**Sample GD-10**	**Sample GD-11**	**Sample GD-12**	**Sample GD-15**	**Sample GD-78**
SiO2 (wt %)	52.39	51.66	49.45	48.72	52.63	48.11	54.26	62.27	49.03
TiO2	2.33	2.03	2.14	2.29	2.55	2.21	1.91	0.78	2.03
Al2O3	15.72	15.96	15.66	15.01	15.62	16.83	15.57	17.04	16.63
Fe2O3	12.29	11.51	12.31	12.65	12.50	11.50	9.68	7.31	12.7
MnO	0.18	0.17	0.18	0.19	0.17	0.17	0.15	0.12	0.13
MgO	3.67	5.25	6.83	6.64	4.12	8.88	4.41	1.59	5.81
CaO	6.79	8.28	9.53	9.97	7.66	8.81	6.77	3.98	8.41
Na2O	3.86	3.41	2.79	2.80	3.54	2.16	3.95	5.71	2.63
K2O	1.99	1.43	0.78	1.03	1.59	2.88	2.00	2.29	0.58
P2O5	0.55	0.23	0.18	0.29	0.48	0.29	0.46	0.23	0.2
LOI	2.01	1.64	1.82	1.22	3.19	4.41	1.98	3.08	1.48
Total	99.9	100.0	99.9	99.7	101.0	102.1	99.3	101.5	99.62
Na2O + K2O (wt %)	5.8	4.8	3.6	3.8	5.1	5.0	6.0	8.0	3.2
$(La/Lu)_N$	8.6	5.2	5.1	5.3	9.7	6.3	7.4	8.4	4.9
V (ppm)	177	244	300	307	242	244	139	56	245
Cr	100	60	150	140	70	550	70	50	0
Co	36.8	45.2	51.1	51	38	49.3	0	0	47.7
Ni	49	48	53	39	30	113	0	0	54
Cu	27	9	23	18	17	28	0	0	43
Zn	146	126	113	120	144	113	0	0	66
Ga	24.5	22	21.9	21.7	23.2	20.4	24.7	29.1	21.7
Rb	53	41.4	19.6	25.8	40.3	72.5	57.9	55.3	15.4
Sr	580	502	479	461	518	740	474	286	388
Y	31	25.6	22	22.8	28.9	24.5	39.2	37.9	22.68
Zr	239	181	140	146	239	177	288	383	126
Nb	24.6	14.9	14.2	14.7	24	12.8	23.8	30.9	13.35
Mo	4	4	3	3	4	4	0	0	2
Sn	3	2	1	2	2	1	3	4	1.2
Cs	3.1	2.68	1.76	2.56	2.79	2.61	3.26	2.62	1.58
Ba	626	363	254	246	474	730	573	973	231
La	30.9	18.8	15.2	15.8	30.1	18.9	38.4	46.9	15.1
Ce	68.4	43	34.8	36.4	66.9	43.7	84.6	101.5	33.5
Nd	38	23.7	20.9	21.6	37.2	25.2	39.3	43.7	21.1
Sm	8.43	5.76	4.58	5.28	7.64	5.69	8.03	8.58	4.8
Eu	2.3	1.73	1.5	1.67	2.26	1.82	2.22	2.04	1.72
Gd	6.87	5.23	4.59	5	6.89	5.14	8.09	7.37	5.84
Tb	1.08	0.77	0.73	0.72	1	0.87	1.13	1.21	0.83
Dy	6.27	5.17	4.39	4.52	5.85	5.22	7.11	6.66	4.75
Ho	1.15	1.04	0.85	0.95	1.08	1	1.38	1.34	0.9
Er	2.85	2.5	2.27	2.49	2.73	2.73	4.18	3.9	2.53
Tm	0.42	0.35	0.32	0.35	0.38	0.33	0.57	0.63	0.35
Yb	2.66	2.39	1.89	2.18	2.35	2.01	3.52	3.71	2.3
Lu	0.36	0.36	0.3	0.3	0.31	0.3	0.52	0.56	0.31
Hf	5.8	4.9	3.7	3.8	5.9	4.6	7	9.6	3.86
Ta	1.7	1.1	1	1.1	1.6	0.9	1.5	2.1	0.8
W	4	4	6	4	5	9	11	8	0.6
Pb	9	8	7	8	8	9	0	0	0
Th	3.96	2.87	1.75	1.84	4.11	2.33	4.99	9.42	1.6
U	1.42	1.12	0.64	0.74	1.49	1.07	1.76	3.62	0.64
Ag	1	1	1	1	1	1	0	0	0
Pr	8.5	5.45	4.41	4.67	8.08	5.45	9.9	11.8	4.57
Tl	0.5	0.5	0.5	0.5	0.5	0.5	0.5	<0,5	0.5

Rock	Dolerite	Gabbro	Gabbro	Diorite Porphyry	Diorite Porphyry	Diorite Porphyry	Trachyte	Trachyte	Trachyte
Bacilândia Intrusions	**Sample GD-79**	**Sample GD-81**	**Sample GD-82**	**Sample GD-23**	**Sample GD-24**	**Sample GD-25**	**Sample GD-04A**	**Sample GD-81A**	**Sample GD-82**
SiO2 (wt %)	46.81	49.11	53.59	63.73	60.38	55.29	60.62	54.74	50.56
TiO2	2.74	1.53	1.10	1.04	1.46	1.93	1.19	1.80	3.23
Al2O3	16.35	18.01	20.08	15.56	16.64	15.93	15.80	15.38	15.91
Fe2O3	13.88	11.63	8.41	7.47	8.38	10.37	8.32	11.60	14.71
MnO	0.13	0.17	0.17	0.13	0.24	0.15	0.13	0.17	0.18
MgO	4.83	13.53	9.55	1.31	2.27	3.54	1.33	2.39	3.18
CaO	6.89	7.64	12.22	2.59	4.95	6.64	4.13	5.79	5.59
Na2O	3.27	1.50	2.31	3.44	2.97	3.54	5.34	3.62	4.39
K2O	1.07	2.18	1.51	3.14	2.87	2.13	2.51	3.05	2.19
P2O5	0.32	0.21	0.14	0.40	0.38	0.34	0.38	0.53	0.77
LOI	0.62	8.47	12.1	1.83	5.25	1.72	1.9	2.43	1.19
Total	96.92	105.75	109.25	99.0	100.67	100.0	100.0	99.3	100.9
Na2O + K2O (wt %)	4.3	3.7	3.8	6.6	5.8	5.7	7.8	6.7	6.6
$(La/Lu)_N$	8.0	7.8	5.1	9.4	5.9	6.9	8.8	7.2	8.8
V (ppm)	251	182	149	48	98	199	58	127	198
Cr	0	850	480	30	40	40	30	40	50
Co	70.9	68.7	0	0	0	0	14.4	28.6	43.8
Ni	67	254	0	0	0	0	17	21	53
Cu	60	40	0	0	0	0	16	18	74
Zn	88	88	0	0	0	0	129	138	198
Ga	24	16.3	11.5	26.3	25.9	25.9	27.1	26.2	27.9
Rb	25.5	58.8	38.6	72.3	71.1	59.8	80.5	94.8	59.1
Sr	664	453	434	185.5	259	506	427	536	742
Y	23.53	17.3	13.7	43.5	54.5	31.6	40	35.4	49.9
Zr	185	145	88	478	396	294	396	275	474
Nb	22.4	10	5.7	36.3	29.6	23.9	32	24.1	44
Mo	2	3	0	0	0	0	5	4	5
Sn	2	2	1	6	5	3	5	3	5
Cs	4.44	5.2	4.84	3.1	1.9	2.57	3.78	4.61	2.97
Ba	356	427	307	890	749	632	1120	1115	662
La	23.1	17.1	9.1	51.8	36.4	31	47.5	32.9	55.7
Ce	52.3	36.8	20.9	115.5	82.2	70.1	99.9	71.3	122.5
Nd	30.6	19.4	12	53.1	39.6	33.9	49.9	37.8	66.6
Sm	6.7	4.26	2.8	10.15	8.28	6.9	9.89	8.63	13.3
Eu	2.22	1.19	1.17	2.71	2.2	2.11	2.44	2.32	3.03
Gd	6.71	3.6	2.84	10.25	9.17	6.87	8.23	7.61	11.45
Tb	0.99	0.57	0.5	1.47	1.62	1.07	1.38	1.06	1.71
Dy	5.19	3.35	2.58	8.23	9.43	6.24	7.65	6.98	10.05
Ho	0.94	0.66	0.5	1.61	1.84	1.04	1.46	1.27	1.88
Er	2.62	1.7	1.61	4.42	5.67	3.35	4.21	3.59	4.8
Tm	0.36	0.25	0.18	0.66	0.78	0.47	0.57	0.5	0.7
Yb	2.2	1.51	1.26	3.99	4.56	2.91	3.75	2.92	4.34
Lu	0.29	0.22	0.18	0.55	0.62	0.45	0.54	0.46	0.63
Hf	5.54	3.5	2.2	12.4	9.7	6.8	10.2	6.7	11.5
Ta	1.4	0.8	0.4	2.5	2.1	1.5	2.3	1.7	2.9
W	1	4	3	37	11	2	6	5	8
Pb	0	9	0	0	0	0	14	10	14
Th	2.3	3.03	1.41	12.45	9.26	5.27	10.05	5.56	8.3
U	0.85	1.38	1.34	4.73	3.93	1.83	3.74	2.26	3.05
Ag	0	1	0	0	0	0	1	1	1
Pr	6.92	4.31	2.53	13.35	9.76	8.19	11.6	8.87	15
Tl	0.5	0.5	0.5	0.5	0.5	0.5	0.5	0.5	0.5

Rock	Trachyte	Trachyte	Syenite porphyry	Syenite porphyry	Syenite porphyry	Syenite porphyry	Syenite porphyry	Lamprophyre
Bacilândia Intrusions	**Sample GD-83**	**Sample GD-84**	**Sample GD-13A**	**Sample GD-101**	**Sample GD-102**	**Sample GD-103**	**Sample GD-104**	**Sample GD-98**
SiO2 (wt %)	60.22	52.01	64.49	66.05	71.07	64.71	68.83	45.20
TiO2	1.56	2.35	0.61	0.48	0.39	0.55	0.72	3.38
Al2O3	15.89	16.11	15.78	15.18	15.67	15.79	15.40	17.17
Fe2O3	8.25	10.28	6.45	5.67	3.48	6.24	4.82	14.54
MnO	0.12	0.15	0.11	0.10	0.06	0.10	0.07	0.22
MgO	3.04	4.66	0.73	0.57	0.47	0.72	0.96	7.11
CaO	6.17	6.70	2.98	2.61	1.62	2.94	2.07	10.72
Na2O	2.57	4.08	5.10	4.98	4.21	4.88	2.86	1.68
K2O	3.10	2.54	3.50	3.71	4.23	3.40	4.87	2.11
P2O5	0.24	0.81	0.23	0.22	0.07	0.24	0.13	0.70
LOI	3.96	2.46	1.69	1.77	1.75	1.85	2.15	3.96
Total	101.3	99.9	100.1	99.7	101.3	99.7	100.9	103.3
Na2O + K2O (wt %)	5.7	6.6	8.6	8.7	8.4	8.3	7.7	3.8
$(La/Lu)_N$	5.7	10.5	8.6	10.6	10.4	9.5	10.9	23.4
V (ppm)	170	171	27	19	27	15	69	376
Cr	40	110	50	40	20	20	20	130
Co	0	0	8	5.9	0	0	0	51
Ni	0	0	21	17	0	0	0	49
Cu	0	0	12	9	0	0	0	19
Zn	0	0	117	111	0	0	0	139
Ga	24.2	23.5	28	27.3	29.8	28.6	30.4	20.1
Rb	64.8	66.2	96.8	105.5	111	94.2	120.5	85.8
Sr	471	668	357	286	123	331	263	1785
Y	33.2	34.4	38.7	35.9	28.5	39.6	27.9	28.1
Zr	218	343	380	363	247	445	229	277
Nb	17.1	30.6	33.9	32.8	35.4	32.6	37	74.8
Mo	0	0	7	5	0	0	0	5
Sn	2	2	5	5	5	4	7	2
Cs	3	3.09	2.04	1.51	1.37	1.67	1.74	5.03
Ba	1145	777	897	780	481	863	888	1945
La	24.4	50.2	53.5	51.7	35.5	51.4	31.6	70.2
Ce	55.6	109	108	104.5	78.3	112	72.7	142
Nd	28.7	49.6	49.3	45.3	34.4	49.3	32.5	63.3
Sm	6.12	9.74	9.36	8.68	6.83	8.66	7.64	10.35
Eu	1.7	2.8	1.97	1.71	0.99	2.15	1.2	2.85
Gd	5.93	8.31	7.48	6.93	6.55	8.46	6.54	7.48
Tb	1	1.25	1.1	1.08	0.96	1.2	0.99	1.05
Dy	6.11	6.52	7.13	6.68	5.63	7.33	5.44	5.66
Ho	1.2	1.37	1.43	1.28	0.88	1.29	0.99	1
Er	3.6	3.55	3.85	3.52	2.8	4.18	2.58	2.65
Tm	0.56	0.56	0.56	0.53	0.37	0.62	0.36	0.34
Yb	3.15	3.17	3.87	3.2	2.3	3.68	2.17	2.18
Lu	0.43	0.48	0.62	0.49	0.34	0.54	0.29	0.3
Hf	5.5	7.1	9.4	9.7	8	10.5	7.4	7
Ta	1	1.5	2.5	2.5	2.7	2.4	2.6	4.8
W	10	1	4	5	1	1	5	4
Pb	0	0	15	16	0	0	0	9
Th	4.37	4.95	11.15	12	11.15	10.6	9.98	6.84
U	1.61	1.83	4.55	4.63	4.83	4.1	4.56	1.76
Ag	0	0	1	1	0	0	0	1
Pr	6.98	12.85	12.1	11.5	8.76	12.55	8.61	16.1
Tl	<0,5	<0,5	0.5	0.5	0.5	0.5	<0,5	0.5

5.0 CONCLUSÕES

Os dados apresentados nesta tese de doutorado permitiram atingir os objetivos principais propostos no plano de pesquisa, quais sejam datar a idade dos diques e de suas rochas encaixantes (Sequência Jaupaci), entender o contexto tectônico em que essas rochas se formaram e a relação de falhas trancorrente com a geração dos diques, granitos tipo-A e fluidos hidrotermais, bem como definir o modelo metalogénetico para o depósito Fazenda Nova, os quais serão abaixo detalhados.

5.1. Evento arco magmático na sequencia Jaupaci e implicações tectônicas regionais.

A evolução do Arco Magmático de Goiás vem sendo reportada nos arcos de Mara Rosa e Arenópolis com dois principais eventos magmáticos: o mais antigo, em um ambiente de arco intra-oceânico com a geração de magmatismo com idade entre 920 e 800 Ma, e posteriormente, um mais recente em um arco continental que ocorreu entre 660 e 630 Ma (Pimentel *et al.,* 2000, Dantas et al 2001; Kroner & Cordani 2003, Brito Neves *et al.,* 2014). Entretanto, os dados de Laux et al., (2005); Matteini et al., (2010); e os apresentados nesta tese apontam um novo evento com intensa atividade magmática ocorrido entre 797 a 750. Esse evento magmático representa boa parte das exposições de rocha na Faixa Jaupaci, apresentando duas idades principais:

- O primeiro evento magmático (~770 Ma) é representado por tonalitos e granodioritos com ilmenita, peraluminosos, calci-alcalinos da Suite Tipo 1. Os isótopos de Nd mostraram idades modelos T_{DM} de 0.86 até 0.91 Ga e ε_{Nd} (T) positivo com valores variando de +4.6 até + 5.4. Baseado nas informações dessa tese foi interpretado que esses magmas são derivados de baixa fusão parcial de um arco juvenil na crosta inferior, composto por rochas sedimentares e basálticas. A fusão ocorre devido ao espessamento da crosta (~25 km), possivelmente em estágios finais de colisão em um ambiente intra-oceânico. Da mesma forma, granitoides peraluminosos (granitos São João e Creoulos, por exemplo) são registrados na parte oriental do Arco de Arenópolis com idades entre 792 e 782 Ma (Laux et al 2005), mostrando que este evento tardio de fusão parcial envolveu boa parte das rochas previamente cristalizadas em ambiente arco oceânico (880-820 Ma).

- O segundo evento engloba magmas félsicos com magnetita e metaluminosos representado pelos granitóides Tipo 2, com idade de 753 ± 12 Ma e os riolitos basais da Sequência Jaupaci datados com 748 ± 10 Ma. Os dados geoquímicos indicam que essas rochas apresentam afinidade adakíticas com fonte proveniente de baixa fusão parcial de crosta juvenil muito espessa (>40 km) em um ambiente de arco continental. Os dados isotópicos de Nd mostram idades modelos T_{DM} um pouco mais antigas, com 1.1 até 1.21 Ga, do que os granitoides peraluminosos Tipo 1. Entretanto a fonte é predominantemente juvenil, sendo indicada pelo o ε_{Nd} (T) positivo, com valores variando de +1.1 até + 2.08, e zircões herdados cristalizados entre 790 e 880 Ma. O mesmo evento é registrado no extremo oeste do Arco de Arenópolis representado por tufos datados por U-Pb em zircão com idade de 749 ± 6 Ma (Guimarães *et al.* 2012). Esses tufos apresentam zircões Paleoproterozoicos e Arqueanos, assim como ε_{Nd} (T) negativo indicando que o evento de 750 Ma envolveu crosta antiga (possivelmente representado pelo gnaisse Ribeirão), suportando a hipótese que este evento ocorreu em um arco continental.

5.2. Evento pós-colisional na Sequência Jaupaci e implicações tectônicas regionais.

Anteriormente, o evento pós-colisional no Arco de Arenopólis era apenas relacionado aos granitos Tipo-A da Suíte Serra Negra. Nesta tese, um extenso mapeamento junto aos dados geoquímicos e isotópicos mostrou que além dos granitos Tipo-A, ocorrem rochas vulcânicas bimodais e os diques das Intrusivas Bacilândia. Desta forma, para englobar todas as rochas supracitadas, propusemos três eventos relacionados temporalmente à geração da Zona de Cisalhamento Moiporá Novo-Brasil: o pré-cinemático (~597-585 Ma), o sin-cinemático (~577-539 Ma) e o pós-cinématico (~511-506 Ma).

- O evento pré-cinemático ocorreu em um ambiente extensional com ascensão mantélica e posterior delaminação da crosta inferior. Associado a esse evento, ocorre o magmatismo bimodal e o primeiro pulso de diques das Intrusivas Bacilândia. No que se refere ao magmatismo bimodal, as vulcânicas máficas são catacterizadas por anfibólio-clorita xisto com assinatura N-MORB, idade modelo T_{DM} de 0.8 Ga e ε_{Nd}(T)

entre +5.2 e +6.7, indicando magmas máficos astenosféricos. Os magmas félsicos são representados por rochas metavulcânicas de composição dacítica à riolítica e granitos tipo-A, apresentando idade U-Pb de 597±10 Ma, idades modelos T_{DM} entre 0.81 Ga e 0.9 e $\varepsilon_{Nd}(T)$ com valores positivos de +2.3 até +6.6. Os dados sugerem que essas rochas félsicas são derivadas de uma mistura de magmas mantélicos com material proveniente da fusão parcial de uma crosta juvenil Neoproterozoica. Tal interpretação é suportada por zircões herdados com idades variando de 778 até 882 Ma. O primeiro pulso das Intrusivas Bacilândia é definido por um pequeno volume de diques de gabros, doleritos e sienitos com idade variando entre 593±5 Ma a 590±5 Ma. A origem desses diques é relacionada com uma baixa fusão parcial de um manto litosférico previamente metassomatizado. Os dados sugerem uma fonte similar das rochas metavulcânicas félsica indicada por $\varepsilon_{Nd}(T)$ positivo com valores entre +3.56 até +4.5, idades T_{DM} variando de 0.75 a 0.88 e zircões herdados com idade de 850 Ma. Quanto às correlações regionais deste evento pré-cinmático, foram feitas algumas comparações pontuais nesta tese baseados nos dados regionais disponíveis, como as rochas da Sequência Iporá ser uma possível continuidade lateral das rochas da Sequência Jaupaci. Entretanto será necessário fazer uma análise isotópica e geoquímica sistemática para confirmar essa hipótese.

- O evento sin-cinématico ocorre em um ambiente transpressional no qual é registrada uma fase deformacional D_n com metamorfismo em fácies xisto verde, desenvolvimento da Zona de Cisalhamento Moiporá-Novo Brasil (ZCMNB), geração de granitos Tipo-A e de um segundo evento de diques das Intrusivas Bacilândia. A ZCMNB foi interpretada como um "*splay*" do Lineamento Transbrasiliano representando uma estrutura translitosférica profunda, que permitiu a interação do manto com a base da litosfera, gerando novos magmas tipo-A. Os granitos tipo-A são alojados ao longo da ZCMNB (além de outras zonas de cisalhamentos subordinadas) e comumente apresentam estruturas miloníticas indicando movimento direcional destral. Tal movimento foi suficiente para justapor os terrenos Arqueano/Paleoproterozoicos do Maciço de Goiás e o Arco Magmático de Arenópolis. Devido a esta justaposição de diferentes

terrenos, os granitos tipo-A deste evento apresentam assinatura isotópica distinta com idades modelos T_{DM} 1.27 – 2.25 Ga e ε_{Nd} (T) negativo com valores variando entre -1.0 até -20.0. A idade dos granitos tipo-A e a formação da ZCMNB foram interpretadas nesta tese variando entre 577 até 539 Ma. O inicio do evento sin-cinemático é marcado por um novo pulso volumoso de diques e *stocks* de traquitos, doleritos, traquitos e sienitos pórfiros, sendo estes dois últimos datados com idades entre 574± 10 Ma e 572± 5 Ma respectivamente. O segundo evento de diques apresenta a mesma assinatura geoquímica e isotópica do primeiro, indicando que são provenientes da mesma fonte. Uma implicação regional de estimar o pico de deformação (e metamorfimos xisto verde da fase Dn) ao evento sin-cinématico com idades entre 579 Ma até 539 Ma é que essa deformação tardia deve estar registrada em outras unidades tectônicas da Faixa Brasília. De acordo com D'el-Rey Silva et al., (2011) estima-se idade entre ~580-540 Ma para uma última deformação (denominada neste trabalho como D_{3S}) na porção meridional da Faixa Brasília, que corrobora essa hipótese discutida neste trabalho.

- O evento pós-cinemático ocorre em um em um ambiente extensional com a geração de granitos tipo-A sem deformação, com idades variando entre 511 até 506 Ma. Apresentam idades modelos entre 0.9 até 1.2 Ga e ε_{Nd} (T) com valores variando de negativo a positivo (-4.0 até +1.0), indicando que neste evento predominou uma fonte juvenil, ao contrário do que se deu no evento sin-sinemático. Ainda neste evento ocorreram os diques de lamprófiros, que podem representar um componente máfico relacionado a esse ambiente extensional. Uma amostra lamprofiro mostrou idade modelo de 0.84 Ga e ε_{Nd} (T) com valor de +1.88.

5.3 O evento de mineralização aurífera no depósito de Fazenda Nova

A mineralização de Fazenda Nova representa um novo estilo de metalogênese aurífera na porção central do Brasil. Os aspectos sobre esta mineralização foram concluídos da seguinte forma:

1- Os doleritos e gabros apresentam assinatura de alto HFSE, LILE, LREE, Nb e Ta típicos de magmas máficos E-MORB. A fonte desses magmas máficos é

proveniente de uma fusão parcial de um manto litosférico previamente metassomatizado. Essa metassomatização do manto pode ter ocorrido tanto em 750 Ma, quando foram gerados os magmas adakíticos, quanto em 597 Ma pela geração de rochas vulcânicas félsicas da Sequência Jaupaci. A geração dos magmas máficos ocorreu em dois eventos: o primeiro de menor volume, em 593± 5 Ma e o segundo, mais volumoso, com idades entre 574±10 Ma e 572±5 Ma. Uma baixa fusão parcial (~8%) foi estimada para geração desses magmas máficos, sendo que tal taxa de fusão foi essencial para a fertilidade de ouro, assim como para o enriquecimento do magma em elementos incompatíveis e voláteis.

2- Os diques de diorito pórfiro, traquito e sienito pórfiro são originados por processos magmáticos como cristalização fracionada, assimilação crustal e *magma mixing*. Tais processos também atuaram de forma crucial na concentração de ouro e outros metais (As Sb e W), assim como na saturação de fluidos hidrotermais.

3- A Falha Bacilândia é uma estrutura NNW de segunda ordem da Zona de Cisalhamento Moiporá-Novo Brasil. A Falha Bacilândia foi interpretada como uma estrutura profunda e canalizou os magmas das Intrusivas Bacilândia, assim como fluidos hidrotermais. A maior atividade desta falha ocorreu em aproximadamente em 572 Ma e está associada à geração de maior volume de magmatismo, assim como aos estágios mineralizantes no depósito de Fazenda Nova.

4- Os fluidos hidrotermais no depósito de Fazenda Nova ocorreram em três estágios inicial, intermediário e tardio; i) o estágio inicial ou mineralizante, que consiste em uma alteração pervasiva com sericitização dos felspatos, biotitização dos minerais máficos e transformação da ilmenita para rutilo/leucoxênio. A alteração pervasiva é acompanhada por *stock-work* de quartzo (eventualmente brechas) e disseminação de sulfeto composta por uma assembleia de arsenopirita-pirrotita-scheelita-stibinita além de apatita e siderita hidrotermal. A arsenopirita desse estágio apresenta formato acicular e frequentemente apresenta inclusões de galena, pirita e ouro, dando este último o caráter refratário do minério. A temperatura estimada para o par de sulfetos arsenopirita-pirrotita foi estimada em 340°C. A esta temperatura o ouro pode ser transportado em soluções hidrotermais como um complexo de bissulfeto ou complexos de tio-arsenatos; ii)

O estágio intermediário é composto *stock-work* de calcita e quartzo com uma assembleia hidrotermal de clorita, epidoto, turmalina e titanita associado a sulfetos como pirrotita-pirita-arsenopirita. A arsenopirita neste estágio é frequentemente tabular, não apresentando inclusões de sulfetos e nem de ouro. A temperatura estimada para o par de sulfetos arsenopirita-pirita foi de 305°C. Isótopos de C-O em veios de calcita desse estágio forneceram $\delta^{13}C$ variando de -9.68 até -11.57‰ e $\delta^{18}O$ com valores variando entre 12.87 a 13.84‰. Tais valores são equivalentes aos de carbonato magmático ou hidrotermal/mantélico; iii) O estágio tardio é composto por veios e brechas compostas apenas por calcita-ankerita sem alteração hidrotermal ou mineralização aurífera.

5- O Depósito de Fazenda Nova foi classificado como *Reduced Intrusion Related* epizonal baseado nos seguintes aspectos: mineralização hospedada em magma reduzido pós-colisional, ocorrência de diques e *stocks* com assinatura mantélica proveniente de um manto metassomatizado, processos magmáticos atuando na concentração de Au e outros metais, textura epizonal de veios como *stock-work* e brechas associado a sulfetos com temperaturas de cristalização entre 340-305 °C indicando um alto gradiente hidrotermal, bem como a associação metálica de Au-As-W-Sb e isótopos de C-O indicando carbonatos de fonte magmática ou mantélica.

Os depósitos auríferos definidos na Faixa Brasília estão relacionados a diversos modelos, tais como: Au-orogênico formado na orogênese Brasiliana (depósito aurífero de Posse) ou previamente em eventos de orogênese Paleoproterozoíca (Oliveira et al., 2004; Jost et al., 2010); o depósito de Chapada como Cu-Au pórfiro com idade aproximada de mineralização de 880 Ma e processos de remobilização durante a orogênese Brasiliana (Oliveria et al., 2015); e o depósito de Zacarias como Au-Ag-Ba VMS com idade aproximada de 900 Ma (Poll 1994). Entretanto todos os depósitos supracitados tem idade mínima de mineralização aurífera de até 630 Ma. O depósito de Fazenda Nova está relacionado a um modelo do tipo *Reduced Intrusion-Related*, onde a idade da mineralização está relacionada ao estágio de maior volume de diques das Intrusivas Bacilândia (~572 Ma), representando, assim, um novo conceito de metalogênese de ouro associada à magmatismo pós-colisional na Faixa Brasília. Outro conceito alcançado na metalogênese de ouro do depósito estudado foi sua relação com a Falha Bacilândia e Zona de Cisalhamento Moiporá-Novo Brasil. Esta última estrutura

foi interpretada como um display N-S do Lineamento Transbrasiliano, mostrando que outros *splays* do Lineamento Transbrasiliano podem apresentar circulação de fluido hidrotermal e mineralização aurífera. A referida hipótese de circulação de fluidos hidrotermais ao longo do Lineamento Transbrasiliano foi documenta por Santos et al,. (2013) em carbonatos hidrotermais no granito Merouca, NE do Brasil.

Os principais guias prospectivos para encontrar depósitos auríferos similares a Fazenda Nova são: i) presença de diques máficos alcalinos reduzidos pós-colisionais com assinatura geoquímica e isotópica de fonte mantélica metassomatizada; ii) coexistência de diques e stocks de composição máfica e félsica, indicando processos magmáticos como cristalização fracionada e *magma mixing* que vão atuar na concentração de metais e elementos voláteis; iii) presença de diques com textura porfirítica que indicará sistemas magmáticos hidratados; iv) existência de zonas de cisalhamentos profundas (por exemplo, utilizando produtos geofísicos regionais) que serão responsáveis por canalizar os fluidos hidrotermais para crosta superior.

6.0 BIBLIOGRAFIA CONSULTADA

Amaro, V. E. 1989. Geologia e Petrologia da Seqüência Metavulcânica de Jaupaci (Go) e lineamentos Associados. Dissertação de mestrado, 298 p. Universidade de Brasília.

Archanjo C.J, Launeau P., Hollanda M.H.B.M., Macedo J.W.P., Liu D. 2009. Scattering of magnetic fabrics in the Cambrian alkaline granite of Meruoca (Ceará State, Northeastern Brazil). *International Journal of Earth Sciences*, v.98, p: 1793-1807.

Bierlein, F.P., Groves, D.I., Goldfarb, R.J., Dubé, B., 2006. Lithospheric controls on the formation of provinces hosting giant orogenic gold deposits. Mineralium Deposita 40,874–887.

Bierlein F.P, Groves D.I, Cawood P.A, 2009. Metallogeny of accretionary orogens—the connection between lithospheric processes and metal endowment. *Ore Geology Reviews* v.36, p: 282–292.

Bonin, B.L., Azzouni-Sekkal, A., Bussy, F., Ferrag, S., 1998. Alkali-calcic and alkaline post-orogenic (PO) granite magmatism: petrologic constraints and geodynamic settings. *Lithos* v.45,p: 45–70.

Botros,2001. Metalogeny of gold in relation to the evolution of the Nubian Shield in the Egypt. *Ore geology Reviews*.v 19,p: 137-164

Brito Neves B.B., Fuck, R.A., Pimentel, M.M 2014. The Brasiliano collage in South America: a review. *Brazilian Journal of Geology*, v. 44(3), p. 493-518

Caby, R., 2003. Terrane assembly and geodynamic evolution of central western Hoggar: a synthesis. Journal Afrincan Earth Science,v. 37, p.133–159.

Cawood, P.A., Kröner, A., Pisarevsky, S., 2006. Precambrian plate tectonics: criteria and evidence. *GSA Today* v.16,p: 4–11.

Cawood, P.A.C., Buchan, C., 2007. Linking accretionary orogenesis with supercontinent assembly. *Earth-Science Reviews* v.82,p: 217–256.

Cawood, P.A.C., Kröner, A., Collins, W.J., Kusky, T.M., Mooney, W.D., Windley, B.F., 2009.Accretionary orogens through time. In: Cawood, J.W., Kröner, A. (Eds.), Earth Accretionary Systems in Space and Time: London, *Geological Society London Special Publication* 318.

Condie, K.C., Chomiak, B., 1996. Continental accretion — contrasting Mesozoic and early Proterozoic tectonic regimes in North America. *Tectonophysics* v.265, p: 101–126.

Cordani, U,G. Pimentel, M,M. Araújo C,E,G. Basei, M,A,S Fuck R.A 2013. The significance of the Transbrasiliano-Kandi tectonic corridor for the amalgamation of West Gondwana. *Brazilian Journal of Geology*, v. 43, p. 583-597.

Dantas, E.L., Jost, H., Fuck, R.A., Brod, J.A., Pimentel, M.M., Menezes, P.R., 2001. Proveniência e idade deposicional de sequências metavulcano-sedimentares da Região de Santa Terezinha de Goiás baseada em dados isotópicos Sm–Nd e U–Pb em monocristal de zircão. *Revista Brasileira de Geociências* v.31 (3),p. 329–334.

Defant M.J. & Drummond M.S. 1990. Derivation of some modern arc magmas by melting of young subducted lithosphere. *Nature*,v. 347,p: 662-665.

D'el-Rey Silva, L.J.H., Oliveira I.L., Pohren, C.B., Tanikazi M.L.N., Carneiro R.C., Fernandes G. L. F., Aragão P. E. 2011. Coeval perpendicular shortenings in the Brasília belt: Collision of irregular

plate margins leading to oroclinal bending in the Neoproterozoic of central Brazil. Journal of South American Earth Sciences v.32 p.1-13.

Doebrich, J.L., Zahony, S.G., Leavitt, J.D., Portacio Jr., J.S., Siddiqui, A.A., Wooden, J.L., Fleck, R.J., Stein, H.J., 2004. Ad Duwayhi,Saudi Arabia: geology and geochronology of a Neoproterozoic intrusion-related gold system in the Arabian shield. *Economic Geology*. v.99, p:713–741.

Doebrich J. L. , Al-Jehani A. M. , Alim A. Siddiqui A.A., Hayes T. S., Wooden J. L , Johnson P. R. 2007. Geology and metallogeny of the Ar Rayn terrane, eastern Arabian shield: Evolution of a Neoproterozoic continental-margin arc during assembly of Gondwana within the East African orogeny. *Precambrian Research* v.158 p. 17–50.

Dostal J., Dupuy C., Caby R. 1994. Geochemistry of the neoproterozoic Tilemsi belt of Iforas (Mali, Sahara) - a crustal section of an oceanic island-arc. *Precambrian Research*, v.65(1-4), p.55-69.

Guimarães, S,B. Moura, M, A. Dantas, E . L., 2012. Petrology and geochronology of Bom Jardim copper deposit. *Brazilian Journal of Geology*, v.42, n.4, 2012, p.841-862.

Ganade de Araújo C.E.., Rubatto D., Hermann J., Cordani U.G., Caby R., Basey M.S. 2014a. Ediacaran 2,500-km-long synchronous deep continental subduction in the West Gondwana Orogen. *Letter for nature* p.8.

Goldfarb, R.J., Groves, D.I., and Gardoll, S., 2001. Orogenic gold and geologic time: A global synthesis: *Ore Geology Reviews*, v. 18, p. 1–75.

Goldfarb, R.J., Baker, T., Dube, B., Groves, D.I., Hart, C.J.R., Gosselin, P., 2005. Distribution, Character, and Genesis of Gold Deposits in Metamorphic Belts. In:*Economic Geology 100th Anniversary Volume*, pp. 407-450.

Griffin WL, O'Reilly S.Y., Afonso J.C., Begg G.C, .2009. The composition and evolution of lithospheric mantle: a re-evaluation and itstectonic implications. *Journal of Petrology* , v.50:p.1185–1204.

Groves, D.I., Goldfarb, R.J., Gebre-Mariam, M., Hagemann, S.G., and Robert, F., 1998. Orogenic gold deposits: A proposed classification in the context of their crustal distribution and relationship to other gold deposit types: *Ore Geology Reviews*, v. 13, p. 7–27.

Groves, D.I., Goldfarb, R.J., Robert, F., Hart, C.J.R., 2003. Gold deposits in metamorphic belts: Overview of current understanding, outstanding problems, future research, and exploration significance: *Economic Geology*, v. 98, p. 1–29.

Hart, C.J.R., McCoy, D., Goldfarb, R.J., Smith, M., Roberts, P., Hulstein, R., Bakke, A.A., and Bundtzen, T.K., 2002, Geology, exploration and discovery in the Tintina gold province, Alaska and Yukon: *Society of Economic Geologists Special Publication* 9, p. 241–274.

Hibbard, J.P., Stoddard, E.F., Secor, D.T., Dennis, A.J., 2002, The Carolina zone: Overview of Neoproterozoic to early Paleozoic peri-Gondwanan terranes along the eastern flank of the southern Appalachians: *Earth-ScienceReviews*, v. 57, p. 299−339

Hronsky, J.M.A., Groves, D.I., Loucks, R.R., and Begg, G.C., 2012, A unified model for gold mineralization in accretionary orogens and implications for regional scale targeting methods: *Mineralium Deposita*, v. 47, p. 339–358.

Jensen E.P., Barton M.D., 2000. Gold deposits related to alkaline magmatism. *Revision Economic Geology* v.13, p:279–314.

Johnson, P.R., Andersen, A., Collins, A.S., Fowler, A.R., Fritz, H., Ghebreab, W., Kusky, T., Stern, R.J., 2011. Late Cryogenian–Ediacaran history of the Arabian–Nubian Shield: A review of depositional, plutonic, structural, and tectonic events in the closing stages of the northern East African Orogen. *Journal of Africa Earth Science*, v.10,p. 1–179.

Jost H.; Chemale F.; Dussin I. A. Martins R. 2010, U--Pb zircon Paleoproterozoic age for the metasedimentary host rocks and gold mineralization of the Crixás greenstone belt, Goiás, Central Brazil. Ore Geology Reviews, v. 37 (2), p.127-139**.**

Kay S.M, Godoy E., Kurtz A. 2005. Episodic arc migration, crustal thickening, subduction erosion and magmatism in the southcentral Andes. Geol Soc Am Bull 117:67–88

Kerrich, R., Goldfarb, R.J., Richards, J., 2005. Metallogenic provinces in an evolving geodynamic framework. In: Hedenquist, J.W., Thompson, J.F.H., Goldfarb, R.J.,Richards, J.P. (Eds.), *Economic Geology 100th Anniversary Volume*. In: Society of Economic Geologists, Littleton, Colorado, pp. 1097–1136.

Kroner, A.Cordani, U,G.,2003. African, southern Indian and South American Craton were not part of Rodinia continent: evidence from field relationship and geochronology: *Tectonophysics*, v.375, n.1-4, p.325-352.

Lang, J.R., Baker, T., Hart, C.J.R., Mortensen, J.K., 2000, An exploration model for intrusion-related gold systems: *Society of Economic Geology Newsletter* v.40, p. 1, 6–15.

Laux, J.H., Pimentel, M.M., Dantas, E.L. Armstrong, R., Junges, S.L., 2005. Two Neoproterozoic crustal events in the Brasília Belt, central Brazil. *Journal of South American Earth Sciences*, v.18 p.183-198.

Loucks RR, Ballard J.R., 2003. Report 2C - Petrochemical characteristics, petrogenesis and tectonic habits of gold-ore-forming arc magmas. Unpublished report for industry-sponsored research project: *Predictive Guides to Copper and Gold Mineralization at Circum-Pacific Convergent Plate Margins*. 69p.

Matteini M., Junges S.L., Dantas E.L., Pimentel M.M., Buhn B. 2010. In Situ Zircon U-Pb and Lu-Hf isotope systematic on magmatic rocks: insight on the crustal evolution Neoproterizoic Goiás Magmatic Arc, Brasília belt, Central Brazil. *Gondwana Research*, v.17: p.1-12.

McCuaig, T.C., Beresford, S., Hronsky, J., 2010. Translating the mineral systems approach into an effective exploration targeting system: *Ore GeologyReviews*, v. 38, p. 128–138.

McGee B. & Collins A., Trindade R.I. 2012. G'Day Gondwana the final accretion of a supercontinent: U–Pb ages from the post-orogenic São Vicente Granite, northern Paraguay Belt, Brazil. *Gondwana Research*,v 21(2-3) p: 316-322.

Mair, J.L., Farmer, G.L., Groves, D.I., Hart, C.J.R., Goldfarb, R.J., 2011. Petrogenesis of mid-Cretaceous post-collisional magmatism at Scheelite Dome, Yukon, Canada: evidence for a lithospheric mantle source for intrusion-related gold systems. *Economic Geology.* v.106, p.451-480.

Martin H. 1999. The adakitic magmas: modern analogues of Archaean granitoids. *Lithos*, v. **46**:411-429.

Martin H., Smithies R.H., Rapp R.J.F., Moyen D., Champion D. 2005. An overview over adakite, tonalite-trondhjemite-granodiorite (TTG) and sanukitoid: relationships and some implications for crustal evolution. *Lithos*,v. **79**:1-24.

Meert, J.G., 2003. A synopsis of events related to the assembly of eastern Gondwana. *Tectonophysics* ,v.362, p.1–40.

Mole, D.R., Fiorentini, M.L., Cassidy, K.F., Kirkland, C.L., Thebaud, N., McCuaig, T.C., and Miller, J., 2013, Crustal evolution, intra-cratonic architecture and the metallogeny of an Archaean craton: *Geological Society, London, Special Publication* 393, SP393-8; DOI 10.1144/SP393.8.

Muller D (2002) Gold-copper mineralization in alkaline rocks. *Mineralium Deposita* v.37:1–3.

Oliveira, C.G., Pimentel, M.M., Melo, L.V., Fuck, R.A., 2004. The Cooper–gold and old deposits of the Neoproterozoic Mara Rosa magmatic arc, central Brazil. Ore Geol. Rev. 25, 285–299.

Oliveira C.G., Bedran de Oliveira F., Della Giustina M.E.S,, Marques G.C., Dantas E.L., Pimentel M.M., Bunh B. M. 2015. The Chapada Cu-Au deposit, Mara Rosa Magmatic Arc, Central Brazil: Constraints on the Mettalogenesis of a Neoproterozoic Large porphyry-type deposit. 2015 , *Ore Geology Reviews*, vol. 72, pp. 1-21.

Patchett, P.J., Chase, C.G., 2002. Role of transform continental margins in major crustal growth episodes. *Geology* 30, 39–42.

Pimentel M.M., Heaman L., Fuck R.A. 1991. U-Pb zircon and sphenc geochronology of late Protcrozoic volcanic arc rock units from southwestern Goiás, Central Brazil. *Journal of South American Earth* Sciences, **4**:329-339.

Pimentel,M.M., Fuck,R.A. and Alvarenga,C.J.S. 1996. Post-Brasiliano (Pan-African) high-K granitic magmatism in central Brazil: late Precambrian/early Paleozoic extension. *Precambrian Research, v.*80:p.217-238.

Pimentel, M.M., Fuck, R.A., Ferreira Filho, C.F., Araújo, S.M., 2000. The basement of the Brasília Belt and the Goiás Magmatic Arc. In: Cordani, U.G., Milani, E.J., Thomaz Filho, A., Campos, D.A. (eds) *Tectonic Evolution of South America*. 31st International Geological Congress, Rio de Janeiro, 195–229.

Pirajno, F., 2007. Mantle plumes, associated intraplate tectono-magmatic processes and ore systems. Episodes v.30, p. 6-19.

Pirajno, F., 2010. Intracontinental strike-slip faults, associated magmatism, mineral systems and mantle dynamics: examples from NW China and Altay-Sayan (Siberia). *Journal of Geodynamics* 50, 325 e 346.

Poll, N.J., 1994. The geology of the Zacarias gold–silver –barite deposit, Goia´s State, Brazil. Unpublished MSc thesis, Colorado School of Mines, USA, 124 p.

Ramos L.N.R.A. Dados gamaespectométricos e magnetométricos aéreos aplicados ao mapeamento geológico e a exploração de ouro na região de Fazenda Nova, porção leste do Arco Magmático de Arenópolis – GO. 2010 . Dissertação de mestrado, 165 p. Universidade de Brasília.

Richards JP, Chappell BW, McCulloch MT (1990) Intraplate-type magmatism in a continent-island arc collision zone: Porgera intrusive complex, Papua New Guinea.*Economic Geology* v.18, p:958–961.

Richards JP (2009) Post-subduction porphyry Cu-Au and epithermal Au deposits: products of the remelting of subduction-modified lithosphere. *Economic Geology* 37:247–250.

Robinson F.A., Foden J.D., Collins A.S., Payne J.L., 2014 , Arabian Shield magmatic cycles and their relationship with Gondwana assembly: Insights from zircon U–Pb and Hf isotopes. *Earth and Planetary Science Letters* v.408 p.207–225.

Rock, N.M.S., and Groves, D.I., 1988, Can lamprophyres resolve the genetic controversy over mesothermal gold deposits?: *Economic Geology*, v. 16, p. 538–541.

Santos, R.V., Oliveira C. G., Parente C.V., Garcia, M.M., Dantas E. 2013. L., Hydrothermal alteration related to a deep mantle source controlled by a Cambrian intracontinental strike-slip fault: Evidence for the Meruoca felsic intrusion associated with the Transbrasiliano Lineament, Northeastern Brazil. *Journal of South American Earth Sciences* v.43, p.33-41.

Sengör, A.M.C., Natal'in, B.A., 2004. Phanerozoic analogues of Archaean oceanic basement fragments — altaid ophiolites and ophirags. In: Kusky, T.M. (Ed.),*Precambrian Ophiolites and Related Rocks. In: Elsevier, Amsterdam*, pp. 671–721.

Sillitoe RH (2002) Some metallogenic features of gold and copper deposits related to alkaline rocks and consequences for exploration. *Mineralium Deposita* v.37:p.4–13.

Storti, F., Holdsworth, R.E., Salvini, F., 2003. Intraplate strike-slip deformation belts.*Geological Society, London, Special Publication* v.210, p.1–14.

Sun W., Zhang H., Ling M., Ding Xing., Chung S.L., Zhou J., X Yang , Fan W.,2010. The genetic association of adakites and Cu-Au ore. *International geology review*, v.53, p.691-703.

Schobbenhaus, C. 1975. Carta Geológica do Brasil ao Milionésimo, Folha Goiânia - SE.22. Brasília: DNPM/Serviço Geológico Do Brasil, 74p.

Stern, R.J., 1994. Arc assembly and continental collision in the Neoproterozoic East African orogen: implications for the consolidation of Gondwanaland. Annual *Review of Earth and Planetary Sciences* v.22, p.319–351.

Tosdal, R.M., and Richards, J.P., 2001, Magmatic and structural controls on the development of porphyry Cu ± Mo ± Au deposits: *Reviews in Economic Geology*, v. 14, p. 157−181.

Thompson, J.F.H., Sillitoe, R.H., Baker, T., Lang, J.R., and Mortensen, J.K.,1999, Intrusion-related gold deposits associated with tungsten-tin provinces: *Mineralium Deposita*, v. 34, p. 323–334.

Thompson, J.F.H., and Newberry, R.J., 2000, Gold deposits related to reduced granitic intrusions: *Reviews in Economic Geology*, v. 13, p. 377–400.

Vauchez, A., Tommasi, A., 2003. Wrench Faults Down to the Asthenosphere: geological and Geophysical Evidence and Thermo-mechanical Effects. In: *The Geological Society, London, Special Publication*, vol. 210, pp. 15e 34.

Vaughan, A.P.M., Sacrow, J.M., 2003. K-rich mantle metasomatism control of localization and initiation of lithospheric strike-slip faulting. *Terra Nova* v.15 (3),p:163–169.

Windley, B.F., 1995. *The Evolving Continents, (3rd edition*). Wiley, New York. 526pp.

Zhmodik, S.M., Postnikov M.M., Buslov., Mironov A.G. Geodinamics of the Sayan-Baikal-Muya Accretion-collision belt in the neoproterozoic-early palezoic and regularities of the formation and locatization of precious-metal mineralization. *Russian Geology and Geophysics*.Vol. 47, No. 1, pp. 183-198.